3 4456 0525564 9
LOCKHEED MARTIN ENERGY RESEARCH LIBRARIES

CENTRAL RESEARCH LIBRARY
DOCUMENT COLLECTION

2

ORNL-4437
UC-4 – Chemistry

CHEMISTRY DIVISION
ANNUAL PROGRESS REPORT
FOR PERIOD ENDING MAY 20, 1969

OAK RIDGE NATIONAL LABORATORY
CENTRAL RESEARCH LIBRARY
DOCUMENT COLLECTION
LIBRARY LOAN COPY
DO NOT TRANSFER TO ANOTHER PERSON
If you wish someone else to see this document, send in name with document and the library will arrange a loan.

OAK RIDGE NATIONAL LABORATORY
operated by
UNION CARBIDE CORPORATION
for the
U.S. ATOMIC ENERGY COMMISSION

Printed in the United States of America. Available from Clearinghouse for Federal Scientific and Technical Information, National Bureau of Standards, U.S. Department of Commerce, Springfield, Virginia 22151
Price: Printed Copy $3.00; Microfiche $0.65

LEGAL NOTICE

This report was prepared as an account of Government sponsored work. Neither the United States, nor the Commission, nor any person acting on behalf of the Commission:

A. Makes any warranty or representation, expressed or implied, with respect to the accuracy, completeness, or usefulness of the information contained in this report, or that the use of any information, apparatus, method, or process disclosed in this report may not infringe privately owned rights; or

B. Assumes any liabilities with respect to the use of, or for damages resulting from the use of any information, apparatus, method, or process disclosed in this report.

As used in the above, "person acting on behalf of the Commission" includes any employee or contractor of the Commission, or employee of such contractor, to the extent that such employee or contractor of the Commission, or employee of such contractor prepares, disseminates, or provides access to, any information pursuant to his employment or contract with the Commission, or his employment with such contractor.

ORNL-4437

Contract No. W-7405-eng-26

CHEMISTRY DIVISION ANNUAL PROGRESS REPORT

for Period Ending May 20, 1969

E. H. Taylor, Director
Sheldon Datz, Associate Director
Ralph Livingston, Associate Director
B. H. Ketelle, Assistant Director

G. E. Moore, Editor of Annual Report

SEPTEMBER 1969

OAK RIDGE NATIONAL LABORATORY
Oak Ridge, Tennessee
operated by
UNION CARBIDE CORPORATION
for the
U. S. ATOMIC ENERGY COMMISSION

LOCKHEED MARTIN ENERGY RESEARCH LIBRARIES

3 4456 0515564 9

Reports previously issued in this series are as follows:

ORNL-2386	Period Ending June 20, 1957
ORNL-2584	Period Ending June 20, 1958
ORNL-2782	Period Ending June 20, 1959
ORNL-2983	Period Ending June 20, 1960
ORNL-3176	Period Ending June 20, 1961
ORNL-3320	Period Ending June 20, 1962
ORNL-3488	Period Ending June 20, 1963
ORNL-3679	Period Ending June 20, 1964
ORNL-3832	Period Ending May 20, 1965
ORNL-3994	Period Ending May 20, 1966
ORNL-4164	Period Ending May 20, 1967
ORNL-4306	Period Ending May 20, 1968

Contents

INTRODUCTION ix

1. NUCLEAR CHEMISTRY 1

^{160}Gd (^{3}He,d) Reactions 1

Neutron Emission in the Fission of ^{213}At 2

Search for the 0^+ Member of the Two-Phonon Triplet in ^{110}Cd 3

Decay of ^{74}As 4

Studies of the Radioactive Decays of ^{152}Eu and ^{154}Eu 4

The Decay of ^{110m}Ag: Gamma-Ray Energy and Intensity Standardization 6

Levels in ^{172}Yb Populated in the Decay of ^{172}Lu 6

New Erbium Isotope, ^{155}Er 7

Decay of ^{89}Nb and ^{89m}Nb 10

Radioactive Decay of ^{192}Au and ^{194}Au 10

Short-Half-Life Rare-Earth Isotopes 13

Alpha Decay of ^{227}U 14

A Computer-Controlled, Iron-Core β Spectrometer 16

Low-Level Gamma-Ray Spectrometer for Lunar Sample Analysis 16

2. CHEMISTRY AND PHYSICS OF TRANSURANIUM ELEMENTS 20

Thermal-Neutron Capture Cross Section and Resonance Integral of ^{245}Cm and ^{246}Cm 20

Thermal Fission Cross Section and Resonance Integral of ^{249}Cf 22

Capture and Absorption Cross Section of ^{253}Cf 22

Delayed-Neutron Energy Spectra and Group Abundances from the Spontaneous Fission of ^{252}Cf 24

Search for ^{258}Fm and Half-Life Limit for Spontaneous-Fission Decay 24

Fragment Energy Correlation Measurements for the Fission of ^{238}U and ^{239}Pu by 8- to 13-MeV Protons 26

The Half-Lives of ^{253}Cf and ^{253}Es 28

States in ^{249}Cm Populated in the Alpha Decay of 17.6-day ^{253}Cf 29

Nuclear Chemistry with Heavy Ions 30

Chemical Properties of the Superheavy Elements. I. Elements 113 and 114, Eka-Thallium and Eka-Lead 30

Lanthanide and Actinide Standard II-III Oxidation Potentials and the Optical Absorption Spectra of Some Lanthanide and Actinide Trihalides in Ethanol 31

Crystal Structure of Americium Trichloride Hexahydrate 32

Crystal Structure of Anhydrous $AmCl_3$ 33

Preparation and Identification of Cyclopentadienyl Complexes of the Actinide and Lanthanide Elements 34

Preparation of Berkelium Metal 35

Szilard-Chalmers Process Using Metal Phthalocyanines for Isotope Enrichment 36

Preparation and Properties of Some Rare-Earth Chelates 36

Gas-Jet System for Rapid Collection of Recoil Nuclei 37

Transuranium Research Laboratory Isotope Separator 37

3. ISOTOPE CHEMISTRY 40

Fractionation of Carbon Isotopes: The COCO System 40

Fractionation of Carbon Isotopes: The CYANEX System 40

^{17}O Facility 41

Chemical Fractionation of Uranium Isotopes 41

Mass Spectrometric Determination of Small Differences in Deuterium Concentration in Water Samples 42

Isotopic Mass Spectrometry 43

Molecular Spectroscopy 44

Spectral Studies of MoF_5 46

4. RADIATION CHEMISTRY 48

Pulse Radiolysis of NO: Production of NO_2 and N_2O_3 and the Production and Relaxation of Vibrationally Excited NO 48

The Use of CO to Detect $O(^1D)$ in the Pulse Radiolysis of O_2 49

Flash Photolysis of Water and Oxygen-Saturated Water 49

Flash Photolysis of Ice 50

Reactivities of Peroxysulfuric Acids with H Atom 51

Kinetic Evidence for a Primary Yield of SO_4^- Radicals in the Radiolysis of Aqueous Sulfuric Acid Solutions 52

Energy Transfer and the Radiolysis of Aliphatic Carboxylic Acids 54

RADIATION AND HOT-ATOM CHEMISTRY OF INORGANIC CRYSTALLINE SOLIDS

Chemistry of ^{38g}Cl Recoils in Neutron-Irradiated Crystalline $KClO_2$, $KClO_3$, and $KClO_4$ 55

Production of ClO_4^- and ClO_2^- Ions in Crystalline $KClO_3$ Irradiated with ^{60}Co Gamma Rays 56

Production of Bromite and Perbromate Ions in Crystalline $CsBrO_3$ Irradiated with ^{60}Co Gamma Rays and the Vibrational Spectrum of BrO_4^- Ion 56

5. ORGANIC CHEMISTRY 57

Preparation and Deamination of 5-*exo*-Phenyl-5-hydroxy-2-*exo*-norbornylamine and 5-*endo*-Phenyl-5-hydroxy-2-*exo*-norbornylamine 57

Deamination of 3-*exo*- and 3-*endo*-Phenyl-^{14}C-3-hydroxy-2-*endo*-norbornylamines 58

Degradation of 2-*exo*-Norborneol-^{14}C 58

POLYMER STUDIES

Equilibria in the System: Poly(Hydroxypropyl Acrylate-co-Tetraethylene Glycol Dimethacrylate), Water, and Electrolyte 59

6. CHEMISTRY OF AQUEOUS SYSTEMS 60

The Thermodynamic Properties of HCl-CsCl-$BaCl_2$ Mixtures 60

On the Existence of the Complex $AgSO_4^-$ in Aqueous Solutions 63

A Monte Carlo Calculation of Some Thermodynamic Properties of Steam Using a Dipole-Quadrupole Potential 64

Free Energies of Electrolyte Mixtures 67

Apparent Molal Volumes of the Lithium and Sodium Halides. Critical-Type Transitions in Aqueous Solution 71

Miscibility in the System Pyridine–Sulfuric Acid–Water 71

Activity Coefficients of NaCl at Saturation in Water Mixtures of Polyglycols and Polyglycol Ethers at 50°C 72

Properties of Sephadex Quaternary Amine Anion Exchangers 74

Diffusion Studies 76

Hyperfiltration with Dynamically Formed Membranes 78

PHYSICAL CHEMISTRY OF POLYELECTROLYTE SYSTEMS

Thermal Effects in Ion-Exchange Reactions with Organic Exchangers: Enthalpy and Heat Capacity Changes 84

Thermodynamic Studies on the Bolaform Electrolytes $[Bu_3N\text{-}(CH_2)_8\text{-}NBu_3]X_2$ in Aqueous Solution 85

7. ELECTROCHEMICAL KINETICS AND ITS APPLICATION TO CORROSION 87

Kinetics of the Formation and Discharge of the Superpassive Film on Iron 87

Electrochemical Behavior of Titanium 89

Properties of the Suspension Electrode 90

Theory of the Suspension Electrode 93

Rhenium-Nickel Suspension Electrode Catalysts 95

Kinetics of Pit Initiation on Titanium in Chloride Solution 96

8. NONAQUEOUS SYSTEMS AT HIGH TEMPERATURES 98

PHASE DIAGRAMS

Limits of Miscibility in Molten-Salt Systems: KBF_4-LiF, Li_2BeF_4-KI, and Li_2BeF_4-KBF_4 98

A Correlation of the Solubility of Cerium Trifluoride in Molten Mixtures of Lithium, Beryllium, and Thorium Fluorides with Solvent Composition 99

MOLTEN-SALT–METAL SYSTEMS

Solubility of Thorium Metal in Molten Lithium Fluoride–Thorium Fluoride Mixtures 101

A Reference Electrode System for Possible Use in Fluoride Melts 102

Solubility of Lanthanum in Molten Lanthanum Triiodide 103

HIGH-TEMPERATURE THERMOCHEMISTRY

The Order-Disorder (λ) Transition in Uranium Dioxide and Other Solids of the Fluorite Type. Effect of Ion Size and Deviation from Stoichiometry 103

Heat Content of Sodium and Potassium Fluoroborates from 298 to 900°K: Heats of Fusion and Transition 106

Heat Capacities and Heats of Fusion of Molten-Salt Reactor Fuel, Coolant, and Flush Salts 106

9. CHEMICAL PHYSICS 107

Spectrophotometry of Solutions over Wide Ranges of Temperature and Pressure 107

Study of the Electronic Structure of Molecules by Means of High-Resolution Electron Spectrometry 108

CALORIMETRY

High-Temperature Enthalpies of the Lead Halides. Enthalpies and Entropies of Fusion 111

The Heat Capacity of Potassium Pertechnetate from 9 to 310°K. Entropy and Free Energy Functions 114

Preparation of K_2TcCl_6 for Calorimetric Studies 115

MICROWAVE AND RADIO-FREQUENCY SPECTROSCOPY

Paramagnetic Resonance Studies of Liquids During Photolysis 115

Paramagnetic Resonance Study of ^{17}O-Labeled NO_2 in Sodium Nitrite Crystals 117

NEUTRON AND X-RAY CRYSTALLOGRAPHY

A Neutron Diffraction Study of Magnesium Chloride Hexahydrate 117

Neutron Diffraction Studies of Calcium Chloride Hexahydrate and Strontium Chloride Hexahydrate 118

Correcting Interatomic Distances and Angles for Thermal Motion 119

Higher-Order Effects in Rigid-Body Motion 122

Crystal and Molecular Structures of Tri(*p*-fluorophenyl)amine and Tri(*p*-iodophenyl)amine 125

Crystal Structure of Sedoheptulosan Monohydrate 129

Diffraction Pattern and Structure of Aqueous Ammonium Halide Solutions 132

Observed Diffraction Pattern and Proposed Models of Liquid Water 136

MOLECULAR BEAM STUDIES

Inelastic Scattering of Alkali Atoms and Ions from Hydrogen Molecules 137

Crossed-Molecular-Beam Studies of Bimolecular Association and Unimolecular Decomposition Reactions 138

"Hot" Atomic Halogen Beams from Sputtering of Silver Halides 140

Crossed-Molecular-Beam Studies of Reactions of Atomic Deuterium with Halogen Molecules 141

MASS SPECTROMETRY AND RELATED TECHNIQUES

Preliminary Mass Spectral Studies of Silane 142

PUBLICATIONS 144

PAPERS PRESENTED AT SCIENTIFIC AND TECHNICAL MEETINGS 150

LECTURES 155

SUPPLEMENTARY ACTIVITIES 157

Introduction

This part of the annual report is again an introduction rather than a summary, but the Table of Contents should serve most of the functions of the latter. A minor change in the report is an expansion of the section on publications and oral presentations to include certain other information about our interaction with outside scientists and organizations.

During the year covered by this report, our earliest members celebrated 25 years with the Laboratory; 25 years ago was near the end of the first year's operation of Clinton Laboratories and the Chemistry Division. It may therefore be amusing, if nothing more, to note some comparisons between then and now, looking at some of our present activities in the perspective of a quarter of a century.

In 1943–44, the chief goal of the whole laboratory was the production of the first two of the man-made transuranium elements, neptunium and plutonium; in 1968–69, new elements were again a major interest of the Chemistry Division and the Laboratory. In 25 years, the atomic numbers of interest had increased by about 10, so that during the past year we have been synthesizing a few atoms of elements above $Z = 100$ while doing macrochemical experiments (synthetic, crystallographic, and optical) on berkelium, californium, and curium. The greatest factor in thus raising the limits of our research has been the High Flux Isotope Reactor with maximum flux of *ca.* 5×10^{15} cm^{-2} sec^{-1} compared with the old Clinton Pile (Oak Ridge Graphite Reactor) with maximum flux *ca.* 5×10^{12}. The most important current development in this direction, however, was the production at the Oak Ridge Isochronous Cyclotron of intense beams of carbon, nitrogen, and oxygen. It is with these that the heaviest elements now available can be made. A major development for the future of synthetic elements was the rapid convergence of plans of several divisions (Electronuclear, Physics, Chemistry) upon an accelerator for heavy ions that has as a major goal the synthesis of superheavy elements, those elements several decades of Z above 100 which have recently been predicted to be sufficiently stable to be detected if formed. The new accelerator would have the capability of accelerating uranium ions to an energy enabling them to penetrate a target uranium nucleus.

As a guide to such experiments and to a search for such elements in nature (their predicted stability makes this a reasonable gamble), extrapolations were made during the year to obtain the chemical properties of elements near $Z = 114$. Element 114 itself, eka-lead, is expected to be almost exclusively divalent and to be somewhat more noble than lead.

Aside from the chemistry of the newest elements and process chemistry (now the province of the Chemical Technology Division), the Chemistry Division of 1943–44 was concerned with both nuclear chemistry and radiation chemistry. These fields still concerned us in 1968–69, indirectly for the same practical reasons. The information being sought and the means employed, however, have evolved remarkably in the intervening years. A fission product radionuclide was then well characterized if its yield, half-life, type of decay, and approximate energy of decay were known. Measurements of radioactivity were made with Geiger-Müller counters or with ionization chambers, and energies were estimated by interposition of different thicknesses of aluminum (of which the custom-rolled sizes can still be identified in the stock room by their exorbitant prices). Today, a decay scheme is unsatisfactory unless it shows all the nuclear energy levels involved, with assignment of spin and parity to each. The G-M counter is gone from the counting room, having been replaced successively by the scintillation counter and by the semiconductor detector, both of which measure the energies of the absorbed particles or quanta as well as their number.

In spite of these technical advantages, nuclear chemists today are limited in one important way over their counterparts in 1943–44. At that time, one element internal to the periodic system remained unknown, but the discovery of promethium among the fission products closed this possibility. Today, one can

find a new element only in the region beyond the end of the periodic table.

Immediate practical considerations still dictate part of our program in nuclear chemistry. The ever-increasing demands on reactors for performance and economy (and for production of transuranium elements) require better knowledge of neutron cross sections, and the nuclides of interest become steadily those of lower abundance or lower yield in fission.

The radiation chemistry done here in 1943–44 was minimal, being confined to gross measurements of H_2O_2 production in the irradiation of water, and some studies of radiation effects on materials (Masonite, for one) and on separation processes and analytical methods. The great boom in it here began about a year later with plans for a homogeneous pile. In 1968–69, radiation chemistry was a major part of the Chemistry Division program, a reflection of the importance of the field to homogeneous reactors and to radiobiology, and of its intrinsic interest. In two parts of the program, analysis of the products of a finite amount of reaction is carried out, as has been done from time immemorial in any kind of chemical kinetics, but the techniques of analysis, both chemical and numerical, typify the changes in the intervening years. In studies of the radiolysis of homologous organic acids, gas chromatography provides rapid, sensitive, and accurate measurement of almost any of the products. In studies of radiolysis of aqueous solutions (25 years have not seen that job completed), modern computing ability makes possible the testing of complex kinetic schemes which could only be talked about 25 years ago, even when comparable data were available. The greatest change, however, is in the pulsed work, in which short-lived intermediates, only guessed at previously, can be produced and measured to good precision in spite of lifetimes shorter than microseconds. A corollary of such developments is the concomitant receding of the final truth – the radiation chemistry of water, for example, shows new complications as new techniques give more penetrating insights. The hydrated electron, one of today's standard primary products of radiolysis, was unsuspected when modern radiation chemistry began.

The work of the Chemistry Division with plutonium and with process chemistry in 1943–44 was almost entirely solution chemistry, but the establishment of Chemistry of Aqueous Systems as a topic of basic research had to wait for slightly more leisure than the pursuit of plutonium allowed. An ion exchange alternative to the bismuth phosphate process was being actively studied 25 years ago, and both fundamental and practical work with ion exchangers has always been a large part of our program. Anion exchange as a separations technique for metals (through complex ions) was started here, and the research included in this report under Chemistry of Aqueous Systems includes numerous studies of ion exchange. A major later influence on our aqueous research was the lamented Homogeneous Reactor; it aroused our interest in higher temperatures even in the basic work. Some of this influence still remains, although the largest part of our pioneering work on aqueous solution thermodynamics at high temperature went with the Reactor Chemistry Division when that separated from us. A new practical focus for all of our aqueous work arose recently with our involvement in desalination and related problems.

Some of our present research, naturally, was not part of our original program; we have entered some other established fields because of their relevance to the Laboratory's interests, and we have helped to establish some new ones because we found we could.

Isotope Chemistry, an example of the former class, was invented during the 1930's and was an important part of the earliest work on atomic energy. The Chemistry Division became involved some 12 years ago as part of the final absorption of some Y-12 activities into ORNL. It is still our laboratory-in-miniature, the only part of the Division in which process development and production accompany research.

Organic chemistry, as practiced here, has two origins, both almost as old as the Laboratory. The use of solvent extraction in early process chemistry obviously required organic chemists; this line led to the present involvement with the Water Research Program through synthesis and study of new or special polymeric materials for membranes or additives, and to involvement with the Transuranium Program through research with metal-organic compounds of the actinides. The part of our organic chemistry that arose from early production and synthetic studies on carbon-fourteen is now chiefly motivated by the power of isotopic techniques to solve problems of mechanism. In this enterprise most of its interaction is with extra-Laboratory groups, but its natural adoption of physical techniques (e.g., NMR) to supplement isotopic methods is bringing it considerable consulting business from other parts of ORNL.

Our program in Electrochemical Kinetics arose from practical problems posed by the aqueous homogeneous reactor, but its detailed course was set more closely by a theoretical prediction about inhibition of corrosion by the pertechnetate ion. The availability of this man-made element for experimental use promoted both experiment and further theoretical development. Both

kinds of research (not, of course, any more confined just to inhibition) are represented in this report. Here, also, the stimulus of a new technology (desalination) can be seen in some of the topics.

Our work in molten salts began with the Laboratory's first interest in these for reactor applications. The experimental techniques developed over many years are now largely at the service of current MSBR problems, although metal–molten-salt solutions, which were the principal interest of this group, continue to receive attention.

The enterprises lumped under Chemical Physics probably have the most tenuous programmatic connection with our past, although their roots are at least partly in the west wing of Building 3550 (née 706-A), our original divisional home. Several lines of research related more to our unique capabilities than to the problems of our technology arose as soon as the needs of the original program were satisfied. The archetype of these is neutron diffraction, pursued by one of our largest groups. The unique capabilities of neutron diffraction for certain structural problems give it a viability quite independent of practical connections, but it has nevertheless profited immensely from certain practical developments. Every increase in reactor flux increases the capability of associated neutron diffractometers; such increases are usually motivated by needs for production (the HFIR) or by other practical considerations. Furthermore, the extensive and precise diffraction data would be almost useless without the high-speed computers obtained originally for reactor physics and other practical calculations.

The microwave spectroscopy group, now concerned exclusively with the study of free radicals by ESR, was organized to take advantage of the Laboratory's production of short-lived isotopes of iodine. The rotational spectra of simple compounds of these furnished values for the nuclear spins and magnetic moments of the various iodine isotopes. The competence in microwave (and radio-frequency) spectroscopy thus developed was applied next to pure quadrupole spectroscopy and then to the present major interest, ESR. The information gained through the latter about free radicals is, of course, of great interest to radiation chemists and to photochemists, free radicals being participants in almost all of the reactions studied by them.

The study of chemical reactions by means of molecular beams is perhaps as distantly related a field as we pursue. It was born here honestly with the intended use of neutron activation as a detection method, and it seems now to be establishing new programmatic ties by the development of fast beams which can be used to study the fundamentals of hot-atom processes.

Thus, to a considerable degree, one can say of the Chemistry Division 25 years later, *plus ça change, plus c'est la même chose.* So far as this reflects continuing attention to the needs of our larger enterprises, this is good. The questions put by technology to chemistry are not usually quickly answered. But the ability to do useful things well and easily can be a comfortable trap. Tennyson, a hundred years before our time, described the reaction of Ulysses to a similar one:

"---; but something ere the end,
Some work of noble note, may yet be done,
Not unbecoming men that strove with Gods.

---. Come, my friends,
'Tis not too late to seek a newer world.

Tho' much is taken, much abides; and tho'
We are not now that strength which in old days
Moved earth and heaven, that which we are, we are, --

Made weak by time and fate, but strong in will
To strive, to seek, to find, and not to yield."

1. Nuclear Chemistry

^{160}Gd(^{3}He,d) REACTION

R. G. Lanier[1] N. R. Johnson
J. B. Ball[2] G. D. O'Kelley
R. K. Sheline[3]

During the last year an experimental study of the (^{3}He,d) reaction on an enriched target of ^{160}Gd using 50-MeV ^{3}He particles was completed. In addition to acquiring more information concerning the level structure of ^{161}Tb, we undertook this study primarily to determine the extent to which the Nilsson model[4] and distorted-wave reaction theory (DWBA)[5] could account for an (^{3}He,d) stripping process on a deformed even-even target.

Data from the ^{160}Gd(^{3}He,d) reaction were taken with the Oak Ridge Isochronous Cyclotron broad-range spectrograph facility at scattering angles of 4, 7, 10, 13, 16, and 21°. A typical deuteron spectrum which exhibits an energy resolution of approximately 40 keV FWHM is shown in Fig. 1.1. Although the data analysis is not yet complete, some preliminary comments concerning the spectral properties of ^{161}Tb can be made.

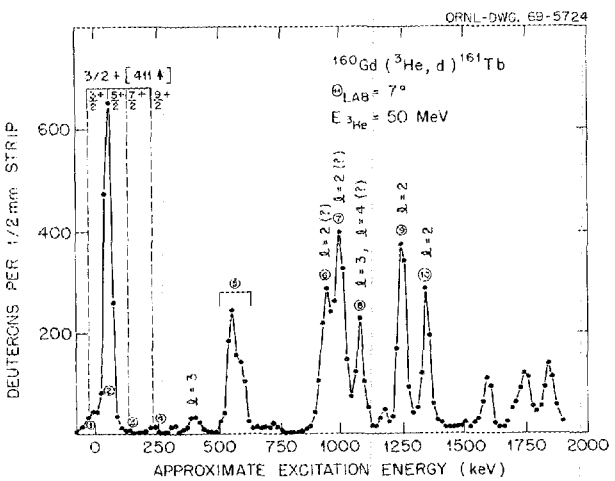

Fig. 1.1. Deuteron Spectrum from the Reaction ^{160}Gd(^{3}He,d)^{161}Tb.

The ground-state spin-parity of ^{161}Tb has been measured to be $3/2^+$ and most probably results from the odd proton being in the $3/2^+$ [411↑] orbit. In Fig. 1.2 are plotted the angular distributions for the population of the first four levels observed in the ^{161}Tb spectra. A DWBA analysis of these angular patterns clearly indicates l = 2 for the deuteron groups 1 and 2; groups 3

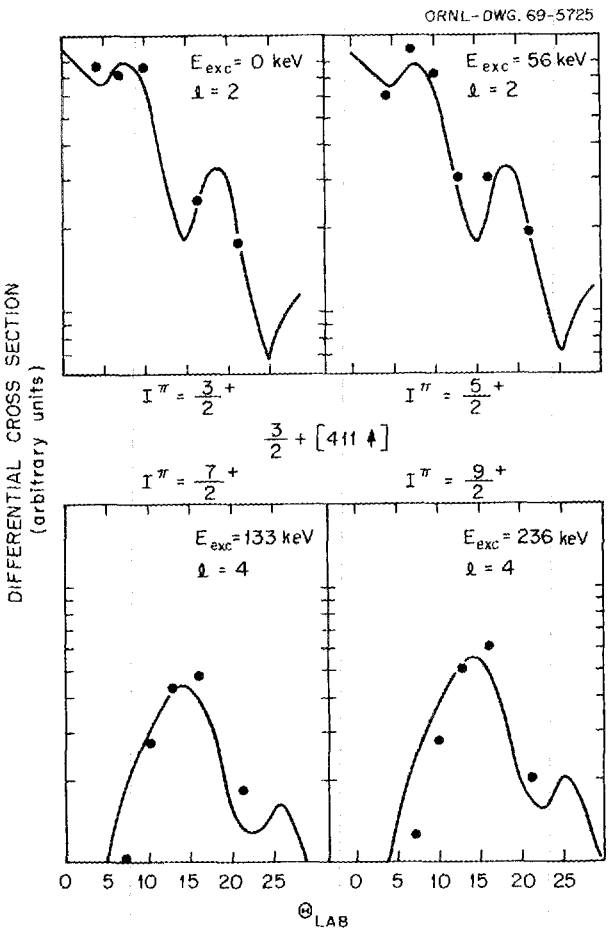

Fig. 1.2. Angular Distributions for the Deuteron Groups Labeled 1 to 4 in Fig. 1.1. The dots are experimental points, and the solid line is the calculated angular pattern from DWBA theory.

and 4 exhibit $l = 4$. The energy spacing of these states, as well as their l-transfer sequence, is consistent with the identification of these levels as members of the $K^\pi = 3/2^+$ ground-state rotational band. Furthermore, the relative cross sections within this band are in generally good agreement with those expected from the rotational states built on the $3/2^+$ [411↑] configuration.

In view of the structure of the ground state, it is expected that a $(K - 2)$ $\gamma = 1/2^+$ vibrational band built on the ground state will be observed somewhere below 1 MeV. The level structures of both ^{157}Tb and ^{159}Tb have been investigated by various decay processes, and in each case an $I^\pi = 1/2^+$ level is observed at approximately 600 keV. Considering these systematics, it is not unreasonable to expect that a similar $I^\pi = 1/2^+$ level will also be observed in ^{161}Tb in the neighborhood of 600 keV. A $1/2^+$ state at this energy can be interpreted as the band head of either the $1/2^+$ [411↓] orbital or the $(K - 2)$ γ vibration, or more reasonably as a mixture of both configurations. Soloviev[6] has shown the character of the 765-keV level in ^{155}Eu and the 423-keV level in ^{165}Ho to be 67 and 95%, respectively, $1/2^+$ [411↓], with most of the remainder being the $(K - 2)$ γ vibration. On this basis alone one might expect that the ^{161}Tb nucleus, with intermediate proton number, might involve a state whose character is 80% $1/2^+$ [411↓], with most of the remaining 20% being the $(K - 2)$ γ vibration.

In Fig. 1.1 the partially resolved complex group (5) appears to be evidence for the population of a band which may contain some $1/2^+$ [411↓] character. Since this population is complex, the angular pattern of the components is not unambiguous; however, there does appear sufficient evidence to warrant the conclusion that the lower-energy component ($E_{exc} \cong 540$ keV) has an angular momentum transfer which is low (e.g., $l \leqslant 2$). Assuming that the complex group is totally due to the population of a set of closely spaced rotational levels arising from the $1/2^+$ [411↓] orbital, the observed intensity appears substantially lower than that expected from the pure configuration. In fact, these intensity considerations indicate that the complex line cannot have more than a 50% admixture of $1/2$ [411↓], thereby suggesting that these partially resolved lines have a character which is predominantly the $(K - 2)$ γ vibration. These comments are somewhat speculative, because all the possible Nilsson states which may contribute to the ^{161}Tb spectrum have not yet been fully explored, but it appears that the intensities of groups 6 and 8 are more in line with what is expected of a band which is predominantly $1/2^+$ [411↓].

[1] U.S. Atomic Energy Commission Postdoctoral Fellow under appointment with Oak Ridge Associated Universities.

[2] Electronuclear Division.

[3] Florida State University, Tallahassee.

[4] S. G. Nilsson, *Kgl. Danske Videnskab. Selskab, Mat.-Fys. Medd.* 29, No. 16 (1955).

[5] R. H. Bassel, R. M. Drisko, and G. R. Satchler, *The Distorted-Wave Theory of Direct Nuclear Reactions. I*, ORNL-3240 (Feb. 9, 1962).

[6] V. G. Soloviev, P. Vogel, and G. Jungklaussen, Dubna preprint No. E4-3051.

NEUTRON EMISSION IN THE FISSION OF ^{213}At

Franz Plasil[1] Robert L. Ferguson
H. W. Schmitt[1]

Information concerning the excitation energy of fission fragments is necessary for a complete study of the energetics of the fission process. The number of neutrons emitted by the fragments as they deexcite is an important measure of this excitation energy. As part of a general survey of fission energetics, we have used an indirect method[2] to determine neutron emission, as a function of fragment mass and kinetic energy, for the fission of the compound nucleus ^{213}At. The indirect determination used here has the advantage that it is not subject to large background corrections, as direct neutron counting would be, and, further, that complete kinetic information is also obtained.

A simplified schematic representation of the experimental arrangement and method of analysis is shown in Fig. 1.3. A thin target of ^{209}Bi was bombarded with 53.25-MeV ^{4}He ions at the Oak Ridge Isochronous Cyclotron. Two silicon surface-barrier detectors were used to measure kinetic energies of fragment pairs and to provide timing pulses for the measurement of the velocity of one of the fragments. Three pulse heights, related to the two fragment energies and to the time of flight, were recorded event by event. These correlated data, with calibrations obtained from a companion experiment on spontaneous fission of ^{252}Cf, were used to calculate, for each event, the post-neutron-emission fragment mass m_1, as given in Fig. 1.3. In the resulting (E_1, E_2) array, a value for the average pre-neutron-emission fragment mass m_1^* was computed for each (E_1, E_2) cell. The derivation of the expression for m_1^* shown in Fig. 1.3 is given in detail in ref. 2. The average number of neutrons ν_1 emitted by a fragment of given mass was then obtained from the difference between pre- and post-neutron-emission masses.

In addition to the neutron-emission results, information was obtained in this experiment on several other

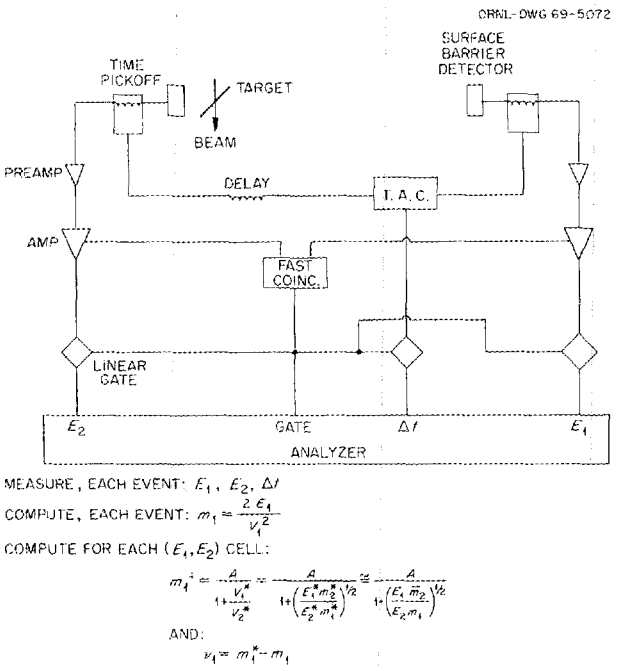

Fig. 1.3. Schematic of Experiment and Analysis for Indirect Determination of Neutron Emission.

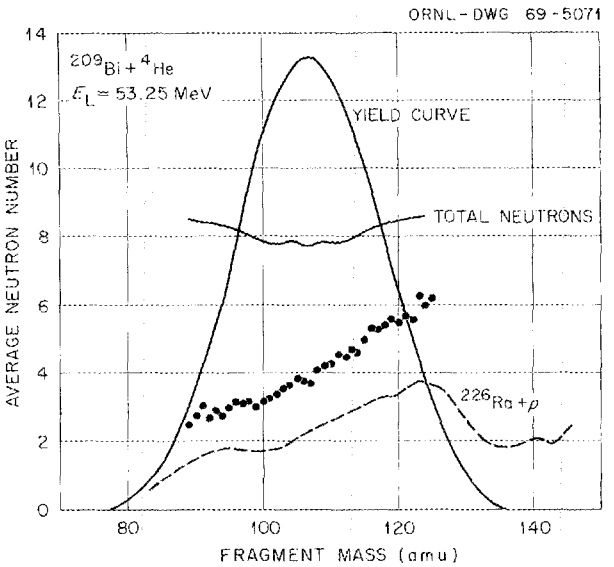

Fig. 1.4. Preliminary Results of the Bombardment of ^{209}Bi with 53.25-MeV ^{4}He Ions. The average number of neutrons emitted by each fragment is represented by the points. The mass-yield distribution from this experiment and previously determined neutron results for proton-induced fission of ^{226}Ra are shown for reference.

features of the system. In Fig. 1.4 are summarized some of the results of a preliminary analysis of the data. These results may be subject to small changes as calibration constants deduced from the ^{252}Cf experiment are refined. The average number of neutrons emitted from single fragments (indicated by the points) rises monotonically from about two neutrons at fragment mass 90 to five neutrons at mass 120. This trend is in accord with trends predicted by the liquid-drop theory of fission,[3] which has been applied with some success in this mass region. Also shown in Fig. 1.4 for reference are results[4] for proton-induced fission of ^{226}Ra, the lightest target for which neutron emission had been studied previously. It can be seen that in the region where the radium system exhibits symmetric mass division, the neutron functions are quite similar in shape. The distribution of neutrons emitted by both fragments together is indicated by the curve labeled "total neutrons." The weighted average of this distribution is ~7.9. The mass-yield curve, which exhibits the expected symmetric distribution, is given primarily for reference.

In addition to these results, two-parameter correlated distributions have also been deduced from the data. These include neutron-emission distributions as a function of fragment mass and total kinetic energy as well as fragment mass-energy relations.

[1] Physics Division.

[2] H. W. Schmitt, R. W. Lide, and F. Pleasonton, *Nucl. Instr. Methods* 63, 237 (1968).

[3] J. R. Nix and W. J. Swiatecki, *Nucl. Phys.* 71, 1 (1965).

[4] E. Konecny and H. W. Schmitt, *Phys. Rev.* 172, 1213 (1968).

SEARCH FOR THE 0$^+$ MEMBER OF THE TWO-PHONON TRIPLET IN ^{110}Cd

M. C. Kelley[1] R. G. Lanier[2]
J. R. Van Hise[1] Noah R. Johnson

In many cases the low-lying states of medium-weight even-even nuclei have been shown to have a collective nature in that they possess the properties of quadrupole surface vibrations about a spherical equilibrium shape. In the quadrupole vibrator model, small interparticle couplings remove the degeneracy of a two-phonon vibration to give triplet levels with spin-parity of 0$^+$, 2$^+$, and 4$^+$ at about twice the energy of the first excited 2$^+$ state. The 2$^+$ and 4$^+$ members of this triplet are seen in many nuclei, but only in a few cases is the 0$^+$ member observed. Even then, it is not always clear that it has the same collective character as the other two members.

For some time we have been involved in searching for these "two-phonon" 0$^+$ states and documenting as

many of their properties as possible. It is felt that by investigating a large number of these cases, we can perhaps observe some systematic pattern of behavior. Such detailed information is necessary for the formulation of a meaningful theoretical description of these states.

In the present experiments we have reinvestigated the decay of 24-sec ^{110}Ag with the use of high-resolution lithium-drifted germanium detectors. The energies in kiloelectron volts (and relative intensities) of the gamma rays observed are 657.6 (100), 815.1 (1.06), 1125.2 (0.42), 1186 (0.066), 1421 (0.026), 1475.4 (0.13), 1630 (0.59), 1674 (0.19), and 1783 (0.22).

Among the gamma rays observed in recent high-resolution measurements[3] of the decay of 250-day ^{110m}Ag were transitions at 818.00 ± 0.04 and 1475.73 ± 0.04 keV. The latter transition, which is known to be the cross-over between the second 2^+ and ground states, agrees well with that observed in our measurements on the 24-sec ^{110}Ag, but there is a large variance in the two values for the other transition. Since ^{110}Ag has a spin of 1^+ and ^{110m}Ag a value of 6^-, we interpret this variance as primarily due to a large population of the two-phonon 0^+ state in the first case and a large population of the second 2^+ state in the latter case. Still a stronger argument that the 0^+ member of the two-phonon triplet is heavily populated in the decay of 24-sec ^{110}Ag is the fact that the ratio of the intensities of the 815.1- and 1475.4-keV gamma rays in the present experiments is 8.1, whereas Brahmavar *et al.*[3] get a ratio of 1.73 for the 818.00- and 1475.73-keV transitions seen in the decay of ^{110m}Ag.

---

[1]Chemistry Department, Andrews University, Berrien Springs, Mich.

[2]U. S. Atomic Energy Commission Postdoctoral Fellow under appointment with Oak Ridge Associated Universities.

[3]S. M. Brahmavar, J. H. Hamilton, A. V. Ramayya, and C. E. Bemis, Jr., *Nucl. Phys.* **A125**, 217 (1969).

DECAY OF ^{74}As

J. H. Hamilton[1] A. V. Ramayya[1]
F. E. Coffman[1] Noah R. Johnson

A reinvestigation of the levels in ^{74}Ge populated by the decay of ^{74}As has revealed a 0^+ state at 1482.6 keV. This is presumably a member of the two-phonon vibrational triplet. Gamma-ray spectral and gamma-gamma directional correlation measurements were performed with Ge(Li) and NaI-Ge(Li) detector arrangements. Eleven transitions from 595.7 to 2198.4 keV were observed and fitted into levels at 595.7 ± 0.1, 1204.3 ± 0.1, 1463.2 ± 1.0, 1482.6 ± 0.5, 1697.3 ± 1.0, and 2198.2 ± 0.5 keV in ^{74}Ge and 634.8 ± 0.1 keV in ^{74}Se.

Directional correlation measurements were performed on the 608-596 keV 2-2-0 cascade and on the 887-596 keV cascade. In the first case, $A_2 = -0.24 \pm 0.04$ and $A_4 = 0.30 \pm 0.05$. These data yielded a $(7^{+3}_{-6})\%$ $M1$ admixture for the 608-keV transition. For the latter correlation, values of $A_2 = 0.6 \pm 0.2$ and $A_4 = 1.3 \pm 0.2$ were found. These values are compatible only with the 0-2-0 cascade, and thus the level at 1482.6 keV has spin zero. Percent feedings and log *ft* values were calculated for decays to ^{74}Ge and ^{74}Se.

---

[1]Physics Department, Vanderbilt University, Nashville, Tenn.

STUDIES OF THE RADIOACTIVE DECAYS OF ^{152}Eu AND ^{154}Eu

L. L. Riedinger[1] Noah R. Johnson
J. H. Hamilton[2]

The onset of nuclear deformation is rather abrupt at the beginning of the rare-earth region of deformed nuclei. The ^{152}Gd nucleus, with 88 neutrons, has been characterized as nearly spherical in shape, partially on the basis of a vibrational-like spectrum. The $N = 90$ nuclei, for example ^{152}Sm and ^{154}Gd, display the low-lying excited states characteristic of rotational spectra and are considered to be deformed. However, these three nuclei are better referred to as transitional, since their properties preclude classifications as well-formed spherical or deformed nuclei. The first excited state of ^{152}Gd occurs at 344 keV, lower than expected for a quadrupole vibration about a spherical shape. The levels of the rotational spectra of ^{152}Sm and ^{154}Gd deviate more widely from the $I(I + 1)$ energy spacings expected for rigid rotators than do the levels in heavier rare-earth nuclei. Also, the quadrupole-vibrational states of the two latter nuclei are found at lower energies than the corresponding levels in the heavier nuclei. These facts indicate that ^{152}Sm and ^{154}Gd are rather "soft" deformed nuclei. Comparative studies of these three nuclei can lead to a wealth of information concerning collective effects in transitional nuclei, and several years ago we therefore initiated experiments on the gamma rays emitted in the radioactive decays of ^{152}Eu and ^{154}Eu.

Gamma rays emitted in the decays of ^{152}Eu and ^{154}Eu have been studied with Ge(Li) and NaI detectors. Energies and relative intensities were derived from singles experiments involving large-volume Ge(Li)

detectors, and assignments of gamma rays to transitions in the level schemes were made with the help of Ge(Li)-NaI coincidence measurements.

A detailed discussion of the complex level properties revealed in these measurements will not be presented here; some preliminary results of these measurements have already been published,[3] as have most of our conclusions[4,5] on the properties of the β and γ vibrational bands. However, we do show in Figs. 1.5–1.7 the level schemes of ^{152}Sm, ^{152}Gd, and ^{154}Gd respectively. Much of the new information deduced from our experimental investigation is reflected in these three figures.

In all, 52 gamma rays were found in the ^{152}Eu decay and 58 in the ^{154}Eu case. Three members each of the β and γ vibrational bands were observed. In addition, the results of the coincidence experiments are used to assign a level at 1649.8 keV as the probable 2^- member of the $K = 2$ band in ^{152}Sm. The properties of this state and of the $K_\pi = 0^-$ and 1^- bands are compared with the properties of the corresponding states in ^{154}Gd. It is found that there is evidently less Coriolis coupling between the negative-parity states in ^{152}Sm than in ^{154}Gd. The members of the $K_\pi = 1^-$ band in the former are not inverted as in the latter, and the $B(E1)$ ratios from the $K_\pi = 0^-$ states in the former are in better agreement with the predictions of the rotational model. The low-energy levels in ^{152}Gd are considered in light of two possible interpretations. We find that it is preferable to consider these states as resulting from quasi rotations and quasi vibrations than to treat them as members of one-, two-, and three-

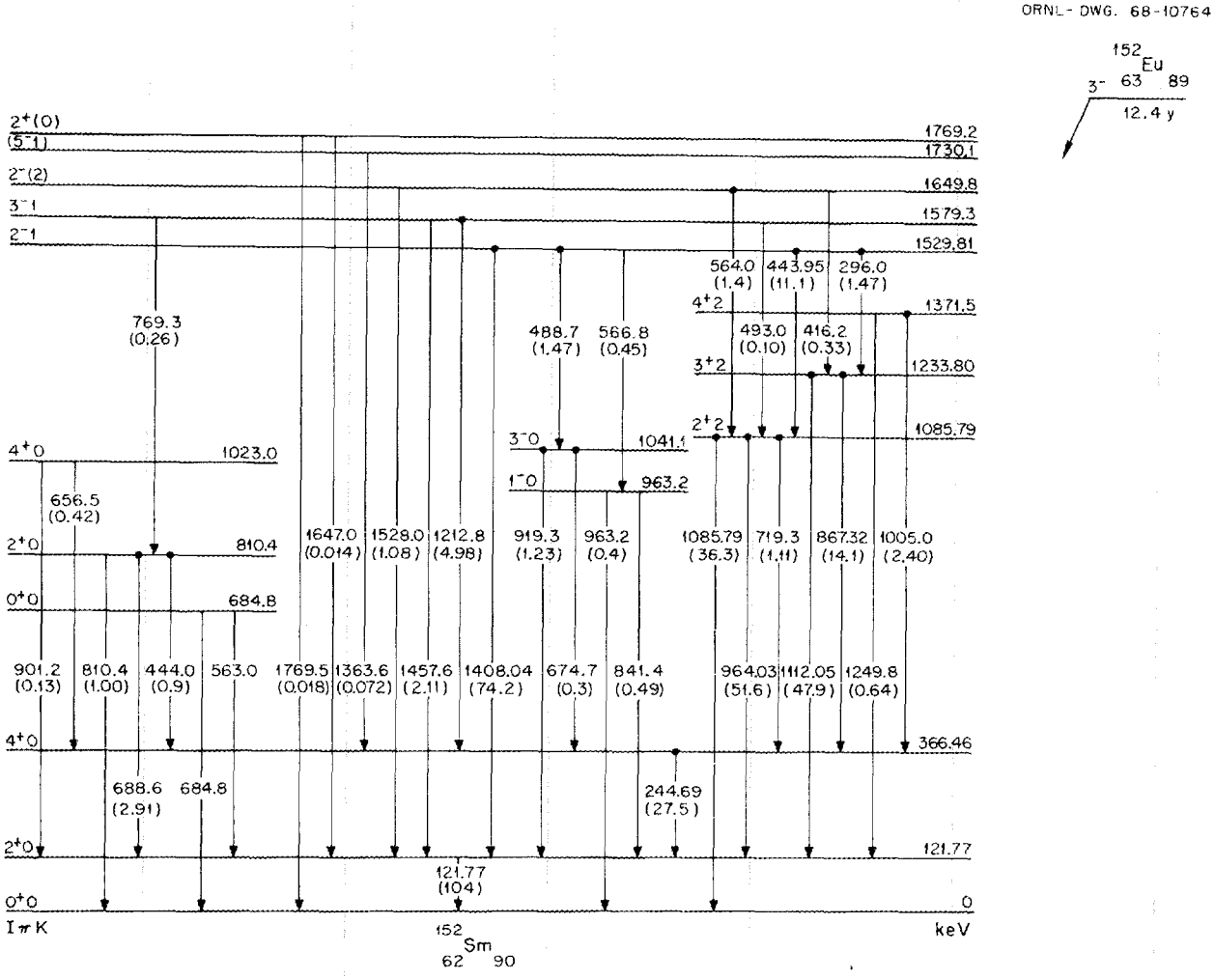

Fig. 1.5. Level Scheme of ^{152}Sm Populated in the Decay of 12.4-year ^{152}Eu. All energies are in keV. The numbers in parentheses below the energies are relative gamma-ray intensities.

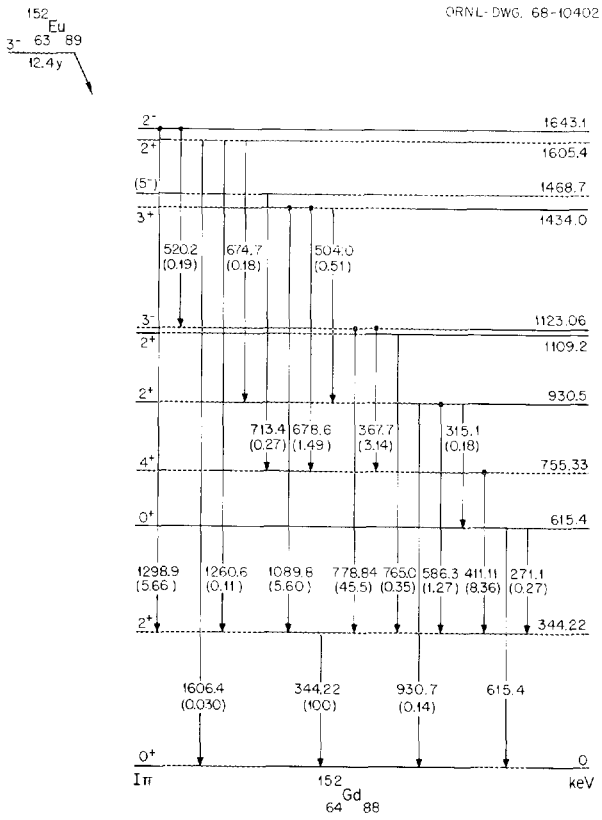

Fig. 1.6: Level Scheme of ^{152}Gd Populated in the Decay of 12.4-year ^{152}Eu. All energies are in keV. The numbers in parentheses below the energies are relative gamma-ray intensities.

phonon vibrational excitations about spherical equilibrium shapes.

---

[1]Oak Ridge Graduate Fellow from Vanderbilt University, Nashville, Tenn., under appointment with Oak Ridge Associated Universities; present address: Niels Bohr Institute, Copenhagen, Denmark.

[2]Physics Department, Vanderbilt University, Nashville, Tenn.

[3]L. L. Riedinger, J. H. Hamilton, and N. R. Johnosn, *Bull. Am. Phys. Soc.* **11** 529 (1966); J. H. Hamilton, L. L. Riedinger, and N. R. Johnson, *Bull. Am. Phys. Soc.* **11**, 407 (1966); L. L. Riedinger, N. R. Johnson, and J. H. Hamilton, *Bull. Am. Phys. Soc.* **13**, 670 (1968).

[4]L. L. Riedinger, N. R. Johnson, and J. H. Hamilton, *Phys. Rev. Letters* **19**, 1243 (1967).

[5]L. L. Riedinger, N. R. Johnson, and J. H. Hamilton, *Phys. Rev.* (in press).

THE DECAY OF ^{110m}Ag: GAMMA-RAY ENERGY AND INTENSITY STANDARDIZATION

S. M. Brahmavar[1] A. V. Ramayya[1]
J. H. Hamilton[1] E. F. Zganjar[2]
C. E. Bemis, Jr.

The energies and intensities of the gamma-ray transitions from the decay of 250-day ^{110m}Ag have been carefully determined with three different systems which use Ge(Li) detectors. All of these transitions fit into the well-known decay scheme of ^{110m}Ag and are suitable for energy and efficiency calibration of Ge(Li) spectrometer systems. Energies (in keV) and relative intensities (in parentheses) for standardization are: 446.77 ± 0.04 (3.5 ± 0.2), 620.22 ± 0.03 (2.9 ± 0.2), 657.71 ± 0.03 (100), 677.55 ± 0.03 (12.2 ± 0.7), 686.80 ± 0.03 (7.4 ± 0.6), 706.68 ± 0.04 (17.2 ± 0.7), 744.19 ± 0.04 (4.4 ± 0.4), 763.88 ± 0.04 (24.0 ± 0.8), 818.00 ± 0.04 (7.8 ± 0.3), 884.67 ± 0.04 (79.2 ± 2.0), 937.48 ± 0.04 (36.5 ± 1.1), 1384.22 ± 0.04 (27.7 ± 0.8), 1475.73 ± 0.04 (4.5 ± 0.2), 1504.90 ± 0.08 (14.8 ± 0.4), and 1562.22 ± 0.06 (1.33 ± 0.06). The adopted transition-energy values below ~1 MeV represent the statistically weighted average value for the three data sets, while the values above ~1 MeV are based not only on the gamma-ray measurements but upon the cross-over-sum relations. The intensities are statistically weighted average values.

Transitions of 566.0, 667.2, 753.0, 785.0, and 1443.0 keV reported by previous workers were not observed. Transitions of 434.00 ± 0.10, 614.37 ± 0.10, and 722.95 ± 0.08 keV were observed but are attributed to the decay of ^{108m}Ag, also present in the various sources used in these experiments.

---

[1]Physics Department, Vanderbilt University, Nashville, Tenn.

[2]Department of Physics and Astronomy, Louisiana State University, Baton Rouge.

LEVELS IN ^{172}Yb POPULATED IN THE DECAY OF ^{172}Lu

M. F. Roche[1] R. L. Hahn
K. S. Toth[1] C. E. Bemis, Jr.

The gamma-ray spectrum of ^{172}Lu, measured with a 35-cm^3 Ge(Li) crystal spectrometer connected to a 4096-channel analyzer, was discussed previously.[2] Fifty-one new transitions in the decay of ^{172}Lu to ^{172}Yb were observed in the spectrum.

ORNL-DWG. 68-10765

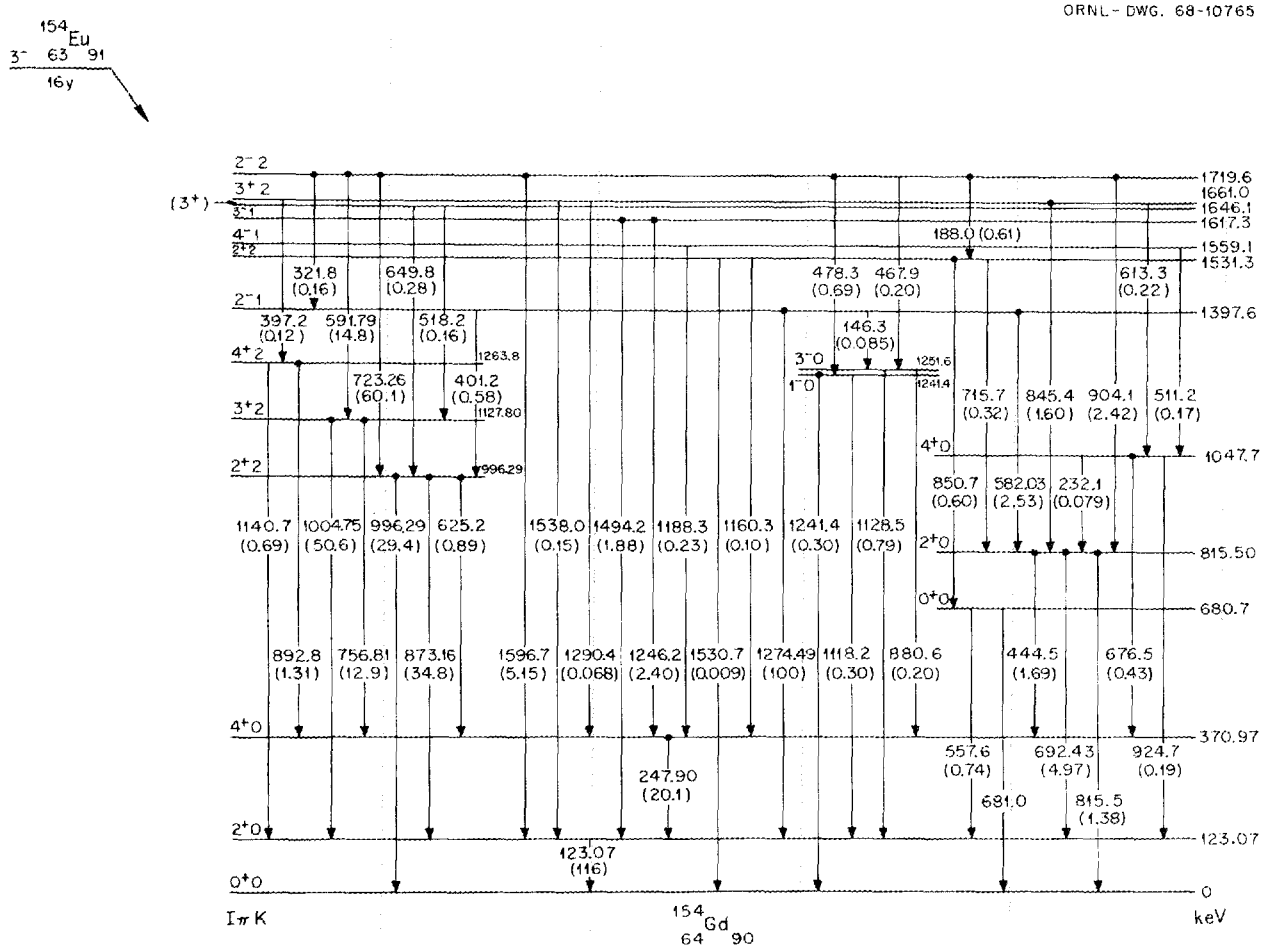

Fig. 1.7. Level Scheme of ^{154}Gd Populated in the Decay of 16-year ^{154}Eu. All energies are in keV. The numbers in parentheses below the energies are relative gamma-ray intensities.

The measured photon intensities were combined with published conversion-electron data[3] to obtain K-shell internal conversion coefficients (ratio of K-shell conversion-electron intensity to gamma-ray intensity). A level scheme consisting of 31 levels was constructed by using sums of transition energies (Fig. 1.8). The levels not previously seen in the decay of ^{172}Lu are at 1476.8, 1608.5, 1633.0, 1706.4, 2181.0, 2213.2, and 2388.3 keV. The first two of these levels in ^{172}Yb had been seen previously[4] in the decay sequence ^{172}Tm to ^{172}Yb. Spin and parity assignments were made with the aid of reduced transition probability ratios and with published results[5] from (d,p), (d,t), and (d,d') reaction studies.

[1] Electronuclear Division.

[2] M. F. Roche *et al.*, *Chem. Div. Ann. Progr. Rept. May 20, 1968*, ORNL-4306, p. 26.

[3] B. Harmatz, T. H. Handley, and J. W. Michelich, *Phys. Rev.* **123**, 1758 (1961).

[4] O. H. Otteson and R. G. Helmer, *Phys. Rev.* **164**, 1485 (1967).

[5] D. G. Burke and B. Elbek, *Kgl. Danske Videnskab. Selskab, Mat.-Fys. Medd.* **36**, No. 6 (1967).

NEW ERBIUM ISOTOPE, ^{155}Er[1]

K. S. Toth[2] M. F. Roche[2]
R. L. Hahn D. S. Brenner[3]

The erbium isotopes with masses from 152 to 154 and neutron numbers from 84 to 86 were first characterized in heavy-ion-induced reactions.[4] The next-heavier erbium nuclide, ^{155}Er, with 87 neutrons, should also, according to the energy systematics of alpha decay, have a detectable alpha-decay branch. Calculations indicated that this nuclide could be

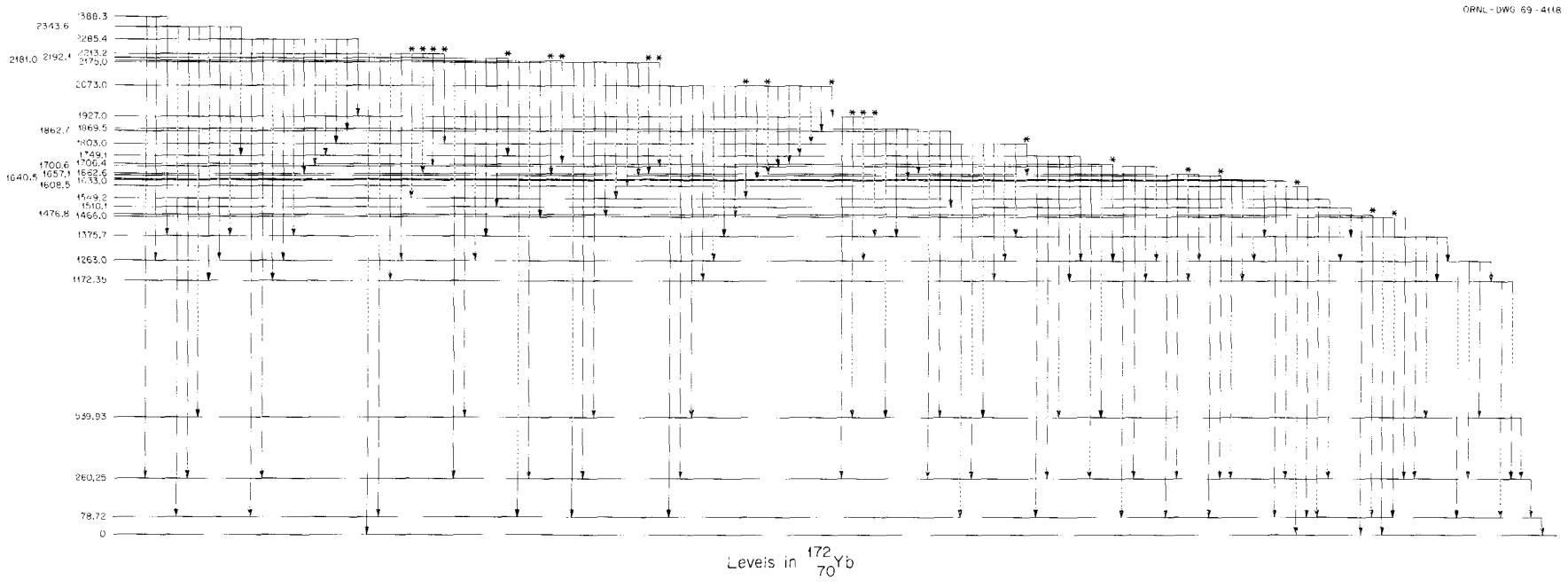

Fig. 1.8. Level Scheme Deduced from the Decay of ^{172}Lu to ^{172}Yb.

produced by irradiating ^{156}Dy with ^{4}He ions in the energy range from 60 to 80 MeV. Because helium ions with these energies are available from the ORIC, a search was undertaken for the alpha activity of this new nuclide.

To facilitate the detection of the short-lived erbium radionuclides, the experiments were performed on line at the ORIC. A target assembly in which beryllium catcher foils were mounted on a remotely controlled wheel behind the enriched ^{156}Dy target was used. Recoil nuclei ejected from the target during irradiation were collected on one of the catchers, which was then automatically moved to an alpha-particle spectrometer. Alpha spectra were taken as a function of time so that peak energies and half-lives could be determined.

Spectra measured from irradiations at three representative energies, 61.8, 70.5, and 72.6 MeV, are shown in Fig. 1.9. The lower portions of the figures represent the counts taken from 0.5 to 18 min after bombardment, while the upper curves were obtained between 35 and 101 min. Note that the spectrum obtained at early counting times is much less complex at 61.8 MeV than at the higher bombarding energies. This observation is consistent with the expectation that ^{154}Er and its daughters would not be produced in substantial amounts at irradiation energies below ~65 MeV. And indeed, above this bombarding energy, ^{154}Er, with 4.5-min half-life and alpha-particle energy of 4.166 MeV,[5] and its electron-capture-decay daughter, ^{154}Ho,[6] with 11.8-min half-life and alpha energy of 3.933 MeV,[5] were clearly seen. The data indicated that ^{150}Dy, the alpha-decay daughter of ^{154}Er, with 7.2-min half-life and 4.23-MeV energy, had also been produced.

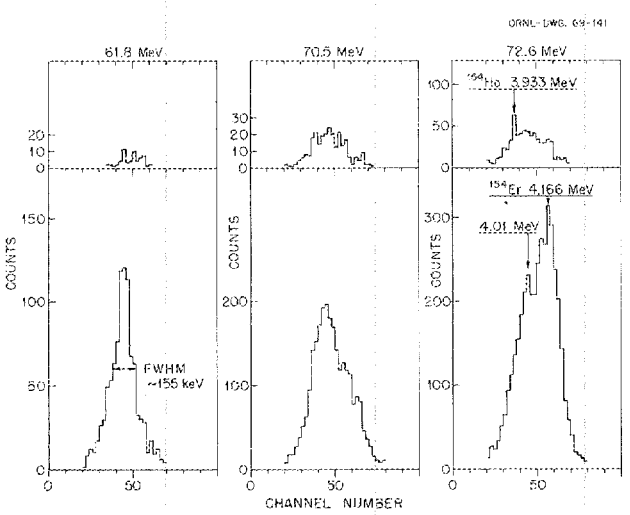

Fig. 1.9. Alpha Spectra from ^{156}Dy Targets After Irradiation with 61.8-, 70.5-, and 72.6-MeV ^{4}He Ions. Lower portions of the figures represent the sum of the first three counts taken between 0.5 and 18.0 min after bombardment; upper portions represent the counts taken between 35 and 101 min.

Analysis of the data from bombardments below the effective threshold for ^{154}Er production indicated that a new alpha emitter had been formed with a half-life of 5.3 ± 0.3 min and an alpha-particle energy of 4.01 ± 0.03 MeV. This energy value is based upon the accurate internal calibration of the spectrometer energy scale with the alpha particles from ^{154}Er, ^{154}Ho, and ^{150}Dy.

Relative measured excitation functions for the new alpha emitter and for ^{154}Er are shown in Fig. 1.10, along with calculated excitation functions[7] for ^{156}Dy(α,xn)$^{160-x}$Er reactions. Because of the agreement of the calculated curves with the measured excitation functions, the new 4.01-MeV alpha particle is assigned to the decay of the previously unknown

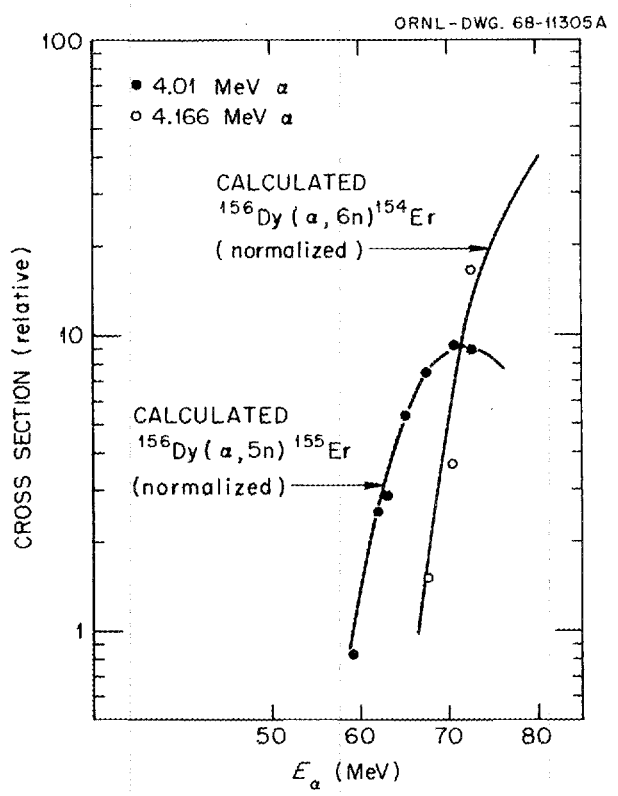

Fig. 1.10. Relative Excitation Functions for the 4.01- and 4.166-MeV Alpha Groups. Excitation functions calculated on the basis of the statistical model for the reactions, ^{156}Dy(α,5n) and ^{156}Dy(α,6n) are indicated by curves normalized to the experimental data points.

nuclide ^{155}Er, which was formed in the ^{156}Dy(α,5n) reaction. This assignment is supported by the fact that this particular nuclide could not be produced in irradiations of the ^{156}Dy target with 20- to 60-MeV protons,[6] where holmium nuclei and lighter products were the only radioisotopes that could be formed.

[1]This work was performed in collaboration with the Electronuclear Division and has also been reported in *Electronuclear Div. Ann. Progr. Rept. Dec. 31, 1968*, ORNL-4404, p. 52.

[2]Electronuclear Division.

[3]Chemistry Department, Clark University, Worcester, Mass.

[4]R. D. Macfarlane and R. D. Griffioen, *Phys. Rev.* **131**, 2176 (1963).

[5]N. A. Golovkov, S. K. Khvan, and V. G. Chumin, p. 27 in *Proceedings of Contributed Papers, International Symposium on Nuclear Structure*, Report D-3893, Dubna, U.S.S.R. (1968).

[6]R. L. Hahn, K. S. Toth, and T. H. Handley, *Phys. Rev.* **163**, 1291 (1967).

[7]I. Dostrovsky, Z. Fraenkel, and G. Friedlander, *Phys. Rev.* **116**, 683 (1960).

DECAY OF ^{89}Nb AND ^{89m}Nb

R. C. Hagenauer[1] E. Eichler
G. D. O'Kelley

Our studies[2] of the decay schemes of ^{89}Nb and ^{89m}Nb were concluded. Sources were prepared by bombardment of $^{90}ZrO_2$ with 27-MeV protons at the ORIC. The niobium fraction was chemically isolated by use of an ion exchange separation procedure.

Gamma-ray singles spectra were determined with 20- and 35-cm^3 Ge(Li) detectors. A 7.6- by 7.6-cm NaI(Tl) crystal was used with a 20-cm^3 Ge(Li) detector to carry out multiparameter gamma-gamma coincidence measurements. We determined beta-ray spectra by using an anthracene beta-particle detector in coincidence with two NaI(Tl) detectors so that only those positrons which annihilated in the anthracene detector would be recorded.

About 50 gamma rays were found to be associated with the decay of ^{89}Nb and 5 with the decay of ^{89m}Nb. Gamma-gamma coincidence relationships, gamma-ray energies, and beta-ray end points were combined to formulate the decay schemes for the ^{89}Nb isomers shown in Fig. 1.11. Careful evaluation of the positron and gamma energies suggests that the $\frac{1}{2}^-$ isomeric state ^{89m}Nb lies only about 70 keV above the $\frac{9}{2}^+$ ground state. A half-life of 66 ± 2 min was obtained for ^{89m}Nb and 122 ± 4 min for ^{89g}Nb.

In Fig. 1.12 we show the levels of ^{89}Zr determined in the present study compared with levels determined in studies of the ^{90}Zr(p,d)^{89}Zr reaction by Ball and Fulmer[3] and Taketani *et al.*[4] An effective-interaction calculation by Ball[5] is included for further comparison. Below 1.8 MeV all experiments are in excellent agreement; at higher energies the results of decay-scheme spectroscopy yield more excited states than the (p,d) reaction data, possibly because of the highly selective nature of the (p,d) reaction.

[1]Oak Ridge Graduate Fellow from the University of Tennessee, Knoxville, under appointment with Oak Ridge Associated Universities. This work is based on a dissertation submitted by R. C. Hagenauer in partial fulfillment of the requirements for the degree of Doctor of Philosophy at the University of Tennessee, March 1969.

[2]R. C. Hagenauer, E. Eichler, and G. D. O'Kelley *Chem. Div. Ann. Progr. Rept. May 20, 1968*, ORNL-4306, p. 8.

[3]J. B. Ball and C. B. Fulmer, *Phys. Rev.* **172**, 1199 (1968) and private communication.

[4]H. Taketani *et al.*, *Phys. Letters*, **27B**, 499 (1968).

[5]J. B. Ball, Electronuclear Division, private communication, 1968.

RADIOACTIVE DECAY OF ^{192}Au AND ^{194}Au

G. D. Benson[1] R. G. Albridge[1]
A. V. Ramayya[1] G. D. O'Kelley
P. V. Rao[2]

The decay schemes of ^{192}Au and ^{194}Au are of great interest because detailed information concerning states excited in ^{192}Pt and ^{194}Pt through the decay of the respective gold parent isotopes can add to knowledge of that region of the nuclear periodic table which marks the transition from deformed to spherical nuclear shapes. Both ^{192}Au and ^{194}Au have been investigated previously by means of the internal-external conversion technique.[3] Since the published spectra contained many unresolved lines, it was difficult to assess the accuracy of the gamma-ray intensities obtained by the internal-external conversion data. It seemed that Ge(Li) gamma-ray detectors, with their excellent resolution at high energies, would yield more accurate photon intensities. One objective of our work was to determine photon intensities with sufficient accuracy to combine them with the internal conversion electron intensities from the magnetic spectrometer data[3] and to calculate internal conversion coefficients for most of the transitions in ^{192}Pt and ^{194}Pt. In addition, it was hoped that coincidence experiments could be performed to place gamma-ray transitions less ambiguously in the decay schemes of interest.

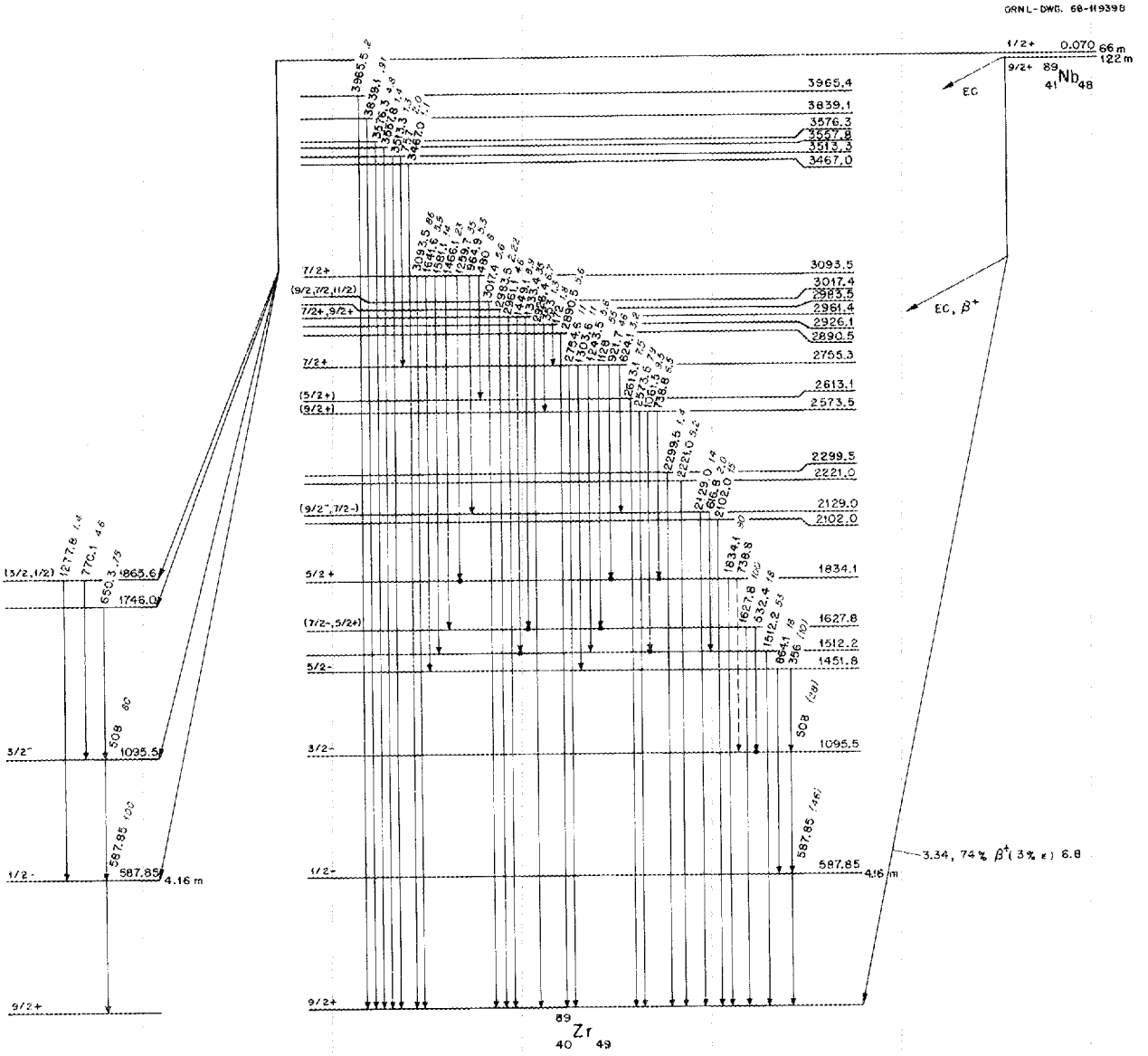

Fig. 1.11. Decay Scheme Proposed for ^{89}Nb and ^{89m}Nb.

ORNL-DWG. 68-11955AR

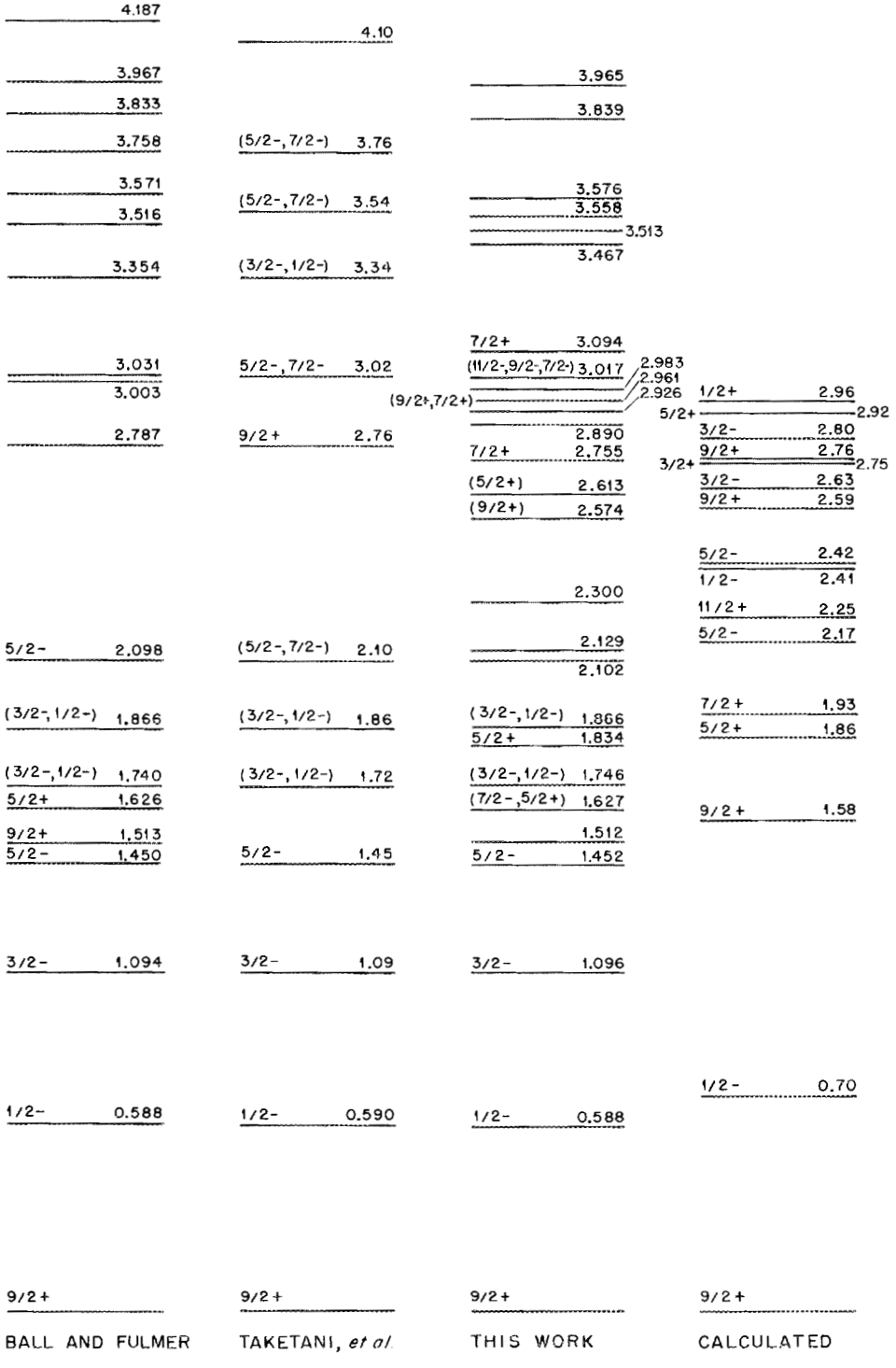

Fig. 1.12. Level Spectra of ^{89}Zr; Comparative data from a study of the decay of the ^{89}Nb isomers (this work), spectroscopy of the ^{90}Zr(p,d) reaction,[3,4] and results of an effective interaction calculation.[5]

Sources were prepared by proton bombardment of platinum metal enriched to 66% in ^{194}Pt. Bombardments were conducted at the ORIC, where the incident proton energy was selected, by adjusting the cyclotron beam energy and the degrading foil thickness, to emphasize either the ^{194}Pt$(p,3n)^{192}$Au or the ^{194}Pt$(p,n)^{194}$Au reaction. Targets were dissolved after bombardment, and a radiochemical separation was used to ensure purity of the gold fraction. Gamma-ray spectra were determined by use of 20- and 35-cm^3 Ge(Li) detectors.

About 100 gamma transitions in the decay of 5-hr ^{192}Au have been characterized in the energy range 0.2 to 3.2 MeV. Gamma-ray intensities have been determined for most of these transitions, and preliminary values of internal conversion coefficients have been calculated. Further work on this problem, including a revised decay scheme, is in progress.

Eighty gamma rays from 160 to 2500 keV were observed in the decay of 40-hr ^{194}Au. Both single-detector and multiparameter gamma-gamma coincidence data were obtained with Ge(Li) detectors. From the energy sums and gamma-gamma coincidence data, a decay scheme with 36 levels in ^{194}Pt was derived. Most of the gamma lines were observed previously by Bergman and Bäckström[3] in their internal-external conversion work. The relative gamma-ray intensities obtained in the present work and the internal conversion electron intensities of Bergman and Bäckström were combined to calculate the conversion coefficients of most of the lines.[4]

---

[1]Physics Department, Vanderbilt University, Nashville, Tenn.

[2]Physics Department, Emory University, Atlanta, Ga.

[3]Au^{192}: B. Nyman *et al.*, *Nucl. Phys.* **88**, 63 (1966). Au^{194}: O. Bergman and G. Bäckström, *Nucl. Phys.* **55**, 529 (1964).

[4]Preliminary reports of this work on levels of ^{194}Pt: A. V. Ramayya *et al.*, *Bull. Am. Phys. Soc.* **13**, 1469 (1968); G. D. Benson *et al.*, *Bull. Am. Phys. Soc.* **13**, 1722 (1968).

SHORT-HALF-LIFE RARE-EARTH ISOTOPES

A. R. Brosi B. H. Ketelle

We have discovered several new isotopes recently as part of a study of the light-rare-earth nuclides on the neutron-deficient side of stability. Because of the short half-lives of these isotopes, we have had considerable difficulty in making definite mass and element assignments. In addition, most of the isotopes have very complex decay schemes, which we have not been able to work out in as much detail as is desirable. As a consequence, the major part of our effort in the last year has been directed toward developing techniques and instrumentation for the study of isotopes with short half-lives.

One of the problems is in the rapidly chemical separation of milligram amounts of rare earths with adjacent atomic numbers. The chemical separations are important both in establishing genetic relationships and in eliminating the complexity of spectra when initially more than one element is present in the source. Recently developed techniques have reduced the time required for the ion exchange separation of neodymium from praseodymium by a factor of 3.

A second problem in working with short-half-life isotopes is that of accumulating sufficient data to reduce statistical errors to an acceptable level. The problem is particularly acute with solid-state detectors because of the energy resolution loss when counting rates are increased to compensate for the short time available for taking data. We have been working with a gated system which rejects pulses that are either outside a region of interest in energy or that occur close enough together in time to overlap in the last stages of our linear amplifier. With this system we have been able to maintain satisfactory energy resolution at counting rates a factor of 10 higher than we could use before.

A third problem in working with short-half-life isotopes is that of accumulating sufficient coincidence data to make deduction of a decay scheme possible. By using the pulse rejection system described above along with higher efficiency detectors and shorter coincidence resolving times, we have been able to increase coincidence counting rates with lithium-drifted germanium detectors by a factor of 40 over the rates achieved with earlier equipment.

A fourth problem in working with short-half-life isotopes is that of rapid pulse-height analysis and storage of data. We are in the process of checking out a "fixed wire" multiparameter analyzer which writes coincidence addresses on magnetic tape while storing samples of single spectra from two detectors in the analyzer memory. The contents of the memory, along with analyzer live time and clock time, can be written on the magnetic tape at a wide range of present intervals. Preliminary work indicates that an enormous amount of information can be stored in a few minutes for later analysis.

ALPHA DECAY OF ^{227}U[1]

R. L. Hahn M. F. Roche[2]
K. S. Toth[2]

The nuclide ^{227}U and its decay products were first characterized by Meinke *et al.*[3] in 1952; since that time no additional work on ^{227}U has been reported.[4] In their experiments, Meinke *et al.* prepared ^{227}U by irradiation of ^{232}Th with high-energy alpha particles followed by rapid chemical separation of uranium. They determined the half-life of ^{227}U to be 1.3 ± 0.3 min, while its daughter all had periods less than 1 sec. With the exception of the 7.43-MeV alpha of ^{211}Po, which was known, the alpha-particle peaks observed in the spectrum were assigned to the members of the decay chain because of the approximate agreement of the experimental energies with values from alpha-decay systematics that were then available.

As those authors pointed out, however, three major problems were encountered in their work. First, it was not a simple task, after the chemical processing, to prepare the thin samples so necessary for accurate alpha pulse-height analysis. Second, in their alpha spectra there were at best approximately equal numbers of counts from 1-min ^{227}U and 9.3-min ^{228}U. Third, the alpha-particle energies from the ^{228}U decay chain are very similar[4] to those reported for ^{227}U. Precise determination of the ^{227}U energies under these conditions was accordingly very difficult.

In the present work, ^{227}U and ^{228}U were produced by irradiating ^{231}Pa with protons from the ORIC. Instead of the 150-MeV alpha particles used for the ^{232}Th$(\alpha,9n)^{227}$U reaction, proton energies of only 35 to 54 MeV were needed to observe the ^{231}Pa$(p,4n)^{228}$U and ^{231}Pa$(p,5n)^{227}$U reactions. By proper selection of the proton energy, the interferences due to the ^{228}U spectrum could be minimized. Also, at these relatively low bombarding energies, competition from other nuclear reactions was not very significant, so that alpha spectra could be obtained without the need of prior chemical purifications.

The target assembly used to collect recoil nuclei rapidly has been described previously.[5] The targets used in these experiments were thin deposits of ^{231}Pa prepared according to a modification of a published procedure.[6] The purified oxide of ^{231}Pa was dissolved in 1 *N* HF, and the solution was adjusted to pH 6 with 1 *N* NaOH and then diluted with 1 *N* NaF. An aliquot was placed in a Lucite plating cell, and the ^{231} Pa was electrodeposited onto a 1-mil-thick platinum foil using a current density of ~550 mA/cm^2 at ~15 V. Typical target thicknesses were ~100 μg/cm^2.

To survey the (p,xn) reactions on ^{231}Pa, irradiations were performed at proton energies from 35 to 54 MeV. A typical alpha-particle spectrum obtained from the 35-MeV bombardment is shown in Fig. 1.13*c*. The major peaks are clearly identifiable as arising from ^{228}U and its daughters and from ^{229}U. Data from the multiple irradiations done at 44 MeV are plotted in Figs. 1.13*a* and *b*. The spectrum obtained within the first 2.5 min after bombardment is shown in Fig. 1.13*a*, while Fig. 1.13*b* shows the peaks observed within the interval from 9 to 20 min after irradiation. At the later counting times, as can be readily seen by comparing the spectra in Figs. 1.13*b* and *c*, the peaks of the ^{228}U chain become prominent. These well-known alpha-particle energies were used as internal standards to calibrate the energy scale of the spectrometer accurately. Members of other decay chains are also indicated in Fig. 1.13*b*.

Figure 1.13*a* demonstrates the presence of a short-lived decay chain with energies different from those of ^{228}U and its descendants. This is the spectrum of ^{227}U and its daughters. Especially striking in the comparison of Figs. 1.13*a* and *b* are the shifts in peak position caused by the decay of the short-lived components. For example, after the 8.67- and 7.99-MeV peaks have decayed away, the 8.78- and 8.05-MeV peaks of ^{228}U are clearly seen in the spectrum. Least-squares analysis of the decay data for the six alpha peaks in Fig. 1.13*a* indicated that they all decay with the same half-life, 1.1 ± 0.1 min, in agreement with the previously reported[3] 1.3 ± 0.3 min.

Table 1.1 lists the alpha-particle energies found in this work and compares them with the results of Meinke *et al.*[3] Some differences from the earlier results are apparent. No evidence was found in the present study for a peak at 7.55 MeV; instead, peaks were observed at 7.33 and 7.70 MeV. In addition, analysis of the decay data indicated that the sum of the intensities of the 7.99- and 7.70-MeV peaks was comparable with the intensities of the other short-lived peaks. Apparently the 7.99- and 7.70-MeV alpha particles are emitted by the same nuclide, with relative emission probabilities of 0.7 ± 0.1 and 0.3 ± 0.1 respectively.

Apart from the noted discrepancies, the present results, although more precise, agree in general with those reported earlier by Meinke *et al.*[3] Moreover, calculated[7] and experimental (p,xn) excitation functions for ^{228}U and ^{227}U also compare favorably and support the assignment. Note that the 7.33-MeV alpha particle is assigned to ^{223}Th, to replace the previously reported 7.55-MeV alpha particle, and that both the 7.99- and 7.70-MeV alphas, as discussed above, are

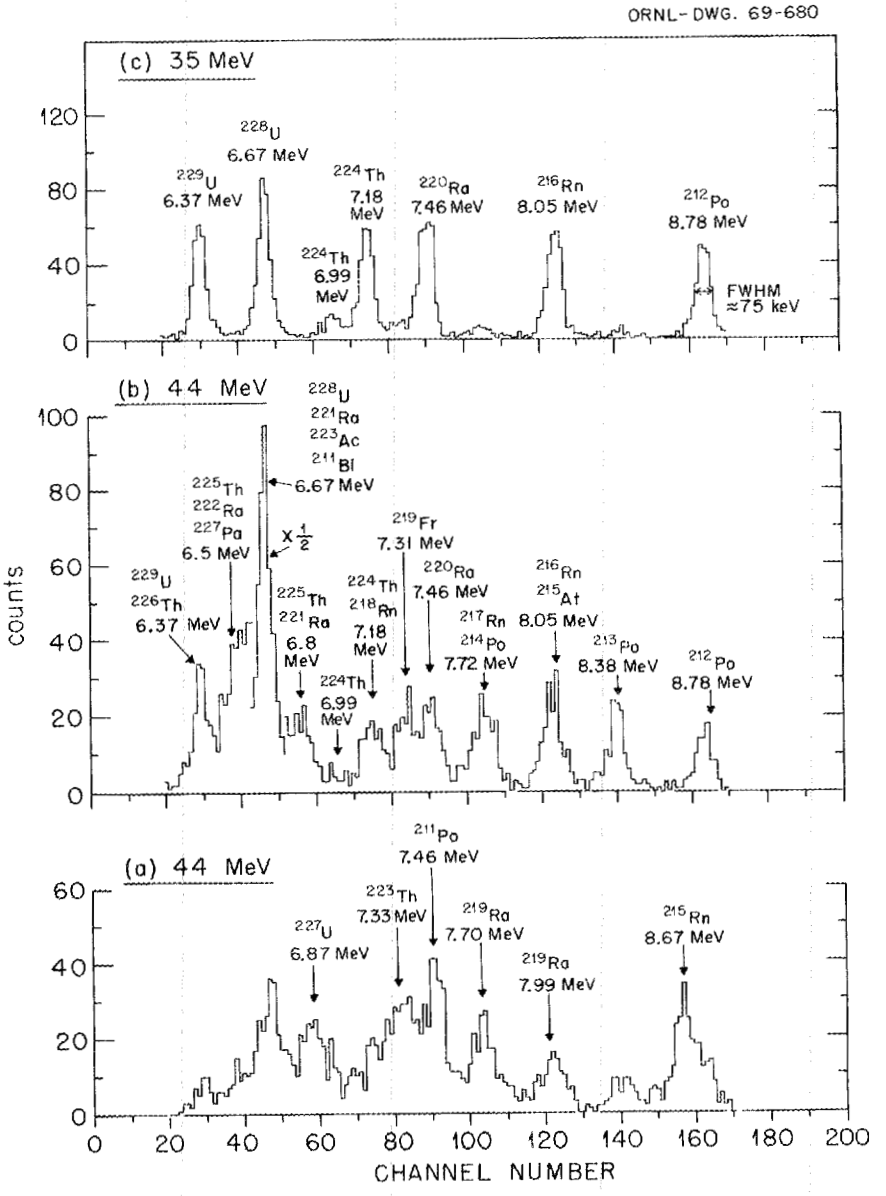

Fig. 1.13. Alpha Spectra Observed from Irradiations of ^{231}Pa with Protons. (*a*) Spectrum taken during the first 2.5 min after bombardment; the proton energy was 44 MeV. (*b*) Spectrum also taken from the 44-MeV irradiation, covering the counting interval from 9 to 20 min after bombardment. (*c*) Spectrum taken during the first 5 min after the 35-MeV irradiation.

Table 1.1. Alpha-Particle Energies in the ^{227}U Decay Chain

Nuclide	Energy (MeV)	
	Meinke *et al.*[a]	This Work
^{227}U	6.8 ± 0.1	6.87 ± 0.02
↓		
^{223}Th	7.55 ± 0.1	7.33 ± 0.02
↓		
^{219}Ra	8.0 ± 0.1	7.99 ± 0.02
		(0.3 ± 0.1)[b]
		7.70 ± 0.02
		(0.7 ± 0.1)[b]
↓		
^{215}Rn	8.6 ± 0.1	8.67 ± 0.02
↓		
^{211}Po	7.43 ± 0.1	7.46 ± 0.02

[a]See ref. 3.

[b]Numbers in parentheses are relative emission probabilities, assuming that the two alpha particles are emitted by the same nuclide.

assigned to ^{219}Ra. These assignments are consistent with the systematic trend generally observed for alpha emitters with neutron number between 128 amd 140: the alpha-particle energy increases with each step down the decay chain.

[1]This work was performed in collaboration with the Electronuclear Division and has also been reported in *Electronuclear Div. Ann. Progr. Rept. Dec. 31, 1968,* ORNL-4404, p. 58.

[2]Electronuclear Division.

[3]W. M. Meinke, A. Ghiorso, and G. T. Seaborg, *Phys. Rev.* **85**, 429 (1952).

[4]C. M. Lederer, J. M. Hollander, and I. Perlman, *Table of Isotopes,* 6th ed., Wiley, New York, 1967.

[5]K. S. Toth *et al.*, "New Erbium Isotope, ^{155}Er," a preceding contribution, this section.

[6]C. Ferradini, *J. Chim. Phys.* **53**, 714 (1956).

[7]I. Dostrovsky, Z. Fraenkel, and G. Friedlander, *Phys. Rev.* **116**, 683 (1960).

A COMPUTER-CONTROLLED IRON-CORE BETA SPECTROMETER

R. G. Lanier[1] N. R. Johnson
F. W. Snodgrass[2]

In the past year the installation of a single-gap iron-core beta spectrometer has been completed. The design of the spectrometer is based on the toroidal double-focusing principle[3] and combines a high transmission efficiency (~2%) with a moderately good momentum resolution (~1%).

The spectrometer assembly has been interfaced with a PDP-8/S digital computer, thereby extending its capabilities significantly. Through the interface facility the computer monitors all incoming data and also controls the magnetic field intensity in the spectrometer. The fact that the system is computer based improves the potential for investigating relatively short-lived sources. In addition to a more rapid acquisition of data, the immediate presence of a computer provides added versatility by accomplishing a substantial portion of the data reduction on site in real time.

The computer software has been written, and the system is now fully automated. For test purposes a number of ^{137}Cs conversion-electron spectra have been run in the automated mode, and in all respects the software appears to be performing the desired functions.

Since the spectrometer has an iron core, hysteresis effects give rise to uncertainties in the energy determination of a particular electron line from one run to another. To reduce this uncertainty to a minimum, it is necessary to recycle the magnet prior to each scan. This process of recycling has also been put under computer control and has been found to be very reliable; compared with manual recycling, computer recycling of the magnet is much more rapid, and the position of the ^{137}Cs *k* line is considerably more reproducible.

[1]U.S. Atomic Energy Commission Postdoctoral Fellow under appointment with Oak Ridge Associated Universities.

[2]Instrumentation and Controls Division.

[3]O. Kofoed-Hansen, J. Lindhard, and O. B. Nielsen, *Kgl. Danske Videnskab. Selskab, Mat.-Fys. Medd.* **25**, No. 16 (1950).

LOW-LEVEL GAMMA-RAY SPECTROMETER FOR LUNAR SAMPLE ANALYSIS[1]

G. D. O'Kelley R. E. Wintenberg[3]
J. S. Eldridge[2] P. R. Bell[4]
V. A. McKay[3] K. A. Richardson[4]
R. T. Roseberry[3] E. Schonfeld[4]

Introduction

The development of high-sensitivity, low-background gamma spectrometer equipment has been essentially completed. The final configuration is that described previously[5,6] except that new detectors of lower background have now been installed in the underground counting facility at the Lunar Receiving Laboratory, Houston, Texas. Most recent work has involved acquisition of spectrum response functions to be used in analysis of the spectra from returned lunar samples.

Data from several meteorites have been recorded to demonstrate the effectiveness of the spectrometer.

Detector Background

As noted previously,[6] the final detector design uses a cylindrical rod of NaI(Tl) 9 in. in diameter and 5 in. long with a 4-in. thickness of pure NaI as a gamma-absorbing light guide interposed between the scintillator and the photomultiplier tubes. In addition, the new detectors were constructed of materials selected for low radioactive contamination. Two of the new detectors were assembled by Harshaw Chemical Company from components fabricated at ORNL. Tests in the ORNL prototype spectrometer demonstrated that the background obtained with these detectors was lower than that of a prototype detector assembled earlier from unselected materials.

Some typical background spectra of one detector in the Lunar Receiving Laboratory (LRL) system are shown in Fig. 1.14. The prominent features of the background are the 1.46-MeV line of ^{40}K, the 2.2-MeV line from neutron capture events in the hydrogen of the plastic inner-mantle scintillator, and a diffuse spectrum above about 2.8 MeV which we have shown to be due largely to alpha particles from heavy-element contamination in the NaI(Tl) crystal. It is seen that the anticoincidence system reduces the background over the entire spectral region. For the spectrum shown in Fig. 1.14 the background rate from 0.1 to 2.0 MeV without anticoincidence is 476 counts/min and with anticoincidence is 78.4 counts/min. It should be emphasized that these backgrounds are for a detector with a volume of about 5200 cm^3.

The LRL counting laboratory is underground, with a 40-ft overburden of earth to adsorb cosmic rays. Hence the intensity of the line at 2.2 MeV, which arises from meson-induced neutrons, is lower by a factor of 5 to 6 than the line intensity observed at ORNL above ground and 840 ft above sea level.

Calibration of the Spectrometer

Because of gamma-ray scattering and absorption in massive samples and because of summing effects in the large detectors, the spectra of radionuclide mixtures are very difficult to analyze. Data are recorded simultaneously in the singles, coincidence, and sum coincidence modes. For analysis it is necessary to record spectra for each nuclide expected to be present in a lunar sample in a variety of sample geometries and sizes.

For preliminary examination of counting data on meteoritic or lunar samples, it is adequate to calibrate the "counting yield" of the system for a particular nuclide by using distributed sources of various sizes. Final data are best obtained from library spectra obtained from dispersing the desired radionuclides, each in a mockup of the same density and physical size as the sample counted. For our preparation of distributed sources, we have used electrolytically reduced iron powder with a bulk density of 3.4 to 3.5 g/cm^3. Small assayed aliquots of each radionuclide were distributed in the appropriate amount of iron powder and mixed thoroughly to ensure homogeneity. Samples of 25, 50, 100, 200, 300, 1260, and 4100 g have been prepared for 12 nuclides.

For a few meteorite samples, actual "phantoms" of the same shape as the specimen have been prepared for assay of uranium, thorium, ^{40}K, and ^{26}Al.

Applications

The gamma-ray spectrometer has been used for quantitative analyses of meteoritic and terrestrial samples. Several of these determinations have been made in connection with exercises at the LRL designed to test the operation of the laboratory under simulated Apollo mission conditions. Three such simulations were held during the period from October 1968 to April 1969. Two examples will serve to illustrate the performance obtained.

Chondritic meteorites have much lower concentrations of uranium and thorium than do most terrestrial rocks. As the chondrites are also generally thought to be characteristic of a primitive stage of cosmic evolution, their concentrations of ^{40}K, uranium, and thorium set practical lower limits for concentrations to be expected in lunar sample analysis.

To demonstrate that our system had the required sensitivity, two olivine-hypersthene chondrites were counted as simulated lunar samples. After 90 min of counting it was possible to detect semiquantitatively ^{40}K, ^{26}Al, and thorium. After several hundred minutes, uranium could also be determined. The results of several long counts are summarized in Table 1.2. Two counts of meteorite sample 2 are shown in order to demonstrate the reproducibility obtained. These measurements were made at the LRL before the installation of the improved detectors mentioned above. The present sensitivity is now even more favorable.

In February 1969, it became possible to analyze a freshly fallen meteorite whose radioactivity closely resembled that expected for lunar samples. The meteorite fell in the state of Chihuahua, Mexico, at 1:05 AM on February 8, 1969, and is called "Pueblito de Allende," after the village where it fell. Samples were

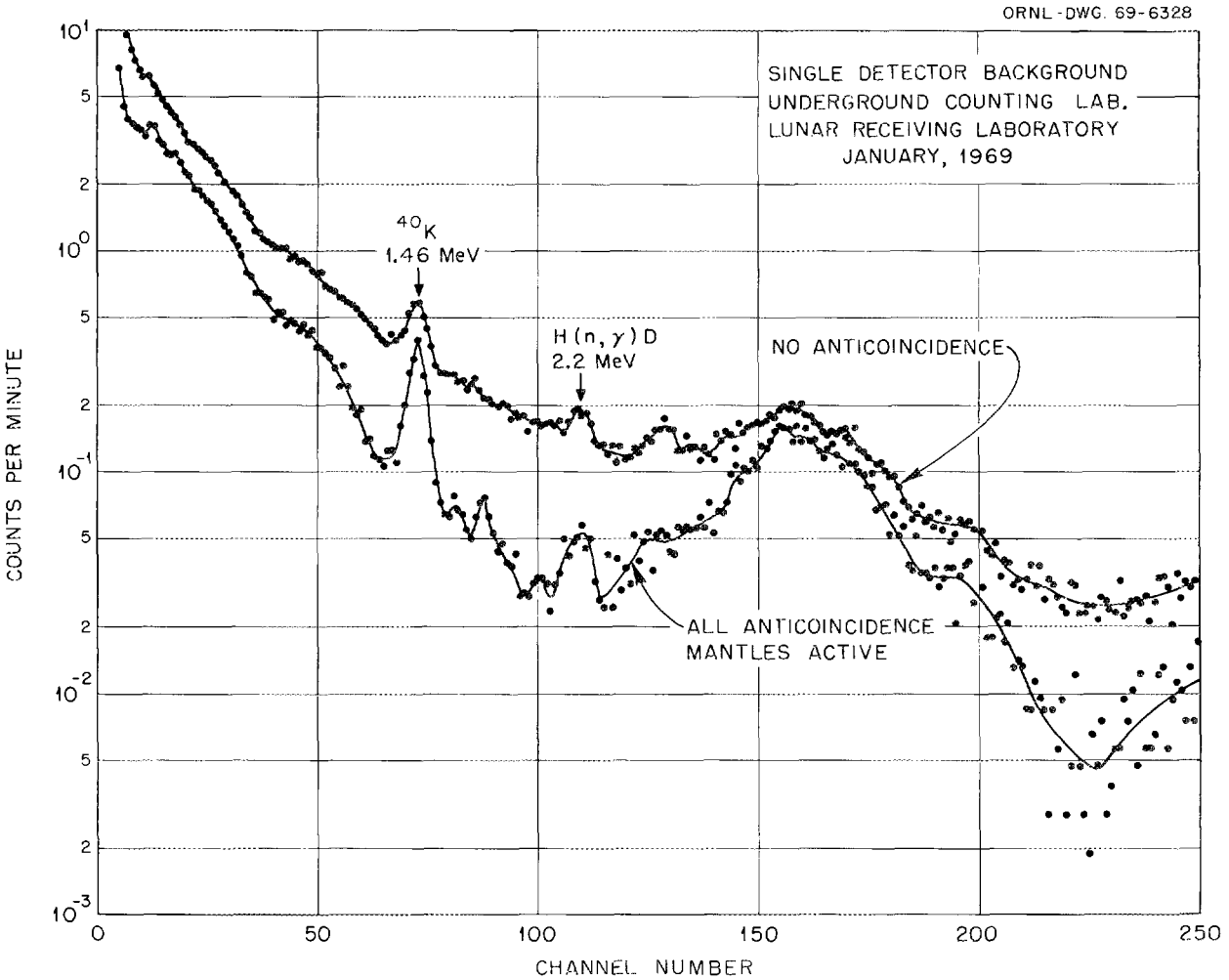

Fig. 1.14. Background Gamma-Ray Spectra in the Underground Counting Facility at the Lunar Receiving Laboratory. Spectra shown are for a single 9- by 5-in. NaI(Tl) principal detector with pure NaI light guide, 4 in. thick (active detector volume ~5,200 cm^3). Upper curve shows spectrum obtained without anticoincidence; lower curve shows the reduction in background when all anticoincidence conditions are met.

Table 1.2. Analysis of Olivine-Hypersthene Chondrites During LRL Simulations[a]

Meteorite No.	Weight (g)	Count Time (min)	^{26}Al (dis min^{-1} kg^{-1})	K (wt %)	U (ppb)	Th (ppb)
1	310	1029	76 ± 3	0.076 ± 0.002	20 ± 8	80 ± 20
2	297	1015	59 ± 3	0.046 ± 0.002	32 ± 9	86 ± 20
2	297	798	59 ± 4	0.045 ± 0.003	22 ± 12	95 ± 30

[a]Errors are statistical only and do not contain any allowances for systematic errors from standards and background.

returned to the LRL, and counting began 101 hr after fall. The first sample of the meteorite introduced into the gamma counter weighed 4180 g; other samples which were analyzed weighed 782, 1259, and 4290 g. Samples of Pueblito de Allende were counted sequentially and frequently throughout February, and with less frequency to the present.

Even though 101 hr had elapsed from time of fall until gamma-ray measurements began, it was possible to identify positively 15-hr ^{24}Na. Other radionuclides identified were ^{22}Na, ^{26}Al, ^{40}K, ^{52}Mn, ^{54}Mn, ^{60}Co, U (^{214}Bi), and Th(^{208}Tl). In addition, ^{7}Be, ^{51}Cr, and ^{56}Co were tentatively identified. A preliminary report on the chemical and physical aspects of the meteorite has been published.[7] Analysis of the counting data is continuing, and detailed information on the radionuclide content will be the subject of a second report.

---

[1]Sponsored by the National Aeronautics and Space Administration through interagency agreements with the U.S. Atomic Energy Commission.

[2]Analytical Chemistry Division.

[3]Instrumentation and Controls Division.

[4]NASA Manned Spacecraft Center, Houston, Tex.

[5]*Chem. Div. Ann. Progr. Rept. May 20, 1967*, ORNL-4164, p. 20.

[6]*Chem. Div. Ann. Progr. Rept. May 20, 1968*, ORNL-4306, pp. 18–21.

[7]E. A. King *et al.*, *Science* **163**, 928 (1969).

2. Chemistry and Physics of Transuranium Elements

THERMAL-NEUTRON CAPTURE CROSS SECTION AND RESONANCE INTEGRAL OF ^{245}Cm AND ^{246}Cm

J. Halperin R. E. Druschel
R. E. Eby[1]

The thermal cross section and resonance integral for radiative capture have been measured for ^{245}Cm and ^{246}Cm, using a cadmium ratio technique together with mass spectrometric analyses of the curium isotopes. The measurement of these cross sections is of special interest in view of the possibility of improved yields of the higher transuranics in a reactor designed to operate at resonance neutron energies rather than thermal neutron energies.

Two irradiations were carried out with calutron-enriched ^{245}Cm (~77%) for periods of two and four days and with ^{246}Cm (~97%) for periods of four and eight days in the ORR at thermal fluxes of ~1.6 X 10^{14} neutrons cm^{-2} sec^{-1}. Approximately 0.3-μg samples of curium were enclosed in capsules of fused silica 6 mm long, and three of these capsules were sealed into a 65-mm-long aluminum capsule for the irradiation. Two of the curium samples were enclosed in 40-mil cadmium cylindrical containers (10 mm in diameter and 10 mm high) placed at the ends of the aluminum container. The third bare curium sample was centered between the two cadmium-filtered samples. A cobalt monitor was placed immediately above and below each curium sample to provide a measure of the neutron flux. The flux monitor consisted of several milligrams of a dilute (0.151 wt %) cobalt alloy of aluminum. Following the irradiation the irradiated curium was electrodeposited onto platinum wire and assayed in a two-stage magnetic-deflection mass spectrometer capable of measuring nanogram samples in the parts per million range. For the analysis the curium samples on platinum wire were deposited in a canoe-shaped rhenium filament, where ions are formed by thermal ionization and are detected with an electron multiplier and a 400-channel analyzer.

The mass spectrometric data and the derived cross-section measurements are summarized in Tables 2.1 and 2.2. The first column lists the irradiation time at constant neutron flux, the third and fourth columns summarize the pertinent mass analysis data, and the fifth and sixth columns list the thermal flux and

Table 2.1. Summary of ^{245}Cm Cross-Section Data

Irradiation Time (min)	Sample No.	Mass Ratio (X 10^3), ^{246}Cm/^{245}Cm Initial	Final	ϕ_{th} (X 10^{-14}) (neutrons cm^{-2} sec^{-1})	ϕ_r (X 10^{-13}) (neutrons cm^{-2} sec^{-1})	I (barns)	σ_{eff} (barns)	σ_{th} (barns)	σ_0 (barns)
2878	1	4.286	4.622		1.89_5	96.4			
	2	4.286	15.62_2	1.68_6	$(1.93_0)^a$		369.6	358.2	341.8
	3	4.286	4.654		1.96_6	102.6			
5760	1	4.294	4.863		1.56_1	101.4			
	2	4.294	25.28_5	1.54_1	$(1.62_8)^a$		365.0	354.2	339.1
	3	4.294	4.919		1.69_4	102.7			
Average						100.8			340.5

[a]Interpolated.

Table 2.2. Summary of ^{246}Cm Cross-Section Data

Irradiation Time (min)	Sample No.	Mass Ratio ($\times 10^3$), ^{247}Cm/^{246}Cm Initial	Final	ϕ_{th} ($\times 10^{-14}$) (neutrons cm^{-2} sec^{-1})	ϕ_r ($\times 10^{-13}$) (neutrons cm^{-2} sec^{-1})	I (barns)	σ_{eff} (barns)	σ_{th} (barns)	σ_0 (barns)
5760	1	0.757	1.378		1.60_3	$122._2$			
	2	0.757	1.504	1.61_4	$(1.67_2)^a$		13.9_4	1.4_5	1.3_9
	3	0.757	1.410		1.74_0	$118._6$			
11520	1	0.757	2.075		1.72_9	$121._6$			
	2	0.757	2.303	1.61_9	$(1.76_5)^a$		14.5_6	1.2_5	1.2_0
	3	0.757	2.133		1.80_2	121.8			
Average						$121._1$			1.2_5

[a]Interpolated.

resonance flux per unit lethargy respectively. The neutron flux values are based upon the ^{59}Co cross-section values of σ_0 (Co) = 37.0 barns and I (Co) = 75.0 barns. The thermal flux is taken as the Maxwellian component of the thermal spectrum and is determined by subtracting from the total reaction rate both the epicadmium portion of the reaction rate and the $1/E$ portion of the rate below the cadmium cutoff. The $1/E$ component of the spectrum is here taken to terminate sharply at $5kT$ (T is the temperature of the Maxwellian neutron distribution). The resonance integral, with a lower energy cutoff of 0.54 eV, is given in column 7. The effective cross section listed in column 8 is the reaction rate per unit thermal flux. The thermal cross section listed in column 9 is the subcadmium reaction rate per unit thermal flux. The 2200 m/sec cross section σ_0 listed in the last column is calculated from σ_{th} on the usual assumption of a $1/v$ dependence in the near-thermal region.[2]

The capture cross sections of both ^{245}Cm and ^{246}Cm were calculated using Eq. (1):

$$\sigma_c^i = \frac{[(N_{i+1}/N_i)_t - (N_{i+1}/N_i)_0\, e^{-\phi t(\sigma_a^{i+1} - \sigma_a^i)}]\,(\sigma_a^{i+1} - \sigma_a^i)}{[1 - e^{-\phi t(\sigma_a^{i+1} - \sigma_a^i)}]}, \quad (1)$$

where i refers to the mass of the nuclide irradiated and $i + 1$ refers to the capture activation product. Thus $(N_{i+1}/N_i)_0$ refers to the experimental mass ratio found in the unirradiated sample and $(N_{i+1}/N_i)_t$ the mass ratio for the irradiated sample. The experimentally measured flux-time product is here ϕt. The absorption cross sections σ_a^i (or I_a^i) and σ_a^{i+1} (or I_a^{i+1}) are input numbers for the calculation.

The results for the ^{245}Cm measurement are summarized in Table 2.1. The cross sections have been corrected (<1%) for a small contribution to the mass ratio due to ^{244}Cm in the sample. The experimental mass ratios are considered accurate to ~1%, although the precision of the measurements made at a given time is considerably better. The uncertainty in the flux measurement exclusive of the spectral model and the cobalt cross sections is about 2%. The uncertainty arising from departures in the neutron spectrum from the model is difficult to evaluate but is here estimated as not exceeding 5%. Since the resonance integral is less than $\frac{1}{3}\sigma_0$, the cross-section variation with energy in the near-thermal region cannot have a $1/v$ dependence. The resonance integral of a hypothetical, pure $1/v$ absorber would be about $0.43\sigma_0$ under the conditions of this experiment. A negative energy resonance is thus suggested by the data. A resonance integral of 101 ± 8 barns and a 2200 m/sec cross section of 340 ± 20 barns are reported here for ^{245}Cm. Smith and co-workers[3] report an absorption cross section of 2210 barns and a fission cross section of 1880 barns for ^{245}Cm. This gives, by difference, a capture cross section of 330 barns, in good agreement with the measurement reported here. There do not appear to be any measurements reported for the resonance integral of ^{245}Cm.

The data for the ^{246}Cm measurements are summarized in Table 2.2. Since the resonance integral is almost a hundredfold greater than the thermal cross section, resonance capture makes up the principal component of the effective cross section in the present experiment. Since the thermal cross section is evaluated by subtracting the resonance response from the total response, this results in taking a small difference between two large

numbers. However, since this difference is taken between experimental values whose precision is appreciably better than their absolute accuracy, the error in the final result is somewhat better than would otherwise obtain. Thus the resonance integral of ^{246}Cm is reported as I (^{246}Cm) = 121 ± 7 barns and the 2200 m/sec cross section value as σ_0 (^{246}Cm) = 1.2 ± 0.4 barns. These results may be compared with values of 103 and 8.7 barns for I and σ_0, respectively, reported by Smith.[3]

---

[1] Analytical Chemistry Division.

[2] R. W. Stoughton and J. Halperin, *Nucl. Sci. Eng.* 6, 100 (1959).

[3] J. A. Smith *et al.*, *Reactor Cross Sections for* ^{242}*Pu-*^{252}*Cf*, DP-Ms-67-111 (Mar. 4, 1968).

THERMAL FISSION CROSS SECTION AND RESONANCE INTEGRAL OF ^{249}Cf

J. H. Oliver J. Halperin

A preliminary measurement has been made of the fission cross section and resonance integral of ^{249}Cf. A particularly pure preparation of the 360-year ^{249}Cf (prepared by milking a ^{249}Bk source) was determined by mass spectrometry to be free of other actinides to parts per million. A 20-pg source of the ^{249}Cf was irradiated in a reactor in contact with Lexan film (biphenol-A polycarbonate plastic) with a suitable flux monitor. The number of fission events was determined by etching the Lexan plastic in a sodium hydroxide medium following the irradiation and then counting the fission tracks under a microscope.

The ^{249}Cf sample was irradiated in an almost pure Maxwellian neutron spectrum in the D_2O tank of the BSR to measure its thermal cross section. The neutron flux was monitored with a dilute alloy of gold in aluminum. The resonance integral was measured in a similar irradiation using a cadmium filter in a pneumatic-tube facility of the ORR. In two irradiations in which some 3000 tracks were counted, a preliminary value of σ_0^F (^{249}Cf) = 1590 barns was measured. This is in good agreement with the value of 1540 ± 70 barns reported by Metta and co-workers,[1] corrected for the current value of the ^{249}Cf half-life. (They actually reported 1735 barns based upon a 320-year, rather than 360-year, half-life.) In two additional irradiations using cadmium filters in which some 4000 tracks were counted, a preliminary value of I^F (^{249}Cf) = 2500 barns is reported.

---

[1] D. Metta *et al.*, *J. Inorg. Nucl. Chem.* 27, 33 (1965).

CAPTURE AND ABSORPTION CROSS SECTION OF ^{253}Cf

C. E. Bemis, Jr. R. E. Druschel
J. Halperin

Although the production of ^{252}Cf is a major goal in the transuranium program, the formation of even higher-mass nuclides is of considerable interest. The 18-day ^{253}Cf is an intermediate for the production of higher nuclides by successive neutron capture in high-flux reactors. A high fission cross section for ^{253}Cf would tend to limit production of higher-mass nuclides. Neutron capture in ^{253}Cf leads to the 60.5-day ^{254}Cf, which decays by spontaneous fission.

A submicrogram preparation of californium containing an appreciable quantity of the 18-day ^{253}Cf recently became available from the mass separator[1] for a cross-section measurement. The sample consisted of a mixture of about 40% ^{253}Cf and 60% ^{252}Cf with negligible quantities of other californium isotopes. The sample was irradiated in the ORR together with cobalt neutron monitors to an integrated thermal flux time of 2.94×10^{19} neutron/cm^2 in a position where the ratio of thermal to resonance flux per unit lethargy was found to be 9.58. By examining a sample of both the irradiated and unirradiated californium with a silicon surface-barrier detector, an alpha pulse-height spectrum containing the alpha groups of ^{252}Cf (6.119 MeV) and ^{253}Cf (5.979 MeV) was obtained. In addition, all pulses corresponding to an energy greater than ~14 MeV were collected at the same time, giving a measure of the spontaneous-fission decay in the sample. The spontaneous-fission activity in the unirradiated sample was due entirely to the 3.1% fission-branching ratio of ^{252}Cf. Following the irradiation the fission activity was enhanced by the 60.5-day ^{254}Cf produced from the ^{253}Cf in the sample:

$$\begin{array}{ccccc} \alpha\uparrow 2.74 \text{ years} & & \alpha\uparrow 15.8 \text{ years} & & \alpha\uparrow 53.4 \text{ years} \\ {}^{252}\mathrm{Cf} & \xrightarrow{(n,\gamma)} & {}^{253}\mathrm{Cf} & \xrightarrow{(n,\gamma)} & {}^{254}\mathrm{Cf} \\ \mathrm{S.F.}\downarrow 85.5 \text{ years} & & \beta-\downarrow 17.8 \text{ days} & & \mathrm{S.F.}\downarrow 60.5 \text{ days} \end{array} \quad . \qquad (1)$$

The alpha activity of the ^{254}Cf was too low in this irradiation to serve as a measure of its production, since its alpha-branching ratio is only 0.31%.

The reactor cross section of ^{253}Cf was evaluated from

$$\phi_{\mathrm{th}}\,\sigma_{\mathrm{eff}} = \frac{A_2}{A_3}\left(\frac{R_T}{R_0} - 1\right) \times \frac{(\Lambda_4 - \Lambda_3)\,(\lambda_2^F/\lambda_4^F)\,(\lambda_3^\alpha/\lambda_2^\alpha)}{(1 - e^{-(\Lambda_4 - \Lambda_3)T})\,(e^{-(\lambda_4 - \lambda_3)t})} \,. \qquad (2)$$

Here the subscripts 2, 3, and 4 refer to the californium isotopes of mass 252, 253, and 254 respectively. The irradiation time is T, and the time following the irradiation is t. The terms λ^F and λ^α refer to the partial decay constants for spontaneous fission and alpha decay, and A_2/A_3 is the experimental ratio of the alpha decay rates of ^{252}Cf to ^{253}Cf. The total removal rate while in the reactor is given by Λ. The term R_0 is the experimental ratio of fission to alpha counts for ^{252}Cf in the unirradiated sample, and R_T is the same ratio for the irradiated sample at time t; ϕ_{th} is the thermal flux based upon the cobalt monitor measurements using a cadmium filter technique. The term σ_{eff} is the effective neutron cross section for radiative capture based upon the thermal flux. The experimental measurements for the irradiation (T = 2728 min at constant neutron flux) are summarized in Table 2.3. The value of t in column 2 is to the midpoint of the measurement, and the value of R is proportional to two fissions per alpha, since the fission process involves the emission of two fragments per decay. One advantage of the formulation of Eq. (2) is that the need for evaluating the alpha counts in the tail of the spectrum is eliminated, since the experimentally measured quantities R and A appear only as ratios. A 10% uncertainty has been assigned to the capture cross-section measurement, and a value of σ_{eff} (^{253}Cf) = 17.6 ± 1.8 barns is reported.

Although the irradiation was too short and was not designed to evaluate the burnout cross section of ^{253}Cf, it is possible to obtain some information bearing on its value. A comparison of the change in ratio of A_2/A_3 (the alpha decay rates of ^{252}Cf to ^{253}Cf) for the measurement of the irradiated and unirradiated samples indicates that (7.5 ± 1.5)% of the ^{253}Cf was transmuted during the irradiation. This implies an effective absorption cross section in our irradiation of σ_{abs}(^{253}Cf) = 2600 ± 500 barns, almost entirely attributable to neutron fission. This value is consistent with earlier approximate estimates of 1000–3000 barns.[2] The capture to fission ratio, α(^{253}Cf), is thus less than 0.01, which is appreciably smaller than any measured value of α for lower mass nuclides.

[1] L. D. Hunt and C. E. Bemis, Jr., "Transuranium Research Laboratory Isotope Separator," this chapter.

[2] *Chem. Technol. Div. Ann. Progr. Rept. May 31, 1968*, ORNL-4272, p. 113, and unpublished work from TRU facility.

Table 2.3. Neutron Capture Cross Section of ^{253}Cf

Sample	t, Time Following Irradiation (min)	Length of Count (min)	Number of Fissions	Number of Alphas, ^{253}Cf	Number of Alphas, ^{252}Cf	R_0	R_T	A_2/A_3	σ_{eff} (barns)
Unirradiated						× 100	× 100		
1	7,847	1391	14,280	13,534	203,455	7.019		15.03	
2	11,649	2664	14,268	12,499	206,416	6.912		16.52	
Irradiated									
3	2,467	3784	29,155	26,687	376,320		7.747	14.10	18.4
4	6,710	1236	13,513	11,311	178,845		7.556	15.81	16.9
5	12,375	4208	19,042	14,361	255,969		7.442	17.88	17.1
								Weighted av	17.6 ± 1.8

DELAYED-NEUTRON ENERGY SPECTRA AND GROUP ABUNDANCES FROM THE SPONTANEOUS FISSION OF ^{252}Cf

E. T. Chulick[1] E. Eichler
P. L. Reeder[1] C. E. Bemis, Jr.

A research program to measure the energy spectrum of delayed neutrons in spontaneous fission is now possible due to the availability of relatively large quantities of 2.646-year ^{252}Cf. The energies of delayed neutrons are of particular importance in the field of fast-reactor kinetics and control, since the accuracy of "neutron-effectiveness" calculations (a parameter of importance in predicting the dynamic behavior of a reactor) is directly related to the accuracy to which the delayed-neutron group energy spectra are known. However, in addition, the measurement of delayed-neutron energies is a novel new form of nuclear spectroscopy, since the emitted delayed neutrons populate discrete nuclear states in the daughter nucleus.

Using an electrodeposited 10-μg ^{252}Cf source and an "endless" tape transport system, we have collected fission fragment recoils on Mylar tape and have rapidly moved the active deposit to the neutron counting system located about 3 m from the vicinity of the source. Transit times from collection to counting were ~0.5 sec. Delayed-neutron group half-lives and group yields were first determined using a BF_3-tube counter system in paraffin moderator. Particular half-life groups were emphasized by an appropriate selection of collection and counting times. Delayed-neutron counting data were accumulated over many collection-counting cycles using a pulse-height analyzer in the multiscale mode to record the decay curves.

The decay curves were analyzed using least-squares fitting techniques and were resolved into four discrete half-life groups. The group abundances and half-lives are listed in Table 2.4, together with earlier values measured by Cox *et al.*[2] We observe a 6.1 ± 1.4 sec half-life group in addition to the groups previously identified by Cox *et al.* The ~6-sec group is well known in other fissioning systems, such as ^{235}U(*n,f*) and ^{239}Pu(*n,f*), and is attributed to the precursor ^{138}I, which is also present in ^{252}Cf spontaneous fission.

Measurements of the delayed-neutron energy spectra were obtained by replacing the BF_3-tube counter system with detectors and instrumentation for time-of-flight neutron spectroscopy. Using an NE-102 plastic scintillator to detect the beta particles preceding delayed-neutron emission and a stilbene scintillator for neutron detection in conjunction with fast photomultipliers and fast timing instrumentation, we are now in the process of recording neutron time-of-flight spectra over a 20- to 30-cm flight path. It has been necessary to use pulse-shape discrimination techniques to reduce sufficiently gamma-ray events in the neutron counting channel and to use pulse "pileup" rejection techniques for the beta-particle detection channel. The delayed-neutron coincidence counting rate is of the order of 1 count/min, thus necessitating long data recording periods. Approximately 30 discrete neutron energy groups are apparent in our spectra with energy widths comparable to our instrumental timing resolution (~1 nsec). We are attempting to identify these energy groups with specific delayed-neutron half-life groups by judicious choices of the collection and counting intervals to emphasize particular half-life periods.

Table 2.4. Delayed-Neutron Energy Spectra and Group Abundances for the Spontaneous Fission of ^{252}Cf

Group Index	Half-Life (sec)	Relative Abundance[a]
Present Work		
1	0.5 ± 0.1	0.17 ± 0.05
2	2.0 ± 0.3	0.30 ± 0.03
3	6.1 ± 1.4	0.22 ± 0.02
4	26.8 ± 1.1	0.31 ± 0.01
Cox *et al.*[2]		
1	0.5 ± 0.4	0.407 ± 0.12
2	2.0 ± 0.4	0.338 ± 0.046
3	20.0 ± 0.5	0.255 ± 0.01

[a]Absolute delayed-neutron yield is 0.0086 ± 0.001 neutron per fission.

[1]Department of Chemistry, Washington University, St. Louis, Mo.

[2]S. Cox *et al.*, *Phys. Rev.* 112, 960 (1958).

SEARCH FOR ^{258}Fm AND HALF-LIFE LIMIT FOR SPONTANEOUS-FISSION DECAY

C. E. Bemis, Jr. E. K. Hulet[1]
R. W. Lougheed[1]

The stability of nuclides with neutron number $N \geqslant 158$ is primarily determined by the spontaneous-fission decay mode. Despite favorable total half-life predictions,[2] these nuclides have never been observed experimentally, presumably because of their extremely short spontaneous-fission half-lives. Because of the im-

portance of the ^{258}Fm spontaneous-fission lifetime in predicting the stability of nuclides with $N \geqslant 158$, we have attempted to produce this nuclide in ultrahigh-flux neutron irradiations.

Approximately 10^8 atoms of 97-day ^{257}Fm were recovered from ^{244}Cm target assemblies and from milligram quantities of ^{252}Cf that had been irradiated in the HFIR as part of the transuranium element production program at Oak Ridge. Extremely careful chemical purification was performed to isolate completely the fermium fraction from the other transuranium element species present in the irradiated materials. The sample was allowed to decay for a period of three weeks to eliminate interference from the 20-hr ^{255}Fm activity also present in the sample.

The ^{257}Fm was deposited on the end of an ultrahigh-purity beryllium rabbit, and a thin film of beryllium metal was flash evaporated over it to prevent mechanical loss of valuable target material. Using the high-speed pneumatic-tube transfer assembly shown in Fig. 2.1, we repeatedly cycled the beryllium rabbit between the center of the HFIR core, located about 30 ft directly below the assembly, and the receiver station. The thermal-neutron flux in the irradiation position was 4.22×10^{15} neutrons cm^{-2} sec^{-1}. Transfer times from the irradiation position to the counting position in the receiver assembly were ~300 msec. A surface-barrier detector in the receiver station in conjunction with a high-speed preamplifier-amplifier-discriminator system was used to detect fission activity. Approximately 800 irradiation counting cycles were performed at various irradiation times ranging from 1 to 6 sec and counting times from 2 to 6 sec.

No fission events could be attributed to the decay of ^{258}Fm. The few fission events that were observed are attributed to the spontaneous fission of ^{257}Fm (SF/α = 2×10^{-3}) because of their random appearance in time after the end of irradiation. Assuming a 10-barn capture cross section for ^{257}Fm and that one fission event from ^{258}Fm was detected, we are able to set an upper limit of ~50 msec on the ^{258}Fm half-life.

The implication of this result on the stability of nuclides toward spontaneous-fission decay in the vicinity of N = 158 is dramatically shown in Fig. 2.2. The assignment of the 0.3-sec spontaneous-fission activity of element 104 to mass 260 by Flerov and co-workers[3] seems particularly suspect in light of the above result.

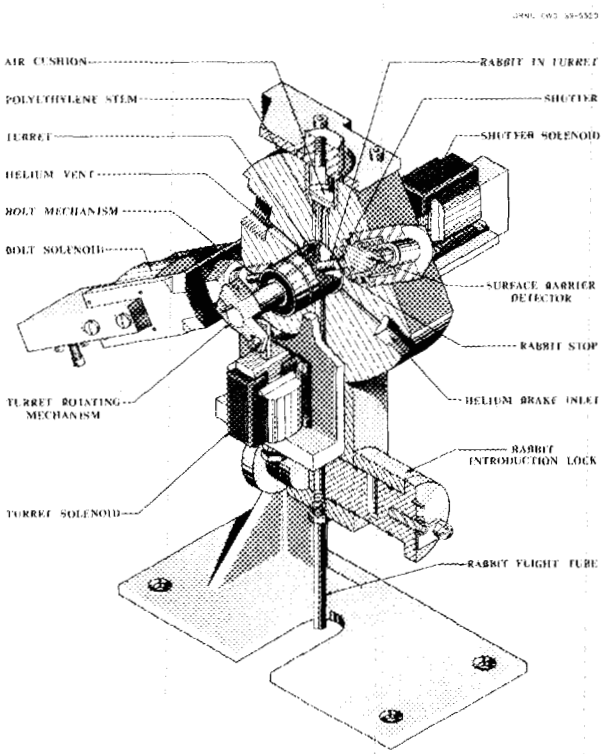

Fig. 2.1. Pneumatic-Tube Receiver Station and Counting Assembly.

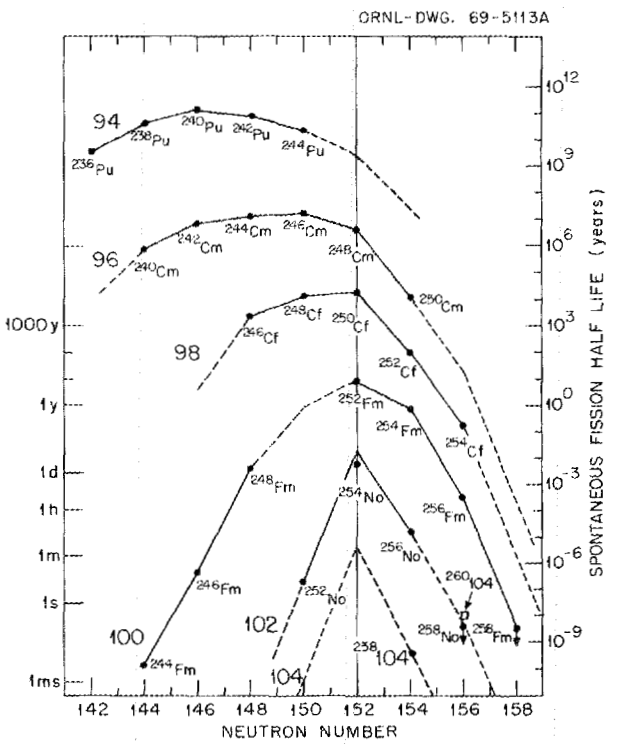

Fig. 2.2. Experimental Spontaneous-Fission Half-Lives for Even-Even Nuclides in the Vicinity of Neutron Number N = 152.

[1]Collaborative research scientists from Lawrence Radiation Laboratory, Livermore, Calif.

[2]V. E. Viola, *J. Inorg. Nucl. Chem.* 30, 2601 (1968) and references cited therein.

[3]G. N. Flerov *et al. Phys. Letters* 13, 73 (1964).

FRAGMENT ENERGY CORRELATION MEASUREMENTS FOR THE FISSION OF ^{238}U AND ^{239}Pu BY 8- to 13-MeV PROTONS[1]

R. L. Ferguson Frances Pleasonton[2]
F. Plasil[2] H. W. Schmitt[2]

As part of a continuing study of the systematics of fragment mass and energy distributions and correlations in nuclear fission, we have carried out two-parameter fragment energy correlation experiments on the proton-induced fission of ^{239}Pu in the proton energy range $8 \leqslant E_p \leqslant 12.5$ MeV. In addition, we have obtained more detailed data in this energy range for the proton-induced fission of ^{238}U than were reported last year.[3]

Experimental details, including experimental techniques and methods of analysis, have been described previously (see ref. 3 and refs. 47–49 therein). It should be noted that references to fragment mass in this work are to the provisional mass μ defined by the equation $\mu_1 = AE_2/(E_1 + E_2)$, where E_1 and E_2 are the measured (post-neutron-emission) single-fragment kinetic energies and A is the mass of the compound nucleus; the symbol μ without subscript is used when no distinction between fragments 1 and 2 is necessary. References to total kinetic energy are to $E_K = E_1 + E_2$, that is, total post-neutron-emission kinetic energy. As shown in the earlier papers indicated above, μ closely approximates the pre-neutron-emission masses, and when neutron emission data are available, the quantities and distributions obtained for μ and E_K may be transformed to obtain accurate results for pre-neutron-emission masses, energies, and mass-vs-energy correlations.

Some of the arrays showing $N(\mu, E_K)$, yield as a function of fragment mass and total kinetic energy, are presented in Fig. 2.3. Asymmetric mass divisions are

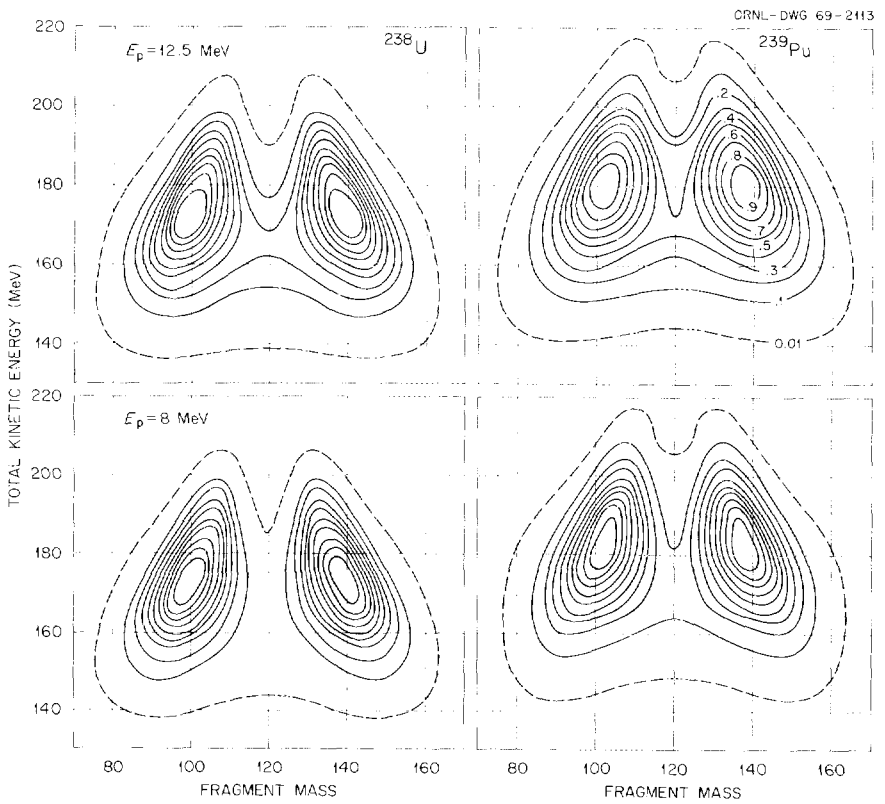

Fig. 2.3. Yields as a Function of Fragment Mass and Total Kinetic Energy for Fission of ^{238}U and ^{239}Pu by Protons of 8 and 12.5 MeV. The contour lines represent fractions of the peak height.

most probable for all cases studied. Certain differences in the arrays, however, are of interest; a brief discussion follows.

It is well established that the yield of mass divisions in the region of symmetry increases with increasing excitation energy. This point is again confirmed for (p,f) reactions on the targets represented in Fig. 2.3, where comparisons between $E_p = 8$ MeV and $E_p = 12.5$ MeV are shown.

We note also that the most probable fragment masses occurring at the highest kinetic energies reached by the contours are in the neighborhood of 130 to 132 amu. We have pointed out this feature of similar arrays in earlier studies, but it is perhaps significant that this feature persists. Qualitatively, the near-doubly-magic nuclei in the region of 132 amu may occur with more nearly spherical shapes than nuclei away from this region; thus the arrays extend to higher kinetic energies in this mass region.

The mass distributions, the average total kinetic energies as functions of fragment mass, and the root-mean-square widths of the total kinetic energy distributions as functions of fragment mass are compiled for $E_p = 8$, 10.5, and 12.5 MeV in Fig. 2.4. In general, these curves follow trends and patterns similar to those reported last year for $^{233}U(p,f)$, $^{235}U(p,f)$, and $^{238}U(p,f)$ for the same proton energy range.[3]

On the basis of the mass distributions previously obtained for $^{238}U(p,f)$ it appeared that, in the curve showing peak-to-valley ratio vs proton energy, a step might occur at $E_p \cong 10$ MeV.[3] As a result of the present series of experiments, points have been obtained at 15 energies for $^{238}U(p,f)$ in the proton energy range $8 \leqslant E_p \leqslant 13$ MeV; the new determinations of peak-to-valley ratio as a function of E_p are combined with the earlier data and are plotted in Fig. 2.5. Only a smooth curve is found. Thus either no onset of additional pre-fission neutron emission occurs in this energy region, or its effects appear only slowly and continuously in this function. Results for the three energies studied for $^{239}Pu(p,f)$ are also included in Fig. 2.5.

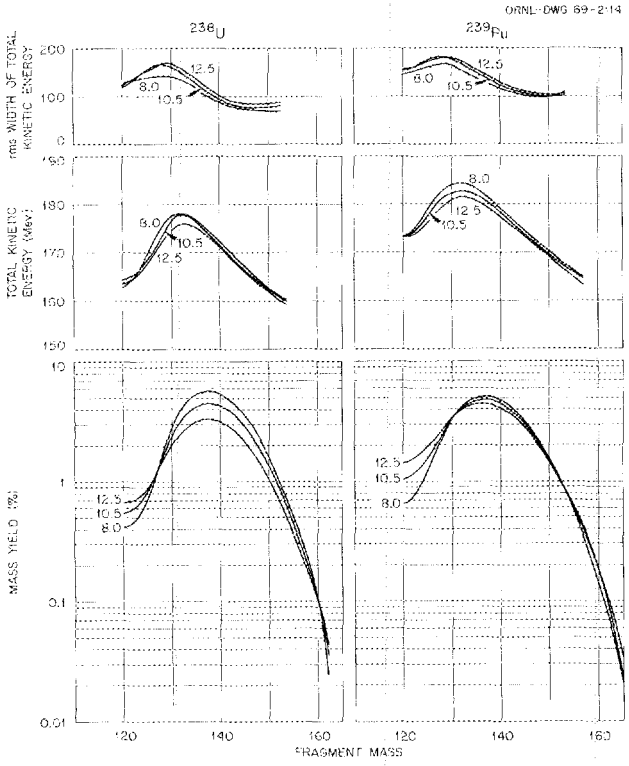

Fig. 2.4. Mass Distributions, Average Total Kinetic Energies as Functions of Fragment Mass, and Root-Mean-Square Widths of the Total Kinetic Energy Distributions as Functions of Fragment Mass for Fission of ^{238}U and ^{239}Pu by Protons of 8, 10.5, and 12.5 MeV. The curves are labeled with the proton bombarding energy.

---

[1] This work was performed in collaboration with the Physics Division and has also been reported in *Phys. Div. Ann. Progr. Rept. Dec. 31, 1968*, ORNL-4395, p. 34.

[2] Physics Division.

[3] *Chem. Div. Ann. Progr. Rept. May 20, 1968*, ORNL-4306, p. 12.

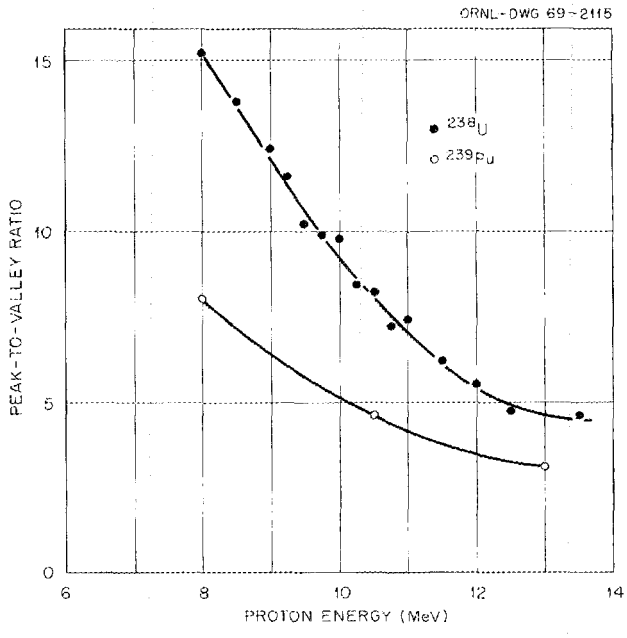

Fig. 2.5. Fragment Mass Distribution Peak-to-Valley Ratios for Proton-Induced Fission of ^{238}U and ^{239}Pu as Functions of Bombarding Energy.

HALF-LIVES OF ^{253}Cf AND ^{253}Es

R. E. Druschel J. Halperin
C. E. Bemis, Jr.

Half-Life of ^{253}Cf

A measurement has been made of the half-life of ^{253}Cf by following the growth and decay of the 20-day ^{253}Es daughter. Californium-253 decays principally by beta emission, although there is a 0.31% alpha-decay branch. It emits a 0.27-MeV beta group and possibly softer negatron groups. A direct measure of the beta decay is made difficult in our samples because the low-energy electrons are emitted in the presence of a large amount of alpha radiation.

A sample of ^{253}Cf was prepared by irradiating ^{252}Cf for 20 hr at a flux of 1.7×10^{14} neutrons cm^{-2} sec^{-1}. Three samples were then prepared from the irradiated californium by electrodeposition onto platinum plates. The alpha-pulse spectrum of each sample was measured with a silicon detector in an evacuated chamber. The ratio of the activity in the ^{253}Es peak (6.640 MeV) to that in the 2.646-year ^{252}Cf peak (6.119 MeV) was then determined by summing the appropriate channels in the spectrum. Since the ratio of two peaks was measured, systematic errors concerning geometry and the evaluation of counts in the tail of the alpha spectrum are not important. Recoil losses in the sample would tend to affect the two nuclides equally and thus also would not alter their ratio. The samples were followed for 142 days, in which ~75 measurements were carried out on each sample. The data were analyzed using a nonlinear least-squares computer program carrying out a two-parameter fit — one parameter involving the initial quantity of ^{253}Cf and the second its radioactive decay constant. The ^{253}Es half-life was set at the best value described in the second part of this experiment. However, the ^{253}Cf analysis is relatively insensitive to the value taken for the ^{253}Es half-life.

The results of the measurements are summarized in Table 2.5. The weighted average of the three measurements is $T_{1/2}(^{253}\text{Cf}) = 17.812 \pm 0.041$ days. To take into account unknown sources of error, we have doubled the uncertainty in the above standard error and report a preferred value of 17.81 ± 0.08 days for the half-life of ^{253}Cf. Metta and co-workers[1] have reported a value of 17.6 ± 0.2 days for the ^{253}Cf half-life based on the measurement of 20 alpha spectra over a period of 84 days. However, they used an older value for the half-life of ^{253}Es of 20.0 days. Correcting their value for the current value of $T_{1/2}(^{253}\text{Es})$ gives 18.0 ± 0.2 days, approximately 1% greater than the value reported here.

Half-Life of ^{253}Es

In support of the ^{253}Cf half-life determination, the alpha-decay half-life of ^{253}Es has been carefully remeasured. A pure sample of ^{253}Es was prepared using an α-hydroxyisobutyric acid separation of an equilibrium mixture of ^{253}Cf and ^{253}Es contained on a Dowex 50 cation exchange column.

The half-life of ^{253}Es was measured in two independent ways, both involving the direct observation of the alpha decay of ^{253}Es. In the first method the gross

Table 2.5. Half-Lives of ^{253}Cf and ^{253}Es

Sample No.	Number of Measurements	$T_{1/2}(^{253}\text{Cf})$ (days)	Standard Error (days)	$T_{1/2}(^{253}\text{Es})$ (days)	Standard Error (days)	Preferred Value (days)
1	75	17.804	0.063			
2	77	17.834	0.069			
3	72	17.796	0.081			
Av		17.812	0.041			$17.81_2 \pm 0.08_2$
1	75			20.465	0.013	
2	75			20.451	0.020	
Av				20.461	0.012	
3	78			20.468	0.026	
4	79			20.509	0.031	
Av				20.485	0.020	
			Weighted mean	20.467	0.012	$20.46_7 \pm 0.02_4$

alpha decay was followed directly using a 2π proportional gas-flow counter. Two plates containing about 3 and 8 pg of ^{253}Es were prepared by electrodeposition. The platinum plates were covered by a 25-μg/cm^2 vacuum-sputtered deposit of gold so as to minimize loss of the einsteinium by alpha recoils. Some 75 measurements of each sample and counter calibrations were carried out over a period of 120 days; a minimum of 10^5 counts were collected in each measurement. The data were analyzed by a nonlinear least-squares computer program in terms of a mixture containing a constant, nondecaying alpha-emitting component together with the ^{253}Es. A three-component fit to the data yielded values for the relative amounts of ^{253}Es, the constant component, and the radioactive decay constant. A mean half-life value of $T_{1/2}(^{253}\text{Es}) = 20.461 \pm 0.012$ days is derived from this measurement.

In the second method, some 18.10-year ^{244}Cm was added to the original sample of pure ^{253}Es from which two electrodeposited and gold-coated samples were prepared as described above. These samples were followed over a period of 120 days by measuring their alpha spectrum with a silicon detector and then determining the ratio of the ^{253}Es (6.640 MeV) to the ^{244}Cm (5.806 MeV) in the spectrum. Initially, in excess of 10^5 counts were accumulated for each nuclide per measurement, but the measurements were eventually limited to 100-min accumulation times; the ^{253}Es counts had dwindled to about 5×10^3 when the experiment was ended. The data were analyzed using a nonlinear least-squares program with a two-parameter fit — the initial ratio of ^{253}Es to ^{244}Cm and the radioactive decay constant for ^{253}Es. The half-life value derived from this measurement is 20.485 ± 0.020 days.

These data are summarized in Table 2.6, in which the weighted average of the two sets of measurements is $T_{1/2}(^{253}\text{Es}) = 20.467 \pm 0.012$ days. However, to take into account unforeseen sources of error, we have doubled the uncertainty in the above standard error and prefer a value of $20.46_7 \pm 0.02_4$ days for the half-life of ^{253}Es. The present value is in good agreement with the relatively recent values of 20.7 days[2] and particularly 20.47 days[3] quoted by Lederer.[4]

Table 2.6. Calculated Alpha Intensities to the Favored $K = 7/2$ Band in ^{249}Cm from the Decay of ^{253}Cf

Transition ($I \to I$)	Predicted Intensities (%)				Experimental Intensity (%)
	$L = 0$	$L = 2$	$L = 4$	Σ	
$7/2 \to 7/2$	83.18	11.41	0.11	94.7[a]	94.7
$7/2 \to 9/2$		4.69	0.18	4.87	5.3 ± 1.9
$7/2 \to 11/2$		0.31	0.06	0.37	
$7/2 \to 13/2$			0.06	0.06	

[a]The calculated relative intensities for the $7/2 \to 7/2$ transition were normalized to the experimental value.

[1]D. Metta *et al.*, *J. Inorg. Nucl. Chem.* **27**, 33 (1965).

[2]Combined Radiochemistry Group of Lawrence Radiation Laboratory (Berkeley and Livermore), Los Alamos Scientific Laboratory, and Argonne National Laboratory, UCRL-14500 (1966) (unpublished).

[3]S. Halvorsen, H. V. Michel, T. Asaro, and I. Perlman, unpublished results (1966).

[4]C. M. Lederer, J. M. Hollander, and I. Perlman, *Table of Isotopes*, 6th ed., Wiley, New York, 1967.

STATES IN ^{249}Cm POPULATED IN THE ALPHA DECAY OF 17.6-DAY ^{253}Cf

C. E. Bemis, Jr. J. Halperin

Further work on the alpha decay of 17.6-day ^{253}Cf has been performed since the initial results were reported for both ^{254}Cf and ^{253}Cf.[1] Using isotopically enriched ^{253}Cf sources, we have identified a weak alpha group at an energy of 5.921 ± 0.005 MeV in addition to the main group at 5.979 ± 0.005 MeV previously reported. Abundances per alpha decay and hindrance factors, HF, based on an alpha-branching ratio of (0.31 ± 0.04)% are: (94.7 ± 0.9)%, HF = 1.5 ± 0.2 for the 5.979-MeV group; and (5.3 ± 1.9)%, HF = 13.2 ± 2.8 for the 5.921-MeV group.

Since alpha-decay hindrance factors less than ≈ 4 in odd-A nuclei indicate favored alpha decay, the 5.979-MeV group populates the $7/2^+$ $7/2$ [613↑] state in ^{249}Cm, the state with the same asymptotic quantum numbers as the ground state of ^{253}Cf. The $9/2^+$ rotational state arising from the $7/2$ [613↑] Nilsson state has been located at an excitation energy of 110 ± 1 keV in ^{249}Cm in the ^{248}Cm(d,p) reaction.[2] The $K = 7/2$ base state was not observed because of interfering levels. We calculate that the $7/2^+$ $7/2$ [613↑] state should lie 60 keV below this known $9/2^+$ rotational state at an excitation energy of 50 ± 1 keV in ^{249}Cm, using the $I(I + 1)$ rule and a rotational energy constant of 6.69 keV. Since alpha decay to the entire $K = 7/2$ rotational band in ^{249}Cm is favored, the 5.921-MeV group populates the $9/2^+$ first rotational state. The energy difference between the two alpha groups, 58 ± 2 keV, is in agreement with the expected energy separation of 60 keV for the $7/2^+$ and $9/2^+$ members of the $7/2$ [613↑] band.

To test our assumption further, we have calculated the relative alpha intensities to states in the $K = 7/2$ favored band using the methods of Bohr *et al.*[3] Assuming that the hindrance factors for the various alpha partial waves ($L = 0, 2, 4$) in favored odd-A alpha decay are the same as for adjacent even-even alpha decay, the relative alpha populations to the rotational states in the favored band are given by the following relationship:

$$P = \frac{P_E}{N} \sum_{L=0,2,4} \frac{C(I_i L K_i 0 | I_f K_f)^2}{HF_{L(e-e)}} ,$$

where P_E is the alpha transition probability calculated from simple barrier penetration theory, N is a constant which we have taken to be unity, C is a Clebsch-Gordon coefficient, and $HF_{L(e-e)}$ is the hindrance factor interpolated from adjacent even-even nuclei. The indices i and f refer to the initial and final states respectively.

We have used relative hindrance factors of 1:3.4:57 for the $L = 0$, 2, and 4 partial waves, respectively, as observed for the alpha groups in ^{252}Cf. The $L = 6$ hindrance factor is ~1200 and was neglected in these calculations. The calculated alpha intensities to the $K = 7/2$ favored band in ^{249}Cm are compared with the experimental values in Table 2.6.

The calculated intensity for the $7/2 \rightarrow 9/2$ alpha transition is within the error limits on the experimental value. We were unable to observe the much weaker $7/2 \rightarrow 11/2$ and $7/2 \rightarrow 13/2$ alpha transitions because of the large low-energy tails from the ^{252}Cf and ^{253}Es activities in the mass-253 sample.

The energy level scheme for ^{249}Cm (Fig. 2.6) is a combination of some of the ^{248}Cm(d, p) work of Friedman[2] and the results of the present work.

[1] C. E. Bemis, Jr., and J. Halperin, *Chem. Div. Ann. Progr. Rept. May 20, 1968*, ORNL-4306, p. 28.

[2] A. M. Friedman, private communication, July 1968.

[3] A. Bohr, P. O. Fröman, and B. R. Mottelson, *Kgl. Danske Videnskab. Selskab, Mat.-Fys. Medd.* 29, No. 10 (1955).

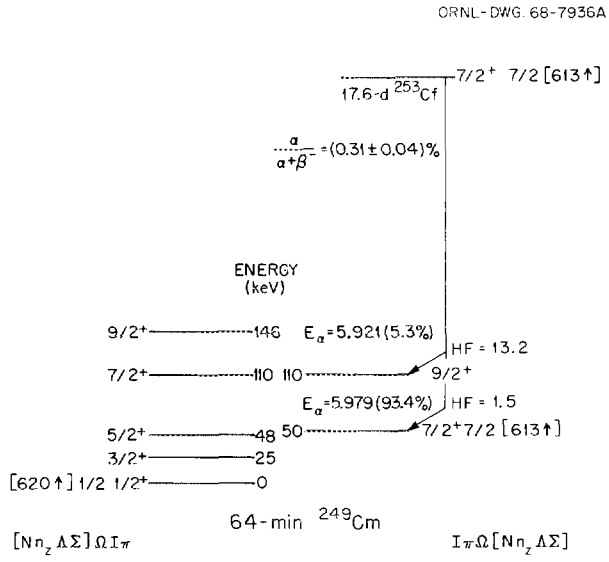

Fig. 2.6. Level Scheme for ^{249}Cm Showing Alpha Decay Pattern of ^{253}Cf.

NUCLEAR CHEMISTRY WITH HEAVY IONS

R. J. Silva, M. Mallory
R. L. Hahn, M. F. Roche[1]
O. L. Keller, C. E. Bemis
K. S. Toth[1], P. F. Dittner

Heavy-ion beams of carbon, nitrogen, oxygen, and neon have recently been produced in the ORIC. Especially significant is the fact that the energies of these beams are sufficiently large, of the order of 100 MeV, to overcome the Coulomb barriers of the heaviest nuclides in the periodic table. Several nuclear-chemical experiments have been initiated with these beams to search for previously unknown radionuclides, such as alpha-emitting ^{241}Cf and ^{240}Cf, among the transuranium nuclei.

Concomitant research has been carried out with lower-energy beams of ^{14}N, ^{16}O, and ^{19}F from the tandem Van de Graaff accelerator [the beam energy in MeV from the tandem is given by the expression $E = (n + 1)V$, where n is the charge state of the ion accelerated and V is the terminal voltage, ~6 MV]. The experiments, which involve irradiations of such light targets as ^{9}Be, ^{27}Al, and ^{62}Ni, are concerned with finding new radionuclides, doing in-beam gamma-ray spectroscopy, and studying nuclear reaction mechanisms.

[1] Electronuclear Division.

CHEMICAL PROPERTIES OF THE SUPERHEAVY ELEMENTS. I. ELEMENTS 113 AND 114, EKA-THALLIUM AND EKA-LEAD

O. L. Keller, Jr., T. A. Carlson
J. L. Burnett, C. W. Nestor, Jr.[1]

A number of theoretical papers[2,3] have appeared recently indicating that islands of nuclear stability exist

around elements 114 to 126. Several laboratories in the United States, Western Europe, and Russia are proposing to build heavy-ion accelerators in order to explore this transactinide region of the periodic table. Work is also progressing here and abroad in the search for the superheavy elements in nature. As an aid in designing the necessary experiments for chemical identification of the accelerator products and to assist in the search for the naturally occurring isotopes of the superheavy elements, we present values for certain physical and chemical properties of elements 113 and 114 predicted on the basis of Mendeleev's periodic system and theoretical calculations.[4]

Element 113 is eka-thallium and element 114 is eka-lead, assuming that the structure of the periodic table continues unchanged. This would be in accord with recent relativistic Dirac-Slater calculations.[5] The properties predicted under this assumption are given in Table 2.7. The ionization potentials were obtained through the use of a relativistic Hartree-Fock-Slater program developed at Oak Ridge.[6] Several years ago Drago[7] explained the tendency toward stabilization of the lower valence in the heavier elements of groups IIIA and IVA as being due to a weakening of the covalent bonds needed to obtain their higher valence states. Extending Drago's arguments to elements 113 and 114, we obtain a most stable valence for element 113 of +1 and for element 114 of +2. We obtained the other values shown in Table 2.7 by extrapolation of the properties for earlier members of the group (such as the Debye θ) or through a theoretical relation using such an extrapolated quantity (such as obtaining the melting point through Lindemann's formula).

Table 2.7. Some Predicted Properties of Elements 113 and 114

	Element 113, Eka-Thallium	Element 114, Eka-Lead
Chemical group	IIIA	IVA
Atomic weight	297	298
Most stable oxidation state	+1	+2
First ionization potential, eV	7.4	8.5
Second ionization potential, eV		16.8
Oxidation potential, V	$M \rightarrow M^{+} + e^{-}$	$M \rightarrow M^{2+} + 2e^{-}$
	−0.6	−0.9
Metallic radius, Å	1.75	1.85
Ionic radius, Å	1.48	1.31
Atomic volume, cm^3/mole	18	21
Density, g/cm^3	16	14
Melting point, °C	430	70
Boiling point, °C	1100	150
Heat of vaporization, kcal/mole	31	9
Heat of sublimation, kcal/mole	34	10
Debye temperature, °K	70	46
Entropy, eu/mole (25°C)	17	20

[1] Mathematics Division.

[2] For an excellent review, see G. T. Seaborg, *Ann. Rev. Nucl. Sci.* 18, 53 (1968).

[3] S. G. Nilsson, S. G. Thompson, and C. F. Tsang, *Phys. Letters* **28B**, 458 (1969).

[4] G. T. Seaborg presented these predicted properties as part of his paper, "Prospects for Further Considerable Extension of the Periodic Table," 157th National ACS Meeting, Minneapolis, Minn., April 13–18, 1969.

[5] J. T. Waber, D. T. Cromer, and D. Liberman, *Ann. Rev. Nucl. Sci.* **18**, 105 (1968).

[6] C. W. Nestor *et al.*, *Relativistic and Non-Relativistic SCF Wave Functions for Atoms and Ions from Z = 2 to 80*, ORNL-4027 (December 1966); for a related paper using a Wigner-Seitz boundary condition see *Phys. Rev.* **174**, 118 (1968).

[7] R. S. Drago, *J. Phys. Chem.* **62**, 353 (1958).

LANTHANIDE AND ACTINIDE STANDARD II-III OXIDATION POTENTIALS AND THE OPTICAL ABSORPTION SPECTRA OF SOME LANTHANIDE AND ACTINIDE TRIHALIDES IN ETHANOL[1]

L. J. Nugent R. D. Baybarz[2]
J. L. Burnett

The standard II-III aqueous oxidation potentials of the lanthanides and some of the actinides have been calculated by means of Jørgensen's refined spin-pairing electronic energy theory[3,4] and measured from the electron-transfer absorption bands of some of the lanthanide and actinide chloride and bromide complexes in anhydrous ethanol solution. The correlation[5,6] between the standard II-III aqueous oxidation potentials and the wave numbers of the lowest-energy electron-transfer bands was established using the potential data for Sm, Eu, and Yb (ref. 7) and our own spectral measurements.

In the lanthanide series the only additional observable electron-transfer band is that for the thulium bromide complex in anhydrous ethanol. The correlation plot yields a standard II-III aqueous oxidation potential of 2.2 V, in very good agreement with the value of 2.4 V calculated from Jørgensen's theory.

In the actinide series there appears to be a shift of +0.8 V from the lanthanide correlation plot. Thus the II-III oxidation potential for an actinide for a given

electron-transfer band position is equal to the potential as read from the lanthanide plot +0.8 V in the halide complexes. The electron-transfer bands have been measured for ^{249}Cf and ^{253}Es bromide complexes in anhydrous ethanol, and from these and the shifted correlation plot, we obtain 1.9 V for the Cf(II)/Cf(III) aqueous oxidation potential and 1.6 V for the Es(II)/Es(III) potential. These values are in excellent agreement with 2.0 and 1.6 V, respectively, calculated from Jørgensen's theory.

---

[1] For greater detail, see L. J. Nugent, R. D. Baybarz, and J. L. Burnett, *J. Phys. Chem.* 73 1177 (1969).

[2] Chemical Technology Division.

[3] C. K. Jørgensen, *Mol. Phys.* **5**, 271 (1962).

[4] C. K. Jørgensen, *Mol. Phys.* 7, 17 (1963).

[5] J. C. Barnes and P. Day, *J. Chem. Soc.* **1964**, p. 3886.

[6] F. S. Dainton, *Chem. Soc. (London) Spec. Publ.* **1**, 18 (1954).

[7] L. B. Asprey and B. B. Cunningham, *Progr. Inorg. Chem.* **2**, 267 (1960).

CRYSTAL STRUCTURE OF AMERICIUM TRICHLORIDE HEXAHYDRATE

J. H. Burns

Although there have been numerous studies of americium compounds by powder x-ray diffraction, there have been few structure determinations by single-crystal methods. Powder and single-crystal photographs have readily shown that $AmCl_3 \cdot 6H_2O$ is isostructural with analogous trichlorides[1] and tribromides of the lanthanides Nd-Lu and the actinide tribromides of U-Am.[2] However, a structure refinement of $AmCl_3 \cdot 6H_2O$ from single-crystal data was needed in order to have a direct determination of atomic parameters.

Large single crystals were grown by evaporation of a solution of Am(III) in 6 *M* HCl, and a suitable specimen was sealed in a thin-walled glass tube for study. X-ray diffraction data were collected with the Transuranium Research Laboratory computer-controlled diffractometer using Mo $K\alpha$ radiation. The space group, $P2/n$, was confirmed, and the monoclinic unit cell was found to have dimensions $a = 9.707(2)$, $b = 6.565(2)$, $c = 8.008(2)$, and $\beta = 93° 39(5)'$. About 1500 reflections were measured and converted to observed structure factors. Starting values for use in least-squares refinement of positions and anisotropic thermal parameters were obtained from the results for $GdCl_3 \cdot 6H_2O$.[3] Rapid convergence was achieved; the final agreement index was 0.039.

An interesting feature of the structure of $AmCl_3 \cdot 6H_2O$ (see Fig. 2.7) is that each Am ion has six O neighbors and two Cl neighbors, forming a complex $Cl_2Am(OH_2)_6$, while the third Cl is not bonded to Am

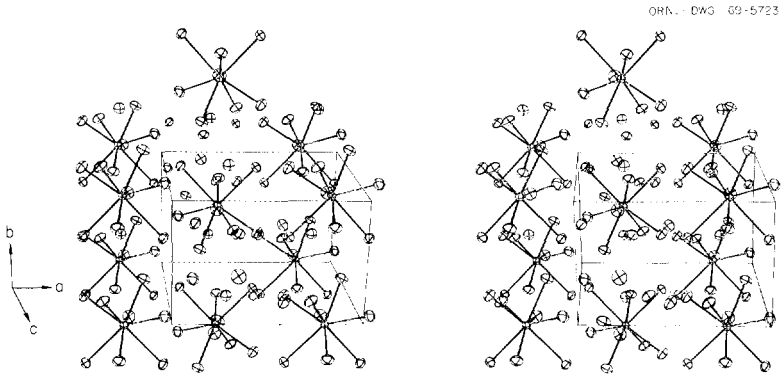

Fig. 2.7. Stereoscopic Drawing of the Structure of $AmCl_3 \cdot 6H_2O$. Atoms are represented by their 50% probability thermal ellipsoids. Bonds are shown only to the americium atoms.

at all but has an irregular octahedron of H_2O molecules around it. Although the H atoms could not be located in this determination, plausible locations for them can be deduced from the O . . . Cl distances and the angles between such interactions. This was pointed out by Marezio *et al.*[3] for $GdCl_3 \cdot 6H_2O$ and applies to the present case also. Accordingly, the six H_2O molecules are oriented with their O atoms toward the Am ion and their H atoms bonded, one to a Cl atom of an adjacent $Cl_2Am(H_2O)_6$ complex and the other to the isolated Cl ion. The relevant interatomic distances are given in Table 2.8.

[1] E. J. Graeber, G. H. Conrad, and S. F. Duliere, *Acta Cryst.* **21**, 1012 (1966).

[2] D. Brown, S. Fletcher, and D. G. Holah, *J. Chem. Soc.* **1968**, p. 1890.

[3] M. Marezio, H. A. Plettinger, and W. H. Zachariasen, *Acta Cryst.* **14**, 234 (1961).

Table 2.8. Bond Distances in the $AmCl_3 \cdot 6H_2O$ Crystal Structure

$Cl_2Am(OH_2)_6$	Bond Distance (Å)	$Cl(OH_2)_6$	Bond Distance (Å)
Am–Cl(2)	2.799	Cl(1)...O(1)[a]	3.246
Am–O(1)	2.471	Cl(1)...O(2)	3.194
Am–O(2)	2.440	Cl(1)...O(3)	3.180
Am–O(3)	2.474		
	Oxygen Contacts		
O(1)–Am	2.471	O(3)–Am	2.474
O(1)...Cl(1)	3.246	O(3)...Cl(1)	3.180
O(1)...Cl(2)	3.178	O(3)...Cl(2)	3.167
O(2)–Am	2.440		
O(2)...Cl(1)	3.194		
O(2)...Cl(2)	3.148		

[a] Dotted lines indicate probable hydrogen-bond interactions.

CRYSTAL STRUCTURE OF ANHYDROUS $AmCl_3$

J. H. Burns J. R. Peterson[1]

The lanthanide trichlorides from $LaCl_3$ to $GdCl_3$ and all the actinide trichlorides studied ($EsCl_3$ is the heaviest) crystallize with the so-called UCl_3 type of structure. In the hexagonal unit cell, space group $P6_3/m$, the metal ions are in sites $\pm(1/3, 2/3, 1/4)$ and the chloride ions are in $\pm(x,y, 1/4; -y, x-y, 1/4; y-x, -x, 1/4)$. Until recently, when refinements with single-crystal data were reported[2] for $GdCl_3$ and for the trichlorides of La, Nd, Eu, and Gd,[3] the only values available for the two variable parameters, x and y, were those estimated to fit x-ray powder diffraction data by Zachariasen.[4] Because these recent results agree with one another but differ considerably from the earlier values, and because no comparable work is available on the actinides, we have studied $AmCl_3$ and plan also to study $CfCl_3$. The important questions of ionic radii and actinide contraction depend on having accurate values for these parameters.

A single-crystal specimen of $AmCl_3$ was prepared by microchemical techniques. About 1 μg of purified ^{243}Am was sorbed on a single Dowex 50-X4 ionexchange resin bead. By heating in air to 1200°C the resin bead was decomposed and the Am converted to the oxide. This spherical sample was placed in a quartz capillary tube attached to a vacuum line and converted to $AmCl_3$ by treatment with anhydrous HCl at 500°C. A nichrome-wound quartz furnace allowed visual observation of the sample during heating. Melting was observed at a nominal temperature of 715 ± 5°; however, the temperature of the sample in the capillary may have been somewhat different than that of the thermocouple. Molten $AmCl_3$ is light amber. A single crystal suitable for x-ray study was grown by slowly cooling the sample under an HCl atmosphere through the melting point. The sample was then sealed off under 1/3 atm of HCl.

X-ray diffraction data were collected with the Transuranium Research Laboratory computer-controlled diffractometer and Mo $K\alpha$ radiation. The unit-cell dimensions were obtained by least-squares refinement of the 2θ values of 12 high-angle reflections; they are given in Table 2.9. Intensities of about 1490 reflections were measured and, after combination of equivalent ones, yielded 382 structure factors. Least-squares refinement of the Cl atomic position and anisotropic thermal

Table 2.9. Crystallographic Data for Some Compounds Having the UCl_3 Structure Type[a]

Compound	a_0	c_0	x_{Cl}	y_{Cl}
UCl_3[b]	7.428(3)	4.312(3)	0.375(15)	0.292(15)
$NdCl_3$[c]	7.399(1)	4.242(1)	0.3878(3)	0.3017(3)
$AmCl_3$	7.382(1)	4.214(1)	0.3877(4)	0.3019(5)

[a] Numbers in parenthesis indicate least-squares standard error in least-significant digit.

[b] Data of Zachariasen, ref. 4.

[c] Data of Morosin, ref. 3.

parameters for Am and Cl gave an agreement index of 0.034. Table 2.9 also lists our final parameters and, for comparison, those of Zachariasen for UCl_3 and of Morosin for $NdCl_3$. It is seen that the UCl_3 parameters would not yield the correct bond lengths for Am-Cl and probably would not for the other actinide trichlorides as well.

In the $AmCl_3$ structure, shown stereoscopically in Fig. 2.8, each Am ion is 9-coordinated by Cl ions arranged as a trigonal prism with capped vertical faces. There are three equatorial Am-Cl bond lengths of 2.914 Å and six apical Am-Cl bonds of 2.873 Å. By comparison of these data with the results for lanthanide trichlorides,[3] an ionic radius of 0.98 Å is derived for Am^{3+}, based on the lanthanide radii of Templeton and Dauben.[5]

[1] Consultant; Chemistry Department, University of Tennessee, Knoxville.

[2] C. Au and R. Au, *Acta Cryst.* **23**, 1112 (1967).

[3] B. Morosin, *J. Chem. Phys.* **49**, 3007 (1968).

[4] W. H. Zachariasen, *The Transuranium Elements* (ed. by G. T. Seaborg, J. J. Katz, and W. M. Manning), National Nuclear Energy Series, Div. IV, vol. 14B, Part II, p. 1473, McGraw-Hill, New York, 1949.

[5] D. H. Templeton and C. H. Dauben, *J. Am. Chem. Soc.* **76**, 5237 (1954).

PREPARATION AND IDENTIFICATION OF CYCLOPENTADIENYL COMPLEXES OF THE ACTINIDE AND LANTHANIDE ELEMENTS

P. Laubereau[1] J. H. Burns

The first organometallic compounds of berkelium and californium, the tricyclopentadienyl compounds $Bk(C_5H_5)_3$ and $Cf(C_5H_5)_3$, have been synthesized, and $Pm(C_5H_5)_3$ has been prepared for the first time in a weighable amount.[2] The syntheses were carried out with microgram quantities of the trivalent ions of the isotopes ^{249}Bk, ^{249}Cf, and ^{147}Pm. The preparative scheme, imposed mainly by the small amounts of available starting materials, was:

M^{3+} in 0.05 *N* HCl; M = Bk, Cf, Pm

↓

M^{3+} on Dowex 50 ion exchange beads

↓ careful ignition at temperatures up to 1200°C

M_2O_3

↓ HCl gas at 500°C

MCl_3

↓ $Be(C_5H_5)_2$ melt at 80°C

$M(C_5H_5)_3$

↓ sublimation under high vacuum at temperatures between 120 and 220°

Purified tricyclopentadienyl compound

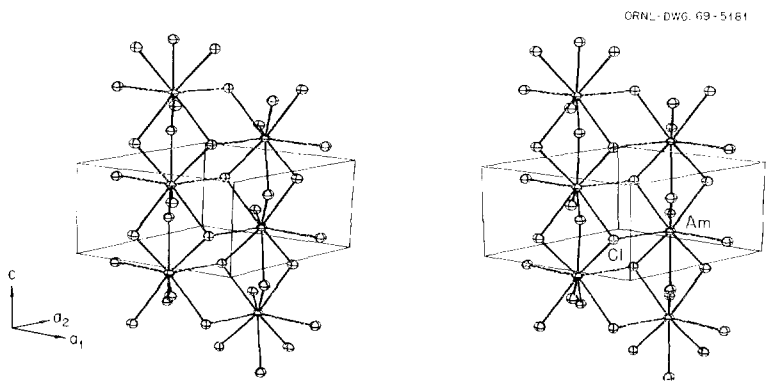

Fig. 2.8. Stereoscopic View of the Structure of $AmCl_3$. Atoms are represented by 90% probability ellipsoids of thermal motion. The *c* axis is vertical.

The first three steps were carried out in carefully cleaned quartz or platinum vessels; leached quartz capillaries under HCl or Ar, or in high vacuum, were used in the final steps. For comparison with these compounds, $Pr(C_5H_5)_3$, $Sm(C_5H_5)_3$, and $Tb(C_5H_5)_3$ were also prepared.

All these tricyclopentadienyl compounds could be sublimed under high vacuum at temperatures from 120 to 220°C; $Cf(C_5H_5)_3$ is garnet red, $Bk(C_5H_5)_3$ is amber, and $Pm(C_5H_5)_3$ is yellow-orange. Ultraviolet and visible spectra of the compounds were obtained,[3] and the extent to which the colors of $Bk(C_5H_5)_3$ and $Pm(C_5H_5)_3$ are influenced by impurities of ^{249}Cf and ^{147}Sm resulting from radioactive decay was determined. The compounds were surprisingly stable toward autoradiolytic decomposition; it was possible to resublime samples with high yield even after a week.

Identification of the microgram quantities of these substances was accomplished by x-ray diffraction methods. Tricyclopentadienylpraseodymium, whose composition was established by chemical analysis of macroscopic quantities, was examined by single-crystal and x-ray powder diffraction techniques to establish its unit-cell dimensions and probable space groups and to obtain its characteristic x-ray powder diagram. All the other $M(C_5H_5)_3$ compounds were found to be isomorphous with $Pr(C_5H_5)_3$ by comparison of either single-crystal or powder diffraction data. Crystallographic data for these compounds are given in Table 2.10; analysis of the crystal structure is under way.

Table 2.10. Crystallographic Data for Tricyclopentadienyl Complexes of Actinides and Lanthanides[a]

Compound	Orthorhombic Unit-Cell Dimensions (Å)		
	a	*b*	*c*
$Bk(C_5H_5)_3$	14.11	17.55	9.634
$Cf(C_5H_5)_3$	14.10	17.50	9.692
$Pr(C_5H_5)_3$	14.21	17.62	9.787
$Pm(C_5H_5)_3$	14.12	17.60	9.756
$Sm(C_5H_5)_3$	14.23	17.40	9.73
$Tb(C_5H_5)_3$	14.24	17.48	9.646

[a]All data are from single crystals. Systematic absences indicate the probable space group to be *Pbcm* or $Pca2_1$. There are eight molecules in the unit cell.

[1]Guest Scientist from Technische Hochschule, Munich, Germany.

[2]F. Baumgärtner, E. O. Fischer and P. Laubereau, *Radiochim. Acta* 7, 188 (1967).

[3]L. J. Nugent, P. Laubereau, G. K. Werner, and K. L. Vander Sluis (to be published).

PREPARATION OF BERKELIUM METAL

J. R. Peterson[1] J. A. Fahey[2]
R. D. Baybarz[3]

The first bulk samples of Bk metal have been prepared by the reduction of BkF_3 with Li metal according to the equation $BkF_3 + 3Li \rightarrow 3LiF + Bk$. The BkF_3 starting material was prepared by hydrofluorination of small samples of BkO_2 (ref. 4) which had been prepared by decomposition of Dowex 50-X4 ion exchange resin beads saturated with 7 to 8 μg of Bk.

The reduction apparatus (Fig. 2.9) consists of a tantalum crucible in which the BkF_3 sample is contained in a 1-mil tungsten-wire spiral. The reductant metal is contained in a small-diameter tantalum tube with crimped ends to minimize exposure to the atmosphere and is placed in the bottom of the crucible.

A typical reduction is carried out in vacuo by heating the crucible (by radiation from an induction shield surrounding the crucible) to ~1025°C for several minutes, followed by an annealing period of several minutes to several hours at 700 to 900°C.

All samples prepared to date have exhibited in their x-ray powder pattern a face-centered cubic phase whose lattice parameter is $a_0 = 4.99 \pm 0.01$ Å. Several samples have shown in addition a double-hexagonal close-packed phase whose lattice parameters are $a_0 = 3.41 \pm 0.01$ Å and $c_0 = 11.05 \pm 0.01$ Å. The error limits are conservative estimates reflecting the preliminary nature

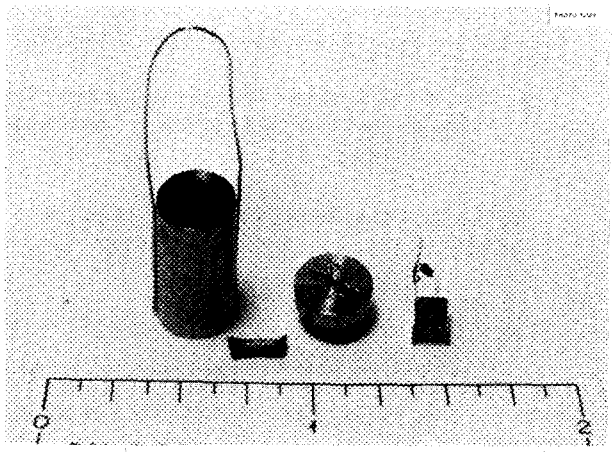

Fig. 2.9. Berkelium Metal Production Apparatus.

Fig. 2.10. Berkelium Metal Sample.

of the results. Present data indicate that the fcc phase is the high-temperature phase with respect to the dhcp phase. Future work will study the relationship between these two phases in greater detail.

A photograph of one of the Bk metal samples is presented in Fig. 2.10.

A recent attempt to prepare Bk metal at the Lawrence Radiation Laboratory (Berkeley) gave a product whose major phase was fcc with $a_0 = 4.99$,[5] in excellent agreement with our results. The apparent melting point of Bk, ~1000°C, indicates that its metallic properties are tending to be more like those of Ce than of its lanthanide analog Tb.

[1] Consultant; Chemistry Department, University of Tennessee, Knoxville.

[2] Graduate student, Chemistry Department, University of Tennessee, Knoxville.

[3] Chemical Technology Division.

[4] J. R. Peterson and B. B. Cunningham, *J. Inorg. Nucl. Chem.* 30, 1775 (1968).

[5] B. B. Cunningham, Lawrence Radiation Laboratory, University of California, Berkeley, Calif., private communication, 1969.

SZILARD-CHALMERS PROCESS USING METAL PHTHALOCYANINES FOR ISOTOPE ENRICHMENT

T. H. Handley[1] B. S. Weaver[2]
W. H. Baldwin

Some actinide isotopes have sufficiently low specific activities (e.g., ^{247}Cm, $t_{1/2} > 10^7$ years) that they can be safely used with a minimum radiation hazard. Such an isotope should be highly enriched and free of short-lived activities. The Szilard-Chalmers process has recently been used with metal-phthalocyanine complexes[3,4] having high thermal and chemical stability to prepare enriched nuclides.[5] Although the stability of these complexes varies greatly with the metal used, we have tested lanthanide phthalocyanines as likely models of the actinide compounds.

Yttrium, lanthanum, europium, and gadolinium phthalocyanines have been prepared by fusion of metal chloride with phthalonitrile and by reaction of the metal chloride and dilithium phthalocyanine in anhydrous media. Unfortunately, the products were too unstable to the extraction agents tested (1 *N* HCl or 5% ammonium citrate) to provide high enrichment factors.

[1] Analytical Chemistry Division.

[2] Chemical Technology Division.

[3] F. H. Moser and A. L. Thomas, *Phthalocyanine Compounds*, Reinhold, New York, 1963.

[4] A. B. P. Lever, *Advan. Inorg. Chem. Radiochem.* 7, 27 (1965).

[5] B. R. Payne, P. Scargill, and G. B. Cook, "Radioisotopes in Scientific Research," *Proceedings of International Conference, Paris, 1957*, vol. 2, p. 154, Macmillan, New York, 1958.

PREPARATION AND PROPERTIES OF SOME RARE-EARTH CHELATES

M. D. Danford C. E. Higgins
W. H. Baldwin

The continuing study of the chelates reported last year[1] has led to an improvement in yield from about 30% to 80% in the reaction

$$La^{3+} + 4Cs(hfa) \rightleftharpoons CsLa(hfa)_4 + 3Cs^+ ,$$

where hfa is the anion, hexafluoroacetylacetone ($CF_3COCHCOCF_3^-$).

Since such chelates are volatile, they have great potential importance in chemical separations, especially of the actinides; but because these elements are available only in limited quantities, their conversion to the chelate form must be quantitative. We have been investigating the effects of hfa^- anion concentration and of acidity on the yield and quality of such chelate products.

Chemical characterization of these chelates also has been undertaken, especially volumetric equivalent weight determinations. Two methods are being investigated: (1) $CsLa(hfa)_4$ in nonaqueous acetic acid forms one equivalent of strong base which can be neutralized with perchloric acid; (2) the acid H(hfa) is liberated

when Cs(hfa), $CsLa(hfa)_4$, or $La(hfa)_3$ in aqueous solution is passed through a strong cation exchange resin in the H^+ form, and can be titrated in the aqueous effluent from the column with standard sodium hydroxide. Other reactions of these chelates are being studied — for example, solvate formation and thermally induced reactions such as occur at the melting point.

[1] M. D. Danford and J. H. Burns, *Chem. Div. Ann. Progr. Rept. May 20, 1968*, ORNL-4306, p. 44.

GAS-JET SYSTEM FOR RAPID COLLECTION OF RECOIL NUCLEI

R. L. Hahn R. Gordin[1]
J. R. Tarrant R. H. Mayer[1]
A. Seidenfeld[1] P. J. Wood[1]

Construction of the gas-jet system previously described[2] has been completed. Energetic recoil nuclei, ejected from a target as a result of a nuclear reaction, are stopped in helium gas in a "high-pressure" chamber (~0.1 to 1 atm); the gas then carries the radioactive nuclides through a very small orifice into a "low-pressure" chamber (~0.2 to 0.5 torr) and deposits them on a foil for assay.

Consideration of the gas flow in the high-pressure chamber has suggested that the time required for efficient collection of the recoils might be markedly reduced. Experiments are under way to test several modifications to the system that are intended to achieve this goal. Recoil nuclei from radioactive decay are being used in these experiments: ^{249}Bk nuclei with recoil energies of 105 keV from the alpha decay of ^{253}Es, and fission fragments with final energies $\lesssim$10MeV (after passing through aluminum) from the spontaneous fission of ^{252}Cf. These energies, 105 keV and 10 MeV, are representative of the wide range of recoil energies that might be expected from actual bombardments at the ORIC.

[1] Oak Ridge Station, School of Chemical Engineering Practice, Massachusetts Institute of Technology.

[2] *Chem. Div. Ann. Progr. Rept. May 20, 1968*, ORNL-4306, p. 37.

TRANSURANIUM RESEARCH LABORATORY ISOTOPE SEPARATOR

L. D. Hunt C. E. Bemis, Jr.

The electromagnetic isotope separator outlined previously[1] was installed and tested at the Transuranium Research Laboratory during the period January–March 1969. The instrument is a one-stage mass analyzer consisting of a 90° homogeneous field sector magnet (field index $n = 1$) with a 150-cm radius.

The entrance and exit of the sector magnet have been shaped to allow collection of ions in a plane normal to the direction of ion beam travel. Ions of the element to be separated are produced by introducing a volatile form of the sample into a gas discharge plasma of the oscillating-electron type. The ions are extracted from the ion source via a potential drop of 10 to 30 kV and are accelerated to the desired energy (90 keV maximum for singly charged ions). The beam is formed and shaped electrostatically using a three-lens system with spherical focusing to adjust the radial divergence, and a lens system with cylindrical focusing to overcome the vertical divergence of the ion beam and to allow a variation of the focused beam height and position at the collector of the separator. The lens system, together with the entire separator, is shown schematically in Fig. 2.11.

The magnetically dispersed ion beams are allowed to impinge on collector foils for direct collection at the full ion energy, or they may be decelerated, refocused, and collected at incident ion energies in the range 1 to 5 keV for those cases in which sample thickness is important.

A periscope system attached to the lens box is used to optically align the ion source with respect to the lens system under operating conditions. Two ion beam scanners in the collection box are used to monitor the ion beam profile in both the horizontal and vertical directions and to aid the operator in adjusting the ion source and lens parameters for optimal separation. A photograph of the entire separator installation is shown in Fig. 2.12.

Initial performance tests on the separator have exceeded our expectations with regard to mass resolution and ion beam current capability. A mass resolution of 2800 ($m/\Delta m$) at full width half maximum height has been obtained for 80-keV Xe^+ ions at total ion currents on the collector of 80 μA. Research separations in the actinide mass region performed to date include the preparation of nanogram samples of 18-day ^{253}Cf at an enhancement factor of ~600 relative to ^{252}Cf. These samples of ^{253}Cf were used in a study of the levels of ^{249}Cm following alpha decay and in measurements of the (n,γ) cross section of ^{253}Cf. Attempts to prepare thin targets of actinide oxides for electron diffraction studies are under way.

[1] L. D. Hunt and C. E. Bemis, Jr., *Chem. Div. Ann. Progr. Rept. May 20, 1968*, ORNL-4306, p. 40.

ORNL-DWG. 69-6336

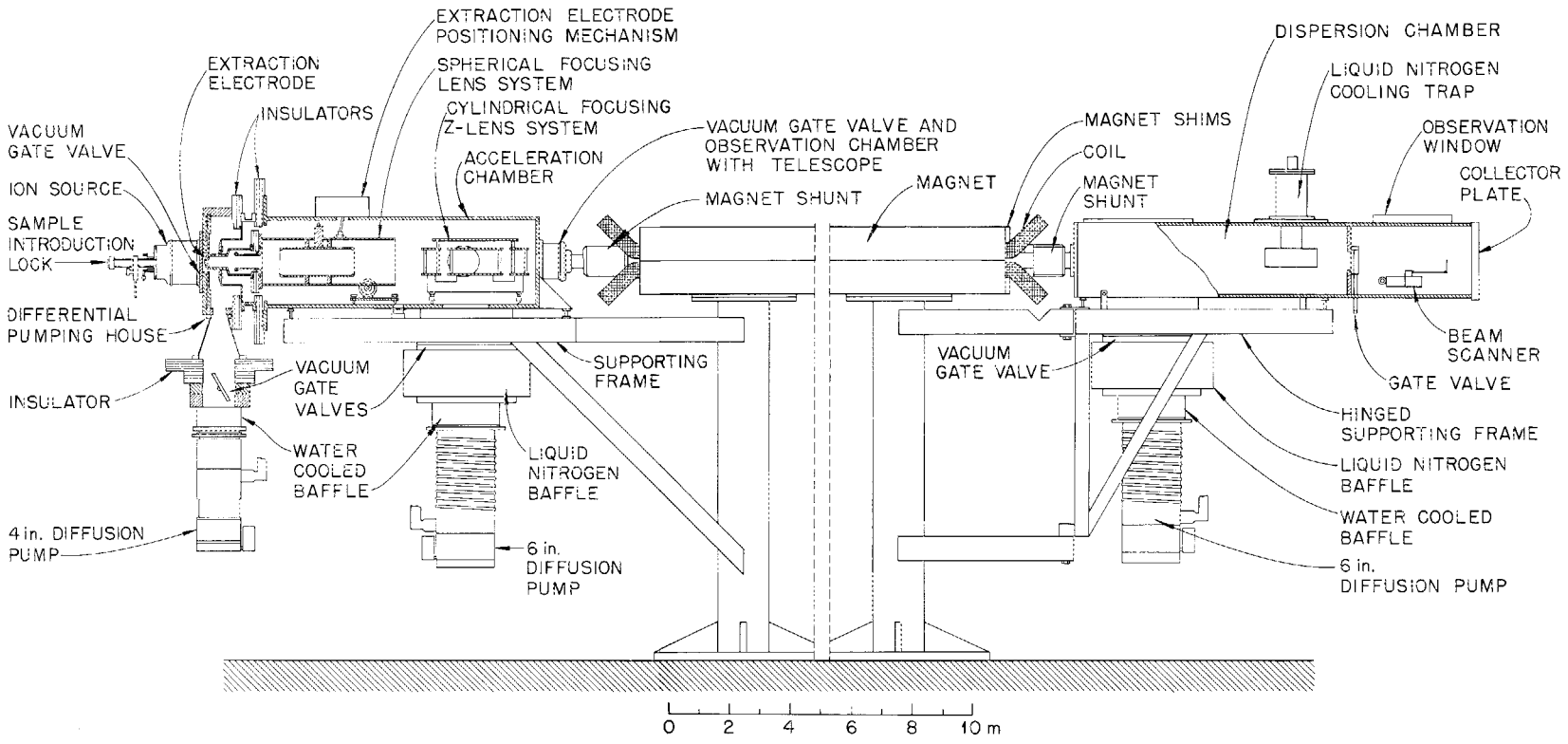

Fig. 2.11. Overall Schematic Drawing of the Isotope Separator Showing Ion Source, Lens System, Magnet, and Collection Region. The ion source end of the separator is enclosed in a glove box for alpha containment.

Fig. 2.12. Photograph of Entire Isotope Separator Installation.

3. Isotope Chemistry

FRACTIONATION OF CARBON ISOTOPES: THE COCO SYSTEM

A. A. Palko

Laboratory studies of the fractionation of carbon isotopes by the COCO process[1] were completed, and cost estimates based on bench-scale observations were made.

In the COCO process, carbon isotopes are fractionated by means of the following isotopic exchange reaction:

$$Cu_2Cl_2 \cdot 8NH_4Cl \cdot {}^{12}CO(l) + {}^{13}CO(g) = Cu_2Cl_2 \cdot 8NH_4Cl \cdot {}^{13}CO(l) + {}^{12}CO(g) \ . \quad (1)$$

Both process streams are readily refluxed by the addition or removal of heat alone:

$$Cu_2Cl_2 \cdot 8NH_4Cl \cdot CO(l) \xrightarrow{\text{heat}} Cu_2Cl_2 \cdot 8NH_4Cl(l) + CO(g) \ , \quad (2)$$

$$CO(g) + Cu_2Cl_2 \cdot 8NH_4Cl(l) \xrightarrow{\text{cool}} Cu_2Cl_2 \cdot 8NH_4Cl \cdot CO(l) \ . \quad (3)$$

All aspects of the system have been well characterized at the bench-scale level.

Our cost studies indicate that the COCO process should be capable of producing 90% pure ^{13}C in amounts of 10, 50, and 200 kg/year for \$29, \$7, and \$2 per gram respectively. The corresponding total plant investments are \$370,000, \$530,000, and \$1,020,000. We believe these costs are realistic; however, they are subject to the experimental confirmation of stage heights assumed for large-diameter exchange columns. Such studies are beyond the scope of the work of the Isotope Chemistry Group. On the basis of the costs cited above, we believe that the large-scale production of ^{13}C in medium and high purities may be accomplished at a lower unit cost by the COCO process than by any other method, except possibly the CYANEX process, described later, which is not yet fully developed.

[1] A. A. Palko, *Chem. Div. Ann. Progr. Rept. May 20, 1968*, ORNL-4306, pp. 48–50.

FRACTIONATION OF CARBON ISOTOPES: THE CYANEX SYSTEM

L. L. Brown A. A. Palko

Laboratory studies of the CYANEX process have been continued. This method of fractionating carbon isotopes is based on the exchange of carbon between an aqueous solution of CN^- and a methyl isobutyl ketone solution of methyl isobutyl cyanohydrin, as shown in reaction (1):

$$R_2C(OH)^{12}CN(org) + {}^{13}CN^-(aq) = R_2C(OH)^{13}CN(org) + {}^{12}CN^-(aq) \ , \quad (1)$$

where $R_2C(OH)CN(org)$ represents methyl isobutyl cyanohydrin dissolved in methyl isobutyl ketone. The single-stage isotopic fractionation factor for this reaction is 1.04 at 25°C.

The immediate objective of the work reported here was to demonstrate the feasibility of thermally refluxing the chemical species involved in reaction (1), that is, to determine the conditions under which reactions (2) and (3),

$$R_2C(OH)CN(org) + K_2CO_3(aq) \xrightarrow{\text{heat}} R_2CO(org) + KCN(aq) + KHCO_3(aq) \ , \quad (2)$$

$$R_2CO(org) + KCN(aq) + KHCO_3(aq) \xrightarrow{\text{cool}} R_2C(OH)CN(org) + K_2CO_3(aq) \ , \quad (3)$$

could be driven to completion by the addition or removal of heat.

The development of an effective contacting device became necessary for this liquid-liquid system. Packed columns, though very efficient for equilibrating gas with liquid and previously used in our studies of

chemical exchange systems, were so inefficient in equilibrating the two liquid phases of the CYANEX system that more effective contactors were required even to obtain laboratory data. Mixer-settlers were constructed and found satisfactory for applications requiring a few theoretical plates but proved too bulky for applications requiring many theoretical plates. Pulsed columns were designed, developed, and shown to be effective contactors for the product- and waste-end refluxers.

The waste-end reflux (reaction 3) was studied in a 1-in.-diam column 16 ft long as a function of mass flow rate, column length, temperature, and solution composition. When equal volumes of the aqueous and organic phases were equilibrated, the CN^- in a 1.0 *M* cyanide solution was transferred quantitatively into the organic phase at 25°C, provided the concentration of HCO_3^- was 35 to 45% greater than that indicated by reaction (3). When the organic to aqueous phase ratio was 2/3, a 1.0 *M* CN^- solution containing only 25% excess HCO_3^- was 99.1% refluxed.

The product-end reflux (reaction 2) was studied in a 1-in.-diam water-jacketed column 8 ft long. Reflux efficiencies of 100% were obtained for 1.0 *M* cyanohydrin solutions when contacted by equal volumes of aqueous solution containing 12 to 33% excess HCO_3^-, provided the reaction temperature was between 74 and 79°C. When the organic to aqueous phase ratio was 2/3, solutions of 1.5 *M* cyanohydrin were refluxed quantitatively at 76°C, with only 25% excess HCO_3^- present. Thus the feasibility of thermal refluxing is no longer doubtful; there remains only the determination of the most desirable operating parameters before an integrated system (product-end refluxer, exchange column, and waste-end refluxer) is demonstrated.

Meanwhile, preliminary cost estimates, based on a conceptual design and available laboratory data, indicate unit costs of \$32, \$8, and \$3 per gram for production rates of 10, 50, and 200 kg/year of 90% pure ^{13}C. Corresponding total plant investments are \$358,000, \$400,000, and \$550,000.

^{17}O FACILITY

D. Zucker

Last year's efforts to improve the heat transfer in the reboilers of column 2 were continued when cleaning and replacement of the reboilers did not provide satisfactory operation of the column. After several unsuccessful corrective measures were taken, the difficulty was discovered to be caused by an erroneous rotameter signal which caused the column to operate under essentially flooded conditions. Rotameter replacement corrected the immediate difficulty, but the isotopic gradient in the distillation cascade was upset by the excessive flow rates in column 2.

Connections were provided for operating the distillation cascade reboilers with building steam in emergencies. A pressure reducer in the steam line is kept set at the operating pressure so that when steam is valved in, the stills continue to function with no disturbance. Minor adjustments can be quickly made. The system works smoothly.

In the past, transfer of process gas between columns of the thermal diffusion cascade depended on thermal convection in two large-diameter tubes, one of which was heated. This design eliminated the need for a transfer pump and contributed to operational stability. However, as a result of this design, there was more holdup in the transfer system than in the thermal diffusion columns. In order to reduce this holdup, we have designed a very dependable positive-displacement pumping system which has only a small fraction of the holdup of the previous transfer system. The component parts of this system have been fabricated, and installation is in progress.

Several of the conditions described above interfered with the normal production of ^{17}O and ^{18}O. Nevertheless, substantial quantities of separated isotopes were prepared. Transfers to Isotope Sales included the following: 14.24 g of $H_2{}^{17}O$ (8% pure), 40.75 g of $H_2{}^{18}O$ (99% pure), 2.76 liters of $^{17}O_2$ (6 to 14% pure), and 5.93 liters of $^{18}O_2$ (99.9% pure). The aggregate value of the isotopic materials transferred during this report period exceeded \$33,300.

CHEMICAL FRACTIONATION OF URANIUM ISOTOPES

A. C. Rutenberg

The redetermination of the isotopic equilibrium constant for the reaction

$$^{238}UCl_4(aq) + {}^{235}U[C_6H_5N(NO)O]_4 = {}^{235}UCl_4(aq) + {}^{238}U[C_6H_5N(NO)O]_4 , \quad (1)$$

where $U[C_6H_5N(NO)O]_4$ represents the uranous cupferride complex dissolved in chloroform, has been completed. The batch equilibrations were performed in the following manner. A cold solution of 0.12 *M* UCl_4 in 1 *M* HCl was vigorously shaken with an equal volume of cold chloroform containing 2.4 moles of cupferron per mole of uranium in a container maintained near 4°C

with an ice bath. About one-half of the contained uranium was extracted into the organic phase. The phases were separated, and the uranium in each phase was recovered, purified, and reconverted to UCl_4. This material was then used to prepare the solution for the subsequent equilibration. The experimental conditions are given in Table 3.1.

Table 3.1. Experimental Conditions for Multistage Uranous Cupferride Batch Equilibrations[a]

Description of Equilibration	Volume of Each Phase (ml)	Contacting Time (min)	Percent of Uranium in Aqueous Phase After Equilibration
Initial	8500	90	59
Second organic	3950	45	51
Third organic	1400	30	51
Fourth organic	675	15	51
Second aqueous	5200	45	52
Third aqueous	2700	30	48
Fourth aqueous	1250	30	53
Fifth aqueous	660	15	54

[a]Both phases were 0.06 *M* in uranium. Aqueous phase was 1 *M* in HCl. At each equilibration, 2.4 moles of cupferron per mole of uranium was added.

The uranium used in the experiment contained 10.08% ^{235}U. This isotopic composition was chosen to obtain the maximum analytical precision from the mass spectrometers used in the isotope ratio determinations. Samples of U_3O_8 prepared from the initial material and from the fourth organic and fifth aqueous phases were analyzed by the ORGDP Mass Spectroscopy Laboratory. The U_3O_8 was converted to UF_6, and appropriate sample pairs were compared alternately using dual-collection techniques to give the ratio of the $^{235}U/^{238}U$ ratios directly. Two mass spectrometers and four analysts were used to minimize operator and machine bias.

The isotopic exchange represented by Eq. (1) concentrated ^{235}U in the aqueous phase. The ratio of $^{235}U/^{238}U$ between the fifth aqueous phase and the fourth organic phase was 1.00034 ± 0.00008 (95% confidence interval). A comparison of these same samples with the starting material gave a separation of 1.00027 ± 0.00004 (95% confidence interval). The single-stage fractionation factor, α, computed from these values was 1.00007 ± 0.00001. This separation factor is very close to the 1.00006 value measured[1] for the isotopic fractionation between an aqueous solution of UO_2^{2+} complexed with ethylenediaminetetraacetate ion and UO_2^{2+} on Dowex 50 ion exchange resin. The small values of the isotopic equilibrium constants measured for these uranium systems, in which the uranium atoms are bonded primarily to oxygen, indicate that the chemical exchange method of isotope separation is not practical for the enrichment of the isotopes of uranium.

[1]A. C. Rutenberg, *Chemical Separation of Isotopes Section Semiann. Progr. Rept. Dec. 31, 1954*, ORNL-1874, p. 23.

MASS SPECTROMETRIC DETERMINATION OF SMALL DIFFERENCES IN DEUTERIUM CONCENTRATION IN WATER SAMPLES

D. A. Lee L. Landau

In connection with other work, we found it necessary to make precise measurements of small changes in the hydrogen-deuterium ratios of certain water samples. This task is very difficult for several reasons. Unlike other isotopes, which are very similar to each other in mass, D is twice as heavy as H. Trajectories of ions through the mass spectrometer and associated effects are therefore much different for H and D. H_2^+ ions react with hydrogen gas to yield H_3^+ ions, which are indistinguishable from HD^+ ions in a low-resolution mass spectrometer. This reaction is pressure dependent; the fraction of H_3^+ formed increases as the pressure increases. Water adsorbed on the walls of glassware and other container materials is an ever-present source of exchangeable hydrogen. This and the adsorption of hydrogen on metals create memory problems both in the preparation of samples and in analysis.

Samples for mass analyses were prepared by the reduction of water to hydrogen in the apparatus shown in Fig. 3.1. Seven-milligram water samples were injected through a septum into the sample inlet section of the apparatus. After deaeration the sample was reduced by recycling it over heated metal for about 20 min. The resulting hydrogen was pumped into a glass break-seal bulb and sealed.

Several metals were used as the reductant for H_2O; their purity was found to be important. Baker Analyzed 10-mesh zinc was the most convenient to use, its chief disadvantage being that it had to be heated almost to its melting point for efficient reduction. This required uniform heating to prevent localized melting and possible restriction of gas flow. Magnesium metal,[1] which has a higher melting point than zinc, reduced water very well at 500°C, but the hydrogen produced

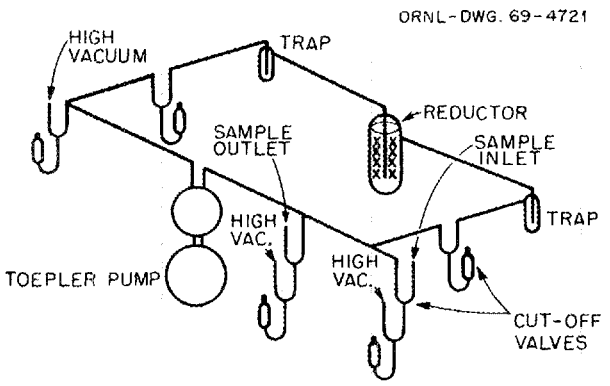

Fig. 3.1. Water Reduction Apparatus.

contained methane and higher-mass hydrocarbons which caused erratic deuterium analyses. Methane undoubtedly came from the reaction of water with carbon impurities in the magnesium, but cleaning the surface of the magnesium did not eliminate the hydrocarbon contamination. Uranium[2] metal reduced water quantitatively at 550° and had the advantage of removing any nitrogen which may have been in the system. Efficiency undoubtedly would have been better at a higher temperature, but this would have required a quartz vessel. Tamiya[3] suggested the use of platinized zinc; however, we found that this gave no advantage over untreated zinc. In fact, the surface of platinized zinc became inactive more quickly than that of the untreated metal. Since 10-mesh unplatinized zinc gave good results, it was preferred.

Since our prime concern was the determination of isotopic separation factors between pairs of samples, we did not try to measure absolute ratios. By using standard reference samples, by maintaining source conditions as similar as possible, and by normalizing all values to a standard pressure by use of a plot relating the rate of change of mass 3 to mass 2 with pressure, acceptable ratio measurements were obtained. Table 3.2 shows an analysis of samples differing from each other in D/H ratio by 1.005. Each number in the table is an average of four to six individual measurements. The samples were separately sealed tubes of hydrogen from one uranium reduction of water fortified in deuterium 1.010 times normal (B samples) and one reduction of water fortified 1.005 times (A samples). It is our aim to improve the procedure so that it will not be necessary to make so many measurements to obtain one ratio.

The analysis of water itself or the conversion of water to phosphine, arsine, ammonia, or methane, and subsequent analysis, did not appear promising.

[1] J. W. Knowlton and F. D. Rossini, *J. Res. Natl. Bur. Std.* **19**, 605 (1937).

[2] A. S. Newton, U.S. Pat. 2,533,138, Dec. 5, 1950; J. Bigeleisen, M. L. Perlman, and H. C. Prosser, *Anal. Chem.* **24**, 1356 (1952).

[3] N. Tamiya, *Anal. Chem.* **32**, 724 (1960).

Table 3.2. Replicate Determinations of D/H Ratios in Water Samples Where (D/H)B ÷ (D/H)A = 1.005

Samples A have a D/H ratio 1.005 times normal, samples B have a D/H ratio 1.010 times normal

Sample	Peak Height at $m/e = 2$ (V)	Peak Height at $m/e = 3$ (V)	$\frac{m/e = 3}{m/e = 2}$ for $m/e = 2$ Set at 75.00
B	75.307	1.1243	0.01491
B	75.503	1.1420	0.01509
A	75.458	1.1366	0.01503
A	75.274	1.1297	0.01499
B′	75.082	1.1414	0.01520
B′	75.220	1.1373	0.01511
A′	75.199	1.1206	0.01489
A′	75.358	1.1211	0.01485
B″	75.289	1.1399	0.01512
B″	75.479	1.1398	0.01507
Average for A samples			0.01494 ± 0.0001 (95% C.I.)
Average for B samples			0.01508 ± 0.0001 (95% C.I.)
Average for B/average for A			1.009

ISOTOPIC MASS SPECTROMETRY

L. Landau

Isotopic analyses of more than 1200 samples of CO, CO_2, O_2, and H_2 were carried out during this report period.

Pairs of CO samples from multistage mixer-settler experiments in the COCO process were analyzed as ratios to determine the extent of ^{13}C enrichment. Carbon dioxide from the oxidation of AgCN in single-stage experiments in the CYANEX system was analyzed for ^{13}C enrichment by the dual-collection ratio method. Samples of CO_2 and of O_2 were analyzed mass spectrometrically at regular intervals to monitor the progress of the Water Distillation Plant and the Thermal Diffusion Plant for the enrichment of ^{17}O and ^{18}O.

Many O_2 samples enriched to more than 99% in ^{18}O were reclaimed by reacting them with hot copper turnings in an evacuated flask. When a sufficient number of samples had been processed, the ^{18}O was recovered by reheating the copper in a stream of H_2

and freezing the resulting $H_2{}^{18}O$ in a trap cooled with liquid nitrogen.

Many H_2 samples were analyzed during the development of a procedure for determining small variations of D in H_2O samples.

MOLECULAR SPECTROSCOPY

G. M. Begun L. C. Brown
R. N. Compton[1]

We have employed infrared, Raman, and mass spectrometric techniques to observe the properties of molecular species which may be of potential use in isotope separation systems and to obtain fundamental information about new or especially interesting molecules.

The recent discovery[2] that XeF_2 oxidizes aqueous BrO_3^- to BrO_4^- prompted us to prepare an appreciable quantity of the previously unknown perbromate ion. We have investigated the infrared and Raman spectra of several perbromate salts. Figure 3.2 shows the Raman spectra of a 0.1 *M* solution of $RbBrO_4$ and of crystalline $RbBrO_4$. The spectra were excited with a continuous-wave helium-neon gas laser emitting approximately 65 mW of radiation at 6328 Å.

Figures 3.3 and 3.4 show the infrared spectra of pressed KBr pellets containing BrO_4^- ions. The spectra show the characteristic tetrahedral-ion pattern analogous to ClO_4^- and IO_4^-. Four Raman bands are seen,

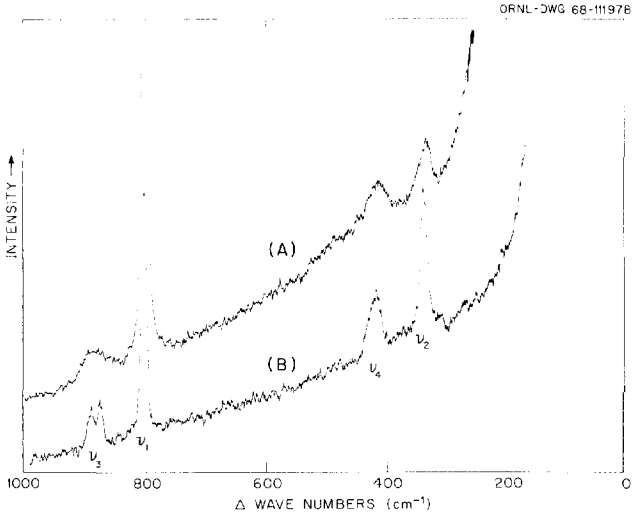

Fig. 3.2. Raman Spectra of Perbromate Ion. (*a*) 0.1 *M* $RbBrO_4$–0.6 *M* HBr aqueous solution; (*b*) crystalline $RbBrO_4$. 6328-Å He-Ne laser excitation.

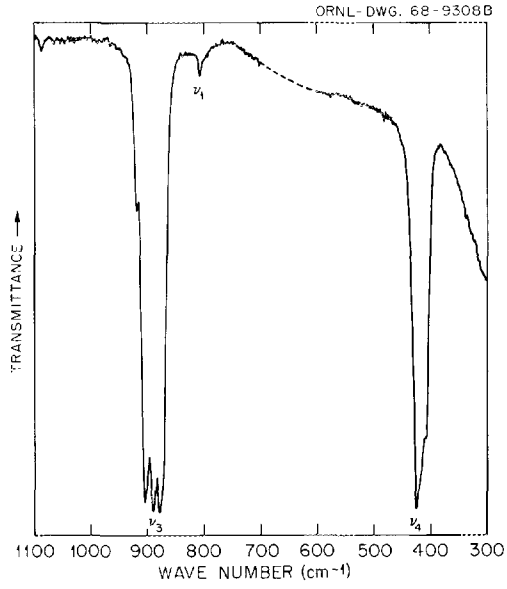

Fig. 3.3. Infrared Spectrum of Solid $RbBrO_4$. KBr pellet.

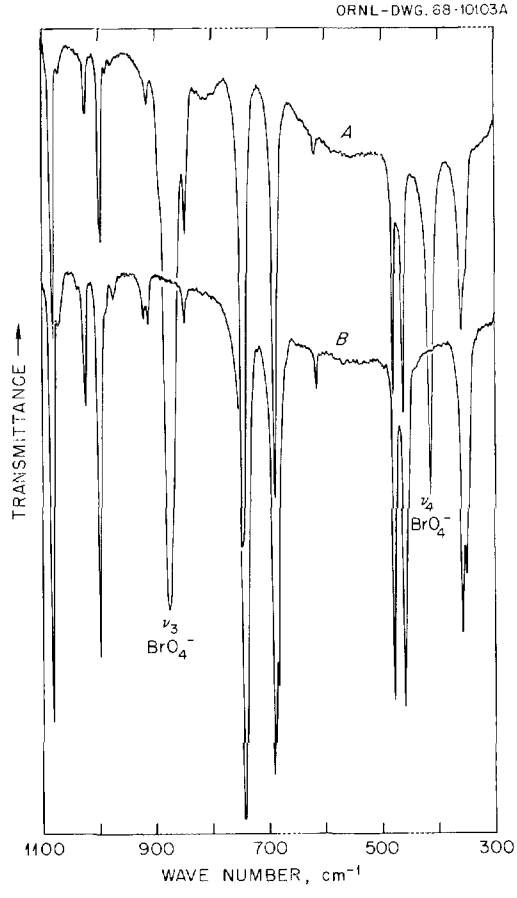

Fig. 3.4. Infrared Spectrum of (*A*) Solid $(C_6H_5)_4AsBrO_4$ and (*B*) Solid $(C_6H_5)_4AsI$. KBr pellets.

Table 3.3. Vibrational Frequencies of BrO_4^- (cm^{-1})

R = Raman, IR = infrared, P = polarized, aq = aqueous

Compound	ν_1 (A_1)	ν_2 (E)	ν_3 (F_2)	ν_4 (F_2)
$RbBrO_4$	802 R	335 R	872, 890 R 879, 890, 904 IR	415 R 410, 420, 426 IR
$RbBrO_4$(aq)	801 R, P	331 R	874 R	410 R
ϕ_4AsBrO_4[a]	799 R		878 IR	410 IR

[a]The ν_3 and ν_4 bands of ϕ_4AsBrO_4 showed no splitting, indicating little or no perturbation of T_d symmetry of the BrO_4^- in this compound.

two of which coincide with the two observed infrared absorptions. The observed frequencies and their assignments, made by analogy with ClO_4^- and IO_4^-, are listed in Table 3.3. The Raman polarization measurements in aqueous solution showed the ν_1 vibration to be very strongly polarized and the other lines to be highly depolarized. The splitting of the ν_3 and ν_4 degenerate frequencies of crystalline $RbBrO_4$ observed in the infrared and partially in the Raman spectra is due to a lowering of the T_d symmetry of the BrO_4^- ion in the crystal site.

Using the symmetry coordinates of Meister and Cleveland[3] and the Wilson F and G matrix method,[4] we calculated valence force constants for ClO_4^-, BrO_4^-, and IO_4^-. These valence force constants (Table 3.4) reproduce the observed frequencies closely. The nonzero force constants used were: f_d, stretching; f_α, bending; $f_{\alpha\alpha'}$, bend-bend interaction between opposite angles; $f_{d\alpha}$ and $f_{d\alpha'}$, stretch-bend interactions. The force constants clearly illustrate the close similarity in bonding between the BrO_4^- and the IO_4^- ions and the considerable decrease in interactions as the central atom increases in size and the oxygens become less crowded.

Xenon hexafluoride was first prepared in 1963. Since that time the compound has been the subject of numerous experimental studies as well as considerable theoretical speculation. Despite this concentration of activity, several aspects of the gaseous XeF_6 molecule are still puzzling. Mass spectral studies of the positive ions produced by electron impact[5] showed the ions XeF_6^+, XeF_5^+, XeF_4^+, XeF_3^+, XeF_2^+, XeF^+, and Xe^+, with the XeF_6^+ ion being very weak. We felt that the negative-ion spectrum and the threshold electron impact excitation spectrum of XeF_6 might give information about dissociation of the molecule and about its electronic energy levels. Since the optical selection rules do not hold for low-energy electron impact excitation, it is possible to observe states in the electron impact spectrum which are optically forbidden.

A Bendix model 14-206 time-of-flight mass spectrometer equipped with a glass-strip electron multiplier was used in these studies. The relative negative-ion yields as a function of energy were recorded using the full energy width of the electron beam (width at half-height, ~0.5 eV). In order to obtain the electron impact threshold excitation spectra of XeF_6, the SF_6 scavenger technique[6] was employed to monitor low-energy electrons

Table 3.4. Valence Force Constants for ClO_4^-, BrO_4^-, and IO_4^- Ions

In millidynes per angstrom

Ion	f_d	f_α/d^2	$f_{\alpha\alpha'}/d^2$	$(f_{d\alpha} - f_{d\alpha'})/d$
ClO_4^-	8.24	0.87	−0.21	0.78
BrO_4^-	6.05	0.46	−0.12	0.39
IO_4^-	5.90	0.30	−0.09	0.07

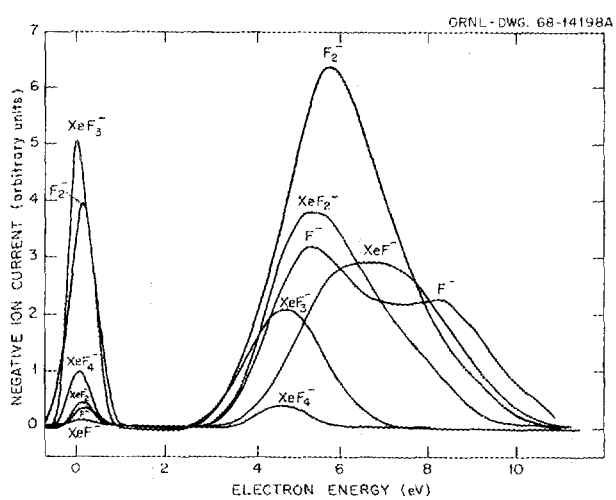

Fig. 3.5. Negative-Ion Current vs Electron Energy for Various Ions in XeF_6.

by the formation of SF_6^- ions in the mass spectrometer ion source.

A scan of the negative-ion mass spectrum of XeF_6 revealed the following ions: XeF^-, XeF_2^-, XeF_3^-, XeF_4^-, F_2^-, and F^-. Figure 3.5 shows the relative abundances of these ions as a function of the energy of the ionizing electrons. At electron energies close to zero, the XeF_3^- ion was the most intense. In the neighborhood of 6 eV excitation energy the F_2^- ion was the most intense, with the XeF_2^- ion next. In the negative-ion cracking pattern of XeF_6 the most abundant ion was F_2^-, indicating that the most probable decomposition products of XeF_6^- were XeF_4 and F_2^-. This conclusion was also indicated by the failure to observe XeF_6^- or XeF_5^- ions. The considerable number of XeF_3^- ions could be produced by the decomposition of XeF_6^- with the formation of F_2 and F simultaneously. We conclude that XeF_6^- and XeF_5^- ions are extremely unstable.

Figure 3.6 shows the threshold excitation spectra of XeF_6 as determined by the SF_6^- difference ion current. For atoms and simple molecules, the threshold electron impact excitation spectrum is often comparable with the ultraviolet spectrum, with the exception that optically forbidden transitions may be seen in the electron impact spectra. Our electron impact data show excitations at 6.0, 7.8, 9.2, and 10.5 eV for XeF_6. Ultraviolet absorption measurements on XeF_6 by J. P. Young and E. T. Arakawa of this Laboratory show the following features: a definite absorption maximum, comparatively weak, at 3.68 eV; a shoulder at 4.9 eV; and broad peaks riding on a high, continuously increasing absorption at approximately 5.5–5.8, 6.9, and 8.8 eV. Absorption continued to increase above 9.5 eV.

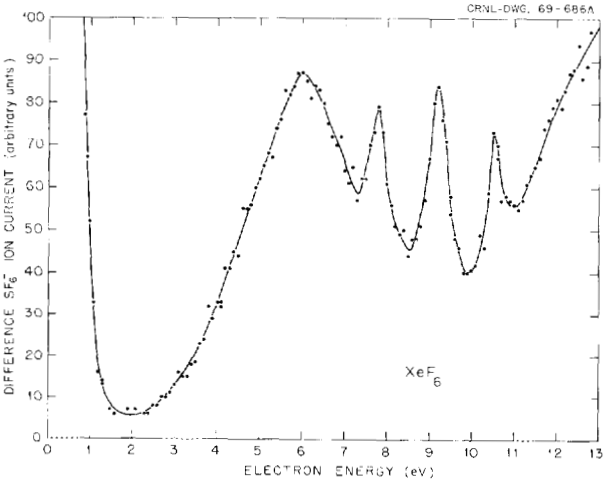

Fig. 3.6. Electron Impact Threshold Excitation Spectrum of XeF_6.

The differences between the electron data and the ultraviolet spectra are not surprising. The ultraviolet spectra are broad and poorly resolved, and in the case of XeF_6 the peaks are superimposed on an intense, continuously increasing absorption. In addition, in electron impact work at low electron energies, the probability of electric quadrupole and singlet-triplet transitions is greatly increased. Because of the many uncertainties involved, we have not proposed assignments of the observed peaks in the electron impact spectrum to definite energy level transitions. While there has been some speculation concerning possible low-lying electronic energy states in XeF_6, we were unable to observe any such states in the region 1 to 3 eV. It seems that the electron impact peaks observed at 6.0 eV and higher must be assigned to transitions to excited levels involving Xe *d*-orbital energy levels unless the overlap of the various energy level groups is greater than that expected. In Fig. 3.6 the rapid rise of the curve around 12 eV may be due to the onset of ionization in the parent molecule. This indicates that the ionization potential for XeF_6 is about 12 eV.

---

[1] Health Physics Division.

[2] E. H. Appelman, *J. Am. Chem. Soc.* 90, 1900 (1968).

[3] A. G. Meister and F. F. Cleveland, *Am. J. Phys.* 14, 13 (1946).

[4] E. B. Wilson, Jr., J. C. Decius, and P. C. Cross, *Molecular Vibrations*, pp. 61 ff., McGraw-Hill, New York, 1955.

[5] M. H. Studier and E. N. Sloth, *Noble-Gas Compounds* (ed. by H. H. Hyman), p. 47, University of Chicago Press, Chicago, Ill., 1963.

[6] R. N. Compton, *et al.*, *J. Chem. Phys.* 48, 901 (1968).

SPECTRAL STUDIES OF MoF_5

A. C. Rutenberg

A study of Raman and infrared spectra of MoF_5 is in progress as a continuation of our program to observe and interpret the vibrational spectra of metal and halogen fluorides. MoF_5 is a yellow solid which melts at 67°C to a viscous liquid which can be supercooled to room temperature. The compound was prepared by treating MoF_6 with powdered Mo metal in an evacuated quartz vessel.

We obtained Raman spectra of the solid with a modified Cary model 81 Raman spectrometer, using the 6328-Å line of a helium-neon laser for excitation. Nine lines were observed. Their locations and relative heights are given in Table 3.5. This is the number of Raman-

Table 3.5. Raman Spectrum of Solid MoF_5

Observed Bands (cm^{-1})	Relative Intensity
192	4
240	7
250	4
287	<1
402	1
696	4
704	3
737	10
759	9

active fundamental frequencies expected for a tetragonal pyramid structure. Such a configuration may be considered the basic unit of the tetrameric structure proposed for solid MoF_5 on the basis of a single-crystal x-ray study.[1] A spectrum was also obtained for liquid MoF_5. Four lines were observed, and there were indications of one or two more peaks. Two of the lines were polarized. The spectrum of the liquid is definitely different from that of the solid. This may be due to ionization of the liquid into MoF_4^+ and MoF_6^-. Salts of these ions are being prepared for comparison.

Attempts were also made to obtain infrared spectra of MoF_5 gas, of MoF_5 as a thick solid film on AgCl windows, and of mineral oil mulls of MoF_5, using AgCl or polyethylene windows and AgCl pellets. Although the cells were loaded in a dry box, all the spectra showed the presence of decomposition products of MoF_5. A major contaminant was $MoOF_4$. Because of the proximity of the impurity peaks to the expected MoF_5 peaks, more elaborate precautions will be necessary to obtain good infrared spectra.

[1] A. J. Edwards, R. O. Peacock, and R. W. H. Small, *J. Chem. Soc.*, p. 4486 (1962).

4. Radiation Chemistry

PULSE RADIOLYSIS OF NO: PRODUCTION OF NO_2 AND N_2O_3 AND THE PRODUCTION AND RELAXATION OF VIBRATIONALLY EXCITED NO[1]

C. J. Hochanadel J. A. Ghormley P. J. Ogren[2]

Nitric oxide is one of the simplest molecules with an unpaired electron and is often used as a scavenger of free radicals in studies of radiation chemistry, photochemistry, and thermal chemical kinetics. Its reactions are of great interest, not only in chemical kinetics, but also in reactor technology, the chemistry of air pollution, upper-atmosphere chemistry, etc.

We studied the pulse radiolysis of pure NO and mixtures of NO with Ar at a total pressure of 1 atm, using 30-nsec pulses of 2-MV electrons. We observed absorptions due to NO_2, N_2O_3, and vibrationally excited NO in the (0,1) and (0,2) gamma bands. In pure NO at 1 atm, most of the NO_2 forms during the pulse, but the formation of N_2O_3 is slower, as shown by the oscilloscope traces in Fig. 4.1. Nitrogen dioxide is produced by the reaction of O atoms with NO, and the pseudo first-order rate constant for formation of NO_2 in an 11% NO-Ar mixture is slightly lower than that calculated from published values.[3] The N_2O_3 comes from the equilibrium $NO_2 + NO \rightleftharpoons N_2O_3$, which is achieved in <1 μsec, orders of magnitude faster than the previously estimated lower limit.[3] The sum of yields of the two products (10.6 ± 0.5 molecules/100 eV) was independent of the pulse dose, but the ratio $G(NO_2)/G(N_2O_3)$ increased with dose. This can be explained by a shift in the above equilibrium caused by the temperature increase produced by the pulse. Superimposed on the broad N_2O_3 band in the ultraviolet were sharp bands at 2362 and 2472 Å, indicating population of the first and second vibrational levels of NO. The formation and relaxation of these levels are shown by the oscilloscope traces in Fig. 4.2. The relaxation lifetime of the first vibrational level was 5.8 μsec for 13% NO in Ar and 1.6 μsec for 41% NO, giving a quenching probability by NO of $(2.1 \pm 0.2) \times 10^{-4}$, compared with $(3.6 \pm 0.4) \times 10^{-4}$ reported by Basco, Callear, and Norrish.[4] The absorption in the (0,2) band at 2472 Å decayed with a lifetime of ~1.4 μsec for 13% NO in Ar, giving a probability for resonant vibration-vibration exchange of only $\sim 10^{-3}$.

ORNL-DWG. 68-11969

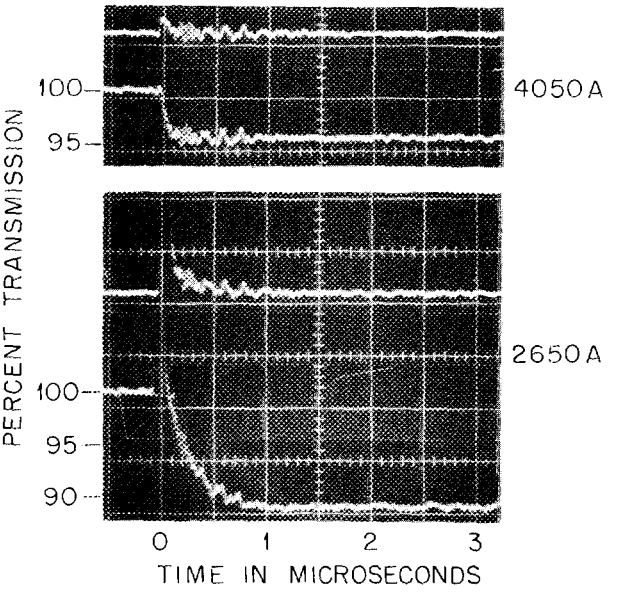

Fig. 4.1. Oscilloscope Traces Showing the Formation of NO_2 (4050 Å) and N_2O_3 (2650 Å) in the Pulse Radiolysis of Pure NO at 1 atm and 25°C.

---

[1] Summary of paper published in *J. Chem. Phys.* **50**, 3075 (1969).

[2] Oak Ridge Associated Universities Research Participant, summer 1968, from Maryville College, Maryville, Tenn.

[3] For a review, see J. Heicklen and N. Cohen, *Advan. Photochem.* **5**, 157–328 (1968).

[4] N. Basco, A. B. Callear, and R. G. W. Norrish, *Proc. Roy. Soc. (London)* **A260**, 459 (1960).

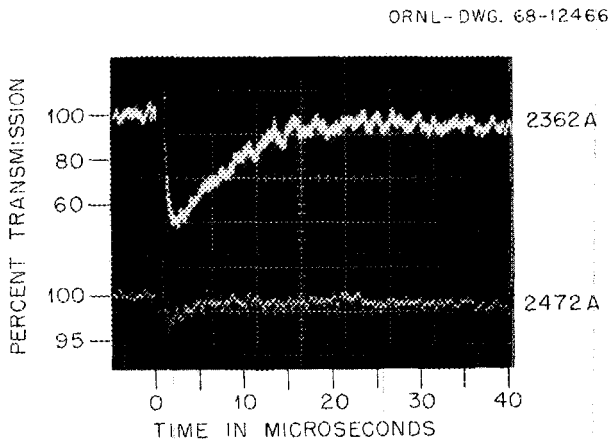

Fig. 4.2. Formation and Decay of Vibrationally Excited NO on Pulsing 13% NO in Argon at a Total Pressure of 755 Torrs at 25°C. The absorptions at 2362 and 2472 Å are the (0,1) and (0,2) bands of the γ system.

USE OF CO TO DETECT $O(^1D)$ IN THE PULSE RADIOLYSIS OF O_2

C. J. Hochanadel J. A. Ghormley
J. W. Boyle P. J. Ogren[1]

In the radiolysis of O_2, excited O atoms, $O(^1D)$ and $O(^1S)$, as well as ground-state atoms, $O(^3P)$, are all possible intermediates. We looked for $O(^1D)$ using CO as a scavenger in the pulse radiolysis of O_2 and O_2-Ar mixtures. The CO reacts rapidly with $O(^1D)$ to form CO_2 and should compete with physical deactivation of $O(^1D)$ by O_2 or Ar, followed by reaction of the $O(^3P)$ with O_2 to form O_3, or with the slower reaction of $O(^1D)$ with O_2 to form O_3 directly.[2] We found little or no effect of CO on the yield of O_3, indicating that $O(^1D)$ atoms are not present.

[1] Oak Ridge Associated Universities Research Participant, summer 1968, from Maryville College, Maryville, Tenn.

[2] M. Clerc and A. Reiffsteck, *J. Chem. Phys.* 48, 2799 (1968).

FLASH PHOTOLYSIS OF WATER AND OXYGEN-SATURATED WATER

J. W. Boyle J. A. Ghormley C. J. Hochanadel

We had previously reported[1] the formation of e^-_{aq} in the flash photolysis of pure water with light above 1600 Å and, by using filters to measure the cutoff, estimated the "ionization potential" of liquid water to be $\leqslant$6.5 eV. In addition to absorption by electrons in the visible, we had also observed absorption in the ultraviolet which started at ~4000 Å and increased with decreasing wavelength down to the limit of our measurements at 1950 Å. We originally attributed this spectrum to the OH radical, although below 2300 Å it did not agree with the spectrum of OH which we obtained by the flash photolysis of H_2O_2 solutions.[2] The answer to this discrepancy was provided by recent results of Nielsen *et al.*,[3] who identified the spectrum of H atoms in the pulse radiolysis of aqueous solutions. We confirmed the absorption by H atoms by comparing the absorptions produced in the flash photolysis of He-purged water and H_2-saturated water. As H_2 converts OH to H, the absorption shifts to shorter wavelengths, and the two species have equal extinction coefficients at ~2100 Å. Our absorption spectrum for H atoms agrees with that of Nielsen *et al.*; absorption starts at ~2400 Å and increases rapidly toward shorter wavelengths.

The effect of oxygen is very important both in the radiolysis of aqueous solutions and in radiobiology. In aqueous solutions the effect has been attributed to scavenging of intermediates such as e^-_{aq} and H. Water saturated with O_2 has an absorption spectrum which extends to much longer wavelengths than that of pure water. We studied the photochemistry of this system by flash photolysis at wavelengths not absorbed by water, expecting O_2^- and OH (via H_2O^+) to be produced initially by a charge-transfer process. We observed an absorption produced during the flash, part of which decayed in about 0.01 sec, leaving a long-lived product with the spectrum of ozone (Fig. 4.3). To obtain the

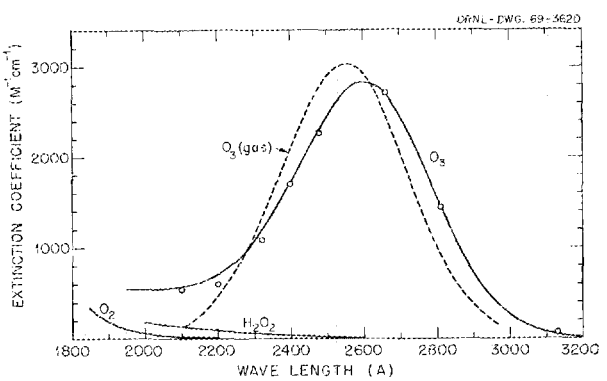

Fig. 4.3. Comparison of the Absorption Spectrum of the Long-Lived Product in the Flash Photolysis of O_2-Saturated Water, ○, with the Absorption Spectrum of O_3 in Water (Solid Curve). The dashed curve is the spectrum of O_3 in the gas phase taken from E. C. Y. Inn and Y. Tanaka, *J. Opt. Soc. Am.* 43, 870 (1953). The lower curves are the spectra of H_2O_2 and O_2 solutions.

spectrum of O_3 in water for comparison, we prepared O_3 by a microwave discharge in pure O_2, dissolved the O_3 in pure water, and measured the spectrum on a model 15 Cary spectrophotometer. The extinction coefficient at the peak (2600 Å) was 2830 M^{-1} cm^{-1}, in good agreement with the value of Kilpatrick *et al.*[4] (2900 M^{-1} cm^{-1}), but lower than Taube's[5] value of 3600 M^{-1} cm^{-1}. In addition to the characteristic absorption, similar to the spectrum in the gas phase or in other media, there is absorption at shorter wavelengths which suggests an electron transfer spectrum similar to O_2 in water.

The formation of O_3 is not consistent with a mechanism in which O_2^- and OH are produced initially, followed by the reactions usually proposed between like and unlike radicals to give H_2O_2 and O_2 as stable products. We propose HO_3 as an intermediate (O atoms, excited O_2 molecules, and H_2O_3 are also possible intermediates), but have not been able to demonstrate directly the reaction of OH with O_2 in neutral solution, either by flash photolysis of solutions of O_2 or H_2O_2 + O_2, or by pulse radiolysis of O_2 solutions. It is well known that the basic form of OH (O^-) reacts rapidly with O_2 to give O_3^-. We did not observe O_3 formation either in the flash photolysis of H_2O_2 + O_2 solutions or in the pulse radiolysis of O_2 solutions, indicating that, with H_2O_2 present, either O_3 is not formed or it reacts rapidly with H_2O_2.

We are investigating further the reactions occurring in the flash photolysis of oxygen solutions and the possible role of ozone in the photolysis and radiolysis of aqueous solutions containing oxygen.

---

[1] *Chem. Div. Ann. Progr. Rept. May 20, 1967,* ORNL-4164, p. 35.

[2] *Chem. Div. Ann. Progr. Rept. May 20, 1966,* ORNL-3994, p. 40.

[3] S. O. Nielsen *et al., Chem. Commun.* **23,** 1523 (1968).

[4] M. L. Kilpatrick, C. C. Herrick, and M. Kilpatrick, *J. Am. Chem. Soc.* **78,** 1784 (1956).

[5] H. Taube, *Trans. Faraday Soc.* **53,** 656 (1957).

FLASH PHOTOLYSIS OF ICE

J. A. Ghormley C. J. Hochanadel

We had previously[1] observed the formation of hydrated electrons in the flash photolysis of pure water at 24°C with photons having energy ≥6.5 eV (1920 Å). The overall reaction

$$2H_2O_{aq} \rightarrow e^-_{aq} + OH_{aq} + H_3O^+_{aq}$$

is endothermic by about 5.8 eV. In order that the hydration energy be available in time, it is likely that the electron must be stabilized in preexisting traps (configuration of suitably oriented water dipoles). It was of interest therefore to examine the possible formation of trapped electrons by the flash photolysis of pure ice. Trapped electrons had been observed by others[2] in the pulse radiolysis of ice at temperatures in the range −10 to −196°C.

The long-wavelength cutoff of ice relative to liquid water is shown in Fig. 4.4. The spectra were measured using a model 15 Cary spectrophotometer purged with nitrogen. On flashing pure ice at −10°C with light above 1600 Å, we observed no absorption by trapped electrons, indicating that suitable traps are not available in ice to allow their formation by photons of this energy. We did observe an absorption spectrum in the ultraviolet (Fig. 4.5) that was produced during the flash. The initial spectrum is very similar to that observed in the flash photolysis of water and is attributed to H and hydrogen-bonded OH radicals. The spectrum of the long-lived component shown in Fig. 4.5 is similar to the OH spectrum in water. The simplest explanation of these results is that the H atoms disappear by reacting with themselves and with part of the OH radicals, leaving the remaining OH radicals to react slowly with H_2 molecules, which are expected to be much more mobile than hydrogen-bonded OH radicals.

---

[1] J. A. Ghormley, C. J. Hochanadel, and J. W. Boyle, *Chem. Div. Ann. Progr. Rept. May 20, 1967,* ORNL-4164, p. 35; *J. Phys. Chem.* in press (1969).

[2] I. A. Taub and K. Eiben, *J. Chem. Phys.* **49,** 2499 (1968).

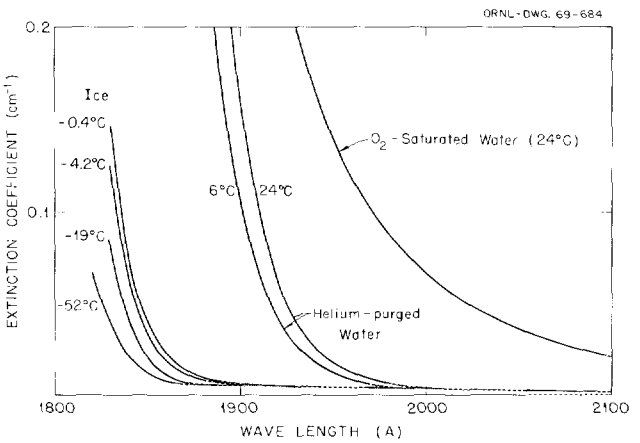

Fig. 4.4. Absorption Spectrum of Ice at Several Temperatures Compared with the Spectrum of Liquid Water. The absorption spectrum of oxygen-saturated water (1.24 × 10^{-3} M) is shown also.

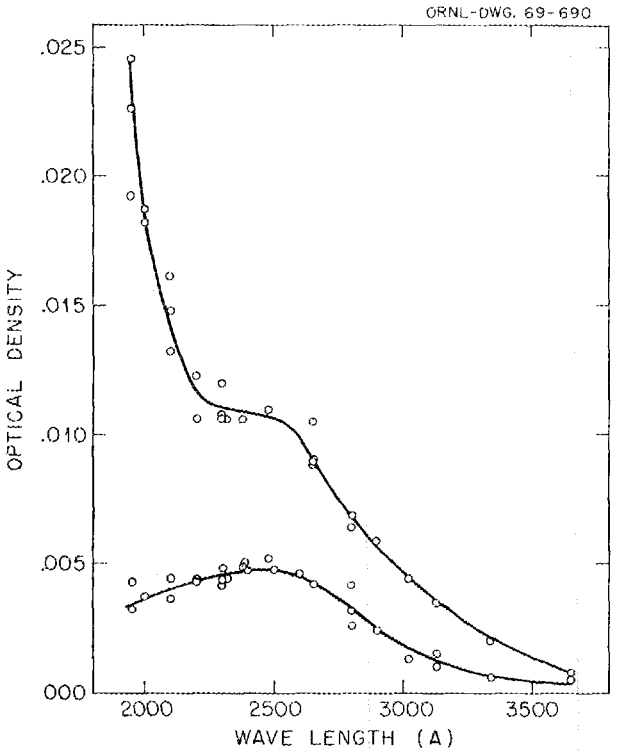

Fig. 4.5. Absorption Spectrum Produced by the Flash Photolysis of Pure Crystalline Ice at −10°C. The upper curve was measured ~40 μsec, and the lower curve ~8 msec after the start of the flash.

REACTIVITIES OF PEROXYSULFURIC ACIDS WITH H ATOM

R. W. Matthews[1] H. A. Mahlman T. J. Sworski

Oxidation of cerium(III) in initially oxygen-free aqueous 4.0 *M* sulfuric acid solutions is induced by ^{60}Co gamma radiation. We proposed[2] a reaction mechanism in which net cerium(III) oxidation was attributed to significant reactions of H atoms with hydrogen peroxide, peroxymonosulfuric acid, and peroxydisulfuric acid in competition with cerium(IV) and oxygen at low concentrations of cerium(IV) and oxygen. To test this reaction mechanism critically, we need to know the relative reactivities of hydrogen peroxide, peroxymonosulfuric acid, peroxydisulfuric acid, cerium(IV), and oxygen with the H atom.

We have determined the relative reactivities of oxygen and peroxysulfuric acids with the H atom by investigating the effects of peroxydisulfuric acid on cerium(IV) reduction by ^{60}Co gamma radiation in air-saturated 4.0 *M* sulfuric acid solutions. Peroxydisulfuric acid is unstable with respect to hydrolysis in 4.0 *M* sulfuric acid solutions: peroxydisulfuric acid hydrolyzes to yield peroxymonosulfuric acid, which further hydrolyzes to yield hydrogen peroxide.[3] Table 4.1 shows the composition of peroxydisulfuric acid solutions as a function of solution age at ambient room temperature. In agreement with Palme,[3] we find the composition to be independent of initial peroxydisulfuric acid concentration.

Table 4.1. Hydrolysis of Peroxydisulfuric Acid in 4.0 *M* Sulfuric Acid

Time (hr)	Percent $H_2S_2O_8$	Percent H_2SO_5	Percent H_2O_2
2.5	79.0	21.0	0
6.0	47.5	52.5	0
16.0	12.8	85.5	1.7

Figure 4.6 shows that $G(Ce^{III})$ decreases with increase in concentration of peroxysulfuric acids until cerium(III) oxidation occurs instead of cerium(IV) reduction. To enable observation of cerium(III) oxidation, all solutions initially contained 0.003 *M* cerium(III). For any particular initial concentration of peroxydisulfuric acid, $G(Ce^{III})$ decreases with increase in age of solution.

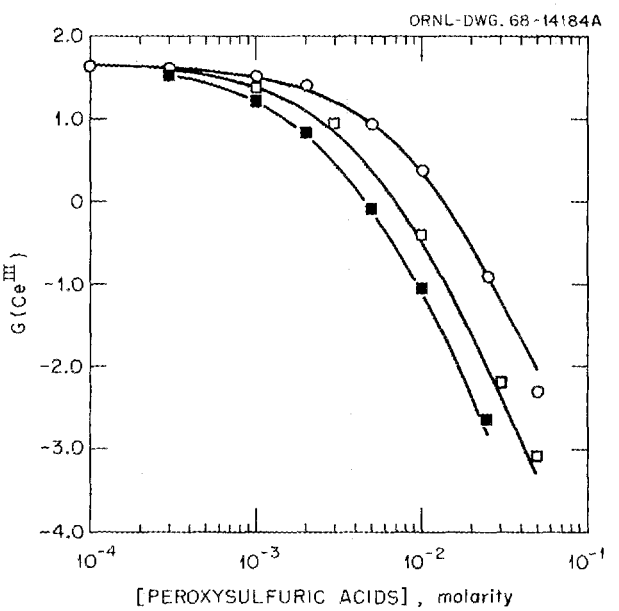

Fig. 4.6. Dependence of $G(Ce^{III})$ on Total Concentration of Peroxysulfuric Acids in Air-Saturated 4.0 *M* Sulfuric Acid. Hydrolysis time of ammonium persulfate solutions: ○, 2.5 hr; □, 6.0 hr; and ■, 16.0 hr.

The experimental data adhere well to Eq. (I),

$$G(Ce^{III}) = G(Ce^{III})^0 - 2G_H \Big/ \left(1 + \frac{k_1[O_2]}{k_3[H_2S_2O_8] + k_4[H_2SO_5]}\right), \quad (I)$$

as evidenced by the theoretical curves in Fig. 4.6. Equation (I) is derived from the following reaction mechanism:

$$H + O_2 \rightarrow HO_2 , \quad (1)$$

$$HO_2 + Ce^{IV} \rightarrow Ce^{III} + H^+ + O_2 , \quad (2)$$

$$H + H_2S_2O_8 \rightarrow H_2SO_4 + HSO_4 , \quad (3)$$

$$H + H_2SO_5 \rightarrow H_2O + HSO_4 , \quad (4)$$

$$HSO_4 + Ce^{III} \rightarrow HSO_4^- + Ce^{IV} . \quad (5)$$

$G(Ce^{III})^0 = 1.66 \pm 0.01$, $G_H = 3.38 \pm 0.12$, $k_3/k_1 = 0.0012 \pm 0.0001$, and $k_4/k_1 = 0.0106 \pm 0.0006$ were obtained by the method of least squares,[4] using an oxygen concentration of 1.33×10^{-4} M reported by Boyle[5] for the air-saturated solution.

---

[1] Guest Scientist from Australian Atomic Energy Research Establishment, Sydney.

[2] R. W. Matthews, H. A. Mahlman, and T. J. Sworski, *J. Phys. Chem.* 72, 3704 (1968).

[3] H. Palme, *Z. Anorg. Chem.* 112, 97 (1920).

[4] M. H. Lietzke, *A Generalized Least Squares Program for the IBM 7090 Computer*, ORNL-3259 (Mar. 21, 1962).

[5] J. W. Boyle, *Radiation Res.* 17, 450 (1962).

KINETIC EVIDENCE FOR A PRIMARY YIELD OF SO_4^- RADICALS IN THE RADIOLYSIS OF AQUEOUS SULFURIC ACID SOLUTIONS[1]

R. W. Matthews[2] H. A. Mahlman T. J. Sworski

Kinetic evidence for a sensibly irreversible reaction of OH radical with sulfuric acid species in aqueous 0.4 M sulfuric acid was previously obtained.[3] The effects of cerium(III) and formic acid concentrations on reduction of cerium(IV) by ^{60}Co gamma radiation were explicable by Eq. (I):

$$G(Ce^{III}) = G(Ce^{III})^* + 2G^*_{OH} \Big/ \left(1 + \frac{k_2[Ce^{III}] + k_3[HSO_4^-]}{k_5[HCOOH]}\right), \quad (I)$$

where $G(Ce^{III})^*$, a function of $[Ce^{III}]$, is the value of $G(Ce^{III})$ at $[HCOOH] = 0$. Equation (I) is based on the following reaction mechanism:

$$H_2O \rightsquigarrow H_2, H_2O_2, H, OH , \quad (1)$$

$$OH + Ce^{III} \rightarrow OH^- + Ce^{IV} , \quad (2)$$

$$OH + HSO_4^- \rightarrow H_2O + SO_4^- , \quad (3)$$

$$SO_4^- + Ce^{III} \rightarrow SO_4^{2-} + Ce^{IV} , \quad (4)$$

$$OH + HCOOH \rightarrow H_2O + COOH , \quad (5)$$

$$COOH + Ce^{IV} \rightarrow CO_2 + H^+ + Ce^{III} . \quad (6)$$

We have reinvestigated the dependence of $G(Ce^{III})$ on cerium(III) and formic acid concentrations, not only in 0.4 M sulfuric acid solution but also in 0.04 and 4.0 M sulfuric acid solutions. For constant concentrations of cerium(III) and sulfuric acid, the dependence of $G(Ce^{III})$ on formic acid concentration adheres well to Eq. (I); values for $G(Ce^{III})^*$, G^*_{OH}, and the kinetic parameter $(k_2[Ce^{III}] + k_3[HSO_4^-])/k_5$ were obtained by the method of least squares.[4]

Figure 4.7 shows that the kinetic parameter is a linear function of the cerium(III) concentration for 0.04 and

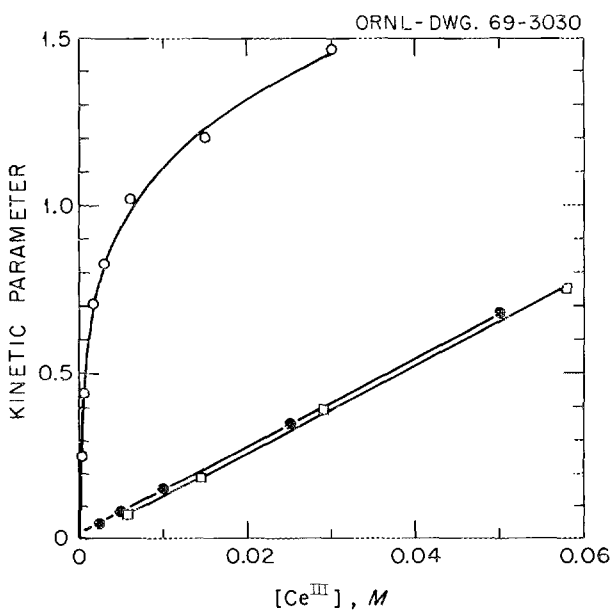

Fig. 4.7. Dependence of the Kinetic Parameter $(k_2[Ce^{III}] + k_3[HSO_4^-])/k_5$ on the Cerium(III) Concentration. Sulfuric acid concentrations: □, 0.04 M; ●, 0.4 M; ○, 4.0 M.

0.4 M sulfuric acid solutions, as required by Eq. (I). For 4.0 M sulfuric acid solutions, however, the dependence of the kinetic parameter on cerium(III) concentration is clearly inconsistent with Eq. (I).

Figure 4.8 shows the dependence of G^*_{OH} on cerium(III) concentration. The increase in G^*_{OH} with increase in cerium(III) concentration for 0.04 M sulfuric acid solutions is just what we expected (see discussion below). Unexpectedly, however, G^*_{OH} is essentially independent of cerium(III) concentration for 0.4 M sulfuric acid solutions and decreases markedly with increase in cerium(III) concentration for 4.0 M sulfuric acid solutions.

Our first attempt to explain quantitatively the unusual results with 4.0 M sulfuric acid solutions was based on the following additions to the above reaction mechanism: (1) the dependence of the kinetic parameter on cerium(III) concentration was explicable by an assumption that reaction (3) was sensibly reversible, as proposed by Wilmarth and Haim[5] and by Mariano and Santos,[6] and (2) the dependence of G^*_{OH} on cerium(III) concentration was explicable by an assumption that there was an unidentified OH radical precursor which could either oxidize cerium(III) or decay by a first-order process to yield OH radical. To test these assumptions critically, we carried out a similar study in 0.4 and 4.0 M sulfuric acid solutions, using 2-propanol instead of formic acid. Although the dependence of the kinetic parameter and G^*_{OH} on cerium(III) concentration in 4.0 M sulfuric acid solutions using 2-propanol is qualitatively similar to that obtained with formic acid, it does not agree quantitatively.

We finally explained the results with formic acid in 4.0 M sulfuric acid solutions by the following additions

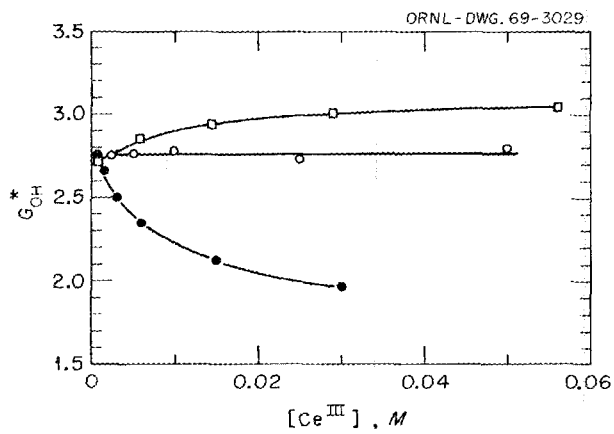

Fig. 4.8. Dependence of G^*_{OH} on the Cerium(III) Concentration. Sulfuric acid concentrations: □, 0.04 M; ○, 0.4 M; ●, 4.0 M.

to the above reaction mechanism: (1) decomposition of sulfuric acid yields SO_4^- as a primary intermediate, as proposed by Boyle,[7]

$$H_2SO_4 \rightsquigarrow H_2S_2O_8, H_2SO_5, SO_4^-, HSO_3 , \qquad (7)$$

and (2) SO_4^- radical reacts with formic acid,

$$SO_4^- + HCOOH \rightarrow HSO_4^- + COOH . \qquad (8)$$

The dependence of $G(Ce^{III})$ on cerium(III) and formic acid concentrations is now given by Eq. (II):

$$G(Ce^{III}) = G(Ce^{III})^* + \frac{2G_{OH}\left(k_5[HCOOH] + \dfrac{k_3 k_8 [HCOOH][HSO_4^-]}{k_8[HCOOH] + k_4[Ce^{III}]}\right)}{k_5[HCOOH] + k_2[Ce^{III}] + k_3[HSO_4^-]} + \frac{2k_8[HCOOH]G_{SO_4^-}}{k_8[HCOOH] + k_4[Ce^{III}]} . \qquad (II)$$

The experimental data with formic acid adhere well to Eq. (II); $G_{OH} = 1.70 \pm 0.02$, $G_{SO_4^-} = 0.97 \pm 0.03$, $k_2/k_5 = 1.9 \pm 0.2$, $k_4/k_8 = 128 \pm 4$, and $k_3[HSO_4^-]/k_5 = 0.066 \pm 0.002$, in addition to seven values of $G(Ce^{III})^*$ for seven cerium(III) concentrations, were obtained by the method of least squares.[4]

Reactions (5), (6), and (8) are replaced for the studies with 2-propanol by reactions (9), (10), and (11) respectively:

$$OH + CH_3CHOHCH_3 \rightarrow H_2O + CH_3COHCH_3 , \qquad (9)$$

$$Ce^{IV} + CH_3COHCH_3 \rightarrow Ce^{III} + H^+ + CH_3COCH_3 , \qquad (10)$$

$$SO_4^- + CH_3CHOHCH_3 \rightarrow HSO_4^- + CH_3COHCH_3 . \qquad (11)$$

To adapt Eq. (II) for the studies with 2-propanol, we replace $k_5[HCOOH]$ and $k_8[HCOOH]$ with $k_9[CH_3CHOHCH_3]$ and $k_{11}[CH_3CHOHCH_3]$ respectively.

The experimental data with 2-propanol also adhere well to Eq. (II); $G_{OH} = 1.64 \pm 0.08$, $G_{SO_4^-} = 1.06 \pm 0.09$, $k_2/k_9 = 0.22 \pm 0.02$, $k_4/k_{11} = 1.46 \pm 0.06$, and $k_3[HSO_4^-]/k_9 = 0.0028 \pm 0.003$, in addition to five values of $G(Ce^{III})^*$ for five cerium(III) concentrations, were obtained by the method of least squares.[4]

Figure 4.9 shows the dependence of $G(Ce^{III})^*$ on the cube root of the cerium(III) concentration in 4.0 M H_2SO_4. These results are consistent with our previous report[3] that $G(Ce^{III})$ decreases linearly with the cube

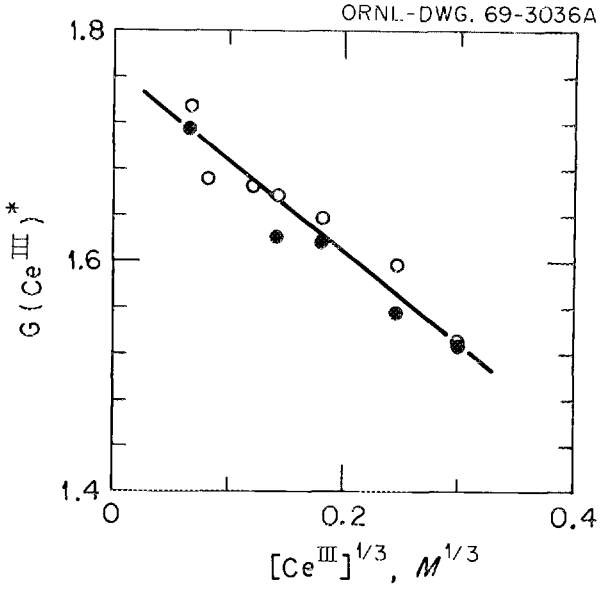

Fig. 4.9. Dependence of $G(Ce^{III})^*$ on the Cerium(III) Concentration in 4.0 *M* Sulfuric Acid Solutions. ○, Formic acid solutions; ●, 2-propanol solutions.

root of the cerium(III) concentration for 0.4 *M* sulfuric acid solutions. The decrease in $G(Ce^{III})$ was attributed to a decrease in $G_{H_2O_2}$, with concomitant increase in G_{OH} owing to reaction of cerium(III) with OH radical and inhibition of H_2O_2 formation by OH radical combination in the spur.

The values for both G_{OH} and $G_{SO_4^-}$ from the studies with formic acid and 2-propanol agree within standard errors. The values for k_4/k_8 and k_4/k_{11} are in good agreement with absolute values of k_4, k_8, and k_{11} reported by Dogliotti and Hayon.[8] These gratifying results indicate the validity of Eq. (II). We must point out, however, that Eq. (II) is admittedly only a good approximation, since we assumed G_{OH} and $G_{SO_4^-}$ to be independent of cerium(III), formic acid, and 2-propanol concentrations.

---

[1] Presented at the 17th Annual Meeting, Radiation Research Society, Cincinnati, Ohio, May 18–22, 1969.

[2] Guest Scientist from Australian Atomic Energy Research Establishment, Sydney.

[3] T. J. Sworski, *J. Am. Chem. Soc.* 78, 1768 (1956); *Radiation Res.* 6, 645 (1957).

[4] M. H. Lietzke, *A Generalized Least Squares Program for the IBM 7090 Computer,* ORNL-3259 (Mar. 21, 1962).

[5] W. K. Wilmarth and A. Haim, *Peroxide Reaction Mechanisms* (ed. by J. O. Edwards), p. 175, Interscience, New York, 1962.

[6] M. H. Mariano and M. L. Santos, *Radiation Res.* 32, 905 (1967).

[7] J. W. Boyle, *Radiation Res.* 17, 427 (1962).

[8] L. Dogliotti and E. Hayon, *J. Phys. Chem.* 71, 3802 (1967).

ENERGY TRANSFER AND RADIOLYSIS OF ALIPHATIC CARBOXYLIC ACIDS

A. R. Jones

Figure 4.10 contains most of the published information on the radiolytic decarboxylation of the homologous series of straight-chain aliphatic monocarboxylic acids. The carbon dioxide yields from alpha-particle radiolysis decrease as a straight-line function of the number of carbon atoms in the acid molecule, and if the plot through behenic acid, C_{22}, were extended it would cut the coordinate of zero production at a point between acids having chains of 26 and 27 carbon atoms. The authors considered it desirable, however, to conclude the study by bombarding melissic acid, C_{30}, both before and after extensive purification. Their dashed line and two final points in the figure were the result. "This last experiment indicates the difficulty of attempting to interpret data based on incomplete experiments on a group of compounds."[1]

In my study of the gamma radiolysis to low conversion of pure members of the same homologous series for the purpose of determining the mechanism of energy deposition in the bond between the carboxyl group and the aliphatic chain, I have found that the decarboxylation yields are not simply expressed, even below C_{22} (Fig. 4.11). These data indicate that the decarboxylation yields for liquid acids asymptotically approach the limiting value of 1.0 found by irradiating at −195°C.

For this work the interesting feature is the efficiency with which the absorbed energy collects in the bond

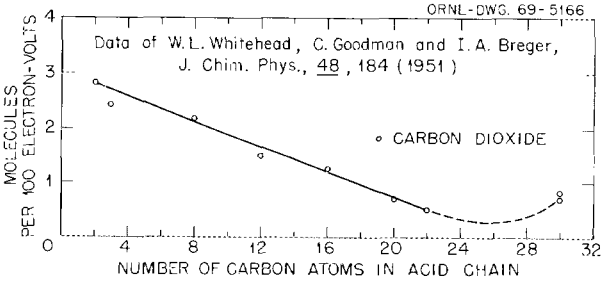

Fig. 4.10. Yield of Carbon Dioxide as a Function of Chain Length for Alpha-Particle Radiolysis of Straight-Chain Aliphatic Monocarboxylic Acids.

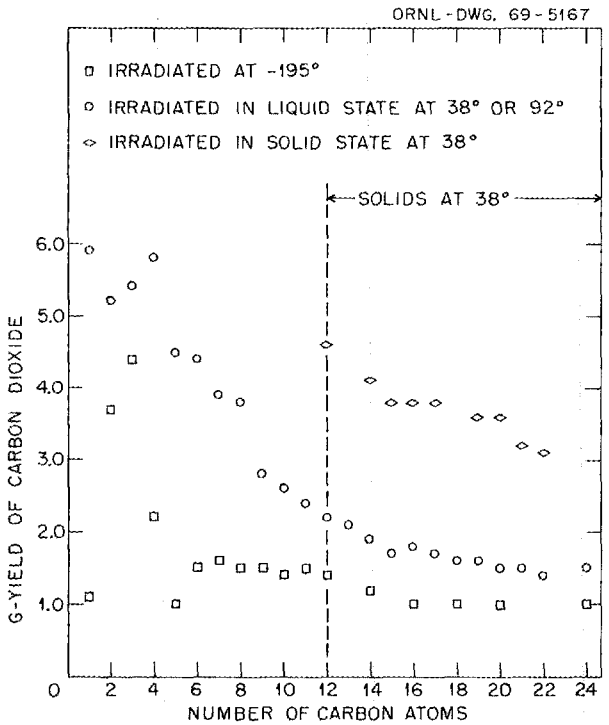

Fig. 4.11. Yield of Carbon Dioxide as a Function of Chain Length for Gamma Radiolysis of Straight-Chain Aliphatic Monocarboxylic Acids.

between the carboxyl group and the aliphatic chain. The decarboxylation yields decrease by a factor of about 5 for the first 22 members of the series in the liquid state, while the carboxyl fraction of the molecule decreases by a greater factor whether one considers electron, volume, or weight fraction. The decarboxylation yields do not appear to be related to the viscosities of the liquids, and irradiation of acids solid at 38° results in greater decarboxylation.

To explain the decrease in the decarboxylation yield by invoking the cage effect and increased back reaction between the fragments R— and —COOH not only appears implausible but ignores the fundamental question: How did the energy accumulate in that bond in the first place?

The only carbon-to-carbon bond breakage which occurs in the parent molecules is that which separates the carboxyl group from the aliphatic chain. Since it is unlikely that the high degree of vibrational energy localization necessary for bond breakage is a result of the accumulation of vibrational energy, one must conclude that the selective bond breakage noted is due to selective localization of electronic energy. This could be the result of (1) some sort of "condensation" of the electronic energy; (2) random absorption of the electronic energy within a molecule, followed by specific inter- or intramolecular energy transfer; or (3) random production of positive ions, followed by charge localization and neutralization by the capture of free electrons at the site of chemical change. The last is apparently excluded, since the specificity and the decarboxylation yields are unaffected by the presence of iodine[2] or water. Intermolecular energy transfer from the hydrocarbon part of the molecules to the R—COOH bond is apparently excluded by the finding that there is no energy transfer from octane to acetic acid when mixtures of these pure substances are irradiated. An intramolecular energy transfer mechanism is supported by the decarboxylation yield of 5.1 found for the radiolysis of the dibasic adipic acid at 38°C. This is almost identical with the yield found for propionic acid. Adipic acid can be considered as constituted of two molecules of propionic acid from the point of view of intramolecular energy transfer.

---

[1] W. L. Whitehead, C. Goodman, and I. A. Breger, *J. Chim. Phys.* 48, 184 (1951).

[2] R. H. Johnsen, *J. Phys. Chem.* 63, 2041 (1959).

RADIATION AND HOT-ATOM CHEMISTRY OF INORGANIC CRYSTALLINE SOLIDS

CHEMISTRY OF ^{38g}Cl RECOILS IN NEUTRON-IRRADIATED CRYSTALLINE $KClO_2$, $KClO_3$, AND $KClO_4$[1]

G. E. Boyd Q. V. Larson

The distribution of recoil 37.5-min ^{38g}Cl among the chlorine valence states following the $^{37}Cl(n,\gamma)^{38}Cl$ reaction at 35° in crystalline $KClO_2$, $KClO_3$, and $KClO_4$ was measured. Anion exchange column separations performed on aqueous solutions of the irradiated solids showed that radiochloride was the principal species formed. The production of $^{38}ClO_2^-$ and $^{38}ClO_2$ was observed for the first time, as was the formation of $^{38}ClO_3^-$ in $KClO_2$ and $^{38}ClO_4^-$ in $KClO_3$. The generation of small amounts of radioperchlorate ion in irradiated $KClO_4$ was confirmed. Radiohypochlorite appeared to be formed in very small yield, if at all. Comparisons of the relative yields of the chlorine valence states produced by ^{60}Co gamma radiation with those for recoil radiochlorine indicated

that the rupture of all the Cl–O bonds in the target anion is much more probable in the "hot-atom" than in the radiation chemical process.

[1] Abstract of published paper: *J. Am. Chem. Soc.* **90**, 5092 (1968).

PRODUCTION OF ClO_4^- AND ClO_2^- IONS IN CRYSTALLINE $KClO_3$ IRRADIATED WITH ^{60}Co GAMMA RAYS[1]

L. C. Brown G. E. Boyd

The production of perchlorate and chlorite ions in crystalline $KClO_3$ irradiated with ^{60}Co gamma rays at about 30°C was demonstrated by infrared absorption measurements. Quantitative determinations of the concentration of ClO_4^- ions in the solid were performed, and the results were compared with chemical analyses for perchlorate in aqueous solutions of the irradiated solid. The concentrations of ClO_4^- in solution and in the crystal were found equal within experimental error. Accordingly, the hypothesis that the perchlorate observed in solution was produced by the hydrolysis of Cl_2O_6 assumed to be present in the solid was unnecessary. Radiolytic yields for the species Cl^-, ClO^-, ClO_2^-, and ClO_4^- were obtained. The concentrations of the first three species appeared to increase linearly with the absorbed dose to a dose as great as 4.4×10^{23} eV per mole of $KClO_3$; the concentration of ClO_4^- ion, however, increased less rapidly than linearly at large doses. Interesting similarities between the radiolytic and thermal decompositions of the alkali-metal chlorates were noted.

[1] Abstract of published paper: *J. Phys. Chem.* 73, 396 (1969).

PRODUCTION OF BROMITE AND PERBROMATE IONS IN CRYSTALLINE $CsBrO_3$ IRRADIATED WITH ^{60}Co GAMMA RAYS AND THE VIBRATIONAL SPECTRUM OF BrO_4^- ION[1]

L. C. Brown G. M. Begun G. E. Boyd

The formation of perbromate and bromite ions in $CsBrO_3$ by ^{60}Co gamma rays at about 30° was demonstrated by infrared absorption measurements on irradiated crystals and by ion exchange column chromatographic separations on aqueous solutions of the radiolyzed solid. Vibrational spectra (infrared and laser-excited Raman measurements) were obtained for BrO_4^- ion in solution and in crystalline $RbBrO_4$ and $(C_6H_5)_4AsBrO_4$. The frequency assignments (cm^{-1}) are: $\nu_1 = 801$, $\nu_2 = 331$, $\nu_3 = 878$, and $\nu_4 = 410$. Force constants derived from these frequencies suggest that there is a close similarity in bonding between BrO_4^- and IO_4^- and that a significant decrease in the nonbonding interactions occurs in the series ClO_4^-, BrO_4^-, and IO_4^- as the size of the central atom increases and the oxygens become less crowded. An unsuccessful search was made for $^{82}BrO_4^-$ ion formed in $^{7}LiBrO_3$ by thermal-neutron capture. The yield of $^{82}BrO_4^-$ ion, if formed, was less than 0.05%.

[1] Abstract of published paper: *J. Am. Chem. Soc.* 91, 2250 (1969).

5. Organic Chemistry

PREPARATION AND DEAMINATION OF 5-*exo*-PHENYL-5-HYDROXY-2-*exo*-NORBORNYLAMINE AND 5-*endo*-PHENYL-5-HYDROXY-2-*exo*-NORBORNYLAMINE

Ben M. Benjamin Clair J. Collins

5-*exo*-Phenyl-5-hydroxy-2-*endo*-norbornyl tosylate[1] was treated with sodium azide in a dimethyl sulfoxide–pyridine solvent mixture. The organic azide was isolated from the reaction mixture and was reduced with lithium aluminum hydride to give 5-*exo*-phenyl-5-hydroxy-2-*exo*-norbornylamine, **1**, mp 105°. The structure of **1** was confirmed by carbon-hydrogen analysis and by interpretation of its nuclear magnetic resonance (nmr) spectrum. The same sequence of reactions was carried out using compounds labeled in the phenyl group with ^{14}C. Compound **1** was deaminated by treating it with sodium nitrite in acetic acid, and the yields of products were determined by chromatographic analysis, nmr spectroscopy, and isotope dilution analysis. The composition of the product mixture and the reaction scheme are shown in Chart I.

In a manner similar to the preparation of **1**, the synthesis of compound **2**, 5-*endo*-phenyl-5-hydroxy-2-*exo*-norbornylamine, mp 118°, phenyl labeled and unlabeled, was carried out starting from 5-*endo*-phenyl-5-hydroxy-2-*endo*-norbornyl tosylate. Chart II shows the product yields and the reaction scheme resulting from the deamination of **2**.

Starting with amine **1**, deamination produced diols **4** and **6** in the ratio 3.4/1 and a small but significant amount of diol **5** resulting from *endo* attack by solvent on the ion A, Chart I. By comparison, deamination of **2** produced diols **4** and **6** in the ratio 0.6/1 and a small amount of the *endo*-diol **7** from ion B, Chart II. These results lead to the conclusion that the first norbornyl ions formed in these deamination processes are classical open-type ions. Nonclassical ions would be expected to give **4** and **6** in the same ratio from **1** and **2**; no products such as **6** or **7** would be anticipated because of bridging on the *endo* side of the intermediate.[2]

The quantity of **7** from amine **1** and of **5** from amine **2** is thought to be insignificant. These yields were determined by the isotope dilution technique, and the very small amount of radioactivity in the reisolated compounds is probably caused by residual occluded labeled impurities. Whether diols **5** and **7** are formed

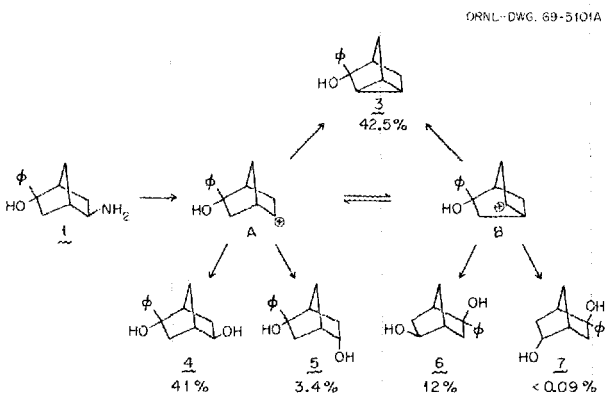

Chart I. Reaction Scheme for the Deamination of 5-*exo*-Phenyl-5-hydroxy-2-*exo*-norbornylamine.

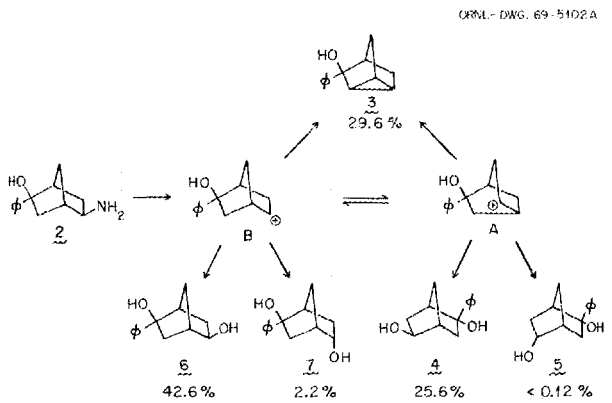

Chart II. Reaction Scheme for the Deamination of 5-*endo*-Phenyl-5-hydroxy-2-*exo*-norbornylamine.

upon deamination of amines **2** and **1**, respectively, is important because their production is related to whether a carbonium ion system colapses from classical to nonclassical after one Wagner-Meerwein shift.

---

[1] B. S. Benjaminov, B. M. Benjamin, and C. J. Collins, *Chem. Div. Ann. Progr. Rept. May 20, 1968*, ORNL-4306, p.66.

[2] C. J. Collins *et al.*, *J. Am. Chem. Soc.* **86**, 4913 (1964).

DEAMINATION OF 3-*exo*- AND 3-*endo*-PHENYL-^{14}C-3-HYDROXY-2-*endo*-NORBORNYLAMINES

V. F. Raaen C. J. Collins

Title compounds **1** and **2** (Chart III) were subjected to deamination with $NaNO_2$ in acetic acid–sodium acetate solutions. Both norbornylamines were labeled with ^{14}C, uniformly distributed in the phenyl substituent. The yields of **3** and **4** were determined carefully by

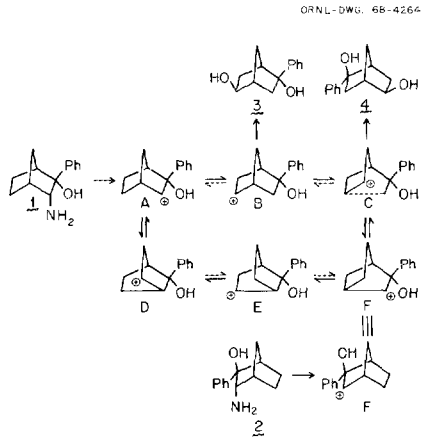

Chart III.

isotope dilution analysis. It was presumed that, if the ratio of **3** to **4** from either reactant was the same, then **B** and **C** could be represented as a single nonclassical ion. If **B** and **C** were classical open unbridged ions (as shown in Chart III), then it was assumed that for diols **3** and **4** formed by the short route, relatively more **3** should be formed from reactant **1** than from reactant **2**. In an earlier investigation[1] the yields of these diols were determined by vapor-phase chromatography. At that time, preliminary results showed that the ratio of **3** to **4** from **1** was about 1.5:1, whereas from **2** the ratio was more than 4:1. The susceptibility of **3** and, especially, **4** to decomposition under the conditions of vapor-phase chromatography raised doubt about the validity of these values.

New results from the isotope-dilution analysis show that the ratio of **3** to **4** from **1** is 1.6:1, and the ratio from **2** is 1.7:1. The relative amounts of diols **3** and **4** formed by the long route (**F→E→D→A→B→C**) as compared with the amounts formed by the short route (**F→C→B**) are not known. More information about the relative contribution of each of these paths will be obtained by labeling with deuterium. For this purpose **2** will be substituted with deuterium in the 5,6-*exo* positions. The labeled compound will be deaminated; the diols, **3** and **4**, will be analyzed for deuterium distribution to indicate the relative contribution from each reaction path.

A procedure was developed for the preparation of high-specific-activity benzene from barium carbonate-^{14}C via acetylene-^{14}C. Benzene-^{14}C was then converted to bromobenzene-^{14}C for use in the preparation of the 2-phenyl-^{14}C-norbornane derivatives needed in the deamination study described above.

---

[1] M. Eckert and C. J. Collins, *Chem. Div. Ann. Progr. Rept. May 20, 1968*, ORNL-4306, p. 67.

DEGRADATION OF 2-*exo*-NORBORNEOL-^{14}C

Charles E. Harding[1] Vernon F. Raaen
Clair J. Collins

In connection with ^{14}C tracer studies of the mechanism of solvolysis of 2-(Δ^3-cyclopentenyl)ethyl and 2-*exo*-norbornyl derivatives, two new degradation procedures have been developed to determine the distribution of ^{14}C. The degradation procedures outlined by Roberts, Lee, and Saunders[2] have two disadvantages: (1) the values for radioactivities are obtained by difference, and (2) with the exception of the 7 position, the values are for paired carbon atoms.

Direct determination of the amount of ^{14}C in the 2 and 3 positions of the norbornyl skeleton was accomplished by photolysis[3] of the labeled norcamphor to 2-(Δ^2-cyclopentenyl)-acetaldehyde, which was oxidized to 2-(Δ^2-cyclopentenyl)acetic acid. The latter compound was then subjected to a Barbier-Wieland degradation. An outline of the procedure is shown in Chart IV.

The amount of ^{14}C in the 1 position of 2-norborneol-^{14}C was determined by a series of reactions similar

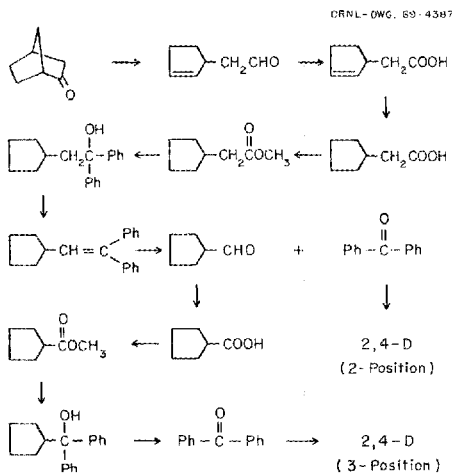

Chart IV.

to those used by Schleyer[4] in his study of the formic acid rearrangement of 2-methyl-2-norbornene. The procedure is outlined in Chart V.

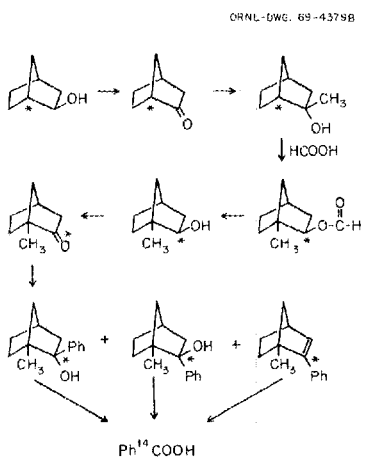

Chart V.

[1]Oak Ridge Graduate Fellow from the University of Tennessee, Knoxville, under appointment with Oak Ridge Associated Universities.

[2]J. D. Roberts, C. C. Lee, and W. H. Saunders, *J. Am. Chem. Soc.* **76**, 4501 (1954).

[3]R. Srinivasan, *J. Am. Chem. Soc.* **81**, 2604 (1959).

[4]P. R. Schleyer, *J. Am. Chem. Soc.* **89**, 3901 (1967).

POLYMER STUDIES

EQUILIBRIA IN THE SYSTEM: POLY(HYDROXYPROPYL ACRYLATE-CO-TETRAETHYLENE GLYCOL DIMETHACRYLATE), WATER, AND ELECTROLYTE[1]

C. E. Higgins W. H. Baldwin

Previously we noted the unusually high degree of swelling when the above-mentioned copolymer was equilibrated with aqueous sodium hydroxide.[2] Since that time we have discovered that both the degree of swelling and the cation exchange capacity vary with the base used. Both effects decrease in the order LiOH = NaOH = CsOH = $(CH_3)_4NOH$ > NH_4OH > pyridine. This copolymer, in which we can control the ion exchange capacity, amount of cross-linkage, and degree of swelling, will be tested as a dynamically formed membrane for beneficiation of contaminated water.

Copolymers of the above type have been shown by Refojo and Yasuda[3] to have an inverse relationship between temperature and the degree of swelling. Cylinders of the copolymer were equilibrated with water at 25° and were then transferred to 0.5 *N* NaCl. When the latter was also at 25°, a 15% reduction in volume occurred, but when at 1°C, a 40% increase in volume occurred. In the latter case the ratio of NaCl to water inside the polymer was 35% less than that outside; however, when the cylinders were warmed to room temperature the exudate was 0.45 *N* in NaCl, compared with the 0.5 *N* starting solution.

[1]Research jointly sponsored by the Office of Saline Water, U.S. Department of the Interior, and by the U.S. Atomic Energy Commission under contract with Union Carbide Corp.

[2]C. E. Higgins and W. H. Baldwin, *Chem. Div. Ann. Progr. Rept. May 20, 1968*, ORNL-4306 p. 71.

[3]M. J. Refojo and H. Yasuda, *J. Appl. Polymer Sci.* **9**, 2425 (1965).

6. Chemistry of Aqueous Systems

THE THERMODYNAMIC PROPERTIES OF HCl-CsCl-$BaCl_2$ MIXTURES

M. H. Lietzke H. B. Hupf[1]
R. W. Stoughton

In this study, emf measurements of the cell

$$\text{Pt-H}_2(p = 1)|\text{HCl}(m_2), \text{CsCl}(m_3), \text{BaCl}_2(m_4)|\text{AgCl, Ag}$$

have been combined with isopiestic measurements of the system CsCl-$BaCl_2$ to calculate the thermodynamic properties of each of the electrolytes in aqueous HCl-CsCl-$BaCl_2$ mixtures. As far as we know, this is the first quaternary system in which this has been accomplished.

The experimental apparatus and the preparation of the electrodes were the same as described previously.[2] The emf measurements were carried out in the temperature range 25 to 175° on solutions of total ionic strength approximately 0.5 and 1.0, in which both the total fractions of acid and salt were varied as well as the ionic strength ratios of the two salts at fixed fractions of total salt. The isopiestic measurements on the CsCl-$BaCl_2$ system were performed at 25° in the ionic strength range 0.2 to 2.0.[3]

The treatment of the experimental data was similar to that described previously.[4] The activity coefficients of HCl calculated for each experimental data point were fitted by the method of least squares using Eq. (1):

$$\log \gamma_2 = -\frac{S_T \rho^{1/2}\sqrt{I}}{1 + 1.5\sqrt{I}} + 2I\left[B_{22} + (B_{23} - B_{22})X_3 + \left(\frac{B_{24}}{3} - B_{22}\right)X_4\right] + 3I^2\left[C_{222} + 2(C_{223} - C_{222})X_3 + 2\left(\frac{C_{224}}{3} - C_{222}\right)X_4\right] + 3I^2\left[2(C_{222} - C_{223} + \frac{C_{234}}{3} - \frac{C_{224}}{3})X_3X_4 + (C_{222} + C_{233} - 2C_{223})X_3^2 + \left(C_{222} + \frac{C_{244}}{9} - \frac{2}{3}C_{224}\right)X_4^2\right] . \quad (1)$$

In this equation the subscripts 2, 3, and 4 refer to HCl, CsCl, and $BaCl_2$ respectively; S_T is the appropriate Debye-Hückel limiting slope at temperature T; ρ is the density of water; I is the total ionic strength of the solution; and the B_{ij} and C_{ijk} may be considered interaction coefficients.

In using Eq. (1) the temperature dependence of the interaction coefficients was expressed as

$$B_{iq} = B'_{iq} + B''_{iq}/T + B'''_{iq} \log T$$

and

$$C_{ijq} = C'_{ijq} + C''_{ijq}/T .$$

The choice of these formulations was consistent with previous studies[4] on other electrolyte mixtures.

The expressions used for describing the logarithms of the activity coefficients of the CsCl and $BaCl_2$, respectively, are shown as Eqs. (2) and (3):

$$\log \gamma_3 = -\frac{S_T \rho^{1/2}\sqrt{I}}{1 + 1.5\sqrt{I}} + 2I\left[B_{33} + (B_{23} - B_{33})X_2 + \left(\frac{B_{34}}{3} - B_{33}\right)X_4\right] + 3I^2\left[C_{333} + 2(C_{233} - C_{333})X_2 + 2\left(\frac{C_{334}}{3} - C_{333}\right)X_4 + (C_{333} + C_{223} - 2C_{233})X_2^2 + \left(C_{333} + \frac{C_{344}}{9} - \frac{2}{3}C_{334}\right)X_4^2 + 2\left(C_{333} - C_{233} + \frac{C_{234}}{3} - \frac{C_{334}}{3}\right)X_2X_4\right] , \quad (2)$$

$$\log \gamma_4 = -\frac{S_T \rho^{1/2}\sqrt{I}}{1+1.5\sqrt{I}} + \frac{4}{3}I\left[\frac{B_{44}}{3} + \left(B_{24} - \frac{B_{44}}{3}\right)X_2 + \left(B_{34} - \frac{B_{44}}{3}\right)X_3\right] + 2I^2\left[\frac{C_{444}}{9} + 2\left(\frac{C_{244}}{3} - \frac{C_{444}}{9}\right)X_2 + 2\left(\frac{C_{344}}{3} - \frac{C_{444}}{9}\right)X_3 + \left(C_{224} - \frac{2}{3}C_{244} + \frac{C_{444}}{9}\right)X_2^2 + \left(C_{334} - \frac{2}{3}C_{344} + \frac{C_{444}}{9}\right)X_3^2 + 2\left(C_{234} - \frac{C_{244}}{3} - \frac{C_{344}}{3} + \frac{C_{444}}{9}\right)X_2X_3\right]. \quad (3)$$

In Eq. (3) the value of S_T has three times the value of S_T in Eqs. (1) and (2). Examination of Eqs. (2) and (3) reveals the fact that there are seven coefficients needed that cannot be obtained from the emf measurements of the HCl activity in the mixtures. These are the coefficients B_{33}, B_{34}, B_{44}, C_{333}, C_{334}, C_{344}, and C_{444}. In order to evaluate these coefficients an independent study of aqueous $CsCl$-$BaCl_2$ mixtures had to be made. In our case we used osmotic coefficient data at 25° on this ternary system.[3]

The values of all the B and C coefficients as obtained by fitting either the emf or the isopiestic data are given in Table 6.1. For the least-squares fit of Eq. (1), values of the logarithm of the activity coefficient of HCl in water and of HCl in HCl-CsCl and HCl-$BaCl_2$ solutions were used.

Table 6.1. Values of the Parameters for Calculating the B and C Coefficients for Eqs. (1), (2), and (3)

$B'_{22} = 1.81352$	$B''_{22} = -59.1680$	$B'''_{22} = -0.624329$
$B'_{23} = 8.92824$	$B''_{23} = -487.292$	$B'''_{23} = -2.95885$
$B'_{24} = 15.4683$	$B''_{24} = -811.730$	$B'''_{24} = -5.20084$
$C'_{222} = 0.0112851$	$C''_{222} = -5.67278$	
$C'_{223} = -0.0420016$	$C''_{223} = 18.6476$	
$C'_{224} = 0.118170$	$C''_{224} = -35.9187$	
$C'_{233} = -0.0513648$	$C''_{233} = 32.4730$	
$C'_{234} = -0.481511$	$C''_{234} = 87.5962$	
$C'_{244} = -0.312727$	$C''_{244} = 236.178$	
$B_{33} = -0.0327076$		
$B_{34} = -0.0369298$		
$B_{44} = 0.0571330$		
$C_{333} = 0.00508436$	at 25°	
$C_{334} = 0.00625010$		
$C_{344} = 0.00439122$		
$C_{444} = 0.00804580$		

Values of the logarithm of the activity coefficient of HCl in the HCl-CsCl-$BaCl_2$ mixtures were computed at $I = 0.5$ and 1.0 as a function of temperature and total ionic strength fraction of salt with varying ionic strength ratios of CsCl to $BaCl_2$, using the parameters in Table 6.1. These values at $I = 1.0$ are shown plotted vs $X_4/(X_3 + X_4)$ in Fig. 6.1. (The plots at $I = 0.5$ are similar except that the effect on the activity coefficient of the HCl is less pronounced.) Hence the left side of the figure corresponds to the HCl-CsCl system ($X_4 = 0$), while the right side corresponds to the HCl-$BaCl_2$ system ($X_3 = 0$). The circles represent the values of log γ_2 taken from previous work[4] on these ternary systems. The crossovers are an indication that the slopes of the Harned rule plots for HCl in the ternary systems have opposite sign: positive for the HCl-CsCl mixtures and negative for the HCl-$BaCl_2$ mixtures.

As can be seen, the addition of the two salts CsCl and $BaCl_2$ has a much greater effect on the activity coefficient of HCl at the same total fraction of salt than adding either salt alone. The greatest effect seems to be in the vicinity where the ratio $X_3/X_4 \cong 1$ in solutions where the total fraction of salt is the highest ($X_2 = 0.25$, $X_3 + X_4 = 0.75$). This enhanced effect is probably due to additional ionic interactions in the quaternary mixture (e.g., the coefficient C_{234} does not occur in the expressions describing either of the ternary mixtures). Moreover, in contrast to the two ternary systems HCl-CsCl and HCl-$BaCl_2$, where Harned's rule applied for the HCl, the coefficients of the X_3^2, X_4^2, and X_3X_4 terms could not be omitted in the HCl-CsCl-$BaCl_2$ system.

Values of the logarithm of the activity coefficient of CsCl and of $BaCl_2$ in the HCl-CsCl-$BaCl_2$ system were also calculated at 25° and $I = 1.0$ as a function of total ionic strength fraction of salt with varying ionic strength ratios of CsCl to $BaCl_2$ using the parameters in Table 6.1. These values are shown plotted vs X_2, the ionic strength fraction of the acid in the mixtures, in Fig. 6.2. Note that the curves for log γ_3 (CsCl) cross over at $X_2 = 0.04$, whereas the values for log γ_4 ($BaCl_2$) do not. Since the values of log γ_3 or log γ_4 on the ordinate axis refer to the CsCl-$BaCl_2$ system ($X_2 = 0$), the crossover is an indication that the slopes of the log γ_3 vs X_4 and log γ_4 vs X_3 plots have opposite signs (positive for the CsCl and negative for the $BaCl_2$). Except for the extreme left portion of the log γ_3 plots ($X_2 < 0.04$), the addition of $BaCl_2$ at constant ionic strength and constant fraction of HCl decreases the activity coefficient of the CsCl. The addition of CsCl

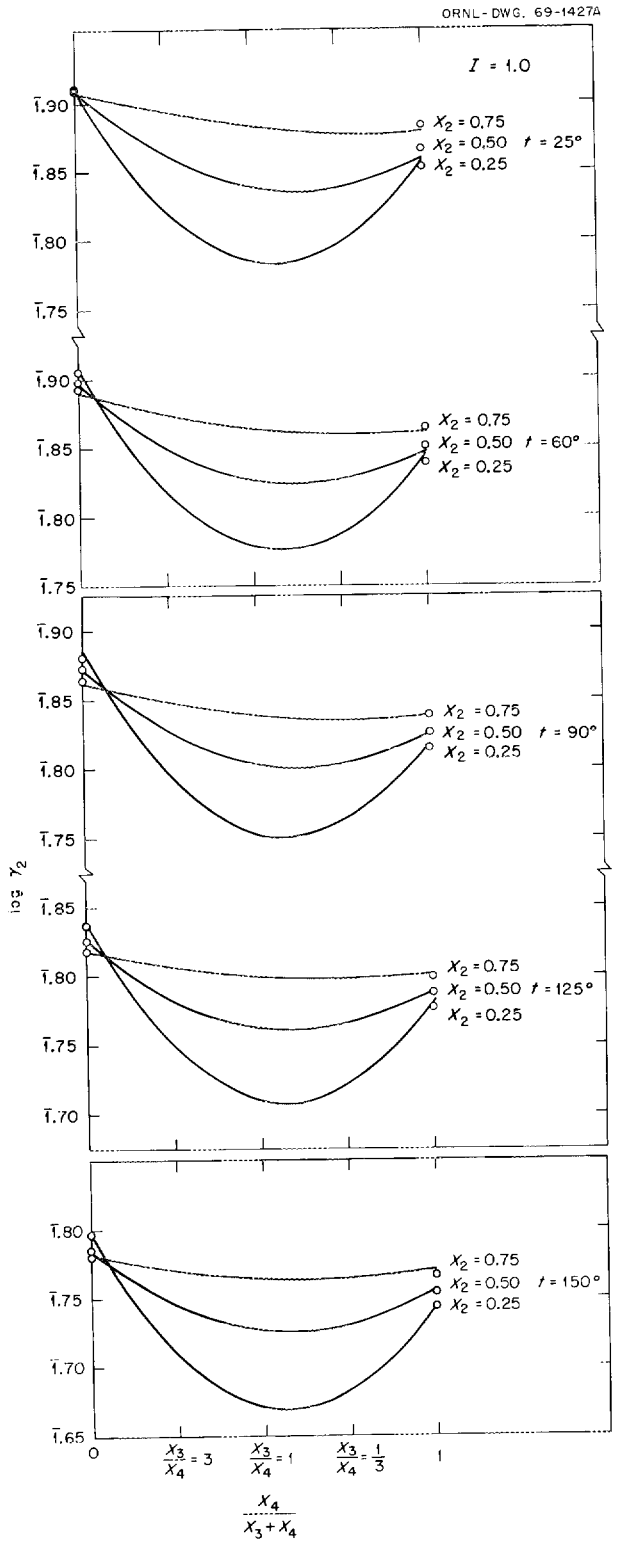

Fig. 6.1. Plots of the Logarithm of the Activity Coefficient of HCl in HCl-CsCl-$BaCl_2$ Mixtures vs $X_4/(X_3 + X_4)$ at $I = 1.0$.

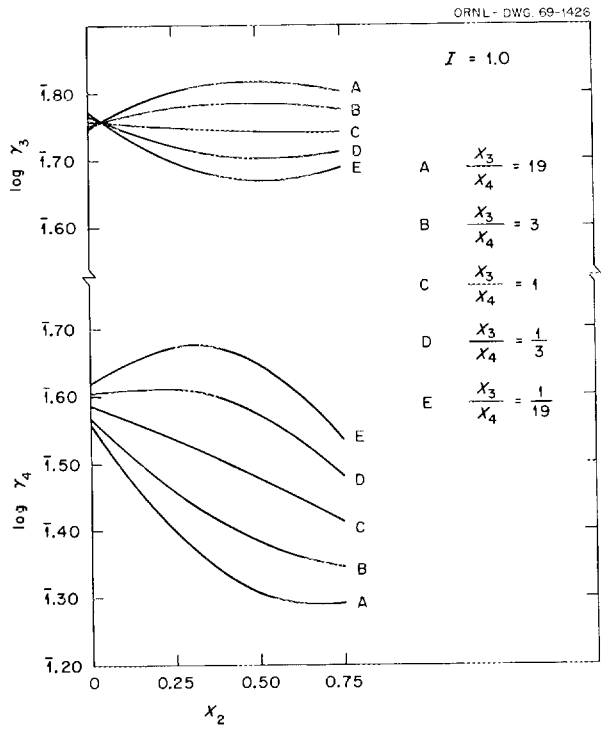

Fig. 6.2. Plots of the Logarithms of the Activity Coefficients of CsCl and $BaCl_2$ in HCl-CsCl-$BaCl_2$ Mixtures vs X_2 at $I = 1.0$ and 25°C.

has a similar effect on the activity coefficient of $BaCl_2$ under the same conditions, as shown by the lower set of curves in Fig. 6.2.

Thus it has been possible by using a combination of emf and isopiestic measurements to calculate the activity coefficient of each component in HCl-CsCl-$BaCl_2$ mixtures. In contrast to the HCl-CsCl and the HCl-$BaCl_2$ mixtures the activity coefficient of the HCl does not obey Harned's rule in the quaternary mixture. The measurements made in the HCl-CsCl-$BaCl_2$ mixtures are entirely consistent with those made previously in the two ternary mixtures.

---

[1] Isotopes Division.

[2] R. S. Greeley *et al.*, *J. Phys. Chem.* 64, 652 (1960).

[3] S. Lindenbaum, private communication.

[4] M. H. Lietzke *et al.*, *J. Phys. Chem.* 69, 2395 (1965); 70, 756 (1966); 71, 662 (1967); 72, 257, 4408 (1968).

ON THE EXISTENCE OF THE COMPLEX $AgSO_4^-$ IN AQUEOUS SOLUTIONS

M. H. Lietzke R. W. Stoughton

In a series of papers the solubility of silver sulfate in aqueous potassium nitrate,[1] potassium sulfate,[1] magnesium sulfate,[1] and silver nitrate[2] solutions was described. In all these systems it was shown that the concentration dependence of the logarithm of the stoichiometric solubility product S could be described in terms of S_0 (the solubility product in the absence of a supporting electrolyte) by an equation of the Debye-Hückel type,

$$\ln S = \ln S_0 + (\Sigma z_i^2) \times S_1 \left[\frac{\sqrt{I}}{1 + A\sqrt{I}} - \frac{\sqrt{I_0}}{1 + A\sqrt{I_0}} \right], \quad (1)$$

on the assumption of complete dissociation of all electrolytes. Here S_1 is the Debye-Hückel limiting slope for a univalent ion; z represents ionic charge, and I represents the ionic strength of the solution. The values of A were found to be essentially temperature independent but ionic strength dependent. The partial molal entropies[3] obtained with the above assumptions agreed closely with those computed from tabulated values of the ionic entropies both at 25 and 100°.

By contrast, we found it necessary to take into account the presence of HSO_4^- in interpreting the solubility of silver sulfate in sulfuric and nitric acids.[4] In these studies we were able to evaluate the HSO_4^- dissociation constant to 225° (ref. 4*c*). This behavior implies a qualitative difference between the complex HSO_4^- and the various other possible ion pairs in the above media.

Recently Hopkins and Wulff[5] reported good agreement between the value of the heat of solution for silver sulfate obtained by direct measurement and the value estimated on the assumption of a "weak" second ionization step. They cite this and additional evidence for the existence of $AgSO_4^-$ ions in aqueous solutions of Ag_2SO_4. They present four values for the standard Gibbs free energy of solution ΔG_1° of silver sulfate (including ours[3]) which average to 6550 ± 30 cal/mole – all based on complete dissociation at finite concentrations. They then present three values averaging 6740 ± 25 cal/mole which they feel have been corrected for the presence of $AgSO_4^-$: (1) a correction of 140 cal/mole on our value[3] of 6595 giving 6735 cal/mole, (2) a value of 6707 cal/mole reported by Pan and Lin[6] from a study with the $Ag(s)/Ag_2SO_4(s)$ electrode, and (3) a value based on the data of Righellato and Davies[7] at two concentrations at 25°.

Regarding item 1, Hopkins and Wulff[5] suggested that our value of the logarithm of the thermodynamic solubility product K_s° obtained in Ag_2SO_4-KNO_3 mixtures should be our best one, since this mixture probably involved the least complications due to ion association. Our value for ΔG_1° in this medium[3] at 25° was, as they claimed,[5] 140 cal/mole different from our average of 6595, but their correction was in the wrong direction. Thus our value should have been cited as 6455, not 6735, cal/mole.

We are uncertain as to the limit of error in the value of Pan and Lin.[6]

In the calculation involving the use of the two data of Righellato and Davies,[7] Hopkins and Wulff[5] obtained a value of ΔG_1° = 6770 cal/mole by using a value of unity for the Debye-Hückel denominator parameter A. While their value of A is not unreasonable, as far as we know it is not known and could vary by as much as from about 0.4 to 2.0. Accordingly we recalculated ΔG_1° using this range of values for A and obtained the range 6875 to 6610 cal/mole for ΔG_1°. Thus we feel that their value could be off by at least as much as 100 cal/mole due solely to the unknown value of A. We do not know how to estimate the other uncertainties.

Hopkins and Wulff[5] point out that our value for the enthalpy of solution at 25° was 4470 cal/mole, compared with two literature values of 4207 and 4215, and imply that this discrepancy results from our not taking into account the presence of $AgSO_4^-$. We feel that our method of calculating ΔH_1° from the temperature dependence of the solubility may easily allow an error of some 200 to 300 cal/mole, particularly at the two extreme temperatures (25 and 200°).

We tried using the value of K obtained by Righellato and Davies[7] (called model A) to see whether this would improve our calculated solubilities in Ag_2SO_4-$AgNO_3$ media at 25°. This model involved fitting three adjustable parameters to four data points by the method of least squares: the Debye-Hückel parameters (A values) for each of the two equilibria and the value of $S_0 = (m_{Ag^+})(m_{AgSO_4^-})$ in the absence of $AgNO_3$.

We then fitted our data[2] at all temperatures by the method of least squares to each of the following models using Eq. (1) only.

Model B. The value of A is assumed to be temperature independent but ionic strength dependent.

Model C. The value of A is assumed to be constant at all temperatures and ionic strengths. A term BI is added to Eq. (1), where B is a function of temperature only.

Model D. This model is similar to model C except that both A and B were assumed to be constant at all temperatures and ionic strengths.

By a statistical analysis of the results we concluded that, on the 95% confidence level, taking the $AgSO_4^-$ complex into account does not provide a significantly better fit of the data than do models B, C, or D. However, on the 90% confidence level, taking into account the $AgSO_4^-$ ion does provide a significantly better fit of the solubility data (compared with models B, C, or D). In this connection it is to be noted that since the model based on the presence of $AgSO_4^-$ contains three adjustable parameters for four 25° data points while the other models have at the most three adjustable parameters for 24 data points from 25 to 150°, the significantly better fit on the 90% confidence level may be only apparent.

We conclude that the question of the existence of the complex $AgSO_4^-$ is still open.

[1] M. H. Lietzke and R. W. Stoughton, *J. Phys. Chem.* **63**, 1183, 1186, 1984 (1959).

[2] M. H. Lietzke and R. W. Stoughton, *J. Inorg. Nucl. Chem.* **28**, 1877 (1966).

[3] R. W. Stoughton and M. H. Lietzke, *J. Phys. Chem.* **64**, 133 (1960).

[4] M. H. Lietzke and R. W. Stoughton, *J. Phys. Chem.* (*a*) **63**, 1188 (1959); (*b*) **63**, 1190 (1959); (*c*) **65**, 2247 (1961).

[5] H. P. Hopkins, Jr., and C. A. Wulff, *J. Phys. Chem.* **69**, 9 (1965).

[6] K. Pan and J-L. Lin, *J. Chinese Chem. Soc.* (Taiwan) **6**, 1 (1959).

[7] E. C. Righellato and C. W. Davies, *Trans. Faraday Soc.* **26**, 592 (1930).

A MONTE CARLO CALCULATION OF SOME THERMODYNAMIC PROPERTIES OF STEAM USING A DIPOLE-QUADRUPOLE POTENTIAL

R. J. Beshinske[1] M. H. Lietzke

In the last 15 years a large amount of effort has been expended in calculating the thermodynamic properties of spherically symmetric molecules by simulating the behavior of an ensemble of these molecules on a high-speed computer.[2-6] No work using a nonspherical potential has been carried out, largely because of three difficulties. (1) A nonspherical potential function is computationally much more difficult than a spherical function to manipulate, and therefore much more computing time is required to evaluate each intermolecular interaction. (2) To specify the position of a molecule, two more coordinates are necessary in the nonspherical case; hence the number of coordinates in the configuration space of the system increases, and many more configurations must be generated to reach equilibrium. (3) Nearly all nonspherical potentials contain a dipole-dipole interaction term which varies as the inverse third power of the intermolecular distance. Such a slowly varying function requires consideration of the interaction of a given molecule with a much larger number of other molecules than is required in the spherical case.

We here report the results of some Monte Carlo calculations of the thermodynamic properties of steam where a nonspherical potential has been used. The results agree favorably with experiment in the region for which the constants in the potential have been fitted to second virial coefficients, thereby demonstrating that the above difficulties are surmountable.

The method that we use is closely related to that developed by Wood and Parker in dealing with a spherical potential.[3] A configuration of N molecules confined within a cube of side L and volume V is represented by N coordinate quintuplets. Three of the numbers in a given quintuplet are the spatial coordinates, x_i, y_i, z_i, of the center of the molecular potential of molecule i. The remaining two numbers are the azimuthal and polar angles, θ_i and ϕ_i, respectively, giving the orientation of the dipole moment vector of molecule i. The initial values of the coordinates are chosen using a pseudorandom number generator from a uniform distribution on the intervals $0 \leqslant x_i < L$, $0 \leqslant y_i < L$, $0 \leqslant z_i < L$, $0 \leqslant \phi_i < 2\pi$, $-1 \leqslant \cos\theta_i \leqslant 1$, where L is taken so that N/L^3 is equal to the number density of the real system being simulated.

The molecules are numbered arbitrarily from 1 to N, and new configurations are generated by moving the molecules sequentially, starting with molecule 1. A molecule is moved by changing each of its coordinates by a random amount. To increase the rate of approach to equilibrium, a limit was placed on the extent to which the molecule could change its position during the move. The spatial coordinates are restricted so that $0 \leqslant \Delta x_i \leqslant L/4$, $0 \leqslant \Delta y_i \leqslant L/4$, $0 \leqslant \Delta z_i \leqslant L/4$, where Δx_i is the change in the x_i coordinate, etc. The angles were allowed to change so that the tip of the dipole moment vector was restricted to a spherical segment of area π about its original position. As the number of configurations becomes large, the probability that a particular configuration will occur in the computer system approaches the probability of occurrence in a petit canonical ensemble, if, as was shown by Wood and Parker, the following procedure is carried out: Taking U_α as the potential energy of the αth configuration, the potential energy difference, $\Delta U_\alpha = U_\alpha - U_{\alpha-1}$, between a newly generated configuration and the

previous one is calculated. If $\Delta U_\alpha \leqslant 0$, the new configuration is allowed. If $\Delta U_\alpha > 0$, a random number R from a uniform distribution on the interval $0 \leqslant R < 1$ is generated. If $R \leqslant \exp(-\Delta U_\alpha/kT)$, where k is the Boltzmann constant and T is the absolute temperature, the new configuration is allowed; if not, the new configuration is ignored, and the system is returned to the previous configuration, which is now considered to have occurred a second time. Whether or not the move of a molecule is allowed, its successor in the ordered sequence of molecules is the next molecule to be moved. Repetition of this procedure generates a Markov chain in the configuration space of the system.

Since N is small (taken to be of the order of 100), the influence of surface effects is avoided by introducing a periodic boundary condition: A molecule is allowed to pass through the wall of the system cube, but, when this happens, it is returned to the cube at a point in the opposite wall corresponding to the exit point (e.g. if $x_i > L$, x_i is replaced by $x_i - L$). In effect, then, the system cube is one cell in an infinite three-dimensional lattice.

The intermolecular potential that we use in our calculations for water is one proposed by Rowlinson,[7]

$$\phi_{ij} = 4\epsilon[(\sigma/r_{ij})^{12} - (\sigma/r_{ij})^6 - A(\sigma/r_{ij})^3 g_{ij} - B(\sigma/r_{ij})^4 h_{ij}] , \quad (1)$$

where r_{ij} is the distance between molecule i and molecule j. The parameters ϵ, σ, A, and B have been evaluated by Rowlinson by fitting second virial coefficients calculated from Eq. (1) to experimentally derived second virial coefficients in a temperature range from 100 to 400°C. The values of these parameters are $\epsilon/k = 356$°K, $\sigma = 2.725$ Å, $A = 0.849$, and $B = 0.4625$. The first two terms in Eq. (1) represent the spherically symmetric part of the potential, assuming a Lennard-Jones relationship. Dipole-dipole interactions are represented by the third term in Eq. (1), where

$$g_{ij} = 3(\mathbf{p}_i \cdot \mathbf{R}_{ij})(\mathbf{p}_j \cdot \mathbf{R}_{ij}) - \mathbf{p}_i \cdot \mathbf{p}_j . \quad (2)$$

In this equation $\mathbf{p}_i$ is a unit vector collinear with the dipole moment of molecule i and pointing from the center of negative charge to the center of positive charge of the molecule. The vector $\mathbf{R}_{ij}$ in Eq. (2) is a unit vector pointing from molecule i to molecule j. Dipole-quadrupole interactions are represented by the fourth term in Eq. (1), where

$$h_{ij} = (1/2)[(\mathbf{p}_i \cdot \mathbf{R}_{ij}) - (\mathbf{p}_j \cdot \mathbf{R}_{ij})]\ [2(\mathbf{p}_i \cdot \mathbf{p}_j) - 5(\mathbf{p}_i \cdot \mathbf{R}_{ij})(\mathbf{p}_j \cdot \mathbf{R}_{ij}) - 1] . \quad (3)$$

The model for which Eq. (1) is an exact representation is one where the quadrupole moment tensor has cylindrical symmetry about the dipole axis. This model may be regarded as consisting of a ring of positive charge located in a plane above a single negative charge where the dimensions of the model are small compared with the intermolecular distance in the total system.[8] This model is an adequate representation of a water molecule if the molecule is considered to be rapidly spinning about an axis passing through the oxygen atom and perpendicularly bisecting a line connecting the two hydrogen atoms.

The potential energy U_α of the αth configuration of the molecules in the system cube may be calculated by summing the interactions of each of the molecules in the cube with all the molecules in a sphere of radius ρ,

$$U_\alpha = \tfrac{1}{2} \sum_i^N \sum_{\substack{j \\ i \neq j}}^{M(\rho)} \phi_{ij}(r_{ij}^{(\alpha)}), \quad (4)$$

where $r_{ij}^{(\alpha)}$ is the value of r_{ij} in the αth configuration. The interaction radius ρ is chosen to be sufficiently large so that there is negligible correlation of the molecules outside the interaction sphere with the central molecule. The range of the interaction sphere may extend beyond the system cube. A partial compensation can be made for the neglect of interactions beyond ρ by assuming a uniform distribution of molecules outside the interaction sphere and integrating the potential over this uniform distribution. In practice, however, this correction has proven negligible for the values of ρ that we have used.

Since, as the number of configurations becomes large, the distribution of computer-generated configurations approaches the distribution in a petit canonical ensemble, we can calculate values of the configurational or excess properties of our system by averaging appropriate functions over a large number of configurations. The excess internal energy is given by

$$\overline{U} = \frac{1}{K} \sum_\alpha^K U_\alpha , \quad (5)$$

where K is the number of configurations. The excess compressibility factor, the deviation of the compressibility factor from the ideal value of unity, is obtained by averaging the virial of forces,[9]

$$\frac{\overline{PV}}{\overline{RT}} - 1 = \frac{1}{K} \sum_\alpha^K \left[-\frac{1}{6NkT} \sum_i^N \sum_{\substack{j \\ i \neq j}}^{M(\rho)} r_{ij}^{(\alpha)} \frac{\partial \phi_{ij}(r_{ij}^{(\alpha)})}{\partial r_{ij}^{(\alpha)}} \right] .$$

We have thus far carried out four calculations at two temperatures and three specific volumes, 150°C and 1937 cm^3/g, 400°C and 306.5 cm^3/g, and 400°C and 26.39 cm^3/g. In all these calculations N, the number of particles per cell, is 64. The pressures under these three sets of conditions are 1, 10, and 100 bars respectively. These values were chosen because they span the temperature range used by Rowlinson to calculate the constants in Eq. (1) and because water vapor behaves nearly ideally under these conditions. The results of the calculations are summarized in Table 6.2. Run 1 was done with a maximum interaction radius equal to the cube edge length L and generated a total of 88,000 configurations. Runs 2, 3, and 4 were done with $\rho = 0.95L$ and generated 90,000 configurations. In each case the first 640 configurations were discarded to minimize the effect of the initial conditions. The approach to equilibrium was monitored by observing the excess compressibility factor as a function of the number of configurations. This is illustrated for run 1 in Fig. 6.3, where the solid line represents averages over the total number of configurations and the isolated points represent subaverages over 1600 configurations each. As can be seen, the system appears to have

Table 6.2. Monte Carlo Calculated Averages and Experimental Values for Some Thermodynamic Properties of Steam

Experimental values from ref. 10

Run No.	T (°C)	V (cm^3/g)	ρ	$(\overline{U}/\overline{RT})_{exp}$	$(\overline{U}/\overline{RT})_{calc}$	Standard Deviation
1	150	1937.	1.00L	−0.027	−0.019	0.03
2	150	1937.	0.95L	−0.027	−0.023	0.03
3	400	306.5	0.95L	−0.038	−0.034	0.03
4	400	26.39	0.95L	−0.438	−0.376	0.08

Run No.	$[(\overline{PV}/\overline{RT}) - 1]_{exp}$	$[(\overline{PV}/\overline{RT}) - 1]_{calc}$	Standard Deviation
1	−0.0081	−0.0086	0.03
2	−0.0081	−0.0071	0.02
3	−0.0134	−0.0131	0.02
4	−0.1505	−0.1343	0.13

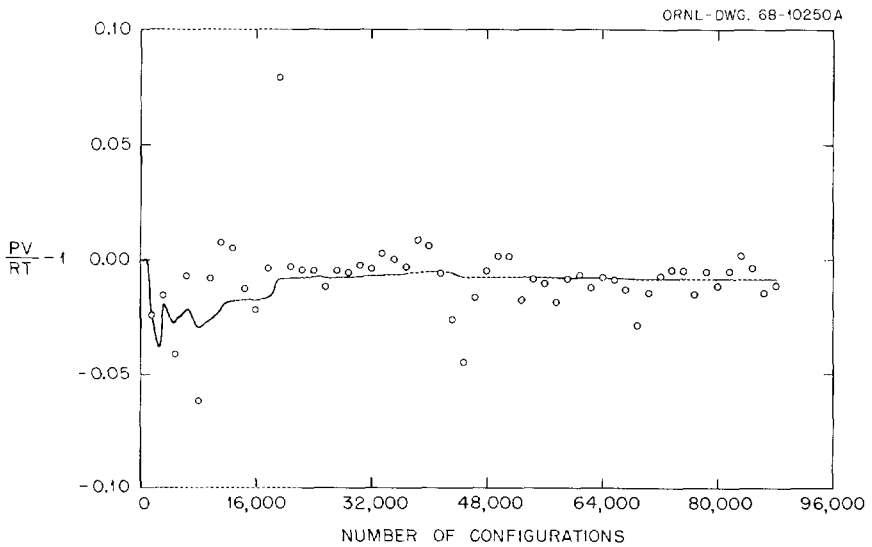

Fig. 6.3. Plot of Excess Compressibility Factor vs Number of Configurations for Run 1. The solid line represents the total average, while the circles represent subaverages over 1600 configurations.

become rather stable after ~70,000 configurations, which requires approximately 5 hr computing time on the IBM 360/75.

The standard deviations appearing in Table 6.2 were determined by calculating the root mean square of the deviations of the subaverages from the total average taken over all the configurations. From a comparison of runs 1 and 2 and from an examination of these standard deviations, the Monte Carlo averages have a precision of about one or two significant figures. To this extent, then, there is favorable agreement between the calculated and experimental[10] values of the excess internal energy and the excess compressibility factor.

---

[1] Department of Chemistry, St. John's University, Jamaica, N.Y.

[2] N. Metropolis *et al.*, *J. Chem. Phys.* **21**, 1087 (1953).

[3] W. W. Wood and F. R. Parker, *J. Chem. Phys.* **27**, 720 (1957).

[4] B. J. Alder and T. E. Wainwright, *J. Chem. Phys.* **31**, 459 (1959).

[5] A. Rahman, *Phys. Rev.* **136**, A405 (1964).

[6] I. R. McDonald and K. Singer, *J. Chem. Phys.* **47**, 4766 (1967). This article gives references to a good deal of the work that we have not cited.

[7] J. S. Rowlinson, *Trans. Faraday Soc.* **47**, 120 (1951).

[8] J. O. Hirschfelder, C. F. Curtiss, and R. S. Bird, *Molecular Theory of Gases and Liquids*, p. 225, Wiley, New York, 1954.

[9] *Ibid.*, p. 135.

[10] R. W. Bain (ed.), *Steam Tables 1964*, Her Majesty's Stationary Office, 1964.

FREE ENERGIES OF ELECTROLYTE MIXTURES

R. M. Rush G. Scatchard[1]
J. S. Johnson, Jr. Y. C. Wu[2]

During the past year, our program concerned with the free energies of multicomponent electrolyte solutions has followed three main lines: (1) additional evaluation of the osmotic and activity coefficients of binary solute mixtures of NaCl, Na_2SO_4, $MgSO_4$, and $MgCl_2$ in water, from emf as well as isopiestic measurements; (2) measurement of the osmotic coefficients in mixed perchlorate solutions; (3) application of the ion-component[3] treatment of Scatchard to the data for the mixtures mentioned in (1), an approach which promises to be more adaptable to estimates of thermodynamic properties of multicomponent systems from data on simpler systems than the method based on expansions of excess free energies in terms of ionic strength.[4]

In the process of developing the computer program for the analysis of our three-component osmotic coefficient results[4] and as a service for other investigators, we have analyzed various data in the literature. The results of this effort have been made available as a topical report.[5] This report gives parameters for the calculation of osmotic and activity coefficients for 22 aqueous mixtures of two electrolytes at 25°C and also tables of osmotic and activity coefficients for these mixtures.

Osmotic and Activity Coefficients of Binary Mixtures of NaCl, Na_2SO_4, $MgSO_4$, and $MgCl_2$ in Water at 25°C[6]

In a previous annual report[7] we discussed the isopiestic measurements made on the six binary mixtures of NaCl, Na_2SO_4, $MgSO_4$, and $MgCl_2$ in water at 25°C. We have completed analysis of the emf measurements made on the NaCl-$MgSO_4$ and Na_2SO_4-$MgCl_2$ systems. These measurements were made with a cation-sensitive glass electrode and a silver–silver chloride electrode without junction and gave values for the activity coefficient of NaCl in these mixtures. The results are shown in Figs. 6.4 and 6.5, where I is the total ionic strength.

The emf results for NaCl-$MgSO_4$ mixtures, both those obtained here and by others, are in good agreement with the results derived from the isopiestic measurements. These results suggest a linear relationship between log $\gamma_{\pm}$ and the ionic strength fractions, y (Harned's rule). This is true for log $\gamma_{\pm}$ for both components, NaCl and $MgSO_4$.

Comparison of the isopiestic and emf results for Na_2SO_4-$MgCl_2$ mixtures is more difficult by the electrolyte-component method since the emf measurements give the quantity log $\gamma_{\pm NaCl}$. With NaCl specified as a component, the system in effect contains four components, except at the two ends (trace NaCl in Na_2SO_4 or $MgCl_2$) and the midpoint (NaCl in $MgSO_4$). It is possible by this method to calculate values of log $\gamma_{\pm NaCl}$ at these three points from the isopiestic results for the NaCl-Na_2SO_4, NaCl-$MgCl_2$, and NaCl-$MgSO_4$ mixtures; these values are shown in Fig. 6.5 by square symbols. The agreement is again quite good.

Two papers describe the results for these six mixtures.[8,9]

Osmotic Coefficients of Mixed Perchlorate Solutions

The isopiestic measurements for the systems $HClO_4$-$UO_2(ClO_4)_2$-H_2O and $NaClO_4$-$UO_2(ClO_4)_2$-H_2O have been completed. The results of a preliminary analysis of the system $HClO_4$-$UO_2(ClO_4)_2$-H_2O are shown in Figs.

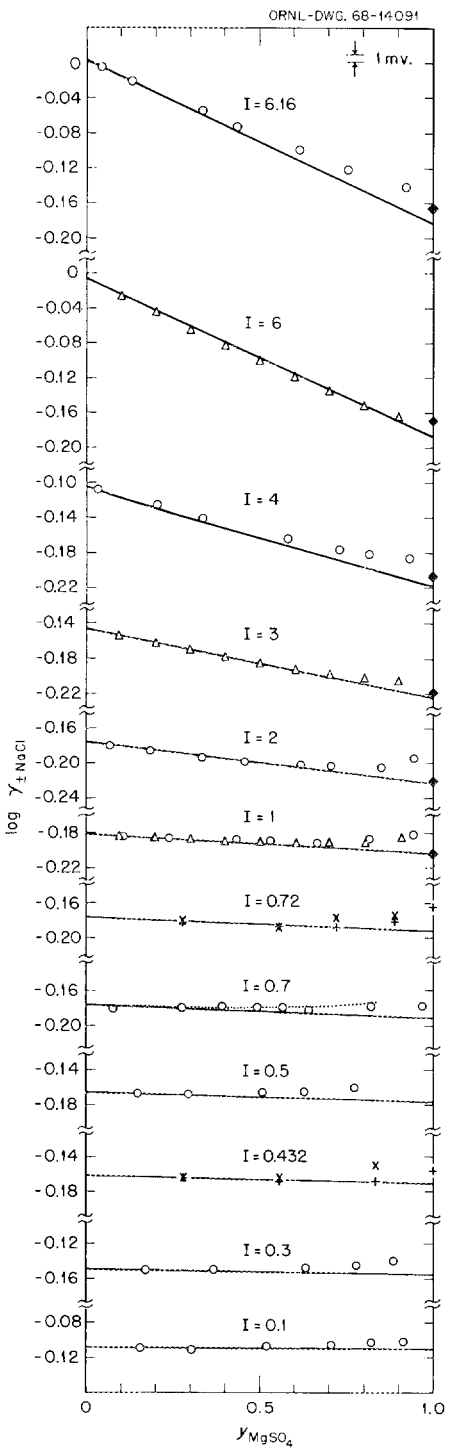

Fig. 6.4. Activity Coefficients of NaCl in $MgSO_4$. ——— , this work, isopiestic; ○, this work, emf; △, this work, emf (Lanier); . . . . . , Gieskes [*Z. Phys. Chem.* (Frankfurt) **50**, 78 (1966)]; +, Platford, isopiestic [*Can. J. Chem.* **45**, 821 (1967)]; x, Platford, emf [*Can. J. Chem.* **45**, 821 (1967)]; ◆, estimate from two-component data.

6.6 and 6.7 The osmotic coefficients obtained from the isopiestic measurements were analyzed by the Scatchard method, described previously.[4,10,11] It appears that this system can be described using only two interaction parameters: $b_{AB}^{(0,1)} = 0.0135$ and $b_{AB}^{(0,2)} = -0.00558$. (These symbols refer to the quantities designated by symbols $\beta_{AB}^{(0,1)}$ and $\beta_{AB}^{(0,2)}$, respectively, in ref. 10.) The results in Figs. 6.6 and 6.7 were calculated using these parameters and are given as values of log (γ/γ^0), where γ is the activity coefficient for the component in question in the mixed solution and γ^0 is

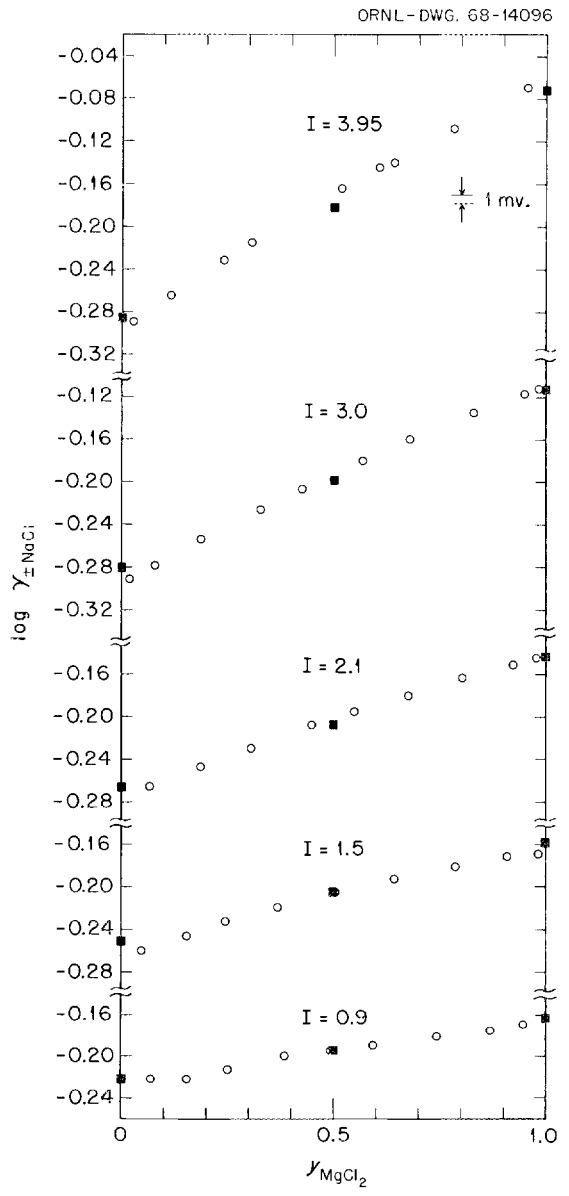

Fig. 6.5. Activity Coefficients of NaCl in the System Na_2SO_4-$MgCl_2$-H_2O. ■, values from other three-component data.

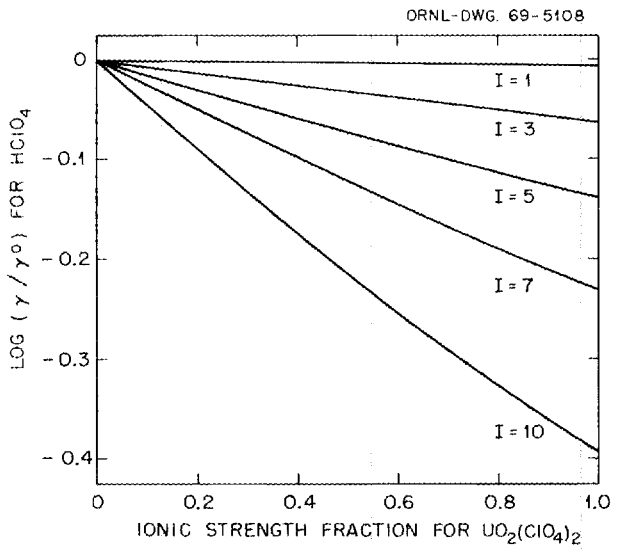

Fig. 6.6. Activity Coefficients of $HClO_4$ in the System $HClO_4$-$UO_2(ClO_4)_2$-H_2O.

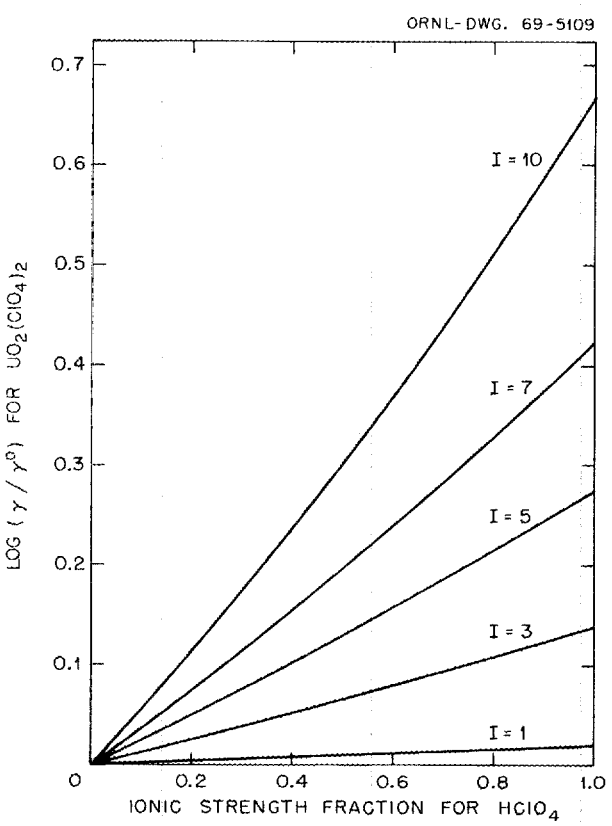

Fig. 6.7. Activity Coefficients of $UO_2(ClO_4)_2$ in the System $HClO_4$-$UO_2(ClO_4)_2$-H_2O.

the activity coefficient for the same component in a pure solution of that component at the same ionic strength. As with the 1:1 perchlorate mixtures we have previously investigated,[11] both components of this system obey Harned's rule reasonably well. Even at high concentrations the curves are close to linear; the deviation from linearity for $UO_2(ClO_4)_2$ at $I = 10$ represents a difference of 5% in $\gamma_{\pm}$.

Our results for $UO_2(ClO_4)_2$-H_2O appeared to be in poor agreement with literature values.[12] The differences in ϕ are as great as 0.08 at the higher concentrations ($I = 13$). The differences are almost negligible (0.004) at lower concentrations ($I = 2$). We rechecked the concentration of the stock $UO_2(ClO_4)_2$ by a different method (ion exchange) and found it to agree with the method previously used (precipitation and weighing as U_3O_8) to within 0.1%. However, at high $UO_2(ClO_4)_2$ concentrations, the water fraction, which is obtained by difference, is low and is therefore quite sensitive to small uncertainties in solute concentration. Since concentrations on the molal scale involve solute/solvent ratios, the effects of analytical errors are magnified at high molality. A change of 0.3% in the solute concentration of the stock solution would bring our results into agreement with those of Robinson and Lim[12] at high concentrations. The apparent differences between the two sets of data do not therefore seem serious.

Experimental work has been started on the systems $HClO_4$-$Ba(ClO_4)_2$-H_2O and $NaClO_4$-$Ba(ClO_4)_2$-H_2O. These results should provide an interesting contrast to those involving $UO_2(ClO_4)_2$. Of the 1:2 perchlorates for which osmotic coefficient data are available, these two represent the extremes in behavior: the osmotic coefficients for $UO_2(ClO_4)_2$ increase rapidly with concentration to a value of 5.2 at $I = 16.5$, while those for $Ba(ClO_4)_2$ increase much more slowly to a value of 1.9 at $I = 16.5$.

Ion-Component Treatment of Free Energy Data

Recently Scatchard has published a treatment of the excess free energies of electrolyte solutions involving the use of ions as components, with concentrations expressed in equivalents.[3] This treatment involves dividing the excess free energy into three parts: (1) that which can be determined from two-ion (single electrolyte) solutions, (2) that which can be determined from three-ion (common ion) solutions, and (3) the residue. For a system involving four ions, it is possible to estimate the excess free energy (and osmotic coefficient) from measurements on the single electro-

lytes and the appropriate mixtures involving common ions.

We have applied this treatment to our measurements on the binary mixtures involving NaCl, Na_2SO_4, $MgSO_4$, and $MgCl_2$ (see above and refs. 7–9). Parameters representing the two-ion solutions were taken from the compilation of Lietzke and Stoughton.[13] Parameters representing the three-ion solutions were derived from our data on the common-ion mixtures NaCl-Na_2SO_4, Na_2SO_4-$MgSO_4$, $MgSO_4$-$MgCl_2$, and $MgCl_2$-NaCl.[8,9] A plot of the deviations of experimental values of the osmotic coefficients for these mixtures from the values using the parameters derived by a least-squares procedure is shown in Fig. 6.8. The deviations are approximately the same as those obtained by the ionic strength method.[8] It is then possible to use these parameters to calculate the osmotic coefficients for the four-ion solutions (NaCl-$MgSO_4$ and Na_2SO_4-$MgCl_2$ mixtures). The deviations of these results from measured osmotic coefficients are shown in Fig. 6.9. It should be emphasized that the calculated results are derived only from data on two- and three-ion solutions, and data for the four-ion solutions were not used in obtaining the calculated values. The fit is reasonably good, though not as good as that obtained by directly fitting the measured values for the four-ion mixtures;[9] most of the points are within 0.003. The worst points are all for one mixture (Na_2SO_4-$MgCl_2$) at the same ionic strength fraction (0.5), and the discrepancy could be caused by an unidentified experimental or computational error.

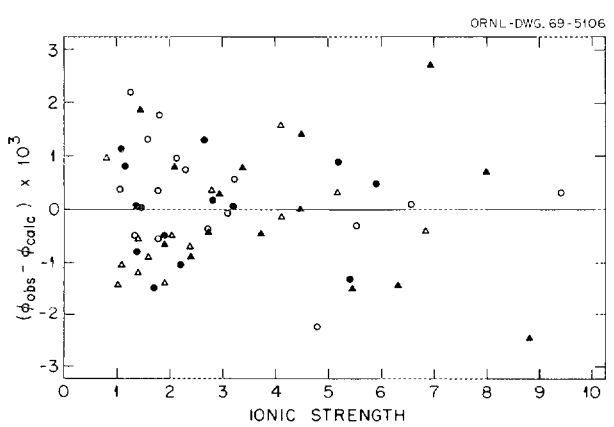

Fig. 6.8. Deviations of Osmotic Coefficients for Three-Ion Systems from Values Calculated from Least-Squares Fit. ○, NaCl-Na_2SO_4; ●, NaCl-$MgCl_2$; △, $MgCl_2$-$MgSO_4$; ▲, Na_2SO_4-$MgSO_4$.

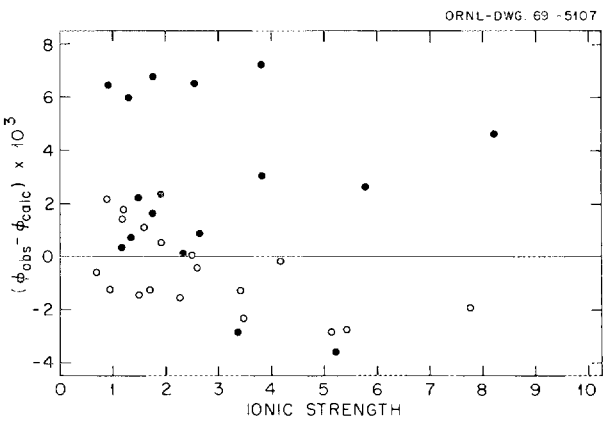

Fig. 6.9. Deviations of Osmotic Coefficients for Four-Ion Systems from Values Calculated with Parameters Derived from Three-Ion Systems. ○, NaCl-$MgSO_4$; ●, Na_2SO_4-$MgCl_2$.

In general, these results are very encouraging for the application of the ion-component treatment. We intend to extend this treatment to the calculation of activity coefficients in the four-ion mixtures.

---

[1] Consultant; Professor of Physical Chemistry, Emeritus, Massachusetts Institute of Technology, Cambridge.

[2] Present address: National Bureau of Standards, Washington, D.C.

[3] G. Scatchard, *J. Am. Chem. Soc.* 90, 3124 (1968); **91**, 2410 (1969).

[4] G. Scatchard, *J. Am. Chem. Soc.* 83, 2636 (1961).

[5] R. M. Rush, *Parameters for the Calculation of Osmotic and Activity Coefficients and Tables of These Coefficients for Twenty-Two Aqueous Mixtures of Two Electrolytes at 25°C*, ORNL-4402 (1969).

[6] Research jointly sponsored by the Office of Saline Water, U.S. Department of the Interior, and U.S. Atomic Energy Commission under contract with Union Carbide Corp. and under Contract No. AT (30-1)-905 with the Massachusetts Institute of Technology.

[7] R. M. Rush *et al.*, *Chem. Div. Ann. Progr. Rept. May 20, 1968*, ORNL-4306, p. 81.

[8] Y. C. Wu, R. M. Rush, and G. Scatchard, *J. Phys. Chem.* **72**, 4048 (1968).

[9] Y. C. Wu, R. M. Rush, and G. Scatchard, *J. Phys. Chem.*, in press.

[10] R. M. Rush and J. S. Johnson, *Chem. Div. Ann. Progr. Rept. May 20, 1967*, ORNL-4164, p. 64.

[11] R. M. Rush and J. S. Johnson, *J. Phys. Chem.* **72**, 767 (1968).

[12] R. A. Robinson and C. K. Lim, *J. Chem. Soc.* **1951**, 1840.

[13] M. H. Lietzke and R. W. Stoughton, *J. Phys. Chem.* **66**, 508 (1962).

APPARENT MOLAL VOLUMES OF THE LITHIUM AND SODIUM HALIDES. CRITICAL-TYPE TRANSITIONS IN AQUEOUS SOLUTION[1]

Fred Vaslow

Measurements of the apparent molal volumes of LiCl, LiBr, LiI, NaCl, NaBr, and NaI have been made, with primary emphasis on obtaining precise values of $\Delta\phi_v/\Delta\sqrt{c}$ at small intervals. Most results were at 25°, a few at 5°, and one at 35°. For LiBr, LiI, NaBr, and NaI, the curves of $\Delta\phi_v/\Delta\sqrt{c}$ vs $\sqrt{c}$ appear to be discontinuous, in a form suggesting a λ-shaped region for the integral curve or inverted for NaBr. Different series of measurements with LiI gave the apparent discontinuity at different concentrations, and one of the four LiI runs did not show the apparent discontinuity. For NaCl the existence of a singularity is not definite, and LiCl showed no sign of a singularity.

It is suggested that these singularities are due to a new kind of transition of the critical type in the solution. Two possible sources of the transition are either a change of solution structure as previously suggested[2] or a change in form of the ion radial distribution function as found by Kirkwood.[3]

---

[1] Abstract of paper to be published in *J. Phys. Chem.*

[2] F. Vaslow, *J. Phys. Chem.* 70, 2286 (1966).

[3] J. G. Kirkwood, *Chem. Rev.* 19, 275 (1936).

MISCIBILITY IN THE SYSTEM PYRIDINE–SULFURIC ACID–WATER[1]

J. Csurny R. J. Raridon

During the study of the activity coefficients of salts in pyridine-water-acid mixtures,[2] it was observed that some pyridine-H_2SO_4-H_2O mixtures gave two-phase systems. A brief study was undertaken to determine the phase diagram of this system. The experimental method was similar to that used previously for the glycerol triacetate–water–salt systems.[3] A mixture of two components (pyridine-H_2SO_4 or pyridine-H_2O) was

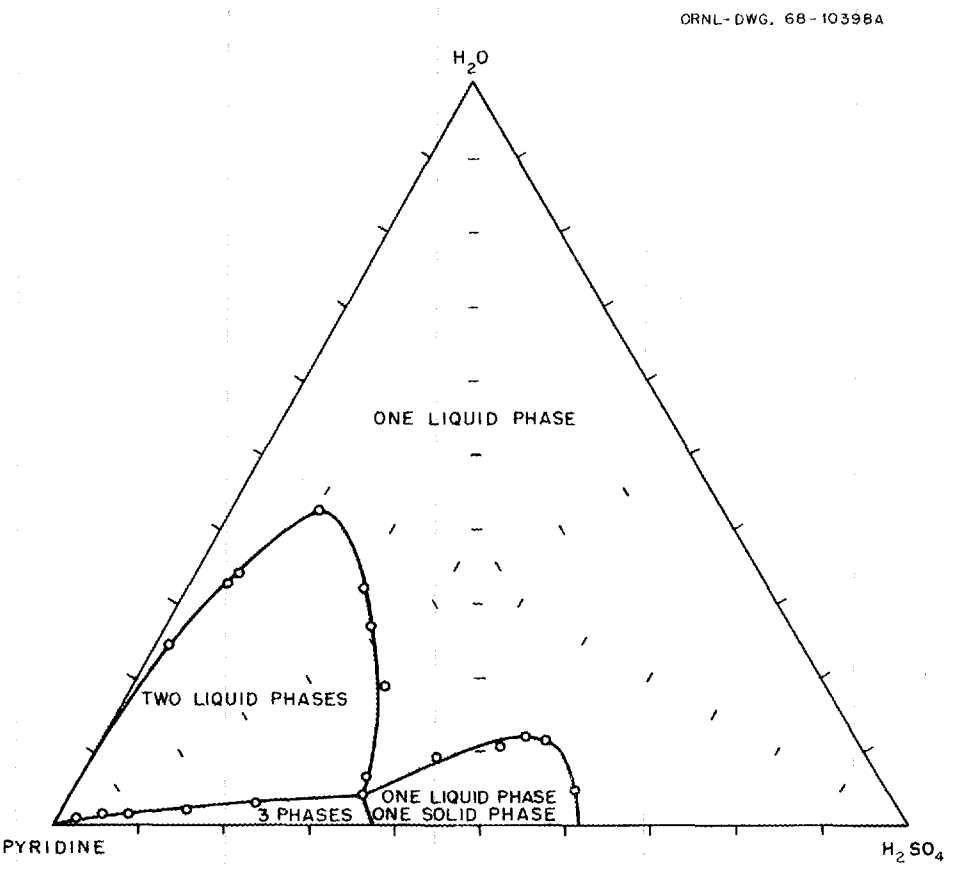

Fig. 6.10. Miscibility in the System Pyridine-H_2SO_4-H_2O at 25°C.

prepared by weight in a flask, and then the third component was added dropwise while the mixture was stirred in a water bath kept at 25°C. When a phase change was observed, the flask was reweighed and the composition of the mixture computed.

The results are shown in Fig. 6.10. Although one liquid phase characterizes most of the system, there is a region where two liquid phases are present. Another region is characterized by a liquid phase and a solid phase; the solid phase had a ratio of two pyridines to one sulfate; that is, it was pyridinium sulfate. There is also a small region where three phases are present, two liquid phases and solid pyridinium sulfate.

---

[1] Work sponsored by the Office of Saline Water.

[2] *Chem. Div. Ann. Progr. Rept. May 20, 1968,* ORNL-4306, p. 97.

[3] R. J. Raridon and K. A. Kraus, *J. Colloid Sci.* **20**, 1000 (1965).

ACTIVITY COEFFICIENTS OF NaCl AT SATURATION IN WATER MIXTURES OF POLYGLYCOLS AND POLYGLYCOL ETHERS AT 50°C[1]

W. H. Baldwin R. J. Raridon
K. A. Kraus

The effect of chain length and functional end groups on the activity coefficient of NaCl in water mixtures of organic compounds has been studied in three homologous series: ethylene glycol and polyethylene glycols, methoxyethanol (methyl Cellosolve) and methoxypolyethylene glycols, and ethylene glycol dimethyl ether and methylated products of polyethylene glycol.

The solubility of NaCl was measured in the organic-water mixtures listed in Table 6.3 using the packed column technique previously described.[2] The results for the different compounds can be compared in terms of an activity coefficient ratio, $\Gamma^* = \gamma_{\pm}^*/\gamma_{\pm}$, where the activity coefficient in the mixed solvent, $\gamma_{\pm}^*$, is computed on the same basis as that in water ($\gamma_{\pm}$), namely, by using the same standard state as in water and expressing concentrations in moles per kilogram of water. Γ^* thus measures the relative selectivity of the medium for salt and water.

If s_{aq} is the solubility in pure water and s_o is the solubility in the water-organic mixture, both expressed in moles per kilogram of solvent, and f_w is the fractional water content of the solvent (kilograms of H_2O per kilogram of solvent), Γ^* is given by

$$\Gamma^* = \gamma_{\pm}^*/\gamma_{\pm} = s_{aq} f_w / s_o \ .$$

Table 6.3. Organic Compounds Studied

Glycols – $HO(CH_2CH_2O)_nH$
Ethylene glycol (EG)
Polyethylene glycol (PEG) – molecular weights 200, 300, 400, 600, and 1000
Monomethyl ethers of glycols – $CH_3O(CH_2CH_2O)_nH$
Ethylene glycol monomethyl ether (EGMME) (methyl Cellosolve)
Diethylene glycol monomethyl ether (DEGMME) (methyl Carbitol)
Polyethylene glycol monomethyl ether (PEGMME) – molecular weights 350 and 750
Dimethyl ethers of glycols – $CH_3O(CH_2CH_2O)_nCH_3$
Ethylene glycol dimethyl ether (EGDME)
Diethylene glycol dimethyl ether (DEGDME)
Triethylene glycol dimethyl ether (TEGDME)
Tetraethylene glycol dimethyl ether (TetEGDME)
Polyethylene glycol dimethyl ether (PEGDME) molecular weights 260, 580, 850, 1230

The value of Γ^* as a function of water content for glycol and polyethylene glycols of different molecular weights is shown in Fig. 6.11. At any given water content Γ^* increases with increasing molecular weight, although the change is small for $f_w > 0.5$. Maxima are observed for EG and PEG 400 and are implied for PEG 200 and 300 for $f_w > 0.10$. Since Γ^* must approach zero as f_w goes to zero, maxima are also implied for PEG 600 and 1000, for $f_w < 0.05$ (i.e., between 95 to 100% organic). Although measurements were not made for PEG 200, 300, and 600 for $f_w > 0.10$, Γ^* values, and hence solubilities, could be estimated for this range with a fair degree of accuracy.

Figure 6.12 shows similar data for the monoethers and diethers. Except for EGMME and DEBMME, the maximum values of Γ^* lie between $f_w = 0$ and 0.05.

The Γ^* values at 5% water for all the compounds are replotted in Fig. 6.13 against the reciprocal of the molecular weight. A reasonably smooth curve can be drawn through the points for each series. The three curves are far apart at low molecular weights but seem to converge to a single point as the molecular weight approaches infinity. At high molecular weights the end groups become less important relative to the long chains of $-CH_2CH_2O-$ groups. One would therefore predict that an infinitely long chain (or film) composed of $-CH_2CH_2O-$ groups and containing 5% water would have a value for Γ^* for NaCl (if it could be measured) of *ca.* 20. Similar extrapolations at 10 and 15% water yield Γ^* values of 6 and 3.5 respectively. These extrapolated values are plotted in Fig 6.14. For

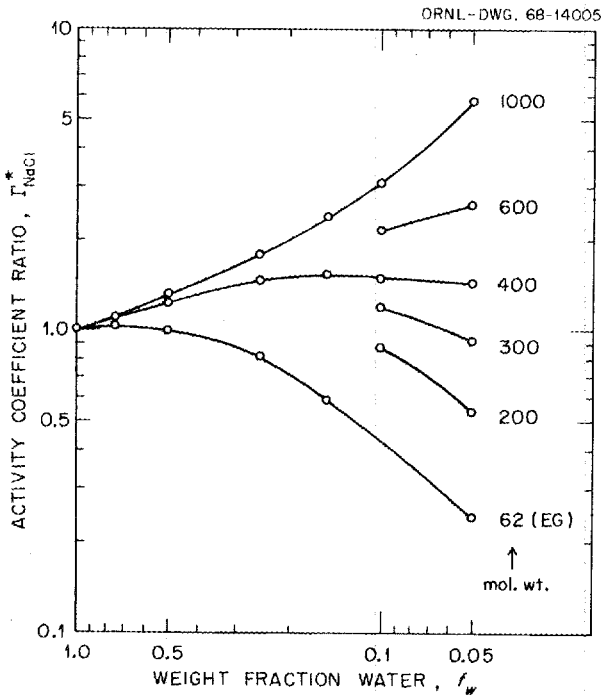

Fig. 6.11. Activity Coefficient Ratios of NaCl at Saturation in Aqueous Solutions of Ethylene Glycol and Polyglycols at 50°C.

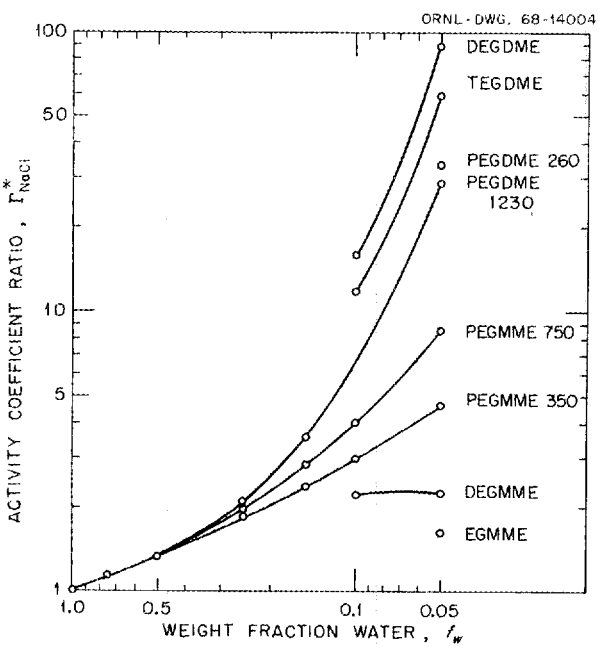

Fig. 6.12. Activity Coefficient Ratios of NaCl at Saturation in Aqueous Solutions of Some Glycol Monomethyl and Dimethyl Ethers at 50°C.

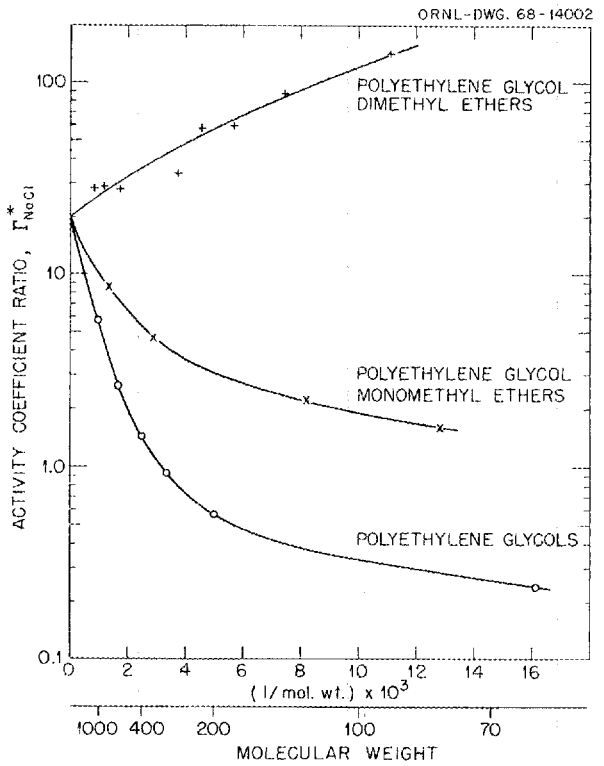

Fig. 6.13. Activity Coefficient Ratios at 50°C of NaCl at Saturation in Solutions of Polyglycols and Polyglycol Ethers Containing 5% Water.

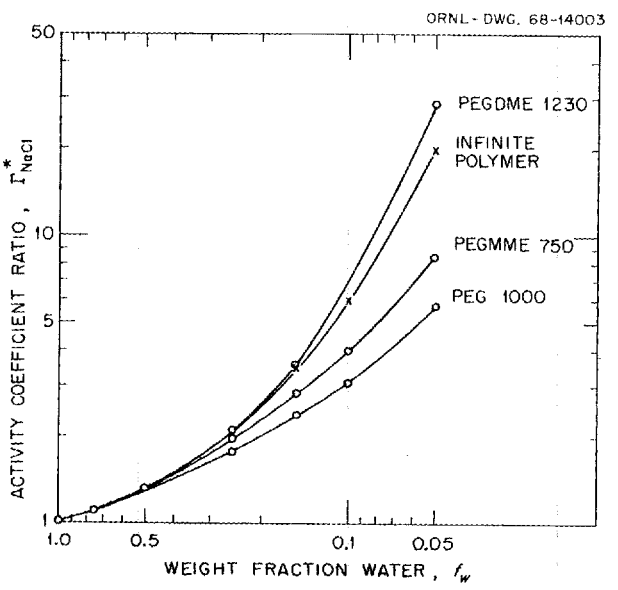

Fig. 6.14. Estimation of NaCl Activity Coefficient Ratio at 50° for Polyethers.

comparison the figure also gives values of Γ^* for a high-molecular-weight dimethyl ether (PEGDME 1230), a monomethyl ether (PEGMME 750), and PEG 1000. The extrapolated values are between those for the monomethyl and dimethyl ethers and relatively close to the latter. For $f_w > 0.15$, Γ^* for the dimethyl ether is probably a good approximation for Γ^* in the infinite polymer.

Knowledge of activity coefficients allows one to calculate the minimum salt rejection by a hyperfiltration membrane based on this infinite polymer. The limiting salt rejection $\mathbf{R}_\infty$ of a membrane at sufficiently high fluxes of water through it is related to a distribution coefficient D^* at the entrance interface by[3]

$$\mathbf{R}_\infty = 1 - \beta D^* .$$

Here β is a coupling coefficient which is presumed to be usually between 0 and 1. The distribution coefficient (for uncharged membranes) is in turn related to the activity coefficient ratio by $D^* = 1/\Gamma^*$. A minimum value of $\mathbf{R}_\infty$ is obtained for $\beta = 1$, where

$$\mathbf{R}_\infty = 1 - 1/\Gamma^* .$$

An infinite polyether membrane containing 25% water ($\Gamma^* \approx 2$) would therefore correspond to $\mathbf{R}_\infty = 0.5$, or a minimum salt rejection of 50%.

---

[1] Work sponsored by the Office of Saline Water.

[2] K. A. Kraus, R. J. Raridon, and W. H. Baldwin, *J. Am. Chem. Soc.* **86**, 2571 (1964).

[3] J. S. Johnson, L. Dresner, and K. A. Kraus in *Principles of Desalination*, K. S. Spiegler, ed., Academic, New York, 1966.

PROPERTIES OF SEPHADEX QUATERNARY AMINE ANION EXCHANGERS

F. Nelson D. C. Michelson

As part of the continuing study of ion exchange materials, some properties of a new quaternary amine anion exchanger were investigated. Column separations of weakly adsorbed elements from more strongly adsorbed ones were carried out. In addition, activity coefficients and distribution coefficients of various salts were determined, and bed volumes of the material were measured in various salt solutions.

The material, designated QAE Sephadex (Pharmacia Fine Chemicals, Uppsala, Sweden), has an aliphatic network containing diethyl-2-hydroxypropylaminoethyl groups as the active exchange sites. This material presumably was designed primarily for separations of high-molecular-weight biochemical substances and hence has a relatively high water content in aqueous solution, in contrast to the moderately cross-linked polystyrene–divinylbenzene resins normally used in chromatographic applications. Two Sephadex preparations in bead form (40 to 120 μ in diameter, dry) and of different water contents (porosities) were studied. They were designated as A-25 and A-50 and had capacities of 3.1 and 3.2 meq per gram of dry resin (chloride form) respectively.

The bed volumes of Sephadex A-25 and A-50 were measured in LiCl solutions as a function of ionic strength. The results are plotted in Fig. 6.15 together with similar data for a Dowex 1 resin cross-linked with 1% divinylbenzene and having approximately the same capacity (2.9 meq per dry gram, Cl^- form). Bed volumes decrease greatly with increasing electrolyte concentration up to about 1 *m* LiCl. At higher concentrations, the bed volume for A-25 remains essentially constant, paralleling the behavior for Dowex 1-X1, while the bed volume for A-50 exhibits a minimum near 2 *m* LiCl and then increases with increasing LiCl concentration.

The bed volume of Sephadex A-50 was measured in solutions of NaCl, Na_2SO_4, and $K_3Fe(CN)_6$, examples

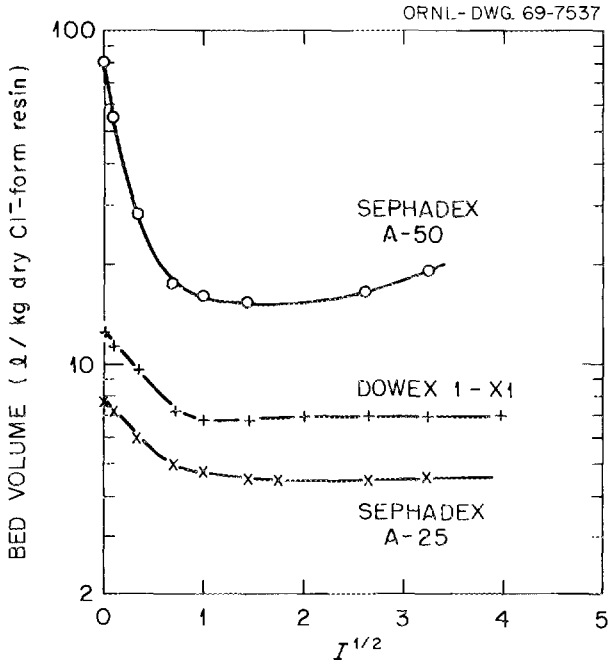

Fig. 6.15. Bed Volume of Various Resins in LiCl Solutions (25°C).

of 1:1, 1:2, and 1:3 electrolytes. The results are shown in Fig. 6.16. Apparently $Fe(CN)_6^{3-}$ is adsorbed strongly by the resin, contracting the network, as evidenced by the rapid decrease in bed volume at low ionic strengths. After contraction, the bed volume changes only slightly with increasing concentration [>0.01 *m* $K_3Fe(CN)_6$]. Bed volumes of A-50 in NaCl and Na_2SO_4 solutions decrease considerably at first with increasing ionic strength but change only slightly at higher concentrations. Up to *ca.* 2 *m*, volumes for NaCl and LiCl beds are very similar. As observed earlier with Dowex 1 resins,[1] the sulfate form of Sephadex A-50 in sulfate solutions has a higher bed volume per unit weight than the chloride form in chloride solutions.

Activity coefficients of NaCl in Sephadex A-25 and of Na_2SO_4 in A-50 were determined by the centrifugation method described earlier[1] and are given in Table 6.4. The activity coefficient ratios, $\Gamma = \gamma_{\pm NaCl(r)}/\gamma_{\pm NaCl}$ and $\gamma_{\pm Na_2SO_4(r)}/\gamma_{\pm Na_2SO_4}$, are not far from unity over a wide range of electrolyte concentrations. As with Dowex 1 resins, exclusion of the salts occurs at low aqueous phase electrolyte concentrations.

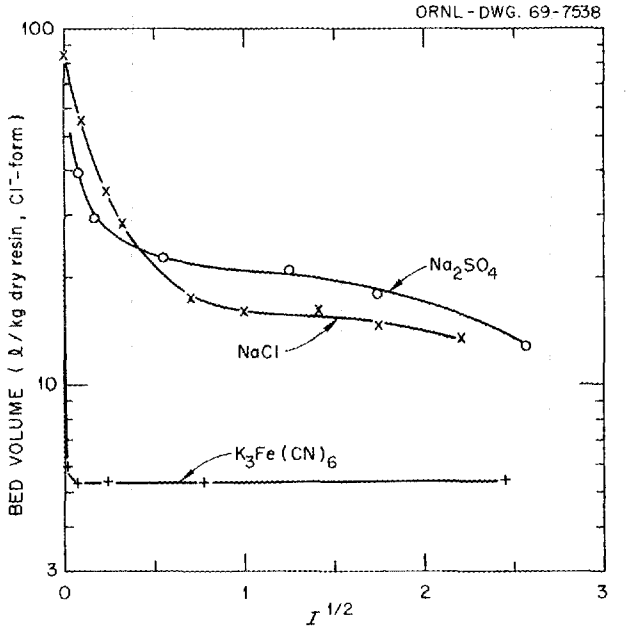

Fig. 6.16. Bed Volume of Sephadex A-50 in NaCl, Na_2SO_4, and $K_3Fe(CN)_6$ Solutions (25°C).

Table 6.4. Activity Coefficients of NaCl and Na_2SO_4

A. NaCl in Sephadex Z-25

m_{NaCl}	$m_{NaCl(r)}$	$m_{Cl(r)}$	$\frac{kg\ H_2O}{kg\ resin}$	$\Gamma = \frac{\gamma_{\pm NaCl(r)}}{\gamma_{\pm NaCl}}$
0.001	0.000013	0.97	3.22	0.28
0.01	0.00062	1.15	2.70	0.37
0.103	0.031	1.39	2.28	0.50
1.00	0.73	2.22	2.08	0.78
5.31	5.1	7.15	1.51	0.88

B. NaCl in Dowex 1-X1

m_{NaCl}	$m_{NaCl(r)}$	$m_{Cl(r)}$	$\frac{kg\ H_2O}{kg\ resin}$	$\Gamma = \frac{\gamma_{\pm NaCl(r)}}{\gamma_{\pm NaCl}}$
0.002	0.000043	0.73	3.97	0.36
0.025	0.0028	0.81	3.61	0.53
0.10	0.0365	1.03	2.93	0.53
1.00	0.816	2.48	1.74	0.79

C. Na_2SO_4 in Sephadex A-50

$m_{Na_2SO_4}$	$m_{Na_2SO_4(r)}$	$m_{SO_4(r)}$	$\frac{kg\ H_2O}{kg\ resin}$	$\Gamma = \frac{\gamma_{\pm Na_2SO_4(r)}}{\gamma_{\pm Na_2SO_4}}$
0.002	0.00069	0.074	21.9	0.38
0.01	0.0063	0.107	15.2	0.39
0.1	0.090	0.224	11.4	0.52
2.0	1.57	1.88	5.0	0.97

Distribution coefficients, D (amount per kilogram of resin/amount per liter of solution), were measured for several elements on Sephadex resins in NaCl solutions containing 0.01 to 0.1 M HCl. The adsorption functions were found to have, as expected, shapes similar to those obtained with Dowex 1 resins. Results for one of the elements studied, Au(III), at trace concentrations in NaCl solutions (containing 0.05 M HCl) are shown in Fig. 6.17. The distribution coefficient is at a minimum near 1 M NaCl for both A-25 and A-50. The adsorbability of Au(III) is lower for A-50 than for A-25, an order that is not surprising since A-50 has a higher water content.

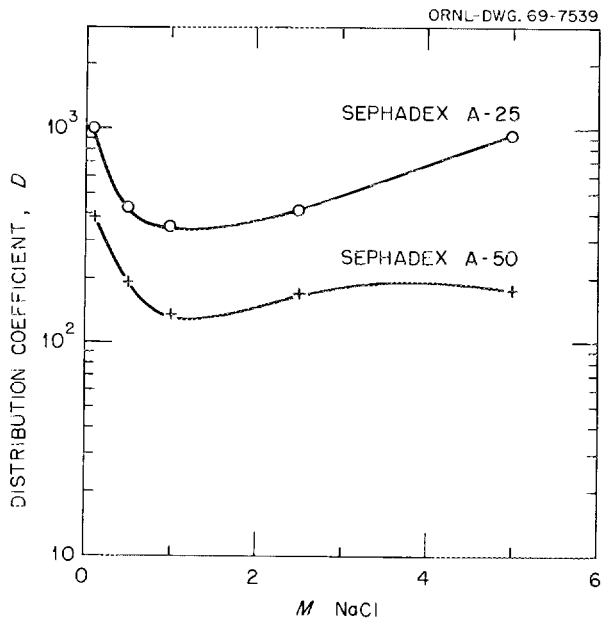

Fig. 6.17. Adsorption of Au(III) By Sephadex Resins in NaCl–0.05 M HCl Solutions (25°C).

Table 6.5. Adsorbabilities of Some Elements by QAE Sephadex (A-25) in 5 M NaCl Solutions Containing 0.01 to 0.1 M HCl

Element	Distribution Coefficient, D
Au(III)	920
Pt(IV)	>>10
Zn(II)	42
Cd(II)	~40
Fe(III)	7
Eu(III)	4
U(VI)	13

Distribution coefficients for several other elements in 5 M NaCl containing 0.01 to 0.1 M HCl are summarized in Table 6.5.

A number of separations of moderately or strongly adsorbed elements from weakly adsorbed elements were carried out with Sephadex A-25 columns using slightly acidified NaCl solutions. The fact that Sephadex resins are unstable in strong acids is useful in some separations involving adsorption and concentration of strongly adsorbed elements (e.g., Au(III), Pt(IV), etc.) from brine solutions. After the concentration step, the column can be treated with a small amount of dilute HCl (0.01 to 0.1 M) to remove excess NaCl. Concentrated HCl is then added and the flow stopped. After 20 to 30 min at 25°C, the column "dissolves," and the adsorbed metals are recovered in a relatively small volume of liquid. Spectrographic analysis for adsorbed metals could presumably be performed directly on the concentrated HCl–Sephadex solution.

[1] F. Nelson and K. A. Kraus, *J. Am. Chem. Soc.* 80, 4154 (1958).

DIFFUSION STUDIES[1]

H. O. Phillips S. B. Sachs[2]
K. A. Kraus

As part of our studies on diffusion in aqueous solutions, the radiometric porous frit method[3] has been adapted for measurements at temperatures from 15 to 85°C. Mainly this has consisted in insulating the reservoir and tubing through which the solution passes. The temperature can be controlled to better than ±0.4° at 85°. Measurements have been made of half-times (τ_d) for Na^+ ion removal from a gold frit in 0.05, 0.10, and 1.0 m NaCl solutions at several temperatures from 15 to 85°. The half-times decreased by a factor of 4 over this temperature range. Self-diffusion coefficients, $\mathcal{D}$, are inversely proportional to the τ_d values, the proportionality constant being the frit calibration factor. To determine whether this factor changes significantly with temperature, the diffusion coefficient data were compared with values calculated by means of the Nernst equation using limiting conductance data for the sodium ion (Fig. 6.18). The ordinate in the figure gives the product of the diffusion coefficient and the viscosity, η, normalized to 25°. The normalized results for Na^+ diffusion closely approximate those calculated from the conductance data, showing that the frit calibration factor is constant, within the still relatively large experimental error.

The self-diffusion coefficients of Na^+ were measured in aqueous solutions of ethylene glycol (EG) and of polyethylene glycol (PEG) over the temperature range 15 to 85°C. The NaCl concentration was 0.1 *m* in all solutions. The results for EG-H_2O mixtures are given in Table 6.6, together with the viscosities of these mixtures. Although the values of $\mathcal{D}$ and η vary widely, the $\mathcal{D}\eta$ products do not change greatly with either temperature or composition. Similar data are given in Table 6.7 for PEG-H_2O mixtures. For these mixtures, however, the $\mathcal{D}\eta$ products are not constant with either temperature or composition.

The results for EG-H_2O and PEG-H_2O mixtures are plotted in Figs. 6.19 and 6.20 as log $\mathcal{D}/\mathcal{D}_{aq}$ ($\mathcal{D}_{aq} = \mathcal{D}$ at f_v = 1.00) vs log f_v. Assuming a linear relationship at high water contents for all temperatures, as seems to be the case at 25°, the slopes $d \log (\mathcal{D}/\mathcal{D}_{aq})/d \log f_v$ for these mixtures decrease with increasing temperature, from *ca.* 1.8 at 15° to 1.0 at 85° for the EG mixtures. The corresponding values for PEG mixtures are 3.8 at 15° and 2.3 at 85°, more than a factor of 2 higher than for EG mixtures. At low water contents the slopes for the EG mixtures are less.

The heat of activation ΔH^* of self-diffusion can be estimated from the data by plotting log $(\mathcal{D}/T)$ vs $(1/T)$ at constant f_v and then measuring the slope of the resulting curve. For EG-H_2O mixtures the curves for various water contents are nearly straight lines, while for the PEG-H_2O mixtures, considerable curvature results. Values for ΔH^* at 25° range from 3.3 kcal at f_v

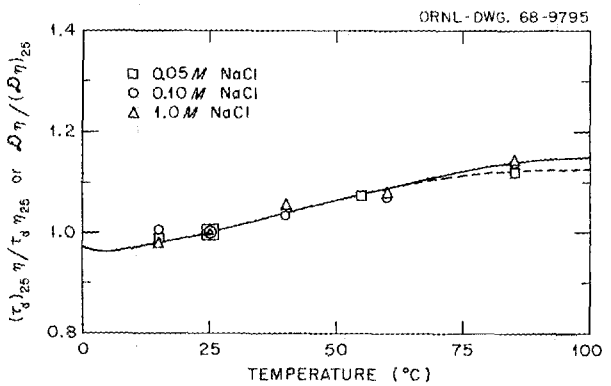

Fig. 6.18. Self-Diffusion Coefficients of Na^+ by the Porous Frit Method as a Function of Temperature. Solid line, Nernst equation; dashed line, Onsager correction (0.1 *M* NaCl).

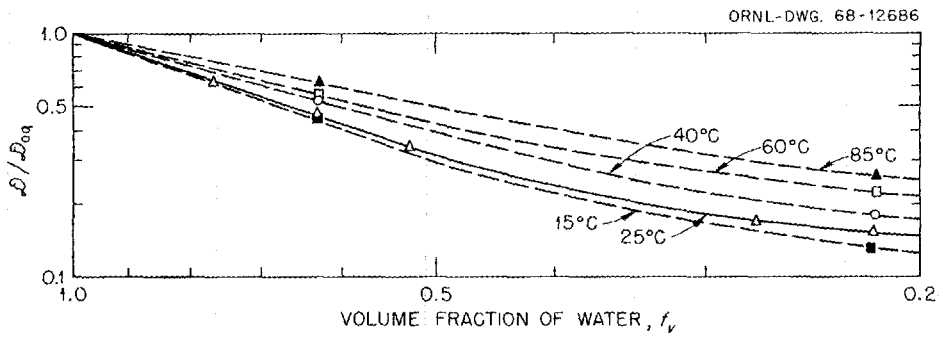

Fig. 6.19. Self-Diffusion Coefficients $\mathcal{D}$ of Na^+ in Ethylene Glycol–Water Mixtures.

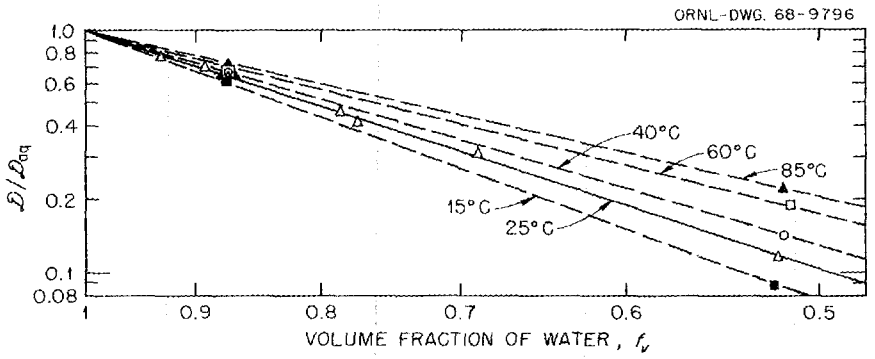

Fig. 6.20. Self-Diffusion Coefficients $\mathcal{D}$ of Na^+ in Polyethylene Glycol–Water Mixtures.

Table 6.6. $\mathcal{D}$, η, and $\mathcal{D}\eta$ for EG-H_2O Mixtures as a Function of Temperature and Volume Fraction of Water (f_v)

f_v	15°	25°	40°	60°	85°
			$\mathcal{D} \times 10^6$ (cm²/sec)		
1.00	10.0	12.8	17.8	25.8	38.2
0.63	4.43	5.93	9.38	14.3	23.6
0.22	1.32	1.94	3.20	5.78	10.0
0	0.54	0.82	1.43	2.84	5.07
			η (centipoises)		
1.00	1.146	0.898	0.660	0.472	0.339
0.63	3.372	2.463	1.639	1.072	0.699
0.22	12.81	8.228	5.017	2.902	1.700
0	27.41	17.54	9.916	5.323	2.893
			$\mathcal{D}\eta \times 10^5$		
1.00	1.15	1.15	1.17	1.22	1.29
0.63	1.49	1.46	1.54	1.54	1.65
0.22	1.69	1.60	1.61	1.68	1.70
0	1.47	1.44	1.42	1.51	1.47

Table 6.7. $\mathcal{D}$, η, and $\mathcal{D}\eta$ for PEG-H_2O Mixtures as a Function of Temperature and Volume Fraction of Water (f_v)

f_v	15°	25°	40°	60°	85°
			$\mathcal{D} \times 10^6$ (cm²/sec)		
0.87	6.16	8.47	12.1	17.3	26.0
0.52	0.88	1.47	2.52	5.07	8.39
			η (centipoises)		
0.87	68.7	44.5	24.8	12.8	6.14
0.52	108.	54.9	24.8	11.2	6.29
			$\mathcal{D}\eta \times 10^6$		
0.87	423	377	299	221	160
0.52	94.9	80.7	62.6	57.0	52.8

= 1 to 6.5 kcal at $f_v = 0$ for EG solutions, and from 4.7 kcal at $f_v = 0.87$ to 7.4 kcal at $f_v = 0.52$ for PEG solutions.

[1] Work cosponsored by the Office of Saline Water.

[2] Guest Scientist from the Weizmann Institute, Rehovoth, Israel.

[3] A. E. Marcinkowsky, F. Nelson, and K. A. Kraus, *J. Phys. Chem.* **69**, 303 (1965).

HYPERFILTRATION WITH DYNAMICALLY FORMED MEMBRANES[1]

J. N. Baird[2]
W. H. Baldwin
J. Csurny
J. A. Dahlheimer[3]
Ellen Elliott[4]
Neva Harrison
C. E. Higgins
J. S. Johnson
K. A. Kraus[5]
J. R. Love[3]
D. C. Michelson
H. O. Phillips
R. M. Rush
S. B. Sachs[6]
A. J. Shor[7]
Warren Sisson[8]
C. G. West
C. G. Westmoreland

The part of the Water Research Program dealing with separations processes remained primarily concerned with salt-filtering properties of layers dynamically formed on porous bodies from materials added to (or already in) feed solutions. Although we continue fundamental studies of membrane transport, there has been a gradual shift of emphasis toward finding membranes and supports of possible usefulness in desalination and pollution control.

Transport Through Ion Exchange Membranes Under Pressure as Driving Force

Test of Equations for Salt Rejection as a Function of Flux. – In last year's report,[9] salt rejections as a function of concentration and charge type of solute,

$$\mathbf{R} = 1 - (m_\omega/m_\alpha) \tag{1}$$

(m_α is the molality of solution in contact with the high-pressure or feed interface α of the membrane, and m_ω is the molality of effluent) were correlated with predictions based on equilibrium distribution of electrolyte between solution and ion exchange phases. The membrane used was dynamically formed of hydrous Zr(IV) oxide and was maintained in anion exchange form by control of feed acidity. For such a test it was necessary that rejections be measured with flux through the membrane high enough for attainment of the maximum rejection[10] of which the membranes are capable, $\mathbf{R}_\infty$. Under this condition, rejection is related to the distribution between solution and membrane by the equation

$$\mathbf{R}_\infty = 1 - \beta D_\alpha^* , \tag{2}$$

where β is the coefficient relating solvent and salt flux and

$$D_\alpha^* = m_\alpha^*/m_\alpha , \tag{3}$$

the asterisk indicating concentration in the membrane phase in moles per kilogram of water.

The phenomenological analysis of hyperfiltration in ref. 10 dealt with neutral membranes, but we have since extended it to ion exchange membranes. The principal difference is that with neutral membranes, the chemical potential gradient of the solute with distance through the membrane, $d\mu_2/dx$, is given by the equation

$$\frac{1}{RT}\frac{d\mu_2}{dx} = \nu\frac{d\ln m^*}{dx} + \nu\frac{d\ln \gamma_\pm^*}{dx}, \tag{4}$$

while for ion exchange membranes it is given by

$$\frac{1}{RT}\frac{d\mu_2}{dx} = \frac{d\ln m^*}{dx} + \frac{(\nu-1)\,d\ln\,[C^* + (\nu-1)m^*]}{dx} + \nu\frac{d\ln\gamma_\pm^*}{dx}, \tag{5}$$

where C^* is the ion exchange capacity in equivalents per kilogram of water, ν is the number of moles of ions per mole of salt, $\gamma_\pm^*$ is the activity coefficient of salt in the membrane phase, R is the gas constant, and T is the absolute temperature. Insertion of the salt chemical potential gradient appropriate for an ion exchanger into the Onsager-type equations for flux of salt and water and integration through the membrane yields

$$\frac{J_1 l}{\mathcal{D}_2^{f*}} = \left[\frac{1}{\nu\beta} + \frac{(\nu-1)^2\, m_\omega}{\nu\beta[m_\omega(\nu-1)+C^*\beta]}\right] \times \ln\frac{1-\beta D_\omega^*}{1-\beta D_\alpha^*/(1-\mathbf{R})} + \frac{(\nu-1)C^*}{\nu[m_\omega(\nu-1)+C^*\beta]} \times \ln\left[\frac{C^*+(\nu-1)\,D_\omega^* m_\omega}{C^*+(\nu-1)\,D_\alpha^* m_\alpha}\right], \tag{6}$$

J_1 being the flux of solvent in kilograms of H_2O per square centimeter per second; l, the membrane thickness; and $\mathcal{D}_2^{f*}$, the diffusion coefficient of salt in the membrane expressed in units appropriate to the molality concentration scale. In the integration the activity coefficient, $\gamma_\pm^*$, was assumed constant; this assumption should be reasonable, at least for low m^*, since capacity and counterions will make the dominant contribution to ionic strength, which will thus be relatively constant with x. Equation (6) at high J_1 leads to the same limiting rejection as given by Eq. (2), which was originally derived for neutral membranes.

Since with dynamically formed membranes, direct measurements of thickness, diffusion coefficients, and capacity are not possible, tests of equations of necessity involve finding whether or not experimental observations made for a range of conditions can be represented by single values of key parameters. Figure 6.21 presents NaCl rejections by a hydrous Zr(IV) oxide membrane as a function of flux for two NaCl concentrations. From the rejections at high flux for these and many other NaCl, as well as $MgCl_2$, concentrations, we earlier concluded[9,11] that for this membrane, the coupling coefficient β was, to a good approximation, 1 and the capacity was 0.45 equivalent per kilogram of water in the membrane. In Eq. (6), C^*, D^*, m_α, m_ω, and $\mathbf{R}$ are related, and the test of the equation is to see if a single value of the ratio $l/\mathcal{D}_2^{f*}$ would give calculated rejections consistent with experiment. The curves calculated for $l/\mathcal{D}_2^{f*} = 2.92 \times 10^5$ (obtained from a nonlinear least-squares fit) are in satisfactory agreement (Fig. 6.21).

Although we cannot separate the values of $l/\mathcal{D}_2^{f*}$ into components, it is of interest that for reasonable estimates,[11] namely, 10 μ for l, 1 for membrane density, and 0.5 for water content, a plausible value of

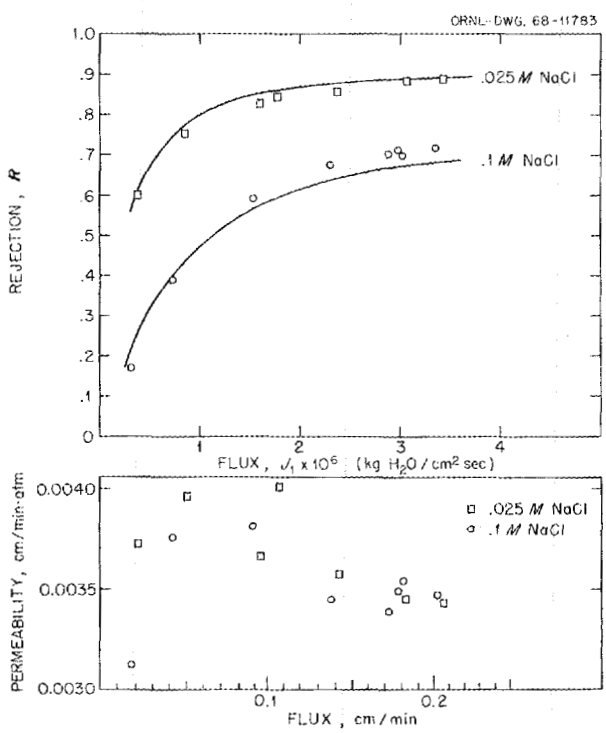

Fig. 6.21. Dependence of Solute Rejection on Flux. Hydrous Zr(IV) oxide membrane; capacity, $C^* = 0.45$; pressures, 100 to 900 psig. Points, experimental; curves, calculated, $l/\mathcal{D}_2^{f*} = 2.92 \times 10^5$.

about 6×10^{-6} is obtained for $\mathcal{D}_2^f(r)$, the salt diffusion coefficient in the membrane, expressed in the familiar units, square centimeters per second.

Additives

The major effort of the program during the past year has been the screening of additives for formation of practical membranes. Emphasis has centered on organic polyelectrolytes, since the pH of optimum rejection of many in this class, in contrast to hydrous oxide membranes, matches better the pH of natural brackish waters. Also, in many cases, the deleterious effect of presence of polyvalent counterions in feed solutions on membrane properties does not seem to be as serious as with the hydrous oxide type, under conditions at which rejections of NaCl are most favorable.

Last year's report[9] discussed studies of the effect of linear charge density of polyelectrolytes on salt rejection. Polyacrylic acid, which has a higher number of ionizable groups per mole of carbon than, for example, polystyrenesulfonic acid, formed membranes of higher rejection than the aromatic polyelectrolytes. Later observations, however, have cast doubt on the attribution of these higher rejections to charge density. Rejections of membranes formed dynamically of poly(maleic acid), which has twice as many carboxyls per chain carbon as poly(acrylic acid), were, if anything, poorer than those of poly(acrylate) membranes. Further, determination of additive rejection, made feasible by a newly acquired carbon analyzer, indicated that polyelectrolytes were by no means completely filtered by membranes formed from them – rejections were in many cases not much better than salt rejections. Passage of such large molecules implies that there must have been sizable imperfections in many of the membranes so far studied. Also, in the few cases studied, salt rejection by polyelectrolyte membranes as a function of concentration have not approached theoretical expectations at low salt concentrations [a slope of 1 in a log (1 – **R**) vs log m plot for a 1:1 electrolyte and a slope of 2 for a 1:2 electrolyte having a divalent coion]; an illustration is given in Fig. 6.22. Such nonideality is consistent with the presence of imperfections, although flaws are not the only reasonable explanation. Until defects are shown not to be present, it is not very profitable to speculate concerning the origin of differences in rejection properties.

More perfect layers should improve performance, and to the extent additives are available or can readily be synthesized, we are now attempting to find what chemical characteristics are conducive to good membrane formation by the dynamic technique and what effects molecular weight and chain branching of polyelectrolytes have on membranes formed from them. We shall give here a few examples of results obtained with recently investigated additives.

Poly(vinylamine). – This additive should form an anion exchange membrane, at least with low-pH feeds, and the order of rejection (Fig. 6.23) $MgCl_2 > NaCl > Na_2SO_4$ experimentally observed for solutions of the same equivalent concentration is in the expected order. Somewhat higher fractions of NaCl and $MgCl_2$ were filtered by membranes supported on a VF Millipore of nominal 0.01 μ pore size (the manufacturer now states that 0.025 μ is a more accurate representation) than on a Millipore of 0.45 μ. However, the rejections reported here are less than those of which the membranes are capable, since they are not corrected for the increase of concentration at the membrane-feed interface because of rejected salt. These experiments were carried out with cells, rather than tubes or other geometry amenable to theoretical analysis,[12] and the results reported are these "observed" rejections,

$$\mathbf{R}_{obs} = 1 - \frac{m_\omega}{m_f} \tag{7}$$

(subscript f indicating the feed concentration) rather than the **R** of Eq. (1), obtained by extrapolation to infinite circulation velocity. The differences between values for the two supports are at least partially accounted for by the higher flux through the support of larger pore size. Sodium sulfate rejection is somewhat

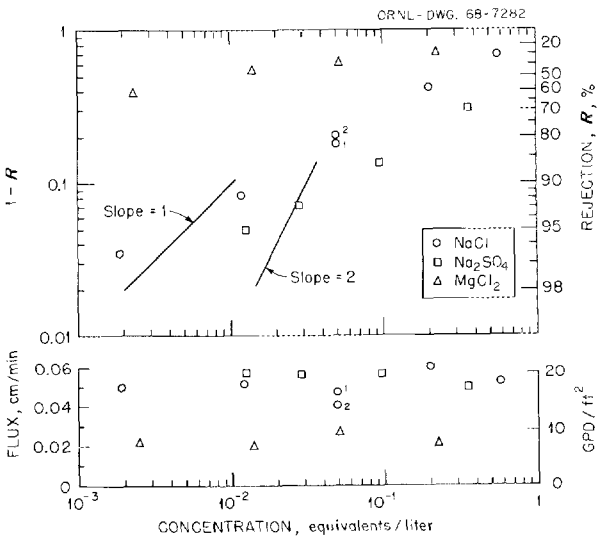

Fig. 6.22. Concentration Dependence of Rejection by a Dynamically Formed Polyacrylate Membrane; 0.3-μ ceramic tube, 68 atm, pH ~7, 1 ppm polyacrylic acid.

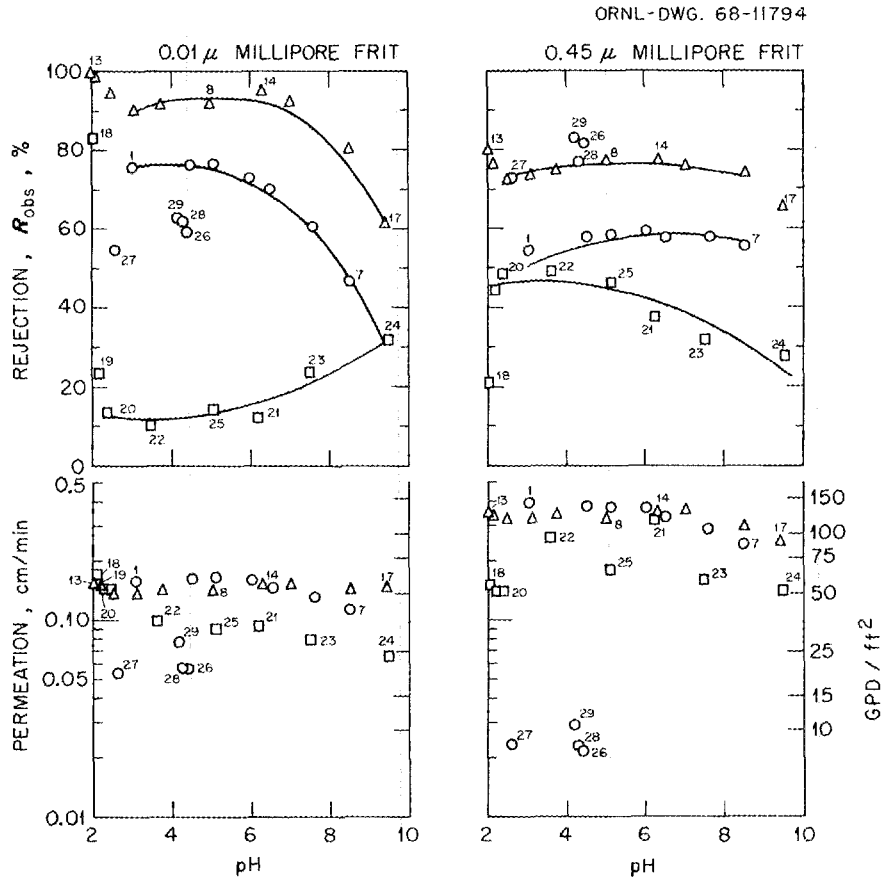

Fig. 6.23. Hyperfiltration Properties of Dynamically Formed Poly(vinylamine) Membranes. 1000 psig, 5 mg/liter additive. ○, 0.05 *M* NaCl; □, 0.025 *M* Na_2SO_4; △, 0.025 *M* $MgCl_2$. Numbers give order of measurements.

anomalous, particularly with the 0.01-μ support; changes in both membranes over the tests are indicated by repeat tests with NaCl at the end of the series (points 26–28).

After the last point in the figure, a few measurements were carried out with a synthetic 2000-ppm natural water, approximating that at Coalinga, California (0.0028 *M* $NaHCO_3$, 0.0096 *M* Na_2SO_4, 0.0018 *M* $CaCl_2$, 0.002 *M* $MgCl_2$). The additive does not appear very promising for practical desalination; R_{obs} of total ions (measured by passage through a chloride form ion exchanger and titration of liberated chloride) was about 50% and of Mg(II) + Ca(II) about 60% for the nominal concentration, and 40 and 55%, respectively, for three times the nominal concentration flux was 15 to 20 gal day^{-1} ft^{-2}.

Starch Sulfate. — This is commercially available (National Starch and Chemical), the type used here having about 1.5 sulfates per hexose unit. It readily forms cation exchange membranes of good flux and of rejections perhaps high enough to be interesting for some purposes when the effect of concentration polarization is considered (Fig. 6.24). As one would expect, the order of rejection is reversed from that observed with poly(vinylamine) with the three salts tested. In a test with Coalinga water, subsequent to those summarized in Fig. 6.24, the membrane on the 0.01-μ support rejected 71% of Ca(II) + Mg(II) and 60% of total ions, at 200 gal day^{-1} ft^{-2}. It appears surprising that the divalent counterions, magnesium and calcium, are more highly rejected than sodium when both are present, although rejections of their chlorides are much lower than those of NaCl from solutions of a single salt; such behavior is frequently encountered, however.

Homogenized Ion Exchangers. — Early in our study of dynamically formed membranes, we found that under some conditions, dispersions of ground low-cross-linked ion exchange beads formed rejecting layers. We have recently carried out further tests of this class. Figure 6.25 summarizes some results obtained with

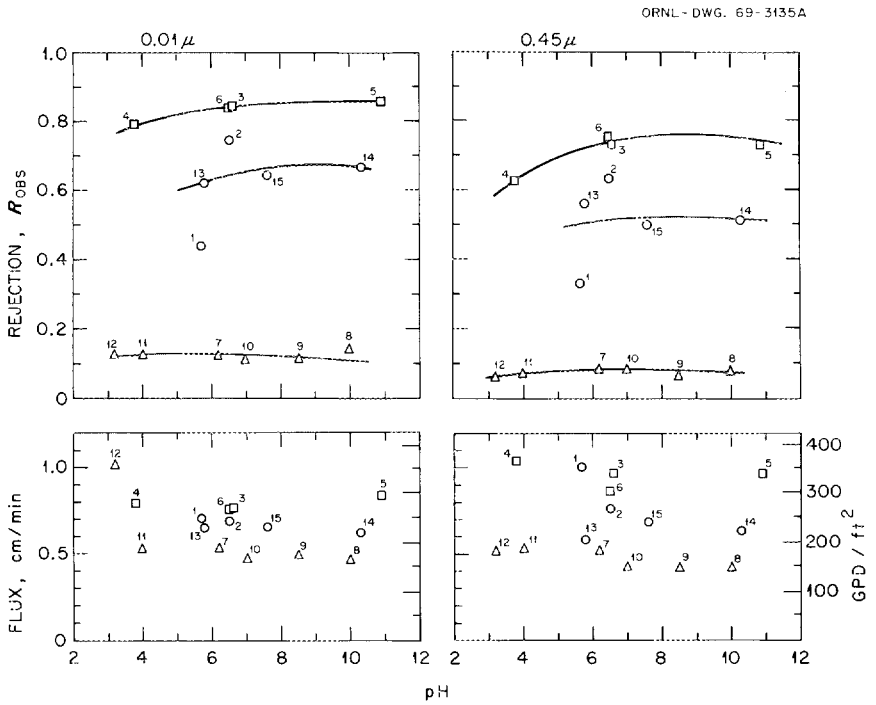

Fig. 6.24. Hyperfiltration with Dynamically Formed Starch Sulfate Membrane. Millipore supports in cells; 10 mg/liter additive; 1000 psig. ○, 0.05 *M* NaCl; □, 0.02 *M* Na_2SO_4; △, 0.035 *M* $MgCl_2$.

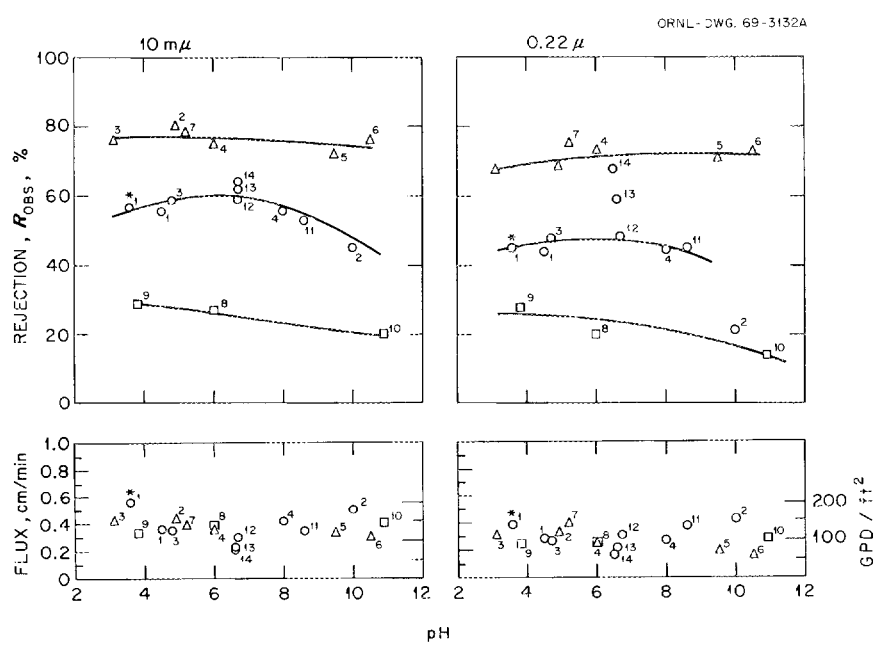

Fig. 6.25. Hyperfiltration with Membrane Dynamically Formed of Pulverized Sephadex A-25 on Millipore, Mounted in Cells. 1000 psig; 1 mg/liter additive. ○, 0.06 *M* NaCl; △, 0.025 *M* $MgCl_2$; □, 0.022 *M* Na_2SO_4. Point 1, 20 mg/liter additive; 13 and 14, +carboxymethyl cellulose.

Sephadex QAE A-25, a dextrin-based anion exchanger, the functional group being a fully quaternized amine. The additive was homogenized with a Waring Blendor before use, and the membrane formed of it had qualitatively the order of rejection properties expected for an anion exchange membrane. Results were similar for supports of 0.01 and 0.22 pore size, the fluxes through both being high. At the end of the series, 1 mg/liter (point 13, Fig. 6.25) and 5 mg/liter (point 14) of carboxymethyl cellulose ("cellulose gum") were added. Rejections of the membrane on 0.22-μ Millipore increased substantially and flux fell; there was a smaller effect on the membrane on 0.01-μ Millipore. Presumably the gum plugged defects in the membrane.

Ion exchange dispersions can be considered as high-molecular-weight branched polyelectrolytes, though their exact nature would be difficult to characterize. The class may be useful in sewage treatment (see below).

Porous Supports

In addition to the investigation of additives, we continue to devote substantial effort to searches for suitable porous supports in two main directions. For experimental purposes, we need to find substrates with which the ultimate rejection potential of membranes formed from a given additive can be quickly and reliably evaluated. The fact, already mentioned, that rejection of high-molecular-weight species is frequently not complete indicates that we have not completely achieved this objective. Uniformity of pore size is important here, and in most cases decreasing pore size, at least in the 0.025-to-1-μ range, seems to improve rejection, sometimes without a penalty of lower flux. Our work in this area involves principally the testing of various commercially available or experimental supports, their cost being a secondary consideration.

The other direction is to search for supports suitable for practical use. Here, important characteristics include, in addition to rejection, low cost per unit area and cheapness of mounting for use; lifetime; flux through the membrane-support systems; and possibility of restoring permeability by backwashing. We have described[9,13] some preliminary studies of the use of fine particulates (commercial filter aids) to coat tubes containing pores of 5 μ and up with a thin layer suitable for membrane formation.

During the past year, we have found that woven fabrics can also be adapted to support dynamically formed membranes by filter-aid pretreatment. The materials most investigated so far have been 1-in.-diam tubes of polyester or cotton manufactured for use as jackets on fire hoses. Although it is not clear that these can be mounted in a way suitable for backwashing, they should otherwise allow great flexibility in the design of practical equipment. Membranes on such supports frequently have high permeabilities. For example, in several separate experiments, polyacrylate membranes were formed on hose pretreated with a diatomite filter aid for later tests in sewage treatment. Initial fluxes were greater than 500 gal day^{-1} ft^{-2} (800 psig), and $\mathbf{R}_{obs}$ for 0.01 *M* NaCl was 40 to 50%. At these fluxes, concentration polarization is high; with allowance for boundary layer buildup, rejections would be in the 80 to 90% range.

Possible Applications Other than Desalination[14]

We have described[9,15] work on effluents from primary treatment of municipal sewage. Membranes in these tests were formed of constituents of the feed, with no extraneous additive. These films typically filtered out 80% of chemical oxygen demand, with fluxes of 50 gal day^{-1} ft^{-2} at less than 500 psig.

We have in the past year carried out a more extensive study with effluents from secondary treatment by the activated sludge process. Here, in addition to determining the lowering of oxygen demand, we were testing whether the dissolved electrolyte added in a normal cycle of community use (about 300 ppm) could be removed. Since salt concentrations are low, a few hundred ppm, and rejection requirements not very high, the dynamic class of ion exchange membranes might be expected to perform well, if other constituents of the feed do not excessively degrade their rejection properties, usually 80 or 90% in this concentration range.

Several dynamic membranes do in fact appear promising, although there are interferences by materials in sewage. Rejections by membranes formed from constituents of secondary effluents alone are in general about 25%, not high enough. Membranes formed of polycationic additives, which form anion exchange membranes, are excessively sensitive to sewage, an observation rather expected, since the bulk of the polymeric contaminants are probably anionic. However, membranes of several polyanionic additives seem to have adequate rejection with secondary effluent feeds — some examples are polyacrylate and pulp mill wastes.

Results of a test lasting over ten days are summarized in Fig. 6.26. The membrane was preformed on a 0.45-μ polyacrylonitrile—polyvinyl chloride support (Gelman Acropore AN 450); the additive was low-cross-linked polystyrenesulfonate ion exchanger homogenized in a Waring Blendor. Sodium chloride was added to facilitate analysis and to simulate partially the effect of

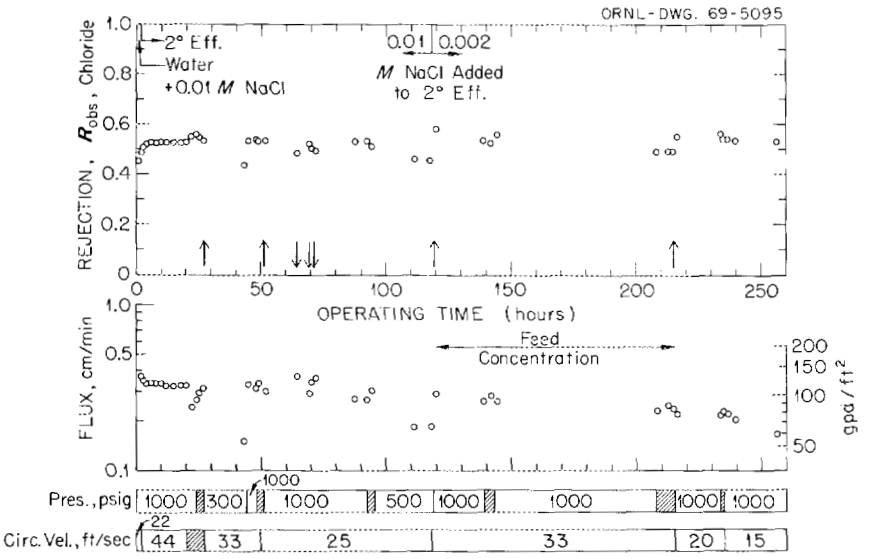

Fig. 6.26. Hyperfiltration of Effluent from Secondary Treatment of Oak Ridge Sewage. Dynamically formed homogenized Dowex 50-X25 membrane. ↓ Shutdown; ↑ feed change; ▨ pressure or velocity excursion.

concentrating the feed stream. At 1000 psig, rejections of 50% were maintained over the course of the run. Fluxes were initially well over 100 gal day^{-1} ft^{-2}. There was a gradual decline in flux over the course of the run, particularly at the lower circulation velocities investigated, but these declines could be partially reversed by operating for a time at a lower pressure and a high circulation rate; after the last point in Fig. 6.15, for example, a pressure excursion raised the flux from 60 to 70 gal day^{-1} ft^{-2}. Organic carbon rejections were mostly 70 to 85%, the product containing 4 to 6 ppm. Rejections of calcium plus magnesium were ~80% and of turbidity, ~95%.

Although much further work will be necessary to determine the practicality of this approach to sewage treatment, these and other results we have obtained are encouraging.

---

[1] Sponsored by the Office of Saline Water, U.S. Department of the Interior.

[2] General Engineering and Construction Division.

[3] Reactor Division.

[4] Oak Ridge Associated Universities Summer Student Trainee from Centre College, Danville, Ky., Summer 1968.

[5] Director's Division.

[6] Guest Scientist from Weizmann Institute, Israel.

[7] Reactor Chemistry Division.

[8] Chemical Technology Division.

[9] *Chem. Div. Ann. Progr. Rept. May 20, 1968*, ORNL-4306, p. 92.

[10] J. S. Johnson, L. Dresner, and K. A. Kraus, in *Principles of Desalination* (ed. by K. S. Spiegler), chap. VIII, Academic, New York, 1966.

[11] A. J. Shor *et al.*, *J. Phys. Chem.* 72, 2200 (1968).

[12] A. J. Shor *et al.*, *Ind. Eng. Chem. Fundamentals* 7, 44 (1968).

[13] J. S. Johnson, Jr., *et al.*, *Desalination* 5, 359 (1968).

[14] Research sponsored by the Federal Water Pollution Control Agency, U.S. Department of the Interior.

[15] H. C. Savage *et al.*, *Water Sewage Works* 116, 102 (1969).

PHYSICAL CHEMISTRY OF POLYELECTROLYTE SYSTEMS

THERMAL EFFECTS IN ION EXCHANGE REACTIONS WITH ORGANIC EXCHANGERS: ENTHALPY AND HEAT CAPACITY CHANGES[1]

G. E. Boyd

Ion exchange equilibria between aqueous electrolyte solutions and organic ion exchangers are temperature dependent, and ion exchange reactions are therefore accompanied by the evolution or absorption of heat. The thermal effect, however, generally is small, so that the enthalpy change, ΔH°_{T}, is best measured with a sensitive isothermal calorimeter. The heat of ion exchange

is itself temperature dependent; hence a change in heat capacity, ΔC_p°, also accompanies ion exchange reactions. For reactions at 298.2°K between equally charged cations in strong-acid exchangers or anions in strong-base exchangers, ΔH° and ΔS° are negative, and the lowering of the free energy, ΔG°, is caused by the enthalpy decrease. However, for reactions between unequally charged ions in which the more highly charged species is preferentially taken up, ΔG° is determined by the entropy change (i.e., $\Delta H^\circ > 0$; $\Delta S^\circ > 0$). Information on the sign and magnitude of ΔH° and ΔC_p° may be used to estimate ion exchange reaction equilibrium constants at temperatures as much as 100° above measurements at room temperature.

Because of the temperature dependence of ΔH_T°, the concept of a lyotropic series in the affinity of ions is not generally valid; there is nothing unique about the sequence at room temperature. The generalization that increased ionic selectivity goes with increased exchanger cross-linking, likewise, is limited because of the balance between the contributions of ΔH_T° and ΔS° to ΔG_T°. Increased selectivity with ion charge is not governed by ΔH_T°, as might be expected if the change in electrostatic energy determined the lowering in the free energy, but rather by ΔS°, which suggests that ion-solvent interactions are of central importance for reactions in hydrogen-bonded solvents.

---

[1] Abstract of paper to be published in proceedings of the International Conference on Ion Exchange in the Process Industries, London, July 16–18, 1969.

THERMODYNAMIC STUDIES ON THE BOLAFORM ELECTROLYTES $[Bu_3N\text{-}(CH_2)_8\text{-}NBu_3]X_2$ IN AQUEOUS SOLUTION

Siegfried Lindenbaum

Thermodynamic[1–4] and transport[5] property measurements on tetra-*n*-butylammonium halides have suggested that cation-cation pairing and aggregation may occur in their aqueous solutions. It has been suggested[6] that the bolaform electrolyte $[Bu_3N\text{-}(CH_2)_8\text{-}NBu_3]X_2$, ($DiBuX_2$), would serve as a model of a Bu_4N^+ cation-cation pair. Partial molal volume measurements[6] with $DiBuX_2$ reproduce the general features of the concentration dependence of the partial molal volumes previously determined for Bu_4NBr solutions. The values obtained and the minima in the partial molal volume vs concentration curves for both systems suggest that these two compounds in aqueous solution have similar properties.

The purpose of this work was to measure the heats of dilution of $DiBuX_2$ aqueous solutions and to compare the results with the heats of dilution of Bu_4NX solutions.[2,7] Apparent molal heat contents, ϕ_L, of $DiBuF_2$, $DiBuCl_2$, and $DiBuBr_2$ are given in Fig. 6.27 as a function of concentration; the data also for Bu_4NF, Bu_4NCl, and Bu_4NBr are reproduced so that the two systems may be compared. The apparent molal heat contents for the divalent bolaform electrolyte are plotted as $\phi_L/2$ vs $2m$. These units represent the heat evolved on dilution per equivalent weight of $DiBuX_2$ as a function of weight normality. The two sets of curves are thus directly comparable. The heat of dilution data for Bu_4NF are the largest of any yet observed for a 1-1 electrolyte for the range of concentrations covered by the measurements. The measurements for Bu_4NF were carried to the concentration limit, which is considerably lower for the fluoride because of the formation of the clathrate hydrate.

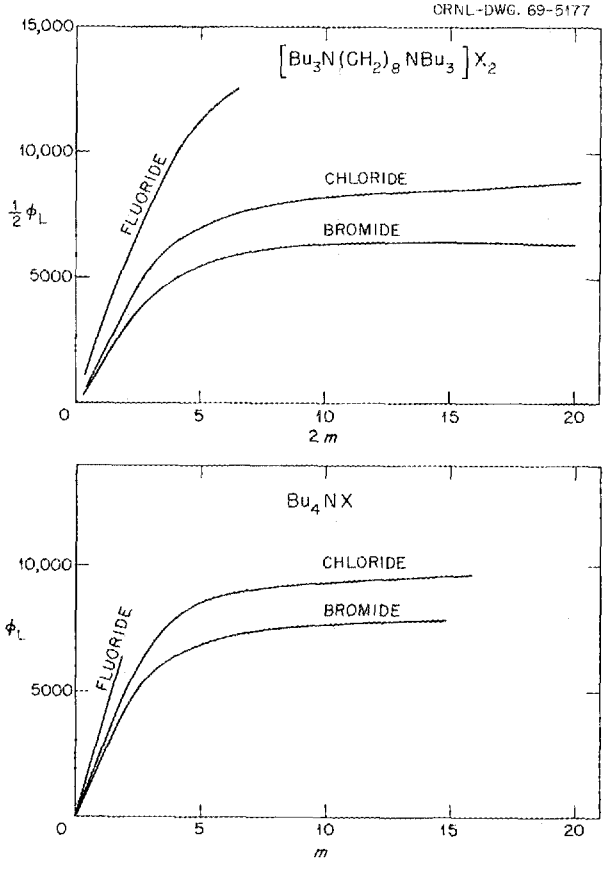

Fig. 6.27. Apparent Molal Heat Contents of Aqueous Solutions of Bu_4NX and $[Bu_3N\text{-}(CH_2)_8\text{-}NBu_3]X_2$, Where X = Fluoride, Chloride, or Bromide. Data for Bu_4NCl and Bu_4NBr are taken from ref. 2.

The ϕ_L curves for the bolaform electrolytes all fall slightly below those of the corresponding univalent salt. The curves are, however, very nearly superimposable after normalization of the coordinates. It has been suggested that the values of ϕ_L for the tetraalkylammonium halides are in large part a measure of the heat evolved due to the promotion of additional hydrogen bonding of the water molecules in the vicinity of the hydrocarbon chains. Whereas a $DiBu^{2+}$ ion has the same length of hydrocarbon chain per unit charge as a Bu_4N^+ ion, less contact of the solvent with the former is possible because one end of a butyl chain is protected. The slightly smaller values of ϕ_L for the bolaform electrolyte are therefore not unreasonable.

This study provides additional evidence for the contention that the thermodynamic properties of aqueous solutions of $DiBuX_2$ are very similar to those of Bu_4NX. However, these data cannot be used as evidence for the existence of cation-cation pairs in Bu_4NX solutions because the contribution to the thermodynamic properties of the solution by such a pair is not known. Small-angle x-ray scattering experiments[8] in fact have provided evidence that such pairing or higher aggregate formation does not occur to an appreciable extent in these solutions.

---

[1] S. Lindenbaum and G. E. Boyd, *J. Phys. Chem.* **68**, 911 (1964).

[2] S. Lindenbaum, *J. Phys. Chem.* **70**, 814 (1966); see also *Chem. Div. Ann. Progr. Rept. May 20, 1968*, ORNL-4306, p. 90.

[3] W.-Y. Wen and S. Saito, *J. Phys. Chem.* **68**, 2639 (1964).

[4] R. H. Wood and H. L. Anderson, *J. Phys. Chem.* **71**, 1871 (1967).

[5] D. F. Evans and R. L. Kay, *J. Phys. Chem.* **70**, 366 (1966).

[6] T. L. Broadwater and D. F. Evans, *J. Phys. Chem.* **73**, 164 (1969).

[7] The heat of dilution data for Bu_4NF are new and will be published.

[8] Performed in collaboration with R. W. Hendricks, Metals and Ceramics Division. To be reported in detail: R. W. Hendricks and S. Lindenbaum, *Metals and Ceramics Div. Ann. Progr. Rept. June 30, 1969*, ORNL-4470.

7. Electrochemical Kinetics and Its Application to Corrosion

KINETICS OF THE FORMATION AND DISCHARGE OF THE SUPERPASSIVE FILM ON IRON

G. H. Cartledge

The last annual report[1] described a well-characterized plateau or inflection in the potential-time curve observed when iron is anodically passivated in a molybdate solution and then placed on open circuit in the presence of small concentrations of iron(II) ions. Since these observations are made at potentials noble to that at which activation sets in spontaneously, the unique surface state was referred to as a superpassive state. In formulating an interpretation of the phenomena, it was assumed that polarization above the normal passivating potential withdraws a certain small number of electrons from the film, thereby raising the average ionic potential, lowering the solubility, and introducing electronic conductivity. The concept was extended to characterize the passive surface state generally.[2]

The processes of charge and discharge may be represented by the equations

$$\underset{\text{discharged}}{\mathrm{FeO \cdot OH}} \rightleftharpoons \mathrm{FeO \cdot OH \cdot \square} + e^- \rightleftharpoons \underset{\text{charged}}{\mathrm{FeO \cdot O \cdot \square}} + e^- + \mathrm{H}^+,$$

which express the assumption that the movement of electrons and protons in opposite directions is involved. The kinetics of these processes is being studied by polarizing iron anodically in several inhibiting media and to various noble potentials and then suddenly switching the potentiostat to a lower potential. The charge passed is obtained by integration of the recorder chart. The sequence of operations in a representative set of experiments is illustrated in Fig. 7.1, the electrolyte being 2.5×10^{-3} f $KTcO_4$ buffered by 10^{-2} f phthalate at pH 5.44. The choice of working potentials of 91 and 291 mV (S.C.E.) for this particular system was determined by the necessity to avoid reduction of the film itself by having the lower potential safely above the activation potential and by the observation that almost the total charge or discharge occurs within 150 mV of this lower potential.

The results may be discussed best by considering, first, experiment a_3, in which the fully charged film was brought back to 91 mV. Figure 7.2, curve 1, shows the current density j plotted logarithmically against q, the charge ($\mu C/cm^2$). Many experiments in different electrolytes showed that the corresponding curves may be represented by a slight modification of an equation

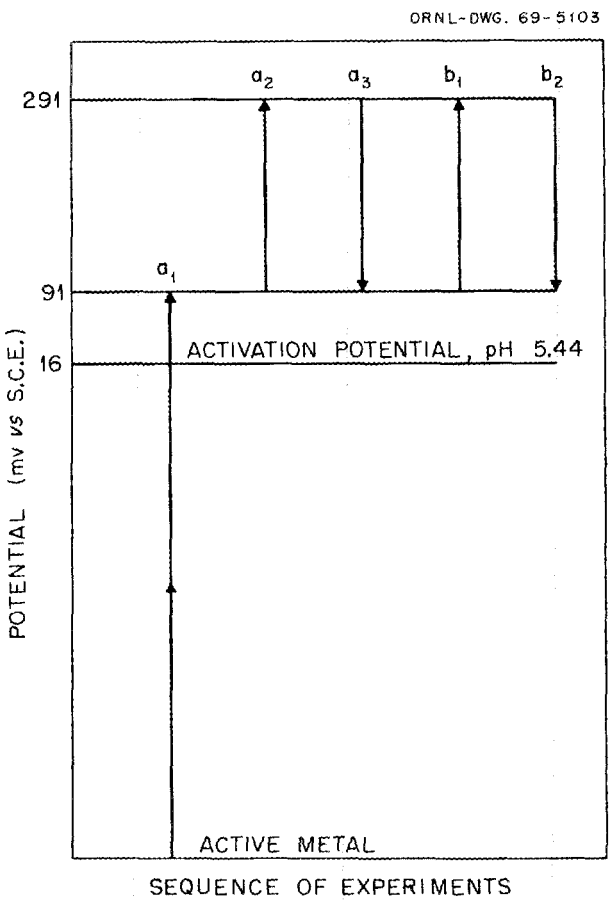

Fig. 7.1. Sequence of Measurements: Formation of Film in a_1 and a_2, Supercharge or Discharge, a_3, b_1, b_2.

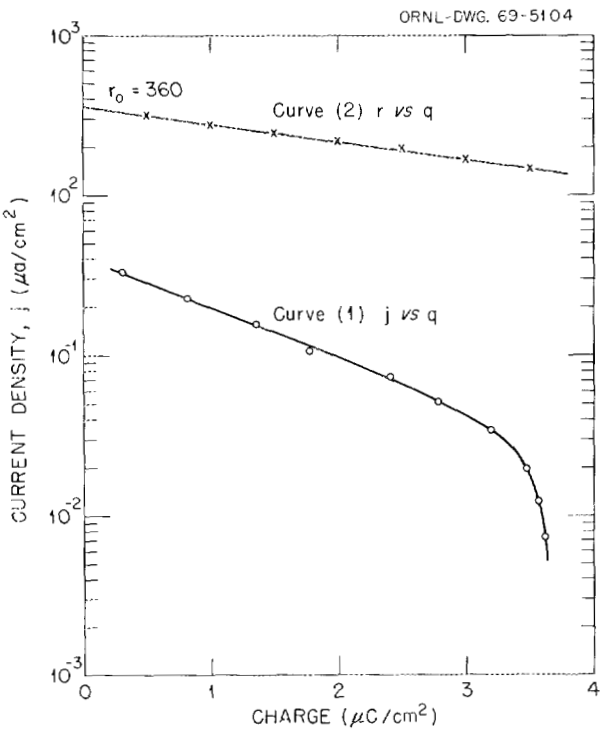

Fig. 7.2. Data from Experiment a_3 and Calculated Values of r. Current density vs charge (curve 1) and values of r calculated from Eq. (2) vs charge (curve 2).

shown previously to express the kinetics of ion exchange between the surface of the passive film and anions in the electrolyte.[3] That equation was derived by incorporation of an activation energy $\Delta H^{\ddagger}$, which increases linearly with the extent of exchange; that is,

$$\Delta H^{\ddagger} = \Delta H_0^{\ddagger} + rq \ , \tag{1}$$

in which q is the extent of the process and r was found to be constant. The rate equation for the present experiments would have the form

$$j = j_0\left(\frac{q_\infty - q}{q_\infty}\right)\exp\left(-\frac{rq}{RT}\right), \tag{2}$$

in which j_0 is the initial current density ($q = 0$) and q_∞ is the total integrated charge ($j \to 0$). These values may be closely estimated from the experimental curve. When test values were inserted into the equation, it was seen that r is not constant but decreases as discharge proceeds. Its variation is accurately expressed by the relation

$$r = r_0 \exp(-lq) \ , \tag{3}$$

in which l is a constant. Curve 2 in Fig. 7.2 shows the exponential dependence of r on q. The complete rate equation therefore becomes

$$j = j_0\left(\frac{q_\infty - q}{q_\infty}\right)\exp\left[-\frac{qr_0}{RT}\exp(-lq)\right] . \tag{4}$$

The factor $(q_\infty - q)/q_\infty$ is required to represent the fact that the current drops either to zero or to a steady-state value j_∞ for different situations. The rates actually come almost to first-order dependence on $q_\infty - q$ during the latter part of a measurement, owing to the dominance of this depletion factor. The applicability of this equation was demonstrated in solutions of several inhibiting anions and over the pH range 6.4 to 4.5, though for experimental reasons the most concordant quantitative results were obtained at pH ~5.5 to 6.0.

In Fig. 7.1, experiments a_1 and a_2 refer to polarizations in which the surface film is being produced by ionization of metal and deposition, most likely as γ-FeO·OH. It is noteworthy that the effective inhibitors diminish the charge required for formation of the film, in comparison with the total charge passed in noninhibited electrolytes.[4] Thus in experiment a_1 the integrated charge from the active metal to a passive potential of +91 mV (S.C.E.) was 3500 μC/cm^2; to carry the potential on to +291 mV in a_2, an additional charge of 900 μC/cm^2 was required, more film having been formed. The charge for step a_3, however, was only 3.9 μC/cm^2, and similar small charges were observed in subsequent steps b_1 and b_2, the bulk of the film remaining essentially unchanged after the potential had once been taken to +291 mV. Further, for steps a_1 and a_2, in which the dominant process is formation of film, the r of Eq. (2) is constant when $j - j_\infty$ is used, the steady-state current density j_∞ being of the order of 0.1 μA/cm^2 or less in well-inhibited solutions. For these film-building polarizations, therefore, the well-known "logarithmic law" of film growth is followed until near the steady state; that is,

$$q = m \log(1 + nt) \ , \tag{5}$$

in which t is the time and m and n are constants. The experiments give additional evidence that the peculiarities associated with passivity derive entirely from an exceedingly small amount of supercharge, in comparison with the total quantity of charge represented by the film, and further that the charge and discharge processes involve a kinetic factor negligibly small in formation of the film itself.

The observed kinetics can be interpreted in terms of the model postulated. When the applied potential is

suddenly lowered, electrons and protons begin returning to the film. Because the mobility of electrons is so much higher than that of protons, however, at the first moments an excess of electrons moves in, thus creating a space charge in the film, the direction of the induced field being such as to impede the flow of electrons but favor the influx of protons. If the latter process is under activation control, this means that the activation energy is initially lowered and increases as the process continues. In a more detailed manuscript now in preparation, it will be shown that the exponential factor of Eq. (4) may be equated with the exponential term in the familiar equation of electrode kinetics, from which it follows that r is a kind of reciprocal capacity, the variation of which results (plausibly) from the variation of the interionic field in the film as its space charge is altered.

[1] G. H. Cartledge, *Chem. Div. Ann. Progr. Rept. May 20, 1968*, ORNL-4306, p. 106.

[2] G. H. Cartledge, *Corrosion* **24**, 223 (1968).

[3] G. H. Cartledge and D. H. Spahrbier, *J. Electrochem. Soc.* **110**, 644 (1963).

[4] G. H. Cartledge, *J. Electrochem. Soc.* **113**, 328 (1966).

ELECTROCHEMICAL BEHAVIOR OF TITANIUM

E. J. Kelly

This report describes progress in determining the mechanisms of titanium corrosion in the active and passive states and in the active-passive transition region (passivation). Additional information on the oxidation of Ti^{III} ions in solution to Ti^{IV} at the passive titanium surface, an important reaction discussed previously,[1] is also presented.

Steady-state current-potential data for titanium in H_2-saturated 1 N H_2SO_4 are given by curve A in Fig. 7.3. Titanium undergoes active-state dissolution in this medium at the corrosion potential E_c. As the electrode potential is made increasingly positive, the anodic current rises to a maximum at the "critical potential" E_m, and then diminishes sharply as the metal is transformed from the active to the passive state. In the active and active-passive transition regions (i.e., in the potential region where curves A and D coincide), titanium is oxidized to Ti^{III} ions in solution. In the passive state the substrate metal is oxidized to form the passive oxide film (TiO_2). In addition to the oxidation of substrate metal, Ti^{III} ions in solution are oxidized to Ti^{IV} at the passive titanium surface, and the current

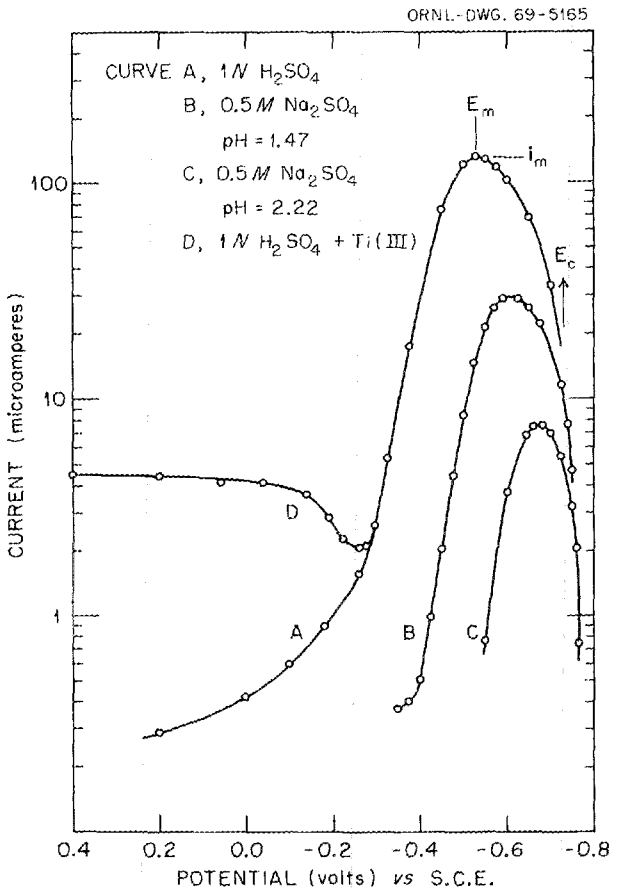

Fig. 7.3. Effects of pH and Ti(III) Concentration on Polarization Behavior of Titanium.

corresponding to this reaction is equal to the difference between curves A and D. As shown previously,[1] the oxidation reaction is first order in Ti^{III}. If at some point along curve D the pH is increased by the addition of NaOH, the rate of oxidation of Ti^{III} increases sharply and becomes dependent upon stirring rate as the reaction passes from activation to mass-transport control. A correspondingly rapid buildup in film thickness is evidenced by a sequence of color changes which is reversed as the Ti^{III} ions are consumed and the system reverts to curve A. These results are consistent with the mechanism given by Eqs. (1) and (2):

$$Ti^{3+} + H_2O = TiO^+ + 2H^+ , \quad (1)$$

$$TiO^+ + H_2O \rightarrow TiO_2 + 2H^+ + e^- . \quad (2)$$

Consequently the current due to the oxidation of Ti^{III} is given approximately by Eq. (3),

$$i = \frac{F\bar{k}_2(D/d)C_{Ti^{III}}}{\bar{k}_2 + (D/d)[1 + (a_H^2 + /K_1)]}, \quad (3)$$

where D is the diffusion coefficient for Ti^{III}, d is the Nernst diffusion layer thickness, and the other symbols have their customary significance. Equation (3) shows the shift from activation to mass-transport control which accompanies the increasing dominance of the first term in the denominator with increasing pH. In either case the reaction remains first order in Ti^{III}. Equations (1) and (2) offer a self-repair mechanism which may account for the failure of titanium to undergo pitting corrosion in sulfate solutions in contrast to halide solutions.

The effect of pH on the dissolution of titanium in the active and the active-passive transition potential regions is illustrated by curves A, B, and C, which show that with increasing pH the dissolution rate decreases and the critical passivation potential E_m becomes increasingly negative. In no instance is a positive Tafel region observed; that is, $(\partial \log i/\partial E)_{pH}$ is not a positive constant. However, at potentials positive to E_m, one observes that $(\partial \log i/\partial E)_{pH}$ approaches a negative limiting value which becomes increasingly negative with decreasing pH. In this same potential region the dissolution rate approaches a second-order dependency on the hydrogen ion activity, an order which diminishes with increasingly negative potential.

In contrast to the preceding observations, other metals which undergo active-state dissolution, such as iron, exhibit positive Tafel behavior and a first-order dependency of the dissolution rate on hydroxyl ion activity.[2] The difference in the behavior of the two metals results from the fact that, in the case of iron, the fraction of the surface occupied by adsorbed reaction intermediates is vanishingly small compared with that occupied by adsorbed water molecules, whereas this is not true for titanium even at the corrosion potential. By analogy to the iron system, a reaction mechanism has been derived for the titanium system, and the resulting equation relating current, potential, and pH fully describes curves A, B, and C of Fig. 7.3. The derived equation accounts for the maximum in i at E_m, the nearly exponential dependence of i_m on E_m, the linear dependence of E_m on pH, the dependence of i on the hydrogen ion activity, and the approach to negative Tafel behavior described above.

[1] E. J. Kelly, *Chem. Div. Ann. Progr. Rept. May 20, 1968*, ORNL-4306, p. 108.

[2] E. J. Kelly, *J. Electrochem. Soc.* **115**, 1111 (1968).

PROPERTIES OF THE SUSPENSION ELECTRODE[1]

R. E. Meyer P. M. Lantz F. A. Posey

The suspension electrode is a relatively little-known type of electrode system in which the electrode is a finely divided catalytic material suspended in a solution of strong electrolyte. The particles of the catalyst, which are usually from 10 to 100 μ in diameter, are charged by intermittent contact with a stationary electrode. Contact may be effected either by stirring the suspended particles or by flow of the suspension past a charging electrode fixed in a channel. The suspension electrode offers several advantages compared with conventional electrode systems. Normally, electrode materials must be selected for a combination of favorable properties, including catalytic activity, mechanical strength, and corrosion resistance. With the suspension electrode the suspended material may be selected primarily for its catalytic activity, and the charging electrode may be selected primarily for its mechanical and corrosion properties. If the suspended material should deteriorate in use, it can easily be replaced without dismantling the cell. In addition, many types of suspended materials have very large active surface areas (e.g., 10 to 50 m^2/g), and therefore increased current densities for certain types of reactions are possible.

Previous publications in the open literature on this electrode configuration are limited to only a few studies of specialized systems, and the factors influencing the magnitude of the current have not been understood. We therefore began a study of the suspension electrode system by examining the kinetics of the hydrogen reaction, using suspensions of Raney catalysts, platinum black, and palladium black.

Current-voltage curves for the hydrogen evolution reaction with the palladium-black suspension electrode are shown in Fig. 7.4. One notes that the current from the suspension electrode is a linear function of the overvoltage. This relation, which had been reported previously by other workers for the suspension electrode system, is surprising at first sight, because normally in electrochemical processes the current is an exponential function of the overpotential. Similar results for the Raney nickel suspension electrode are shown in Fig. 7.5. We have also shown that the slopes of the current-voltage curves are identical for both the anodic and the cathodic process with the hydrogen electrode reaction, as may be seen in Fig. 7.6. The slope of this line has been found to be a function of the nature of the catalytic material, the solution conduc-

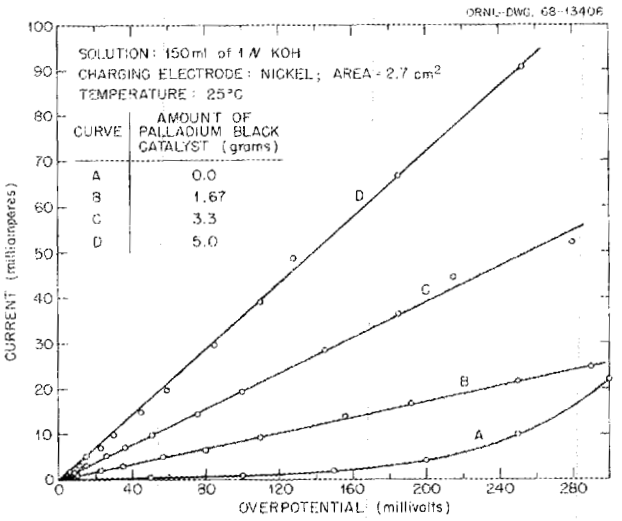

Fig. 7.4. Effect of Catalyst Concentration on Polarization of the Palladium-Black Suspension Electrode.

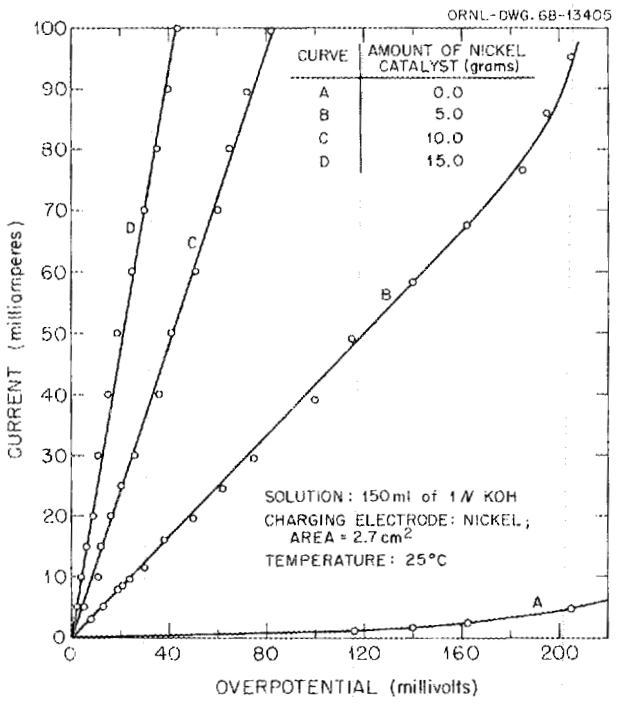

Fig. 7.5. Effect of Catalyst Concentration on Polarization of the Raney Nickel Suspension Electrode.

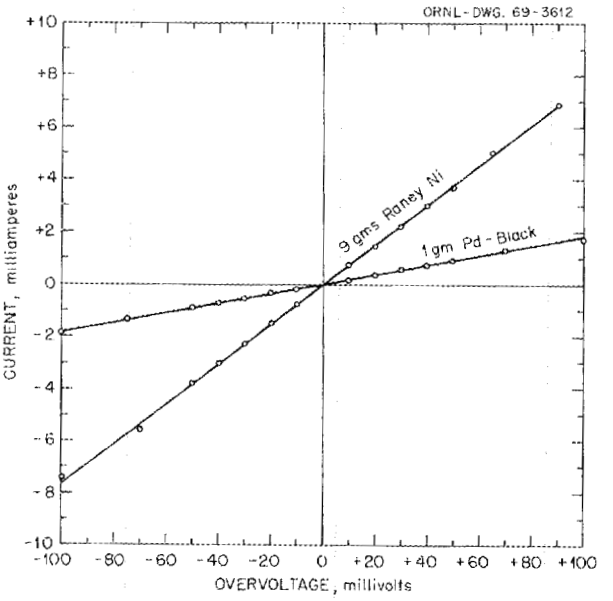

Fig. 7.6. Anodic and Cathodic Current-Voltage Characteristics of the Hydrogen Reaction in the Suspension Electrode System. Solution: 0.3 *N* KOH, 25°C; cell capacity: 150 ml.

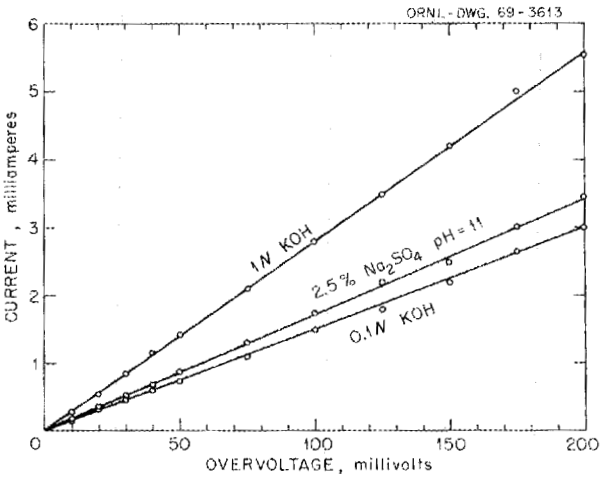

Fig. 7.7. Oxidation of Hydrogen in the Palladium-Black Suspension Electrode System. 1 g Palladium black in 150 ml.

tivity, and the geometric and hydrodynamic factors which control the frequency and duration of contact between the particles and the charging electrode. The effect of solution conductivity is illustrated in Fig. 7.7. The sodium sulfate solution in Fig. 7.7 has a conductivity only slightly greater than that of 0.1 *N* KOH and of course a considerably different pH. This and other experiments in which the composition of the solution was changed showed that the pertinent variable is the solution conductivity. In general, a change of conductivity by a factor of 10 changes the current by a factor

of from 2 to 4 at constant electrode potential, catalyst concentration, and stirring conditions.

These results were confirmed by observations of individual pulses due to contact of catalyst particles with the charging electrode by use of an oscilloscopic technique. On lowering the concentration of the catalyst to a few milligrams per liter and on reducing the size of the charging electrode, it was possible to reduce the frequency of contact events to only a few per second, and indivudual pulses could then be observed. Some typical pulses are shown in Fig. 7.8. Most of the pulse shapes were characterized by a sharp increase to a peak current followed by a somewhat slower decay. The duration of the pulses for our stirring conditions was generally of the order of 1 msec. Many pulses were examined, and average pulse heights were determined as a function of overpotential and solution conductivity. Some results of these measurements are shown in Figs. 7.9 and 7.10. These experiments confirm the linear relation between current and overpotential and the increase in current with conductivity.

A satisfactory model for the suspension electrode system was developed based on the following assumptions: (1) individual catalyst particles are highly porous and behave like miniature porous electrodes; (2) the resistance of the electrolyte is the predominant factor in determining the overpotential during the course of a current transient; (3) since most of the overpotential lies within the solution phase, the potential at the metal-solution interface on the catalyst particles departs only a few millivolts from the equilibrium potential (this fact is ultimately responsible for the linear relation observed between current and overpotential); and (4) the effective rate constant at the surface is very large during the important first few milliseconds of the charging transient. Details of the theoretical model are described in the following section of this report. Studies are in progress on the possibility of enhancing the

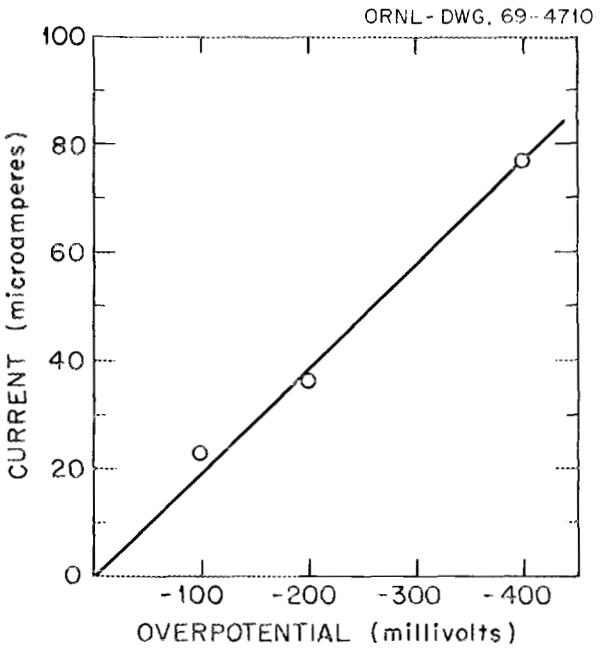

Fig. 7.9. Effect of Overpotential on Pulse Height for Contact of Individual Catalyst Particles with Charging Electrode. Palladium catalyst, 0.3 *N* KOH.

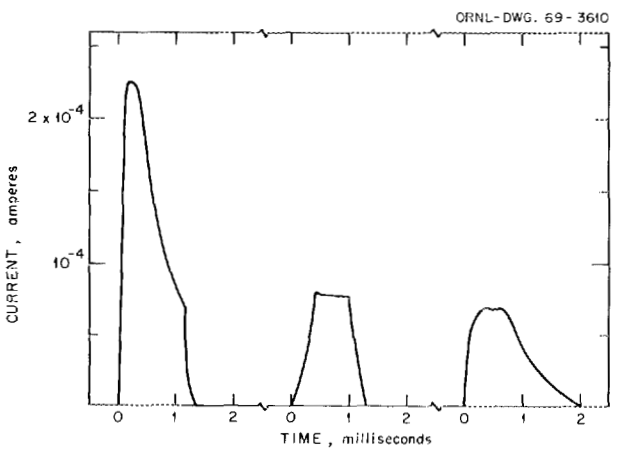

Fig. 7.8. Pulse Shapes for Charge Transfer to Individual Suspension Particles. Palladium-black catalyst, platinum charging electrode, 1 *N* KOH, −200 mV overvoltage.

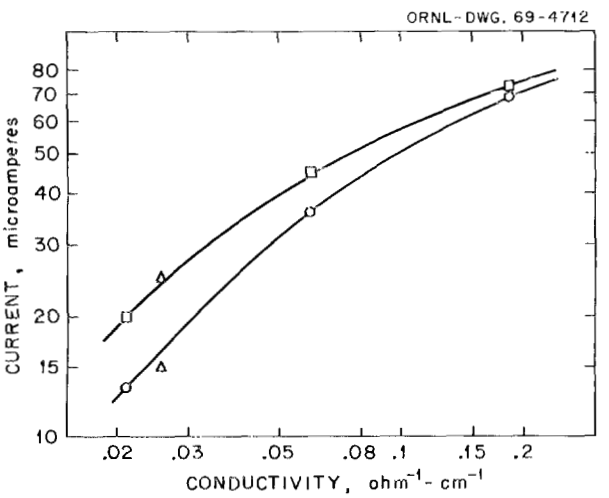

Fig. 7.10. Effect of Solution Conductivity on Pulse Height for Contact of Individual Catalyst Particles with Charging Electrode. □, KOH solutions; ○, repeat; △, Na_2SO_4, pH = 10.

current output of other reactions by use of a suspension electrode system.

---

[1] Research jointly sponsored by the Office of Saline Water, U.S. Department of the Interior, and by the U.S. Atomic Energy Commission under contract with Union Carbide Corporation.

THEORY OF THE SUSPENSION ELECTRODE[1]

F. A. Posey R. E. Meyer

A theoretical model of the suspension electrode was developed which explains a number of the principal experimental observations. The current output of the suspension electrode has been found to vary linearly with the potential of the charging electrode over wide limits (cf. preceding report). Observations on current transients due to contact of single catalyst particles with the charging electrode have shown the existence of a maximum in the current transient which cannot be accounted for simply by the charging of the double layer. It was possible to account for these facts by considering current, potential, and concentration transients which would occur at the surface of a hemispherical catalyst particle on contact with the charging electrode. However, detailed predictions of the simple hemisphere model could not account for the variation of current with solution conductivity, for the magnitude of the current observed on individual particles, or for the variation in the shape and time constant of the current transient with change in electrode potential. These and other observations led to the conclusion that most of the current observed during a transient arises from reaction on the internal surfaces of the catalyst particles, which are known to be highly porous and to possess very large surface areas of high catalytic activity. Therefore a model for the suspension electrode was developed which considers the nature of the current transient due to reaction in the pores of a catalyst particle in contact with the charging electrode.

A schematic cross-sectional diagram of a cylindrical pore of radius a (cm) and length l (cm) in a catalyst particle is shown in Fig. 7.11. The current density of the hydrogen evolution reaction which occurs on the walls of the pore is assumed to be given by the following equation of conventional form:

$$j(x,t) = j_0 \left\{ \left[\frac{C(x,t)}{C_0} \right] e^{+(\beta_a F/RT)\eta(x,t)} - e^{-(\beta_c F/RT)\eta(x,t)} \right\} , \quad (1)$$

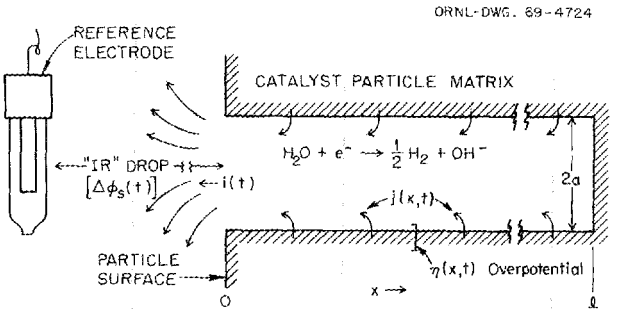

Fig. 7.11. Schematic Diagram of Pore Model for the Hydrogen Evolution Reaction in the Suspension Electrode System.

where $j(x,t)$ is the current density (A/cm^2) at a distance x (cm) from the mouth of the pore ($0 < x < l$) at time t (sec), j_0 is the exchange current density of the hydrogen reaction (A/cm^2), $C(x,t)$ is hydroxide ion concentration (moles/cm^3), C_0 is initial hydroxide ion concentration (moles/cm^3), β_a and β_c are transfer coefficients of the anodic and cathodic processes, $\eta(x,t)$ is interfacial overpotential (V), and RT/F is the thermal volt equivalent (V). Since a one-dimensional model is used and $a << l$ for most cases of interest, any reaction at the base of the pore (at $x = l$) may be neglected. Current due to reaction on the external surface of the catalyst particle, which is only a small fraction of the total surface involved, is also neglected.

The total current flowing from the mouth of the pore, due to the distributed current density along the pore, is given by Eq. (2),

$$i(t) = S \int_0^l j(x,t)\, dx , \quad (2)$$

where $i(t)$ is total current (A) at time t and S is the surface area of the pore per unit length (cm^2/cm). In the case of a cylindrical pore of radius a, $S = 2\pi a$. The flow of current $i(t)$ in the bulk electrolyte surrounding the catalyst particle causes an "IR" drop, $\Delta\phi_s(t)$ (V), which may be assumed to be given to a good approximation by Eq. (3),

$$\Delta\phi_s(t) = \frac{i(t)}{\pi a \sigma} , \quad (3)$$

in which σ is the conductivity of the electrolyte (ohm^{-1} cm^{-1}). During the time of contact of the catalyst particle with the charging electrode (which is held at the constant potential E by a potentiostat), the potential constraint is given by Eq. (4),

$$E = \eta(0,t) + \Delta\phi_s(t) \ , \tag{4}$$

where E is the potential of the charging electrode referred to the hydrogen electrode potential (V), $\eta(0,t)$ is the interfacial overpotential at the pore mouth (V), and $\Delta\phi_s(t)$ is given by Eq. (3). It is evident that large values of $i(t)$ will cause $\eta(0,t)$ to be small compared with E. This fact is ultimately responsible for the linearity of current-potential curves in the suspension electrode system, since the reaction in the pores of a catalyst particle is constrained to take place at small values of overpotential, thus implying linearity between current density and overpotential.

Solution of the appropriate mass transport equations for the case of a binary electrolyte (KOH, in this case) leads to Eqs. (5) and (6),

$$\frac{\partial [C(x,t)/C_0]}{\partial t} = D_0 \frac{\partial^2 [C(x,t)/C_0]}{\partial x^2} - \frac{SD_K}{VF(D_K + D_{OH})C_0} j(x,t) \ , \tag{5}$$

$$\frac{\partial}{\partial x}\left\{\left[\frac{C(x,t)}{C_0}\right]\frac{\partial \eta(x,t)}{\partial x}\right\} = \frac{S}{V\sigma} j(x,t) + \frac{RT}{F} \cdot \frac{(D_K - D_{OH})}{(D_K + D_{OH})} \cdot \frac{\partial^2 [C(x,t)/C_0]}{\partial x^2} \ , \tag{6}$$

in which D_0 is the so-called "salt" diffusion coefficient given by $D_0 = 2D_K D_{OH}/(D_K + D_{OH})$, where D_K and D_{OH} are diffusion coefficients of potassium and hydroxide ions (cm^2/sec); $\sigma = F^2(D_K + D_{OH})C_0/RT$ is the initial conductivity of the electrolyte in the pore (ohm^{-1} cm^{-1}); and V is the volume of electrolyte inside the pore per unit length (cm^3/cm). The parameter V may also be regarded as the average cross-sectional area of electrolyte in the pore (for a cylindrical pore $V = \pi a^2$). As usual in problems of this type, the first term in Eq. (6) is an Ohmic contribution to the field, and the second term is essentially a junction potential.

Equations (5) and (6) must be solved simultaneously, subject to the appropriate initial and boundary conditions, which are given by Eqs. (7) to (9):

$$C(x,0) = C_0 \ , \tag{7}$$

$$\eta(0,t) = E - \frac{S}{\pi a \sigma} \int_0^l j(x,t)\, dx \ , \tag{8}$$

$$\left.\frac{\partial \eta(x,t)}{\partial x}\right|_{x=l} = 0 \ . \tag{9}$$

The boundary condition of Eq. (8) is obtained by combination of Eqs. (2) to (4). The solution of this set of equations leads ultimately to the current transient which would be observed in such a system and to the current density, concentration, and overpotential distributions in the pore as a function of time. A general analytical solution is not available, due to the nonlinearity of Eqs. (5) and (6) and to the complexity of the boundary condition of Eq. (8), but a number of important special cases have been solved explicitly which allow insight into the behavior of the system.

When the exchange current density (j_0) is large enough so that exponentials in Eq. (1) may be expanded to first-order terms [$\eta(x,0) \ll RT/F$], it is possible to obtain an exact solution of Eqs. (5) and (6) for the initial current due to reaction in a single pore on contact of a catalyst particle with the charging electrode. The resulting expression for the initial current is given by Eq. (10),

$$i(0) = E \frac{\sqrt{i_0/R_0\Phi}\, \tanh\sqrt{i_0 R_0/\Phi}}{1 + (1/\pi a\sigma)\sqrt{i_0/R_0\Phi}\, \tanh\sqrt{i_0 R_0/\Phi}} \ , \tag{10}$$

in which $i_0 = Sj_0 l$ is the total exchange current of the reaction inside the pore (A), R_0 is the "resistance" of the solution inside the pore ($R_0 = l/V\sigma$), and $\Phi = RT/(\beta_a + \beta_c)F$. This relation shows that over a certain range of operation, especially for large values of solution conductivity, the initial current will be proportional to the square root of the solution conductivity. Such a relationship has been observed repeatedly in studies on current transients which occur during contact of individual catalyst particles with the charging electrode.

Solutions of Eqs. (5) and (6), together with the initial and boundary conditions of Eqs. (7) to (9), have been obtained by numerical integration, using parameters thought to be typical of the experimental measurements. Figure 7.12 shows the current transient for reaction in a cylindrical pore calculated for a particular set of parameters, which are given in the figure. One notes the existence of a maximum in the current transient; this type of transient occurs frequently, as mentioned above. The maximum in the current appears at approximately 10^{-4} sec, a value which is typical of those observed experimentally. The increase in current corresponds to the increase in solution conductivity

with time inside the pore as a consequence of the production of hydroxide ions by the (cathodic) hydrogen evolution reaction. Increase of solution conductivity allows the current density distribution to penetrate to greater depths along the pore, thus enhancing the total current output. With time, however, the increase in hydroxide ion concentration increases the rate of the anodic process to such an extent that the net (cathodic) current density begins to decrease. Reaction inside the pore is propagated in a "wave," in a manner very similar to charging of the double layer in a porous or capillary electrode.

The mass transport relations have also been solved explicitly for quantities of interest in the case of a large excess of inert electrolyte. The conclusions drawn from the present treatment do not depend on the unique form of the rate law of Eq. (1). Alternative reaction mechanisms, such as those involving adsorbed hydrogen atoms on the catalyst surface, can also lead to transients having similar properties and to similar relations among output current, electrode potential, solution conductivity, etc.

Immediately following loss of contact of a catalyst particle with the charging electrode, the overpotential on the surface and in the pores of the particle will tend to return to zero, corresponding to the state of equilibrium which normally exists on isolated catalyst particles in the solution. One of the interesting aspects of the suspension electrode system is that reaction proceeds on the surface and in the pores of a particle both during and following contact with the charging electrode. Optimum utilization of the potentialities of the suspension electrode system will require a knowledge of the time required for a particle to return to the equilibrium state which exists prior to impact with the charging electrode.

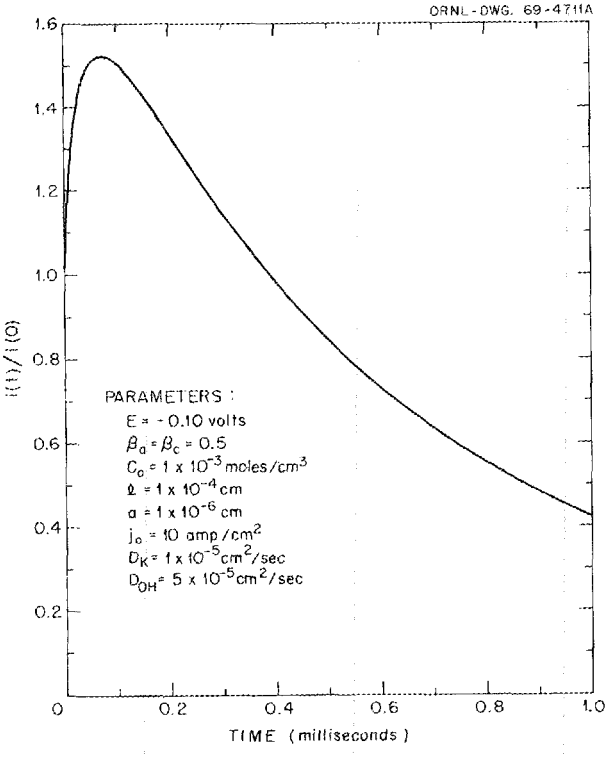

Fig. 7.12. Calculated Current Transient for Hydrogen Reaction in Cylindrical Pore of Catalyst Particle in the Suspension Electrode System.

[1] Research jointly sponsored by the Office of Saline Water, U.S. Department of the Interior, and by the U.S. Atomic Energy Commission under contract with Union Carbide Corporation.

RHENIUM-NICKEL SUSPENSION ELECTRODE CATALYSTS[1]

P. M. Lantz R. E. Meyer

The effectiveness of the suspension electrode for enhancing the current output of the hydrogen evolution reaction in concentrated alkaline solutions is due principally to the catalytic activity of the suspended material. The catalytic activity of rhenium, supported by finely divided carbon or alloyed with metals such as nickel and platinum, has been particularly outstanding in hydrogenation and oxidation reactions.[2] In addition, rhenium displays unusually high resistance to such catalyst poisons as nitrogen, sulfur, and phosphorus. The relative effectiveness of alloys of rhenium and nickel for catalysis of the hydrogen evolution reaction has been studied in 1 *N* KOH solution at 25°C. It was found that hydrogen overvoltage decreases as the rhenium content of rhenium-nickel alloys approaches 40%, but increases with further increase of rhenium content to 100%. At constant electrode potential the current output of a 40% rhenium–nickel electrode was found to be approximately 5 and 30 times greater than for pure rhenium and nickel respectively. Experimental Raney rhenium-nickel alloys are being prepared to assess the usefulness of this material in the suspension electrode system.

[1] Research jointly sponsored by the Office of Saline Water, U.S. Department of the Interior, and by the U.S. Atomic Energy Commission under contract with Union Carbide Corporation.

[2] W. H. Davenport, V. Kollonitsch, and C. H. Kline, *Ind. Eng. Chem.* **60**(11), 10 (1968).

KINETICS OF PIT INITIATION ON TITANIUM IN CHLORIDE SOLUTION[1]

D. V. Subrahmanyam[2] F. A. Posey

Studies were conducted on the kinetics of initiation of pitting corrosion on commercial titanium (type 55A). Galvanostatic (constant current) anodization transients were measured in 1 *M* NaCl + 10^{-4} *M* HCl and in 1 *M* NaCl + 10^{-2} *M* HCl solutions at 25°C as a function of anodic current density. Estimates of the thickness of the passive oxide layer were obtained at various points along the anodization transients by use of capacity measurements. Capacities were measured by application of a square wave of current (10^3-10^4 Hz) to the electrode and observation of the resulting potential "sawtooth" wave on an oscilloscope.

A typical anodization transient and corresponding measurements of the film thickness during the transient are shown in Fig. 7.13. Film thickness was found to vary linearly with electrode potential during the anodization transient; this behavior is typical of metals on which film growth takes place at constant field strength. For the transient shown in Fig. 7.13, field strength was close to 10^6 V/cm, and in all cases studied the field had the same order of magnitude. After a certain time the electrode potential more or less suddenly drops to a potential which is called the pitting potential. Stable pit growth seems not to be possible at potentials below the pitting potential, and the pitting potential is essentially independent of the current passed through the electrode surface. Pitting potentials are to be understood as average potential values exhibited by an electrode undergoing pitting corrosion. In many cases, large fluctuations of potential are detectable on devices such as a strip-chart recorder, which normally possess restricted bandwidths. Oscilloscopic observations show that there are, in addition, potential fluctuations which occur in the millisecond range. The origin of such rapid potential fluctuations is not known with certainty; possibly the influence of natural convection and of formation of gaseous reaction products on potential and concentration distributions inside the pits must be considered.

It was found during the oscilloscopic capacity measurements that rapid potential fluctuations, which consist individually of a very fast drop followed by a somewhat slower return, take place even at potentials several volts below the final pitting potential. The first few events are small in amplitude (only a few millivolts) and may be spaced many seconds apart, depending on applied current, initial film thickness, etc. As the film thickness and electrode potential increase, the frequency and amplitude of these rapid potential fluctuations increase considerably until the final pitting potential is attained.

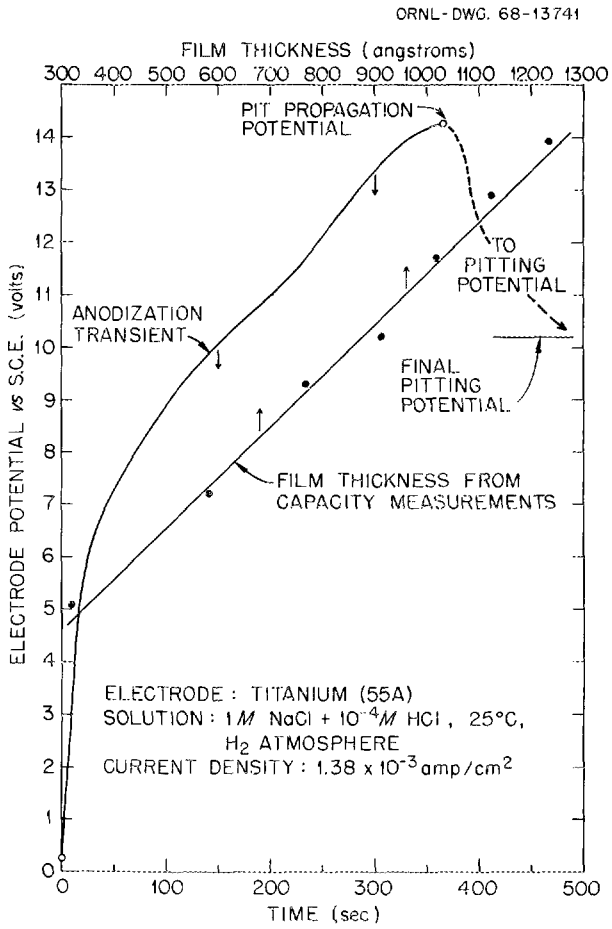

Fig. 7.13. Variation of Electrode Potential and Film Thickness with Time During Anodization of Titanium (Type 55A).

The observations suggest that pit initiation actually occurs much earlier during anodization of titanium in chloride solutions than had been supposed. Pits formed at low potentials and relatively small oxide layer thicknesses appear not to be stable, however, and repassivation takes place very quickly. Measurements of film thickness show that oxide layers of the order of 1000 Å in thickness are formed before stable pit formation becomes possible. Such film thicknesses may be needed to provide a sufficiently confined "column" of electrolyte at sites of incipient pit formation, so that the interacting forces of diffusion and migration can lead to formation of both an acid electrolyte in the pit and a sufficient *IR* drop in the electrolyte phase in order that the metal at the base of the pit can remain in

the active region of corrosion during the growth process. During the ascending branch of the anodization transient, the potential is determined almost exclusively by the film formation reaction and by oxidation reactions (production of O_2 and/or Cl_2) at the oxide-solution interface. However, as the film thickness increases, repassivation of incipient pits becomes more difficult, and an appreciable fraction of the applied anodic current begins to be involved in the pit growth process so that finally the electrode potential is no longer determined by the film formation process but by the pit growth process. The pit propagation potential and the pit propagation time therefore signal this change of potential control.

It is apparent from the curvature of the anodization transient in Fig. 7.13 that the film formation process is not 100% efficient. The capacity measurements have allowed this matter to be studied in more detail, and a typical set of results is shown in Fig. 7.14. Efficiency of the film formation process varies both with electrode potential and with applied current density. Other experiments have shown that the pH of the solution is an additional variable. Anodization efficiency is quite low at current densities below about 1 mA/cm^2. Use of larger current densities leads to increased efficiency of the film formation process. The minimum in the efficiency-potential curves which appears at 9 to 11 V is characteristic of all systems studied. It corresponds to a maximum in the current due to the oxidation reactions which lead to formation of gaseous O_2 and/or Cl_2. Such a maximum in the oxidation current may be a result of two opposing tendencies: (1) the rate of an anodic process tends to increase with increasing electrode potential, and (2) the film thickness also increases with increasing potential and thus may affect transport and/or surface concentrations of electrons and/or holes which are involved in the oxidation processes leading to formation of gaseous products. At potentials of 12 V or higher, a further drop in anodization efficiency always

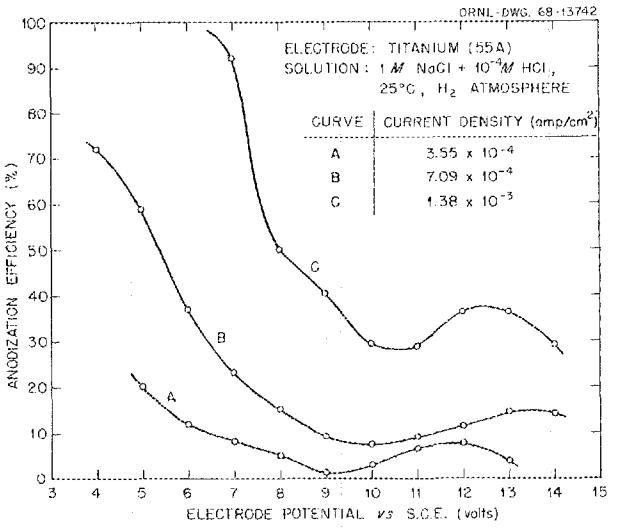

Fig. 7.14. Effect of Anodic Current Density and Electrode Potential on Efficiency of Film Formation on Titanium in Chloride Solution.

takes place as the pit propagation potential is approached. This final drop in efficiency is probably associated with the increased fraction of the anodic current devoted to the pit growth process in this region of the transient. As the potential of the system approaches the final pitting potential, most of the current is then involved in the growth of stable pits. Further experiments will attempt to explore the phenomena described above in greater detail.

---

[1] Research jointly sponsored by the Office of Saline Water, U.S. Department of the Interior, and by the U.S. Atomic Energy Commission under contract with Union Carbide Corporation.

[2] Guest Scientist from the Indian Institute of Science, Bangalore; present address: Department of Metallurgical Engineering, Ohio State University, Columbus.

8. Nonaqueous Systems at High Temperatures

PHASE DIAGRAMS

LIMITS OF MISCIBILITY IN MOLTEN-SALT SYSTEMS: KBF_4-LiF, Li_2BeF_4-KI, AND Li_2BeF_4-KBF_4

A. S. Dworkin M. A. Bredig

The System KBF_4-LiF

In the phase diagram of the reciprocal salt system NaF-KBF_4, containing cations and anions all of unit charge but of widely differing sizes, the NaF liquidus has been interpreted in terms of a large positive deviation from ideality.[1] It was then predicted and has now been confirmed that replacement of NaF by LiF would bring about separation into two liquids. In this system the more-stable ion pairing is [Li^+ (charge/radius ratio $z/r \approx 1.15$), F^- ($\approx$0.85)] and [K^+ ($\approx$0.65), $(BF_4)^-$ ($\approx$0.40)].

At 840°C the miscibility of molten LiF and KBF_4 is indeed small, the two conjugate monotectic liquids containing 3 and 99% LiF in equilibrium with solid LiF (Fig. 8.1). The observed slight variance of the monotectic temperature with composition may be caused by the formation of some KF through dissociation of KBF_4. The eutectic point lies at 564°C and about 0.5% LiF. No attempt was made to determine the predictably high temperature of complete miscibility because of the large BF_3 dissociation pressure involved.

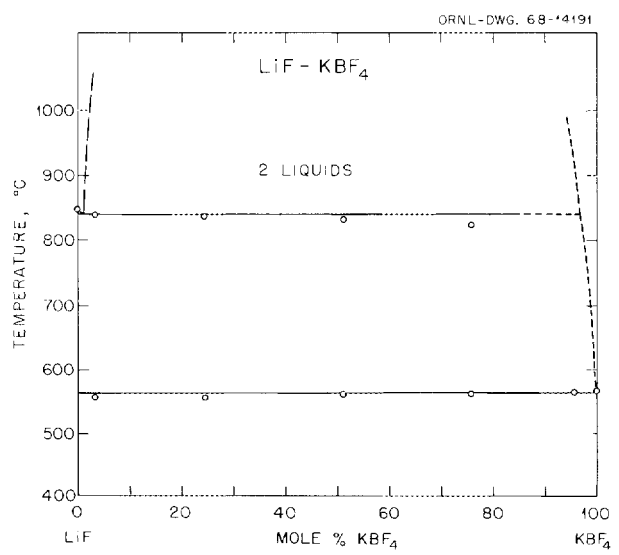

Fig. 8.1. The System LiF-KBF_4.

The System Li_2BeF_4-KI

This system contains as the more-stable ion pairs [Li^+ ($z/r \approx 1.15$), $(BeF_4)^{2-}$ ($\approx$0.85)] and [K^+ ($\approx$0.65), I^- ($\approx$0.50)]. We have been able roughly to delineate the region of two conjugate liquids as well as the eutectic and monotectic equilibria (Fig. 8.2). At a critical solution (consolute) temperature of 945°C (above which only one liquid phase exists) the critical solution contains 53% KI. At 665°C the two conjugate monotectic liquids contain 7 and 98% KI in equilibrium with solid KI. The observed large variance of the monotectic temperature, a decline with decreasing KI concentration, may be caused by the presence of excess BeF_2 in the Li_2BeF_4 sample used (LiF-BeF_2, 66-34 mole %). However, it must also be recognized that the system is a reciprocal *pseudo*-binary one and that even without excess BeF_2 the compositions of the two liquid phases are likely to be more complicated than shown in Fig. 8.2. The eutectic point lies at about 450° and 4 mole % KI. Large supercooling effects and our observation of what may be a metastable phase of the Li_2BeF_4 with added KI made the establishment of the eutectic approximate at best.

The System Li_2BeF_4-KBF_4

The more-stable ion pairs are [Li^+($z/r \approx 1.15$), $(BeF_4)^{2-}$ ($\approx$0.85)] and [K^+($\approx$0.65), $(BF_4)^-$ ($\approx$0.4)]. With the similarity in z/r for BF_4^- and I^- the eutectic and monotectic equilibria in the system were expected, and found, to be very similar to those reported above for the Li_2BeF_4-KI system. At 554°C the two conjugate monotectic liquids contain about 5 and 98% KBF_4 in equilibrium with solid KBF_4. The eutectic point lies at about 450° and 4 mole % KBF_4. Because of

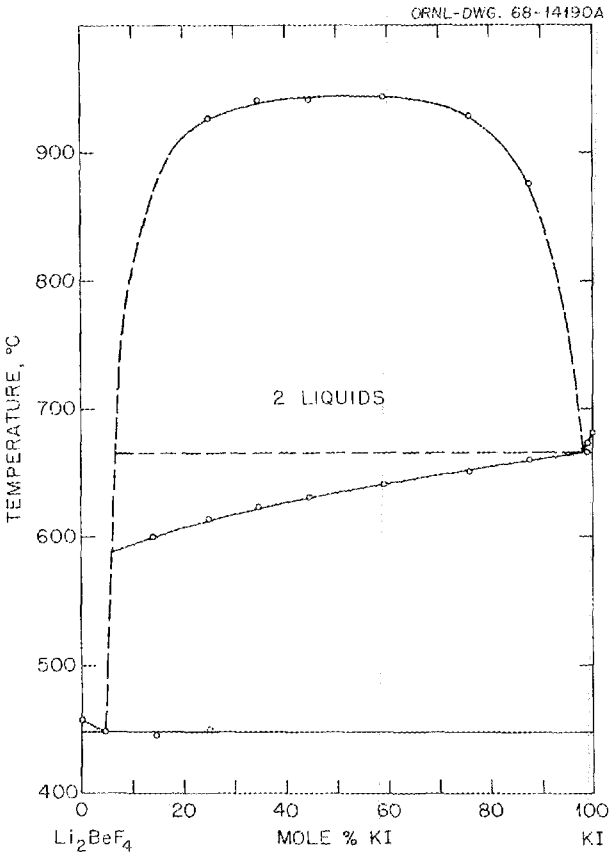

Fig. 8.2. The System Li_2BeF_4-KI.

expected high BF_3 gas pressures, no attempt was made to determine the consolute temperature, but it is probably not too different from that found in the Li_2BeF_4-KI system. The difficulties described above in establishing the monotectic and eutectic equilibria for the Li_2BeF_4-KI system were again encountered in almost identical fashion for the Li_2BeF_4-KBF_4 system.

The much greater miscibility in the Li_2BeF_4-$NaBF_4$ system indicated from the liquid-liquid distribution studies of Bamberger *et al.*[2] is due to the smaller size of the sodium ion. Further delineation of the entire two-liquid region may be desirable, possibly by the technique of thermal analysis. In the present study it was the only method thus far employed. More detailed knowledge may be gained by the use of additional techniques such as sampling at temperature or quenching with subsequent analysis of the separated phases (high-temperature centrifuge?). More studies of simpler systems such as LiF-KI, LiF-KBr, LiF-CsCl, etc., may also be desirable to further our basic quantitative understanding of the phenomenon of liquid-phase separation in molten-salt systems.

---

[1] M. A. Bredig, *MSR Program Semiann. Progr. Rept. Feb. 29, 1968*, ORNL-4254, pp. 167–68.

[2] C. E. Bamberger *et al.*, *MSR Program Semiann. Progr. Rept. Feb. 29, 1968*, ORNL-4254, pp. 171–73.

CORRELATION OF THE SOLUBILITY OF CERIUM TRIFLUORIDE IN MOLTEN MIXTURES OF LITHIUM, BERYLLIUM, AND THORIUM FLUORIDES WITH SOLVENT COMPOSITION

M. A. Bredig

Preliminary attempts[1] to relate the solubility of CeF_3 in LiF-BeF_2-ThF_4 mixtures to solvent composition had given unsatisfactory results. I found the molar ratio of ThF_4 to BeF_2 to be the dominant factor in the results of Fredricksen, Gilpatrick, and Barton.[1] The smooth lines of Fig. 8.3 show the nearly linear dependence of the solubility (s) of CeF_3 = 100 × CeF_3/(CeF_3 + LiF + BeF_2 + ThF_4) on u = ThF_4/(ThF_4 + BeF_2), in accordance with the empirical equations:

$$s(600°C) = 0.50 + 2.60u - 0.40u^2 ,$$

$$s(700°C) = 1.60 + 4.23u - 0.88u^2 ,$$

$$s(800°C) = 3.80 + 5.80u - 0.80u^2 .$$

The only significant deviation from these equations among the *ternary* solvents occurred with mixture 8 (LiF-BeF_2-ThF_4: 75.0-17.9-7.1 mole %, u = 0.28, marked with a plus sign in Fig. 8.3), with the characteristically high "free LiF" content b = [LiF] − 2[BeF_2] − 3[ThF_4] of 18 mole % LiF. The definition of b involves the assumption that BeF_2 and ThF_4 exist in the molten mixtures as BeF_4^{2-} and ThF_7^{3-} respectively.[2] The significance of b as a second parameter in the solubility behavior is further demonstrated by the similar deviations from the equations above with two of the *binary* solvents, namely, mixture 14 (LiF-BeF_2: 72.7-27.3 mole %, u = 0) and mixture 11 (LiF-ThF_4: 80-20 mole %, u = 1), both having similarly high "free LiF" content, b = 18 and 20. The correspondence of the excess CeF_3 solubilities in these three solvents is depicted in Fig. 8.3 by the dashed lines for each of the temperatures 600, 700, and 800°C.

An attempt has been made to rationalize the observed dependence of the CeF_3 solubility in mixtures of LiF, BeF_2, and ThF_4 on solvent composition in terms of

ORNL-DWG. 69-688AR2

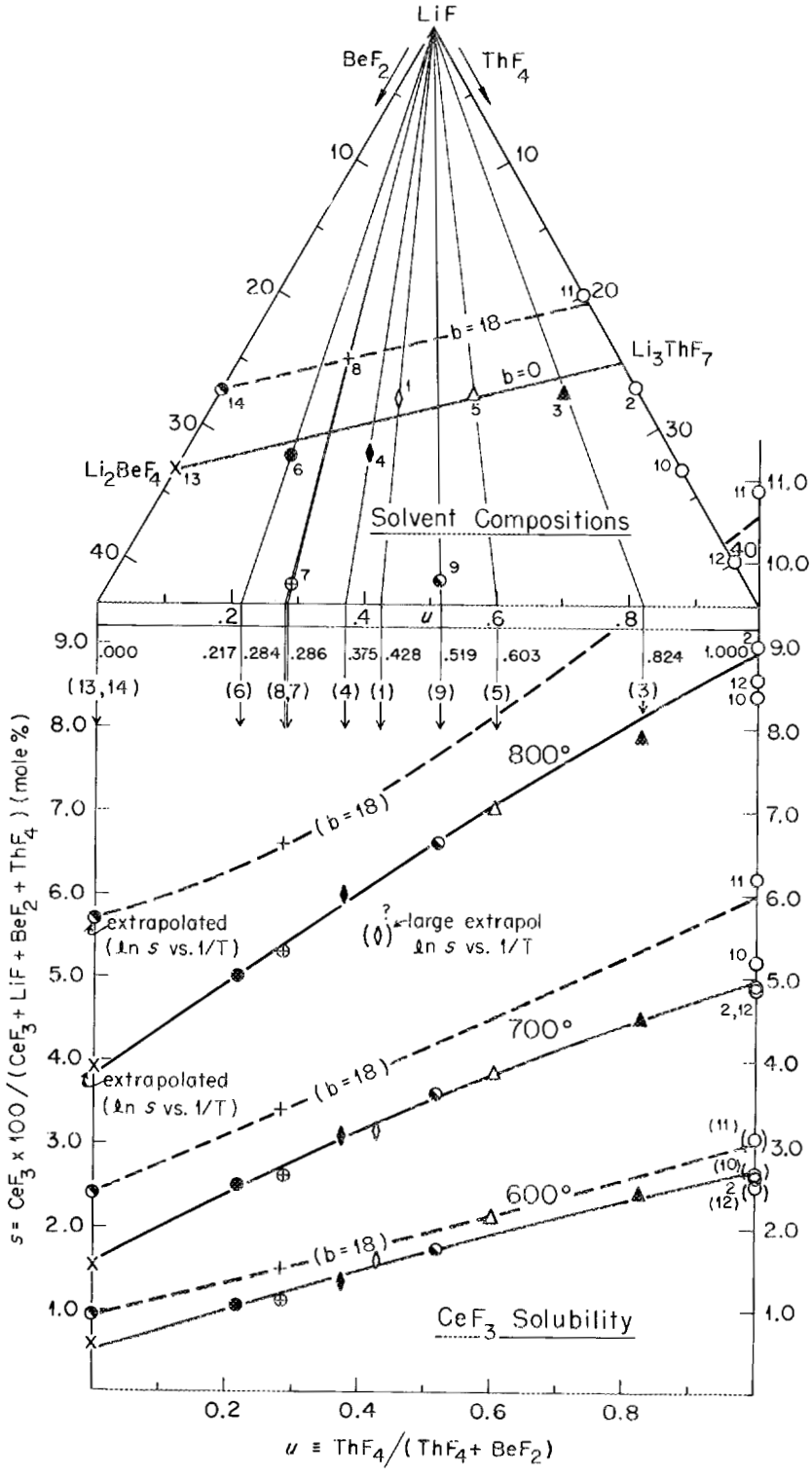

Fig. 8.3. Solubility of Cerium Trifluoride in Lithium, Beryllium, and Thorium Fluoride Mixtures as a Function of the Thorium-Beryllium Ratio.

charge and size of the constituent ions. The dependence reflects the significance of the greater availability of F^- ions for interaction with Ce^{3+} in melts richer in LiF. This is indicated by the considerable negative deviation from ideality in the LiF-CeF_3 phase diagram: values, measured or extrapolated, for the CeF_3 concentrations of the CeF_3 liquidus at 600 to 800° exceed those estimated from the known entropy of fusion of CeF_3 [8.62 cal (°C)$^{-1}$ mole^{-1} at the melting point of CeF_3] by factors of from 4 to 2 respectively. In LiF-BeF_2 mixtures containing 25 to 50 mole % BeF_2, the solubility is very much smaller than ideal. This positive deviation from ideality can be attributed to the much weaker interionic forces between the singly charged Li^+ ions and the relatively large BeF_4^{2-} anions (cf. also the low melting points in the LiF-BeF_2 system) as compared with the forces between the triply charged Ce^{3+} and the relatively small F^- ions. Although molten Li_3ThF_7 contains even larger complex anions, ThF_7^{3-}, it exhibits a CeF_3 solubility intermediate between that in LiF and that in Li_2BeF_4. This apparent anomaly can be attributed to the fact that the Ce^{3+} ion, with a charge-to-size ratio, or "ionic potential," $z/r \cong 3$, competes for F^- ions much more successfully with Th^{4+} ($z/r \cong 4$) than with Be^{2+} ($z/r \cong 6$).

---

[1] J. A. Fredricksen, L. O. Gilpatrick, and C. J. Barton, *Solubility of Cerium Trifluoride in Molten Mixtures of LiF, BeF_2, and ThF_4*, ORNL-TM-2335 (January 1969).

[2] M. A. Bredig, MSR-68-75 (Apr. 26, 1968) (internal memorandum).

MOLTEN-SALT–METAL SYSTEMS

SOLUBILITY OF THORIUM METAL IN MOLTEN LITHIUM FLUORIDE–THORIUM FLUORIDE MIXTURES

H. R. Bronstein M. A. Bredig

We have corroborated the finding of Barton and Stone[1] that with inert-gas stirring of a melt of LiF-ThF_4 (73-27 mole %), the immersion of a thorium rod in the melt causes extensive attack of the nickel container by the dissolved thorium. Two nickel-rich phases of the five known intermetallic nickel-thorium compounds have been positively identified as products of this attack: $ThNi_2$ as the major, and $ThNi_5$ as a minor, constituent. The great importance of the stirring reflects the low solubility of the thorium metal in the salt melt.

With an improved analytical technique involving the mass-spectroscopic determination of the hydrogen produced when samples taken at temperature are dissolved in aqueous acid, the solubility of thorium metal in molten LiF-ThF_4 (73-27 mole %) at 620°C has been firmly established as 0.1 mole %. The particular form in which the thorium metal dissolves in the melt is as yet undetermined. Russian workers, using electrochemical techniques,[2-7] claim to have demonstrated the presence of ionic species of lower valency when beryllium, zirconium, or thorium metal is equilibrated with alkali halide melts containing the normal chlorides of those metals.

If, on dissolving in the LiF-ThF_4 melt, the thorium metal forms an ion of lower valency, $Th^{(4-n)+}$, an inert metal electrode such as tantalum should assume the same potential in that melt as a thorium metal electrode, because the potential-determining process occurring at each electrode is the same:

$$Th^{(4-n)+} \rightleftarrows Th^{4+} + ne^- . \qquad (1)$$

However, a dissolution mechanism other than the formation of a thorium species of lower valency might conceivably also yield a zero potential difference. This is the reaction

$$Th^0 + 4LiF \rightarrow ThF_4 + 4(Li^+ + e^-) , \qquad (2)$$

where the electron may be considered to have *F*-, or color-, center-like properties. At equilibrium the potential developed will be the same for the thorium electrode and for an inert metal electrode:

$$E^\circ_{Th^0/Th^{4+}} - \frac{RT}{4F} \ln a_{Th^{4+}} = E^\circ_{(Li^+ + e^-)/LiF} - \frac{RT}{F} \ln \frac{a_{LiF}}{a_{(Li^+ + e^-)}} .$$

In two experiments the potential developed initially between a thorium electrode and a tantalum electrode placed in an LiF-ThF_4 (73-27 mole %) melt at 620°C was 950 mV. This potential remained constant for approximately 20 min; then a slow downward drift commenced, terminating after 8 hr in a potential difference of essentially zero. For an explanation of the zero potential, the second solution model is not considered a very likely one, since available thermodynamic data for reaction (2) would predict a quantity of color centers two orders of magnitude smaller than that found analytically (4 × 0.1 mole % "Th metal"; cf.

above). Therefore, though very tentative in the absence of positive spectroscopic evidence, the assumption of a thorium species of lower valency, stable only in minor concentrations, seems to be at present the better explanation for the results obtained.

---

[1] C. J. Barton and H. H. Stone, *Reduction of Iron Dissolved in Molten LiF-ThF$_4$*, ORNL-TM-2036 (November 1967).

[2] M. V. Smirnov and L. E. Ivanovskii, *Zh. Fiz. Khim.* **31**, 802 (1957).

[3] M. V. Smirnov and V. A. Chemezov, *Dokl. Akad. Nauk SSSR* **120**, 122 (1958).

[4] M. V. Smirnov and N. Ya. Chukreev, *Russ. J. Inorg. Chem. (English Transl.)* **4**, 1168 (1959).

[5] N. I. Kornilov and N. G. Ilyushchenko, *Electrochem. Molten Solid Electrolytes (English Transl.)* **5**, 71 (1967).

[6] V. Ya. Kudyakov *et al.*, *At. Energ.* (USSR) **24**, 448 (1968).

[7] M. V. Smirnov and L. D. Yushina, *Izv. Akad. Nauk SSSR, Otd. Khim. Nauk*, No. 11, 1285 (1956) and No. 2, 251 (1959). See, however, R. Srinivisan and S. N. Flegas, *Can. J. Chem.* **42**, 1315 (1964).

A REFERENCE ELECTRODE SYSTEM FOR POSSIBLE USE IN FLUORIDE MELTS

H. R. Bronstein

A knowledge of the activity of the ThF_4 in the fuel salt mixture LiF-BeF_2-ThF_4 (72-16-12 mole %) of the projected MSBR would be of value for fuel reprocessing studies. The most obvious and direct method for the determination of this quantity is by an emf study of a cell of the type

$$Th^0 | LiF, BeF_2, ThF_4(x) | \text{reference electrode} .$$

However, although thorium metal has a very slight solubility [0.1 mole % in the molten LiF-ThF_4 (73-27 mole %) solvent at 600°C],[1] the consequences of its continuous reaction with some reference electrodes and of its alloying with a container material such as nickel would cause serious difficulties. The above considerations would almost immediately eliminate the use of the $(H_2, HF)|F^-$ electrode as a reference electrode, since nickel is the most convenient metal for use with this gas mixture. The $(H_2, HF)|F^-$ reference electrode[2] is also inconvenient to use since it requires an HF-H_2 gas mixture of accurately known composition and, in addition, has the serious fault that hydrogen as a reactive, rapidly diffusing gas is difficult to confine to the vicinity of the electrode. Therefore a cell must be designed in which contact of the reactive dissolved species of thorium[1] with the reference electrode is eliminated and in which a container material such as tantalum is used which is not attacked by the subvalent species.

Such a cell might be

$$(-)\ Th^0 \left| \begin{array}{c} ThF_4, LiF, BeF_2 \\ \text{(liq)} \end{array} \right| \begin{array}{c} \text{Ta frit of} \\ \text{fine porosity} \end{array} \left| \begin{array}{c} \text{single-crystal} \\ CaF_2 \text{ disk} \end{array} \right| \begin{array}{c} (NiF_2 + Ni) \\ \text{pellet} \end{array} (+) .$$

The melt would be held in an open tantalum crucible with the single-crystal CaF_2 disk making contact with the melt at the surface of a tantalum frit of extremely fine porosity welded into the bottom of the crucible. The CaF_2 crystal in turn is in contact with the pellet of an NiF_2-Ni mixture (50-50% by volume), which is the reference electrode. The solid-solid junction[3] CaF_2 vs NiF_2-Ni provides no difficulty since the solid CaF_2 conducts virtually 100% by the mobile F^- ion at the temperature of the experiment (600°C). Since the free energy of formation of NiF_2 is well established,[3] the NiF_2-Ni makes a suitable reference electrode. The magnitude and stability of the liquid-solid junction potential must be established. Although a minimum of liquid contact will be permitted by the tantalum frit, some reaction of the melt with the CaF_2 will occur nevertheless.

The $Be^0|LiF, BeF_2$ electrode was used in place of $Th^0|ThF_4, LiF, BeF_2$ in a test cell at 600°C since the activity coefficients of BeF_2 in this melt are known.[4] The voltage of the cell on initial contact of the melt with the CaF_2 crystal was 1.870 V, in agreement with the theoretical value of 1.900 V considering that the free energy of formation of BeF_2 is not known to better than ±1.0 kcal.[3] However, this potential was constant for only 10 min, and then a slow downward drift began. A somewhat steady potential of approximately 1.35 V was attained after a period of 12 hr, which implies a total potential for the liquid-liquid and liquid-solid junctions of the order of 0.5 V. However, since the liquid formed on the surface of the CaF_2 crystal did not provide a stable contact, any movement of the cell caused wild fluctuations in the potential, which after some time returned to 1.35 V.

The experience with this cell demonstrates that a system using the solid $CaF_2|NiF_2$, Ni reference electrode is feasible in a molten salt if the liquid-solid junction is modified. This will be done in the following manner utilizing an apparatus previously described.[5] The LiF-BeF_2 melt with the Be metal electrode will be

contained in a tantalum capsule and will make contact with a communicating liquid, a saturated solution of CaF_2 in LiF-NaF (60-40 mole %), through the tantalum frit welded into the side of the capsule.[5] Into the communicating liquid a single crystal of CaF_2 will be placed as part of the reference electrode system. The cell may be written

$$(-)\ Be^0 \left| \begin{matrix} LiF\text{-}BeF_2 \\ (liq) \end{matrix} \right| \begin{matrix} Ta \\ frit \end{matrix} \left\| \begin{matrix} LiF\text{-}NaF\ CaF_2 \\ (sat'd\ liq) \end{matrix} \right| \begin{matrix} CaF_2 \\ solid \end{matrix} \left| \begin{matrix} (NiF_2 + Ni) \\ pellet \end{matrix} \right. (+) .$$

Experience has shown that a stable and constant liquid-junction potential, independent of changes in concentration in the bulk solution, can be maintained by the tantalum frit method if the junction is made within the frit.[5]

---

[1] H. R. Bronstein and M. A. Bredig, preceding report, this section.

[2] B. F. Hitch and C. F. Baes, Jr., *MSR Program Semiann. Progr. Rept. Aug. 31, 1968*, ORNL-4344, p. 167.

[3] R. J. Heus and J. J. Egan, *Z. Physik. Chem.* (Frankfurt) 49(1-2), 38–43 (1966).

[4] B. F. Hitch and C. F. Baes, Jr., *EMF Study of LiF-BeF$_2$ Solutions*, ORNL-4257 (July 1968).

[5] H. R. Bronstein, *Chem. Div. Ann. Progr. Rept. May 20, 1966*, ORNL-3994, p. 100; *J. Phys. Chem.* 73, 1320 (1969).

SOLUBILITY OF LANTHANUM IN MOLTEN LANTHANUM TRIIODIDE

H. R. Bronstein

The solubility limits of the rare-earth metals in their molten halides as determined by an emf technique[1] are in good agreement with values obtained by other methods,[2] with the exception of the La-LaI_3 system. In the La-LaI_3 system the emf technique gave a value of 25 mole % La^0, in contrast to the value 33 mole % obtained from phase equilibrium studies.[3] This discrepancy has now been resolved. The lower value represented not the solubility of La metal at 835°C but the highly temperature-sensitive solubility of LaI_2 at 813°, just below its melting point. The error was caused by an unsuspected temperature gradient of 22°C within the emf apparatus. This gradient was not detected earlier, nor did it affect results in the other rare-earth metal-halide systems, because there only the temperature-insensitive solubility of the metal was involved.

---

[1] H. R. Bronstein, *Chem. Div. Ann. Progr. Rept. May 20, 1966*, ORNL-3994, p. 98 and *May 20, 1967*, ORNL-4164, p. 97.

[2] *Chem. Div. Ann. Progr. Rept. May 20, 1968*, ORNL-4306, Table 8.1, p. 121.

[3] J. D. Corbett *et al.*, *Discussions Faraday Soc.* 32, 79 (1961).

HIGH-TEMPERATURE THERMOCHEMISTRY

THE ORDER-DISORDER (λ) TRANSITION IN URANIUM DIOXIDE AND OTHER SOLIDS OF THE FLUORITE TYPE. EFFECT OF ION SIZE AND DEVIATION FROM STOICHIOMETRY

M. A. Bredig[1]

In a study of the causes for the abnormally low entropy of fusion of several salts AB_2 possessing the fluorite type of crystal structure, I attributed the fusion behavior to an exceptionally high entropy of the solid as the result of gradual (CaF_2, $SrCl_2$, K_2S) or sudden ($SrBr_2$, $BaCl_2$) disordering and distribution of the B ions over two types of lattice positions, namely, ($\frac{1}{4}$ $\frac{1}{4}$ $\frac{1}{4}$ fcc; $\frac{3}{4}$ $\frac{3}{4}$ $\frac{3}{4}$ fcc) and ($\frac{1}{2}$ $\frac{1}{2}$ $\frac{1}{2}$ fcc).[2] This disordering process was reflected in a very distinct maximum of the heat capacity in each of the solids CaF_2, $SrCl_2$, and K_2S and in an unusually large entropy for the first-order transition in solid $SrBr_2$ and $BaCl_2$. I also predicted the occurrence of a heat capacity maximum in oxides of the fluorite type of structure, particularly the dioxides of uranium and thorium, and noted indications of an abnormal entropy in the excellent measurements of the enthalpy of UO_2 up to 2350°K by Conway and Hein.[3] More recently, these were extended by Hein and Flagella,[4] Hein, Sjodahl, and Szwarc,[5] and Hein, Flagella, and Conway[6] to and beyond the melting point, above 3100°K. A theoretical treatment of the data was given by Szwarc[7] in terms of the formation of Frenkel lattice defects, that is, of a rather limited concentration of interstitial oxygen ions and ion vacancies. However, in this interpretation, a salient feature of the data was not considered. This is the occurrence of a pronounced, sharp maximum in the heat capacity of UO_2 at a temperature of 2670°K ("λ-point"), entirely analogous to those found in other compounds of the fluorite type,[2,8] such a maximum is characteristic of the cooperative process of a second-order, or λ, transition, for example, the disordering of *all* the oxygen ions. This significant and predicted[2] aspect of the high-temperature behavior of uranium dioxide has been examined in some detail and is briefly discussed in the following.

1. Excess enthalpy, H_{ex}, representing the difference between the experimental enthalpy[7] and a "lattice enthalpy," H_l, according to Szwarc's equation

$$H_l = -5602 + 17.78T + 1.02 \times 10^{-3} \times T^2 ,$$

is plotted in Fig. 8.4 against absolute temperature T. A sharp break in H_{ex} is very obvious at 2670°K. (One experimental point, at 2774°K, showing excessive deviation, is disregarded in accordance with "Chauvenet's criterion"). Clearly apparent are the systematic deviations (negative below and positive above 2600°K) of the experimental points from the dotted line depicting the relationship

$$\ln H_{ex} = 14.83/2R + \ln(\sqrt{2} \times 71{,}300) - 71{,}300/2RT,$$

proposed by Szwarc. Obviously, the use of this equation for an interpretation of the high-temperature excess enthalpy in terms of Frenkel defects only, with an alleged enthalpy of defect formation of 71.3 kcal/mole and a corresponding entropy of 14.83 eu, is not justified. Figure 8.5 clearly shows the very sharp and pronounced maximum in C_p at 2670°K, followed by a region of high excess heat capacity rising from 12 to 18 cal (°K)$^{-1}$ mole^{-1} up to the melting point. Since the theory of the formation of a relatively small number of Frenkel defects does not provide for the occurrence of such a maximum, the latter is definite proof for the existence, in UO_2, of a different, namely a cooperative, process such as the destruction of long-range order, in this case undoubtedly of the oxygen ions.

2. An evaluation of the area under the curve for the excess heat capacity vs ln T up to the λ point at 2670°K yields an entropy of approximately 2.7 eu. This is slightly larger than R ln 3 = 2.18, expected from a simplified theory of the disordering process. If absence of electronic excitation is assumed, the small difference of one-half of one entropy unit may be

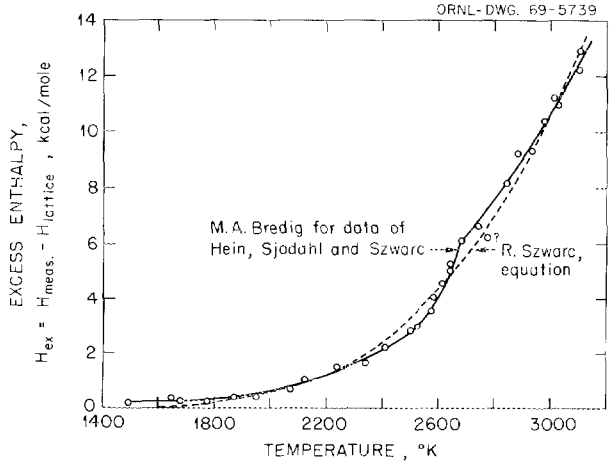

Fig. 8.4. High-Temperature Excess Enthalpy and Second-Order Transition in Uranium Dioxide.

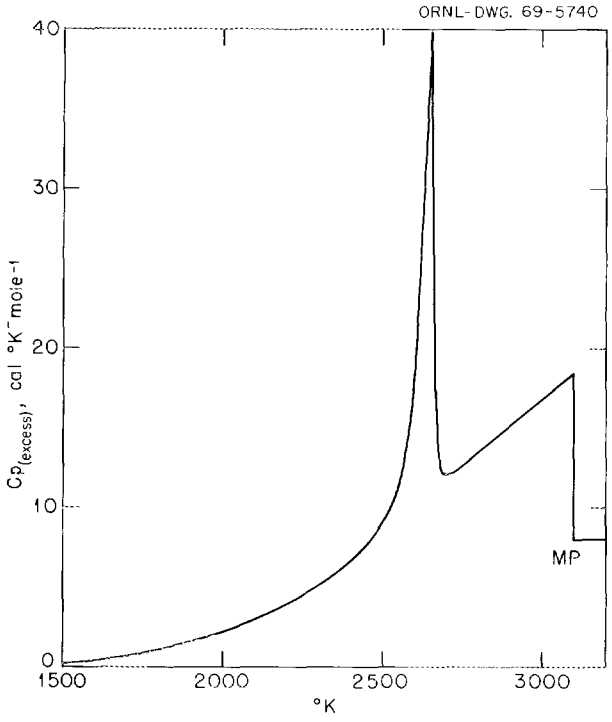

Fig. 8.5. High-Temperature Heat Capacity and Second-Order Transition in Uranium Dioxide.

attributable to the onset of some Frenkel defect formation, possibly also reflected by the high excess heat capacity between the transition and melting temperatures. New enthalpy and entropy values might be derived for this process after due consideration of the order-disorder transition.

3. Most recently, Leibowitz, Mishler, and Chasanov[9] also have reported some high-temperature enthalpy measurements on UO_2. Although duly cautious because of the precision statistics of their data, they found a transition indicated at a temperature of 2800 to 2850°K, about 150° higher than shown for the results of Hein *et al.* A possible interesting cause for the discrepancy, if real, may be the excess oxygen content of 0.015 O^{2-} per mole of UO_2, five times higher than 0.003, reported for the preparation giving the lower λ-point temperature. It is conceivable that for oxygen contents greater than $UO_{2.05}$, the λ point may reach the melting-point temperature and disappear. Such behavior might also occur in CaF_2-YF_3, $SrCl_2$-$NdCl_3$, or K_2S-K_3P and various other similar solid solutions.

4. It was recently noticed by Busey[1] that the compounds of the fluorite type for which the order-disorder transition had been observed might arrange themselves into two groups, namely, those with the excess entropy for the temperature range between the

onset of the transition and the melting point amounting to a value close to $R \ln 3 = 2.18$ (CaF_2: 2.3; $SrCl_2$: 2.35 eu)[2] and those with a considerably higher excess entropy (K_2S: 4.0, ref. 2*c*; PbF_2: 3.6 eu).[8] It appears now that SrF_2 and BaF_2, with excess entropies estimated by me from data of Gant and Smith[10] to be 4.5 and 6.0, can be placed in the second group. On the other hand, $SrBr_2$ (ref. 2*a*) and $BaCl_2$ (ref. 2*a*), with transition entropies of 3.16 and 3.44, belong to the former group, if from these values is subtracted a likely small contribution to ΔS_{tr} of about one entropy unit, resulting from the change in the nonconfigurational *lattice* entropy in the *first*-order transition of these two salts. It seems, furthermore, that the principal factor in this behavior is the ratio in the sizes of the two ions, A and B, of the AB_2 compounds, the size of the A ion equaling exactly the size of the void in the fluorite structure being filled by the B ion on disordering. Figure 8.6 shows how S_{ex} increases with increasing radius ratio, $R = r(A) : r(B) = r(void) : r(B)$, above $R \cong 1$, which might well be the critical value of R. The ionic radius ratios used in this diagram were derived from the partial set of new average crystal radii given by Tosi and Fumi[11] in combination with cubic lattice constants.

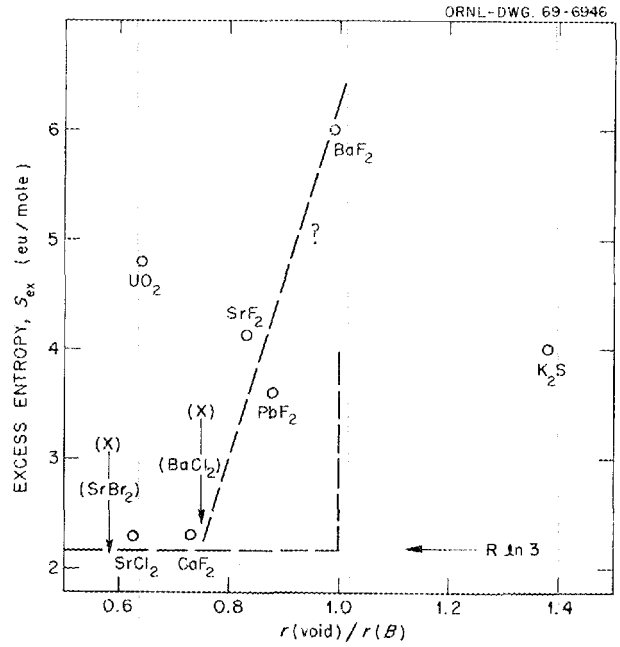

Fig. 8.7. Same as Fig. 8.6, but with Traditional Radii.

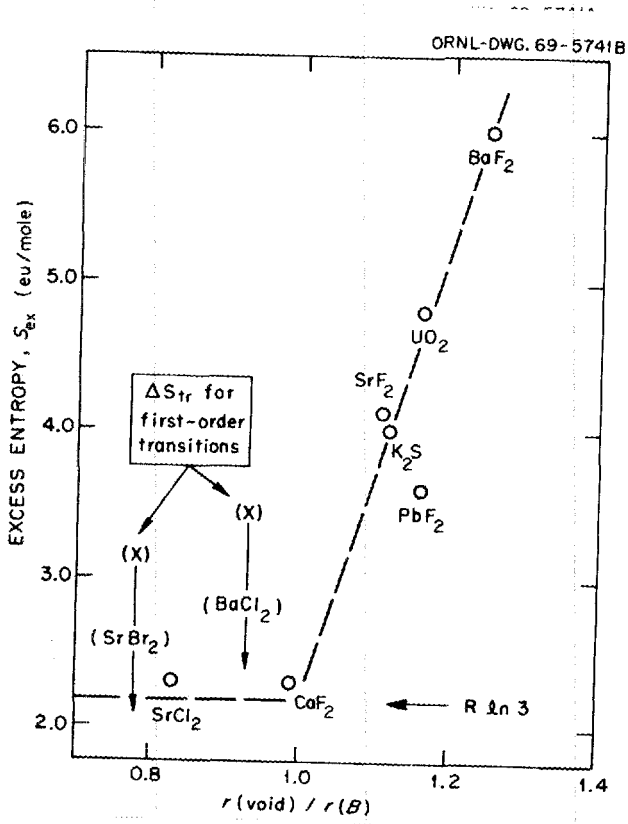

Fig. 8.6. High-Temperature Excess Entropies in Compounds of the Fluorite Type of Structure in the Range Between Transition and Melting Temperatures as a Function of Ionic Size. New ionic radii.

It seems noteworthy that traditional radii would eliminate both UO_2 and K_2S from the correlation with the other compounds (see Fig. 8.7). Furthermore, the rise in excess entropy would occur at a radius ratio of no apparent significance, 0.75, rather than unity.

---

[1] R. H. Busey and A. S. Dworkin have contributed greatly through helpful discussions.

[2] A. S. Dworkin and M. A. Bredig, (*a*) *J. Phys. Chem.* **67**, 697 (1963); (*b*) *J. Chem. Eng. Data* **8**, 416 (1963); (*c*) *J. Phys. Chem.* **72**, 1277 (1968).

[3] J. B. Conway and R. A. Hein, *J. Nucl. Mater.* **15**, 1 (1965).

[4] R. A. Hein and P. N. Flagella, GEMP-578 (Feb. 16, 1968).

[5] R. A. Hein, L. H. Sjodahl, and R. Szwarc, *J. Nucl. Mater.* **25**, 99 (1968).

[6] R. A. Hein, P. N. Flagella, and J. B. Conway, *J. Am. Ceram. Soc.* **51**, 291 (1968).

[7] R. Szwarc, *J. Phys. Chem. Solids* **30**, 705 (1969); in Eq. (15) of this paper a "+" sign has been omitted after $\Delta S_F/2R$.

[8] C. W. Linsey, R. A. Gilbert, and R. H. Busey, "High Temperature Enthalpies of the Lead Halides. Enthalpies and Entropies of Fusion," this report.

[9] L. Leibowitz, L. W. Mishler, and M. G. Chasanov, *J. Nucl. Mater.* **29**, 356 (1969).

[10] Private communication from F. A. Gant to A. S. Dworkin, used here with the kind permission of Prof. D. F. Smith, University of Alabama.

[11] M. P. Tosi and F. G. Fumi, *J. Phys. Chem. Solids* **25**, 45 (1964).

HEAT CONTENT OF SODIUM AND POTASSIUM FLUOROBORATES FROM 298 to 900°K: HEATS OF FUSION AND TRANSITION

A. S. Dworkin M. A. Bredig

Sodium fluoroborate is the main component of a proposed coolant mixture for a molten-salt reactor. We have measured the high-temperature heat contents of $NaBF_4$ and KBF_4 both to obtain information for reactor technology and to explore the interesting transition behavior of the solid fluoroborates.

The copper-block drop calorimeter used for the measurements has been described previously.[1] The salts were sealed in an inner platinum liner to prevent attack on the Inconel capsules especially designed for our heat content apparatus.

The following equations represent our measured heat content data for $NaBF_4$ and KBF_4 in calories per mole:

$NaBF_4$

$$H_T - H_{298} = -3820 + 3.148T + 3.703 \times 10^{-2} T^2 - 1.217 \times 10^5 T^{-1}; 298\text{–}516°K; \pm 0.3\%$$

$$\Delta H_{transition} = 1610 \pm 30 \text{ cal/mole}; 516°K$$

$$\Delta S_{transition} = 3.13 \text{ eu}$$

$$H_T - H_{298} = 9785 + 36.48T; 516\text{–}679°K; \pm 0.1\%$$

$$\Delta H_{fusion} = 3250 \pm 30 \text{ cal/mole}; 679°K$$

$$\Delta S_{fusion} = 4.78 \text{ eu}$$

$$H_T - H_{298} = -8605 + 39.52T; 679\text{–}750°K; \pm 0.1\%$$

KBF_4

$$H_T - H_{298} = -6325 + 15.62T + 1.943 \times 10^{-2} T^2 - 1.737 \times 10^4 T^{-1}; 298\text{–}556°K; \pm 0.2\%$$

$$\Delta H_{transition} = 3300 \pm 40 \text{ cal/mole}; 556°K$$

$$\Delta S_{transition} = 5.93 \text{ eu}$$

$$H_T - H_{298} = -7800 + 34.95T; 556\text{–}843°K; \pm 0.2\%$$

$$\Delta H_{fusion} = 4300 \pm 40 \text{ cal/mole}; 843°K$$

$$\Delta S_{fusion} = 5.10 \text{ eu}$$

$$H_T - H_{298} = -7710 + 39.94T; 843\text{–}900°K; \pm 0.1\%$$

Although the entropies of fusion of the two salts are similar, the entropy of transition of KBF_4 is much larger than that of $NaBF_4$ (5.93 eu to 3.13 eu). This can be understood qualitatively on the basis of the differing structures of the low-temperature solids, whereas the high-temperature solids both presumably have the cubic structure. Less energy is required for the structural change in $NaBF_4$ from the orthorhombic $CaSO_4$ (pseudocubic) structure to the high-temperature cubic form than for the change in KBF_4 from the orthorhombic $BaSO_4$ (pseudotetragonal) structure. The lattice constants[2] change in $NaBF_4$ from 6.25, 6.77, and 6.82 to an estimated 7.0, while in KBF_4 the change is from 7.84, 5.68, and 7.38 to 7.26.

---

[1] A. S. Dworkin and M. A. Bredig, *J. Phys. Chem.* 64, 269 (1960).

[2] R. W. G. Wykoff, *Crystal Structures*, vol. 3, 2d ed., pp. 19, 50, 56, Interscience, New York, 1965.

HEAT CAPACITIES AND HEATS OF FUSION OF MOLTEN-SALT REACTOR FUEL, COOLANT, AND FLUSH SALTS

A. S. Dworkin

Estimates and/or experimental data for the solid and liquid heat capacities and heats of fusion of seven salt mixtures of interest to the Molten-Salt Reactor Program were evaluated for a report on physical properties of molten salts.[1] Listed with the tables containing the physical properties are estimated uncertainties, sources of data, methods of estimation, and some discussion. The validity of our methods of estimation was confirmed by comparison with our measurements[2] as well as with those for a number of other mixtures containing fluorides of lithium, beryllium, and thorium.

---

[1] S. Cantor (ed.), *Physical Properties of Molten-Salt Reactor Fuel, Coolant, and Flush Salts*, ORNL-TM-2316 (August 1968).

[2] A. S. Dworkin and M. A. Bredig, *Chem. Div. Ann. Progr. Rept. May 20, 1968*, ORNL-4306, pp. 124–25.

9. Chemical Physics

SPECTROPHOTOMETRY OF SOLUTIONS OVER WIDE RANGES OF TEMPERATURE AND PRESSURE

W. C. Waggener A. J. Weinberger
R. W. Stoughton

Analysis of the familiar broad 0.96- and 1.15-μ absorption bands of liquid water was completed, and the results were discussed.[1] Our theoretical model assumes that the complex (but well-understood) vibrational-rotational spectrum of gaseous H_2O is replaced in the liquid state by a collision-broadened spectrum. Perturbation of the vibrational energy levels of individual absorbing molecules by the close approach of their neighbors and by the specific (H-bonding) intermolecular association among them controls the shape of the liquid spectrum.

We have shown[2] that bands in the CO_2 spectrum can be fitted satisfactorily to Lorentz distribution functions with the dependence of intensity on density as required by the Lorentz theory for broadening as expected for nonassociated molecules. However, liquid H_2O, which is much more highly associated than CO_2, gives bands having a highly Gaussian contour. Our curve-fitting computer program, which incorporates mixed Gauss-Lorentz distribution functions (in which one of the adjustable parameters is the fraction Gauss profile), has successfully resolved the H_2O spectrum over the temperature range 0 to 250°.[3] Changes in component band parameters (viz., position and intensity of maximum, half-intensity bandwidth, and fraction Gauss profile) with temperature are generally monotonic; however, the occurrence of qualitative differences in temperature dependence indicates a high degree of specificity. For example, in Fig. 9.1 the integrated intensities of four of five components of the 1.15-μ band and three of four components of the 0.96-μ band decrease with decreasing temperatures (increasing density); however, the most intense component of each of the composite bands does the opposite. One of the most interesting observations from the plots of the component band parameters vs temperature in Fig. 9.1 is that the most pronounced changes in slope occur between 90 and 120°C. Although the slopes in general are relatively large in the 0 to 90° region, there are no significant breaks in the curves; the observed behavior of both composite bands, according to our model, results from the qualitative differences among the components. Above 120° the slopes are generally relatively small, and the profiles of some of the component bands change from pure Gaussian to pure Lorentzian, as one might expect for decreasing intermolecular association. We believe the qualitative differences observed in

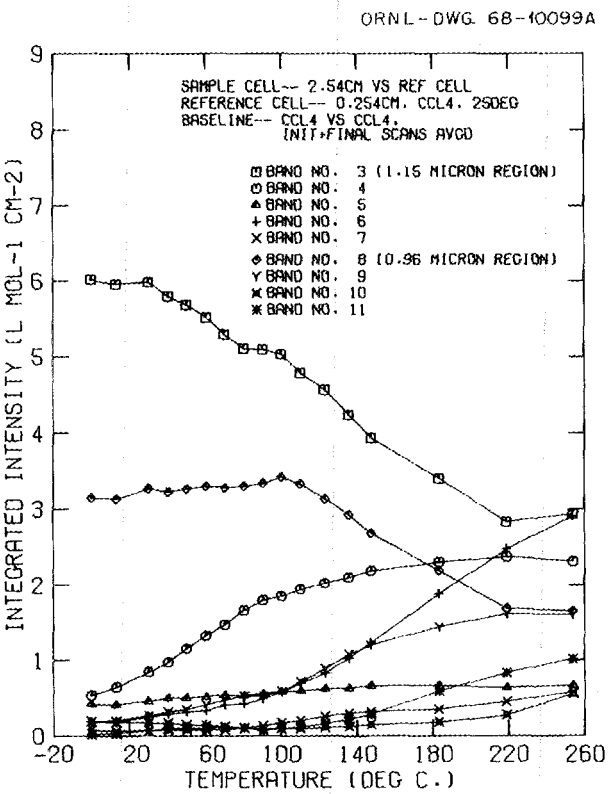

Fig. 9.1. Temperature Dependence of the Integrated Intensities of the Components of a Synthetic 11-Band Fit of the Absorption Spectrum of Liquid H_2O. 0.86–1.34 μ.

temperature dependence among the components of each band cluster reflect the effect of Fermi resonances and intermolecular coupling within each cluster in producing shifts in frequency and intensity which vary with temperature in a complex way.

Measurements of the spectrum of liquid anhydrous H_2S from 0.6 to 2.2 μ at temperature intervals from the critical point (100°C) to the freezing point (−83°C) have been completed, and we are attempting resolution of the prominent bands centered at 1.6 and 1.9 μ by the same methods used in the analysis of the H_2O spectrum. Our spectra are the first reported for liquid H_2S at any temperature.

The most significant accomplishment was confirmation of the unexpected, highly non-Lorentzian character of the near-infrared spectrum of anhydrous liquid H_2S. The spectrum of this congener of H_2O is very similar to it, and the rotational-vibrational bands in the gaseous state have been analyzed in detail.[4] Though its molecular weight is almost twice that of H_2O, its freezing point (−82.9°) and critical point (100.4°) are indicative of relatively weak intermolecular forces; we had hoped that a comparison of the effect of temperature upon the parameters of the (111) band in liquid H_2S at 1.6 μ with the same parameters of the much-studied (111) band in liquid H_2O near 1.2 μ would differentiate the role of the H bond in affecting the (111) band of H_2O. By estimating the small contribution of the 1.9-μ band in the 1.6-μ region, we were able to get a very satisfactory five-band least-squares fit of our 75° data. The vibrational model was identical with that for H_2O, and there was a similar lack of close correlation of the positions and intensities of the five components with the five vibrational band cluster in the gas. The bands ranged from 0.78 to 1.00 in fraction Gauss profile with half-widths averaging nearly 150 cm^{-1} (35 cm^{-1} would be expected if H_2S behaved like CO_2). It is extremely surprising and interesting to us that the close qualitative similarities between the near-infrared spectra of gaseous H_2O and H_2S persist in the liquid state. Indeed, our studies indicate that the significant difference between the H_2S and H_2O vibrational band clusters, which include the strong (111) transition, lies in the breadths of the corresponding components rather than in the character of their respective profiles, which are both highly Gaussian. In the case of H_2O (strong H bonds) the average breadths are almost 2.5 times that observed in H_2S (weak H bonds).

We have taken an initial look at liquid chloroform prior to studying its spectrum over the orthobaric fluid region from the freezing point (−63.5°) to the critical point (263°). The spectrum of this extremely weakly H-bonded solvent is simpler and more susceptible to band analysis than *n*-hexane and cyclohexane, which we already have measured. Two scans, one at room temperature and one near the freezing point, have been made over the wavelength range 0.6 to 2.5 μ using a 2.54-cm cell. The second, third, and fourth harmonics of the single C-H stretching vibration stand out clearly. The $3\nu_1{}^{C\text{-}H}$ band, at 1.15 μ, is free from other transitions and has the proper intensity for close examination of its profile and composition. The half bandwidth (~60 cm^{-1}) and maximum absorbance (~1.3) are little changed by temperature between 25 and −63°. We are preparing to analyze this band and expect that it will have a highly Lorentzian shape.

---

[1] W. C. Waggener, A. J. Weinberger, and R. W. Stoughton, "Mathematical Resolution of the 0.86–1.34 μ Absorption Spectrum of Liquid H_2O at Temperatures from 250° to 0°C," presented at the 156th National Meeting, American Chemical Society, Atlantic City, September 1968.

[2] W. C. Waggener, A. J. Weinberger, and R. W. Stoughton, *J. Phys. Chem.* **71**, 4320 (1967).

[3] W. C. Waggener, A. J. Weinberger, and R. W. Stoughton, *Chem. Div. Ann. Progr. Rept. May 20, 1968*, ORNL-4306, p. 131.

[4] H. C. Allen, Jr., and E. K. Plyler, *J. Res. Natl. Bur. Std.* **52**, 205 (1954); *J. Chem. Phys.* **22**, 1104 (1954).

STUDY OF THE ELECTRONIC STRUCTURE OF MOLECULES BY MEANS OF HIGH-RESOLUTION ELECTRON SPECTROMETRY[1]

T. A. Carlson W. E. Moddeman[3]
B. P. Pullen[2] W. E. Bull[4]
G. K. Schweitzer[4]

A new high-resolution electron spectrometer has been built for studies in chemical bonding. This spectrometer incorporates in its design two double-focusing electrostatic plates; it and preliminary results on the *KLL* Auger spectra of simple gaseous molecules have been described.[5] We now have investigated the electronic structure of a series of molecules using the 21.21-ev He resonance line to induce photoionization. The molecules studied were CO, CH_4, SiH_4, GeH_4, BF_3, BCl_3, SF_6, CF_4, SiF_4, CH_3F, CHF_3, XeF_2, NF_3, CF_3Cl, and CH_3Cl.

Turner *et al.*[6] have demonstrated the effectiveness of photoionization for investigating the electronic structure of molecules. When photoionization occurs, the simple relationship holds:

$$E_b = E_{h\nu} - E_e \,, \qquad (1)$$

where E_e is the measured kinetic energy of the photoelectron, $E_{h\nu}$ is the energy of the photon, and E_b is the difference in energy between the ground state of the molecule and the various states of the positively charged ion. When transitions occur to the ground state of the singly charged ions (usually the highest observed energy for the photoelectron), we have a measure of the binding energy of the molecular orbital. Since the He resonance line has a natural width of about 1 mV, it is thus possible to make studies with high resolution, in practice to the order of 0.02 eV. Binding energies of all orbitals up to the limit of 21.21 eV as well as the accompanying vibrational spectra of the positive ions can be studied. A few examples will be given in this report to illustrate the types of information that can be obtained.

Figure 9.2 shows three bands arising from the first three filled molecular orbitals of a diatomic molecule, carbon monoxide. The first vibrational line in each band, at 19.69, 16.65, and 14.08 eV, represents the binding energy of the orbital. The remaining lines arise from Franck-Condon transitions to excited vibrational states in the singly charged molecular ion and agree well with the Franck-Condon factors obtained from optical spectra. In fact optical and photoelectron spectroscopy supplement each other, and in certain areas photoelectron spectroscopy offers special advantages — namely, in obtaining absolute values of binding energies of the neutral molecules, particularly the more tightly bound orbitals, and in examining the vibrational levels of singly charged ions.

Turning to a more complex molecule, BF_3, which contains six degrees of freedom, we find five bands lying below 21.21 eV. The energy values agree well with the theoretical eigenvalues obtained by Davies[7] for the $e'(\sigma)$, $e''(\pi)$, $a_2'(\sigma)$, $e'(\sigma)$, and $a_1'(\sigma)$ electronic states. The total spectrum is shown in Fig. 9.3 along with an inset of the fine structure arising from the loss of an electron from the $a_1'(\sigma)$ electronic level.

The two bands observed for CH_3F, which are shown in Figs. 9.4 and 9.5, illustrate another aspect of photoelectron spectroscopy, namely the presence or absence of vibrational structure. The fine structure in Fig. 9.4 indicates that the singly charged electronic state of the molecule is stable and suggests that the spacings between the vibrational levels of the nine different modes of vibration are quite similar. On the other hand, Fig. 9.5 shows a broad band with no associated fine structure; thus the singly charged species is not stable, and a predissociated state results.

Figures 9.6–9.8 show the photoelectron spectrum of CH_4. Two broad bands with associated fine structure are observed, resulting from the removal of an electron from the triply degenerate states. The two broad bands

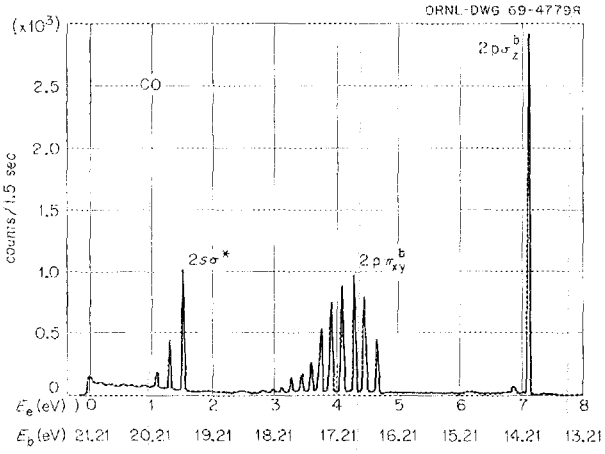

Fig. 9.2. Photoelectron Spectrum of CO Resulting from Ionization by the Helium Resonance Line (21.21 eV). E_b = (21.21 − E_e) eV, where E_e is the measured kinetic energy of the electron. The lowest energy line in each of the three bands corresponds to the binding energy of the molecular orbital designated in the figure by the appropriate symbol. The remaining lines correspond to excited vibrational states of the singly ionized molecule.

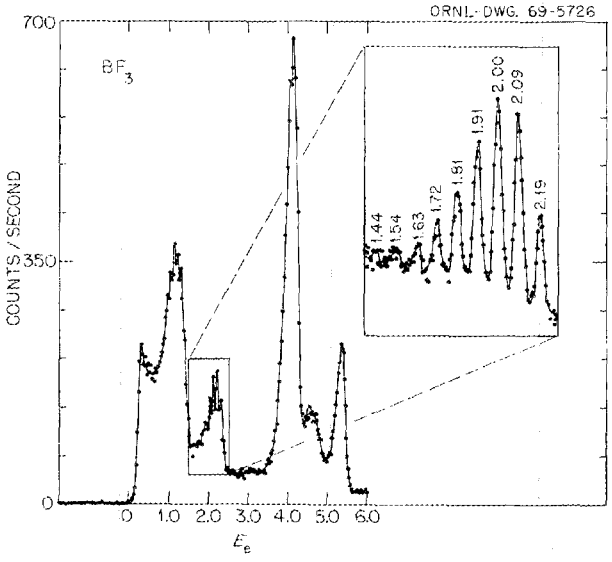

Fig. 9.3. Photoelectron Spectrum of BF_3 Resulting from Ionization by the Helium Resonance Line. The inset gives the details of one of the bands.

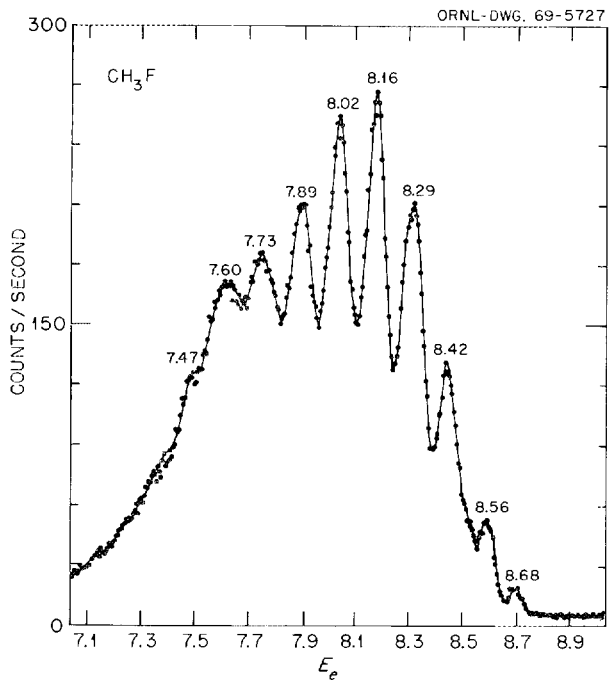

Fig. 9.4. Photoelectron Spectrum Resulting from Ionization of the First Molecular Orbital of CH_3F (i.e., the Least Tightly Bound Orbital) by Means of Irradiation with the Helium Resonance Line.

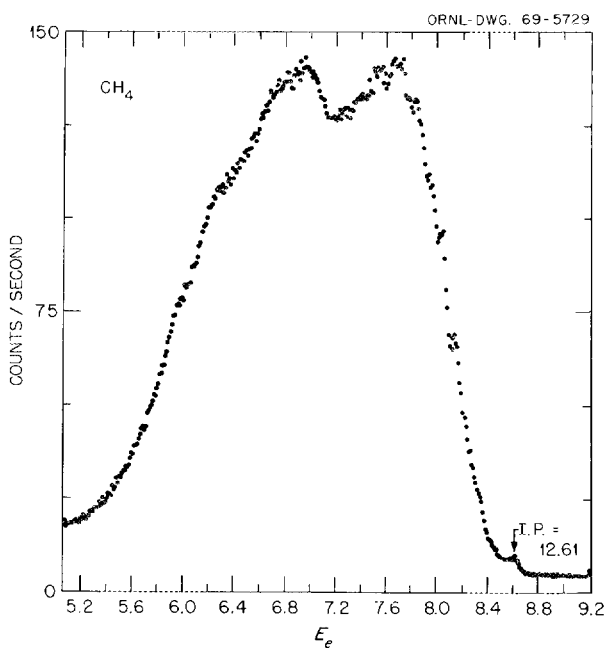

Fig. 9.6. Photoelectron Spectrum Resulting from Ionization of the First Molecular Orbital of CH_4. The double maximum arises from transition to two different electronic states of CH_4^+. The appearance potential for CH_4^+ is given at 12.61 eV.

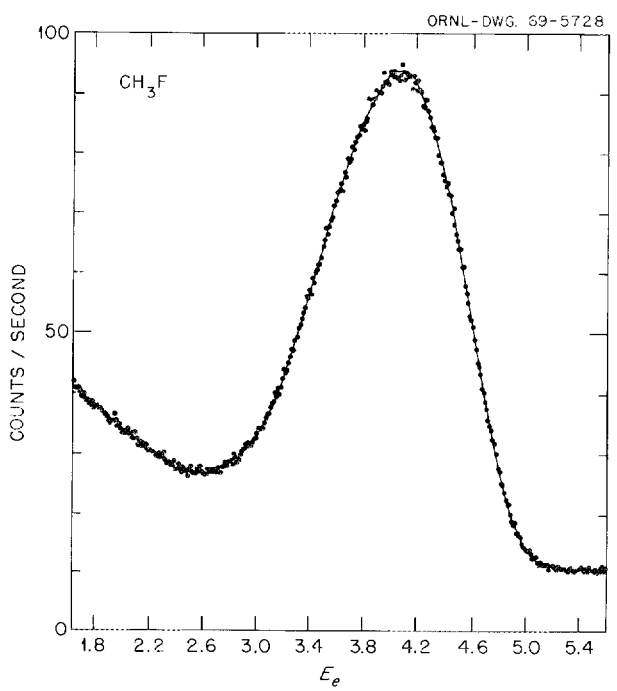

Fig. 9.5. Photoelectron Spectrum Resulting from Ionization of the Second Molecular Orbital of CH_3F by Means of Irradiation with the Helium Resonance Line.

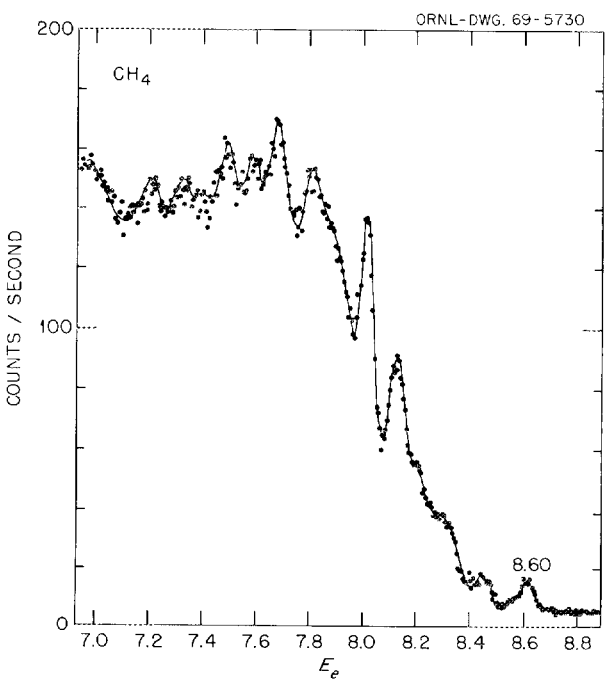

Fig. 9.7. Details of the Photoelectron Spectra of CH_4 (cf. Fig. 9.6) Showing the Fine Structure Associated with the Lower Kinetic Energy Part of the Band.

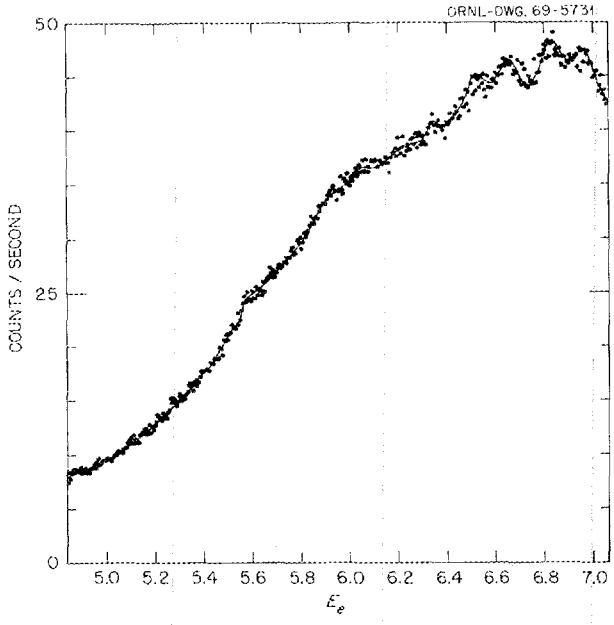

Fig. 9.8. Details of the Photoelectron Spectra of CH_4 (cf. Fig. 9.6) Showing the Fine Structure Associated with the Higher Kinetic Energy Part of the Band.

are believed to be associated with Jahn-Teller distortions in the positive ion. Double bands and associated fine structure also have been observed in the spectra of SiH_4 and GeH_4.

Of particular interest is the presence of vibrational structure above the dissociation level of CH_4^+, since lines have been observed in interstellar space that have been postulated[8] to arise from transitions in CH_4^+. Evidence for such levels is not available from optical studies, but photoionization gives an excellent opportunity to answer this question. Figures 9.7 and 9.8 do indeed show vibrational lines associated with CH_4^+, particularly for the first band, but also in the second band corresponding to binding energies possibly as high as 15.6 eV.

---

[1] Work carried out jointly with the Physics Division.

[2] Oak Ridge Graduate Fellow from the University of Tennessee, Knoxville, under appointment with Oak Ridge Associated Universities.

[3] Physics Division; graduate student from the University of Tennessee, Knoxville.

[4] Department of Chemistry, University of Tennessee, Knoxville.

[5] T. A. Carlson *et al.*, *Phys. Div. Ann. Progr. Rept. Dec. 31, 1968*, ORNL-4395, p. 87.

[6] D. W. Turner, *Advan. Phys. Org. Chem.* **4**, 31 (1966).

[7] D. W. Davies, *Chem. Phys. Letters* **2**, 173 (1968).

[8] G. H. Herbig, *IAU Symposium No.* **31**, p. 85 (1967); G. Herzberg, *ibid.*, p. 91.

CALORIMETRY

HIGH-TEMPERATURE ENTHALPIES OF THE LEAD HALIDES. ENTHALPIES AND ENTROPIES OF FUSION

C. W. Linsey[1] R. A. Gilbert R. H. Busey

An examination of the high-temperature thermodynamic properties of PbF_2, $PbCl_2$, $PbBr_2$, and PbI_2 in the JANAF tables[2] reveals that some of the tabulated properties are based upon rather sparse information or upon data of low precision. These compounds can be prepared in high purity and are thus eminently suited to high-precision thermal measurements. Their low melting points make them tractable for fused salt studies. There are claims in the literature that $PbCl_2$,[3-5] $PbBr_2$,[4] and PbI_2[3,6] exhibit solid-solid phase transformations.

The need for accurate high-temperature thermodynamic data on all the lead halides and our interest in phase transformations in the solid state prompted the high-temperature enthalpy measurements briefly reported here. The measurements were made by drop calorimetry in our high-precision Bunsen ice calorimeter using a furnace with a massive silver core for temperature uniformity.

The lead chloride, bromide, and iodide samples were purified by passing the respective halogen and hydrogen halide gases up through the molten salt contained in a large quartz tube with a fritted filter disk in the bottom; the melt was then purged with argon and filtered through the fritted disk, which removed insoluble impurities. Lead fluoride exists in two modifications at room temperature, orthorhombic and cubic (fluorite structure), the latter a metastable form.[7] A sample of the cubic material was obtained from Harshaw as a clear single crystal. The orthorhombic lead fluoride sample was Baker and Adamson reagent-grade material which was used without further purification. Samples of the lead halides were sealed in gold capsules, which in turn were encapsulated in Nichrome V. A small amount of helium gas was added to both capsules to aid in rapid heat transfer. Nichrome V and gold capsules of the same weight were used for all samples. The relative enthalpy of the "empty" Nichrome V capsule with its gold capsule inside was determined in a separate series of measurements.

From the enthalpy data just below the melting point on PbI_2, PbF_2, and $PbBr_2$, the liquid-soluble—solid-insoluble impurity was determined to be 0.044, 0.049, and 0.006 mole % respectively. The $PbCl_2$ sample melted so sharply that similar data could not be

obtained. Chloride analyses gave 25.509 and 25.513% (theoretical, Cl = 25.496%).

The orthorhombic to cubic transition in PbF_2 is highly irreversible, and the enthalpy of the transition cannot be observed by drop calorimetry. The enthalpy of the transition at room temperature, 240 ± 9 cal/mole, was determined by solution calorimetry; that is, the enthalpy of the transition was determined by the difference in the enthalpy of solution of the two modifications in 1 *M* $Fe(NO_3)_3$, a solvent which rapidly dissolves PbF_2. The enthalpy measurements on orthorhombic PbF_2 are incomplete, but preliminary data indicate that the orthorhombic to cubic transition temperature lies between 305 and 325°C.

The high-temperature enthalpy data for cubic PbF_2, which has the fluorite structure,[7] revealed a lambda-type transition. The heat capacity derived from the enthalpy data is given in Fig. 9.9; the transition shown, with a heat capacity maximum at about 445°C, is an order-disorder transition. Other compounds with the fluorite or antifluorite structure also exhibit an order-disorder transition just below their melting points.[8] In the present case the transition represents a positional disordering of the F^- ions in the lattice. It may be shown that the entropy of the transition due to positional disordering only (i.e., disordering of the F^- ions to give a "static" disordered state) is $R \ln 3 = 2.18$ cal deg^{-1} $mole^{-1}$. The estimated entropy of transition in cubic PbF_2, based on the estimated "normal" heat capacity (dotted curve in Fig. 9.9), is 3.6 cal deg^{-1} $mole^{-1}$. The excess entropy above $R \ln 3$ indicates a degree of disorder greater than the "static" one and may be attributed to increased translational freedom of the F^- ions in the lattice. The latter should be manifested by a marked increase in the thermal and electrical conductivity in the solid above the transition. A cursory search of the literature reveals such measurements have not been made on solid PbF_2.

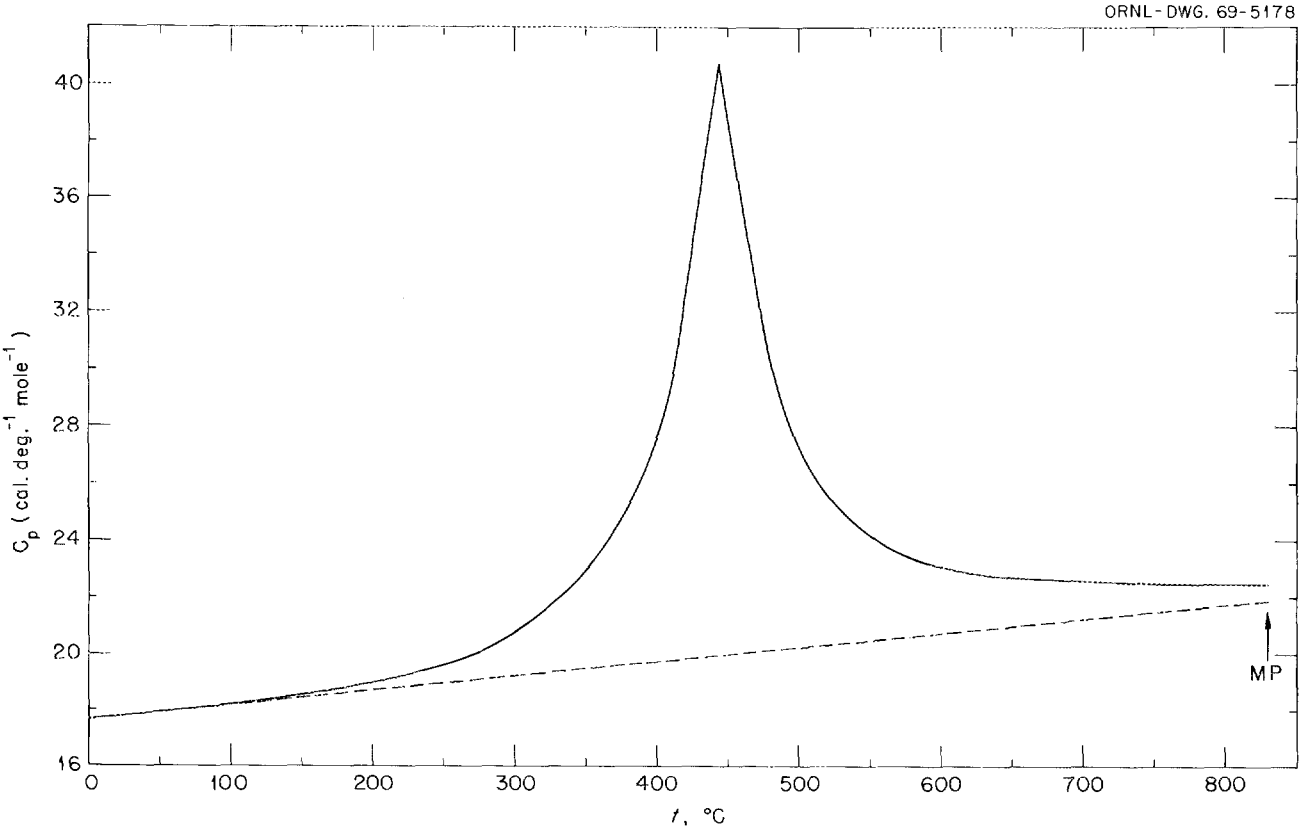

Fig. 9.9. Heat Capacity of the Cubic Modification of PbF_2 Derived from High-Temperature Enthalpy Data. The dotted curve is an estimate of the "normal" molar heat capacity.

No solid-solid transitions were observed in $PbCl_2$, $PbBr_2$, or PbI_2.[9] The following equations represent the enthalpies observed:

$PbCl_2$

Solid (273.15 – 771°K):

$$H_T - H_{273.15} = 14.99T + 4.33 \times 10^{-3}T^2 - 8.058 \times 10^4 T^{-1} - 4126.0$$

$$C_p = 14.99 + 8.66 \times 10^{-3}T + 8.058 \times 10^4 T^{-2}$$

Liquid (771 – 1000°K):

$$H_T - H_{273.15} = 7.818T + 1.1791 \times 10^{-2}T^2 + 2114.1$$

$$C_p = 7.818 + 2.358 \times 10^{-2}T$$

$PbBr_2$

Solid (273.15 – 644°K):

$$H_T - H_{273.15} = 13.82T + 5.81 \times 10^{-3}T^2 - 1.525 \times 10^5 T^{-1} - 3647.1$$

$$C_p = 13.82 + 1.162 \times 10^{-2}T + 1.525 \times 10^5 T^{-2}$$

Liquid (644 – 925°K):

$$H_T - H_{273.15} = 26.80T - 5904$$

$$C_p = 26.80$$

PbI_2

Solid (273.15 – 683°K):

$$H_T - H_{273.15} = 16.06T + 3.08 \times 10^{-3}T^2 - 5.969 \times 10^4 T^{-1} - 4397.4$$

$$C_p = 16.06 + 6.16 \times 10^{-3}T + 5.969 \times 10^4 T^{-2}$$

Table 9.1. Thermodynamics of Fusion of the Lead Halides

Compound	ΔH_{fusion} (kcal/mole)		ΔS_{fusion} (cal deg^{-1} mole^{-1})		Melting Point (°K)	
	This Work	Literature	This Work	Literature	This Work	Literature
PbF_2	3.5[a]	1.8[b]	3.2[a]	1.6[b]	1103[a]	1095[b]
		4.2[c]		3.85[c]		1091[c]
		3.7[d]		3.4[d]		1098[d]
$PbCl_2$	5.25	5.7[b]	6.81	7.4[b]	771	771[b]
		5.7[c]		7.42[c]		768[c]
		5.2[e]		6.72[e]		774[e,f]
		5.3[f]		6.8[f]		774[e,f]
$PbBr_2$	3.93	5.[b]	6.10	7.8[b]	644	643.2[b]
		5.1[c]		7.96[c]		640[c]
PbI_2	5.60	5.2[b]	8.20	7.6[b]	683	685[b]
		3.87[c]		5.69[c]		680[c]
		6.1[g]		8.9[g]		685[g]

[a]Tentative result, subject to slight revision.

[b]F. D. Rossini *et al.*, *Selected Values of Chemical Thermodynamic Properties*, Circular 500, National Bureau of Standards, U.S. Government Printing Office, Washington, D.C., 1952.

[c]M. Blanc and G. Petit, *Compt. Rend.* **248**, 1305 (1959).

[d]Von C. Schmitz-Durmont and G. Bergerhoff, *Z. Anorg. Allgem. Chem.* **283**, 314 (1956).

[e]A. Alim, P. Kurtz, and W. D. Van Vorst, *J. Chem. Eng. Data* **13**, 24 (1968).

[f]H. Bloom and S. B. Tricklebank, *Australian J. Chem.* **19**, 192 (1966).

[g]I. G. Murgulescu, S. Sternberg, and M. Terzi, *Electrochim. Acta* **12**, 1121 (1967).

Liquid (683 – 880°K):

$$H_T - H_{273.15} = 25.95T - 4203$$

$$C_p = 25.95$$

The enthalpy of fusion, entropy of fusion, and melting point obtained for each salt are given in Table 9.1. For comparison purposes, values from NBS Circular 500 and more recent results from the literature are also given.

[1]Oak Ridge Graduate Fellow from North Texas State University, Denton, Tex., under appointment with Oak Ridge Associated Universities.

[2]*JANAF Thermochemical Data*, The Thermal Laboratory, Dow Chemical Co., Midland, Mich.

[3]T. Sumarokova and T. Modestova, *Russ. J. Inorg. Chem.* (English Transl.) 1(10), 96 (1956).

[4]T. Modestova and T. Sumarokova, *Russ. J. Inorg. Chem.* (English Transl.) 3, 245 (1958).

[5]T. P. Modestova, *Russ. J. Inorg. Chem.* (English Transl.) 5, 804 (1960).

[6]Z. G. Pinsker, L. I. Tatarinova, and V. A. Novikova, *Acta Physicochim. URSS* 18, 378 (1943).

[7]R. W. G. Wyckoff, *Crystal Structures*, vol. 1, Interscience, New York, 1963.

[8]A. S. Dworkin and M. A. Bredig, *J. Phys. Chem.* 72, 1277 (1968).

[9]It should be pointed out that the samples of these compounds were prepared from the molten state. If these salts have a high-temperature modification which is metastable at room temperature, similar to the situation in PbF_2, then the data here presented apply to this high-temperature modification.

THE HEAT CAPACITY OF POTASSIUM PERTECHNETATE FROM 9 TO 310°K. ENTROPY AND FREE ENERGY FUNCTIONS

R. H. Busey R. B. Bevan, Jr. R. A. Gilbert

An earlier measurement[1] of the low-temperature heat capacity of potassium pertechnetate, $KTcO_4$, was made on a small sample (~9 g) which the thermal measurements showed to contain 0.83 wt % (8.6 mole %) water. Such a large amount of water, presumably entrapped in the crystals as brine holes, resulted in an intolerable uncertainty in the heat capacity data. A knowledge of the thermodynamic properties of this compound is so basic to the chemical thermodynamics of technetium that these heat capacity measurements have been repeated using a normal size (~72 g) high-purity sample.

The $KTcO_4$ was prepared from NH_4TcO_4 by addition of ~105% of the stoichiometric amount of KOH in aqueous solution. The mixture was digested in a platinum dish for several hours and finally taken to dryness to expel all ammonia. The $KTcO_4$ produced was purified by two to three recrystallizations from water. The final recrystallized product was dried in air at 450 to 475°C for an hour. A portion of the sample was used for high-temperature heat content observations reported earlier.[2,3]

Table 9.2. Thermodynamic Properties of $KTcO_4$

In calories per degree per mole

T (°K)	C_p°	S°	$(H^\circ - H_0^\circ)/T$	$(F^\circ - H_0^\circ)/T$
20	1.73	0.611	0.453	0.158
50	9.11	5.114	3.473	1.640
100	16.87	14.077	8.425	5.652
150	21.64	21.881	12.086	9.795
200	24.86	28.573	14.899	13.674
298.15	29.50	39.415	18.982	20.433
310	29.96	40.573	19.393	21.181

The low-temperature heat capacity measurements were made in an adiabatic-type calorimeter.[4] No anomalous behavior in the heat capacity of $KTcO_4$ was expected or observed in the temperature range studied. Table 9.2 summarizes the thermodynamic properties.

These new heat capacity observations indicate that some impurity (or impurities) in addition to the water was present in the earlier sample of $KTcO_4$ and justify our skepticism of the earlier results. The entropy at 298.15°K derived from the earlier and the present measurements is 39.74 and 39.42 cal deg^{-1} mole^{-1} respectively. The latter result should be correct to at least ±0.1 cal deg^{-1} mole^{-1}.

The new value for the entropy of $KTcO_4$ at 298.15°K requires a small revision in the entropy of the TcO_4^-(aq) ion previously computed from solubility and heat of solution measurements on this compound.[5] The revised value is $S^\circ[TcO_4^-(aq)] = 47.6$ cal deg^{-1} mole^{-1}. This result is still based upon an estimate[6] of 7.4 cal deg^{-1} mole^{-1} for the entropy of technetium metal. No significant change in the free energy of formation of TcO_4^-(aq) previously obtained[5] results from this revised entropy.

[1]R. H. Busey and Q. V. Larson, *Chem. Div. Ann. Progr. Rept. June 20, 1957*, ORNL-2386, p. 26.

[2]R. A. Gilbert and R. H. Busey, *Chem. Div. Ann. Progr. Rept. May 20, 1966*, ORNL-3994, p. 110.

[3]R. H. Busey and R. A. Gilbert, *Chem. Div. Ann. Progr. Rept. May 20, 1967*, ORNL-4164, p. 103.

[4]R. H. Busey, R. B. Bevan, Jr., and R. A. Gilbert, *J. Phys. Chem.* 69, 3471 (1965).

[5] R. H. Busey and R. B. Bevan, Jr., *Chem. Div. Ann. Progr. Rept. June 20, 1960*, ORNL-2983, p. 8.

[6] J. W. Cobble, W. T. Smith, Jr., and G. E. Boyd, *J. Am. Chem. Soc.* 75, 5777 (1953).

PREPARATION OF K_2TcCl_6 FOR CALORIMETRIC STUDIES

R. B. Bevan, Jr. R. H. Busey

An extensive program has been initiated to determine several thermochemical properties of the potassium hexahalotechnetates, K_2TcX_6, and their ions in aqueous solution, TcX_6^{2-}, where X represents F, Cl, Br, or I. The thermodynamic properties of interest are: low-temperature heat capacity, solubility in dilute HX acid solution, enthalpy of solution in dilute acid, enthalpy of hydrolysis, and enthalpy of oxidation to TcO_4^-(aq). Such measurements will yield the entropies and the enthalpies and free energies of formation of the salts and their ions. Since these paramagnetic salts with three unpaired electrons in the ground state (t_{2g}^3 configuration) are expected to become antiferromagnetic at low temperatures, the heat capacity measurements will establish the Néel temperature, where the transition from a paramagnetic to an antiferromagnetic state occurs.

It is highly desirable to have a method of preparing these compounds in large amounts (~100 g), in high yield and as simply as possible in order to recover the technetium from a reaction mixture easily; the operations must be performed in a glove box with double containment of solutions. We report here a preparative procedure for K_2TcCl_6 which involves very simple operations and is, or can be made, quantitative. The bromide or iodide complex is readily made from K_2TcCl_6 by successive evaporations with hydrobromic or hydriodic acid respectively.[1] The fluoride complex may be prepared from K_2TcBr_6 by reaction with KHF_2 melt.[2]

Our preparative procedure for K_2TcCl_6 takes advantage of the fact[3] that the TcO_4^- ion is reduced by concentrated HCl to $TcCl_6^{2-}$. A batch method is used to keep the volume of solution handled to less than 1 liter. Approximately 10 g of $KTcO_4$ and an equimolar amount of KCl are digested in ~200 cc of concentrated HCl at 70 to 80°C for ~48 hr. This is probably longer than necessary, but complete reduction must be ensured. The K_2TcCl_6 crystals are dissolved and recrystallized from hot 6 *M* HCl. The mother liquor may be concentrated to obtain additional high-purity product. The crystals are collected in a sintered-glass filter funnel, washed with 3 *M* HCl, and finally rinsed with 95% ethyl alcohol. The product so obtained is dried in an oven at ~80°C for 2 hr.

A Mohr titration for Cl^-, made on a sample from a pilot batch preparation, indicated the purity was 99.91%.

[1] J. Dalziel *et al.*, *J. Chem. Soc.* (London), p. 4012 (1958).

[2] K. Schwochau and W. Herr, *Angew. Chem. Intern. Ed. Engl.* 2, 97 (1963).

[3] R. H. Busey, *Chem. Div. Ann. Progr. Rept. June 20, 1959*, ORNL-2782, p.13.

MICROWAVE AND RADIO-FREQUENCY SPECTROSCOPY

PARAMAGNETIC RESONANCE STUDIES OF LIQUIDS DURING PHOTOLYSIS

Ralph Livingston Henry Zeldes

Electron paramagnetic resonance spectra have been studied at room temperature during the photolysis of solutions containing oxalic acid and esters of oxalic acid. It was found that radicals result from the one-electron reduction of oxalic acid and its esters by other radicals which are known[1] to be good electron donors. For instance, aqueous solutions containing only oxalic acid, oxalic acid and H_2O_2, or oxalic acid and isopropyl alcohol give no spectra. On the other hand, aqueous solutions containing oxalic acid, isopropyl alcohol, and H_2O_2 give spectra which include a very strong, sharp line which we attribute to reduced oxalic acid, $HOOCCOOH^{\dot{-}}$, or its protonated form $HOOC\dot{C}(OH)_2$. In the absence of oxalic acid, this solution gives[2] $(CH_3)_2\dot{C}OH$, a good one-electron donor, produced from isopropyl alcohol by the abstraction of H by the radical $\dot{O}H$ which results from photolysis of H_2O_2. Upon adding oxalic acid, the spectrum from $(CH_3)_2\dot{C}OH$ becomes progressively weaker and the spectrum from reduced oxalic acid becomes stronger. Similar chemistry is observed with many other solutions which contain good electron-donor radicals.

It was found that esters of oxalic acid are also one-electron acceptors, and radicals are produced from dimethyl oxalate and diethyl oxalate. These show hyperfine couplings, respectively, from six and four equivalent protons. The equivalence does not necessarily mean that the radical is in the ionic form rather than the protonated form, as rapid proton exchanges

could make the couplings equivalent in the protonated form:

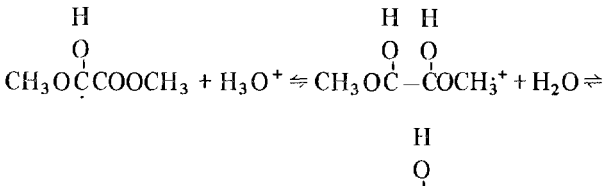

Similar radicals were produced from the monomethyl and monoethyl esters in solutions of the diesters as they hydrolyzed. A number of monoester radicals were prepared from acidified solutions made up with oxalic acid and the desired alcohol and containing the equilibrium concentration of monoester. Accurate g values and proton hyperfine couplings were measured.

In our previous work we had seen spectra whose hyperfine lines seemed to have strengths indicating the spin states were not in thermal equilibrium with the solutions. There was the possibility, however, that the observed line heights were anomalous due to variable widths of the hyperfine lines. In our work with oxalic acid, we saw spectra due to $(CH_3)_2\dot{C}OH$ and $CH_3\dot{C}HOH$, both used as electron donors, whose line heights were very anomalous. For this reason we examined solutions in which these radicals were produced and in which the amount of oxalic acid was progressively increased, thus shortening the mean chemical lifetime of the donor radicals. The line strengths became more anomalous as oxalic acid was added, and it is now quite clear that the effect cannot be attributed to variable widths. A solution containing much oxalic acid even had some hyperfine lines of $(CH_3)_2\dot{C}OH$ due to induced emission and some to induced absorption. For some nuclear magnetic states, there were more radicals in the higher-energy electron spin state than in the lower. These radicals were produced with magnetic spin states distributed far from the equilibrium distribution. By shortening the chemical lifetime, we were able to see the anomalous intensities before they became normal through thermal relaxation mechanisms.

An anomalous spectrum was found for one of the several radicals formed by photolyzing concentrated aqueous solutions of tartaric acid. This spectrum consisted of eight lines, of which seven were clearly resolved from the spectra of other radicals. The lines were of comparable strength and of the usual width found in solution studies ($\approx$0.1 G), but all of the lines were inverted; they resulted from induced emission rather than absorption. The multiplicity of lines comes from hyperfine interactions with three inequivalent protons with strengths 17.47, 9.20, and 0.79 G. The g value is 2.00312. A comparison of these values with those found for a radical made by abstracting hydrogen from ethylene glycol[3] indicates that this new radical is $HOOCCH(OH)\dot{C}H(OH)$, tartaric acid lacking one of the carboxyl groups.

Spectra for three other radicals (with normal absorption lines) were measured in tartaric acid solutions. A single line arose from the approximately 0.05% oxalic acid present as an impurity and was clearly the radical produced by electron transfer discussed above. Another more complex spectrum arose from a radical tentatively identified as $HOOCCH_2\dot{C}HOH$. A third set of lines was attributed to $HOOC\dot{C}HCHO$, and it is proposed that this radical is formed from the radical showing the emission spectrum by a pinacol-like rearrangement exactly like that found in acid solution for the radical from ethylene glycol.[2] This mechanism terminates the life of the radical showing the emission spectrum in a time comparable with or shorter than the thermal relaxation time. Preliminary results indicate that the electron spin population for the emission spectrum not only is inverted but is very highly polarized as well.

Aqueous tartaric acid solutions have also been photolyzed in the presence of strong mineral acid. One of the effects is a reduction to zero of the weaker hydrogen hyperfine interactions attributed to hydroxyl hydrogens. The effect is caused by acid-catalyzed exchange of the hydrogen and is consistent with the identifications made for the radicals. The addition of oxalic acid to tartaric acid has also been studied. Electron transfer to the oxalic acid causes the spectra from all radicals to become weaker, except the emission spectrum.

A variety of short-lived radicals formed by abstracting hydrogen from esters of orthoacids and related compounds has been studied in solution at room temperature. The abstraction of hydrogen was accomplished by photolyzing a solution of the ester with either hydrogen peroxide or acetone. Included in the study were dimethyl and diethyl carbonate, trimethyl and triethyl orthoformate, methylal, acetone dimethyl acetal, trimethyl and triethyl phosphate, tetraethyl orthosilicate, and trimethyl borate. Hyperfine couplings and g values were measured. Phosphorus couplings were obtained in the phosphates and that of ^{11}B in the borate. Comparisons of hydrogen couplings of both organic and inorganic acids show highly systematic trends. A similar study is under way on simple aliphatic acids, hydroxyacids, and their esters.

[1] A. L. Buley and R. O. C. Norman, *Proc. Chem. Soc.*, p. 225 (1964); R. O. C. Norman and R. J. Pritchett, *J. Chem. Soc.* (B), 378 (1967).

[2] R. Livingston and H. Zeldes, *J. Am. Chem. Soc.* 88, 4333 (1966).

[3] R. Livingston and H. Zeldes, *J. Chem. Phys.* 44, 1245 (1966).

PARAMAGNETIC RESONANCE STUDY OF ^{17}O-LABELED NO_2 IN SODIUM NITRITE CRYSTALS

R. W. Holmberg Z. Luz[1]

Electron paramagnetic resonance spectra of the free radical NO_2 labeled with ^{17}O have been studied in single crystals of $NaNO_2$. Sodium nitrite containing several percent ^{17}O was irradiated at 77°K with gamma rays from a ^{60}Co source, and EPR observations were made at this temperature. The positions of the ^{14}N hyperfine lines which were studied earlier[2] and the positions of ^{17}O hyperfine lines were measured as a function of crystal orientation. A typical spectrum from a labeled NO_2 molecule consists of a strong triplet of lines from ^{14}N with each of these flanked by six weaker lines from the lesser abundant ^{17}O. Because of the low abundance of ^{17}O, spectra were seen in which only one of the oxygens was labeled. The crystal orientation was determined by comparing the ^{14}N line positions with spectra determined earlier.[2] The principal values of the ^{14}N hyperfine tensor and the g tensor were redetermined here and were found to be in close agreement with the previous work. The hyperfine tensor for ^{17}O in NO_2 was evaluated from the data. Both of the oxygens of the NO_2 were found to be equivalent, and the magnitudes of the principal values of the ^{17}O tensor were found to be 4.3, 54.9, and 1.7 G. These results, and the ^{14}N tensor, were analyzed in terms of a simple molecular orbital treatment of the NO_2 molecule. The distribution of spin density throughout the molecule was estimated, and the results were compared with theoretical predictions. A detailed report of this work has been submitted to the *Journal of Chemical Physics* for publication.

[1] Visiting guest scientist from the Weizmann Institute of Science, Rehovoth, Israel.

[2] H. Zeldes and R. Livingston, *J. Chem. Phys.* 35, 563 (1961).

NEUTRON AND X-RAY CRYSTALLOGRAPHY

A NEUTRON DIFFRACTION STUDY OF MAGNESIUM CHLORIDE HEXAHYDRATE

P. A. Agron W. R. Busing

The alkaline-earth hydrates form a large family of crystalline compounds made up of monatomic ions and water molecules which make only weak hydrogen bonds to the anions. It may soon be possible to understand their structures in terms of a relatively simple electrostatic model.[1] A neutron diffraction study of $BaCl_2 \cdot 2H_2O$ has been reported previously,[2] and incomplete results on $SrCl_2 \cdot 6H_2O$ and $CaCl_2 \cdot 6H_2O$ are presented in the following report. We describe here the results of a neutron diffraction study of $MgCl_2 \cdot 6H_2O$. The crystal structure of this compound was determined by Andress and Gundermann[3] using x-ray diffraction techniques. Our work serves to locate the hydrogen atoms and to improve the precision of the parameter values. There is no significant disagreement between the two sets of results.

$MgCl_2 \cdot 6H_2O$ crystallizes with monoclinic symmetry $C2/m$, two formula units per cell. The lattice parameters were redetermined by least-squares refinement based on x-ray diffractometer measurements of the Bragg angles for 12 high-angle reflections using Cu $K\alpha_1$ radiation (λ = 1.54051 Å). They are a = 9.8607(2) Å, b = 7.1071(2) Å, c = 6.0737(2) Å, and β = 93.758(2)° at 23°C.

Neutron diffraction intensities were measured for 813 independent reflections, corrected for absorption, and used for least-squares refinement, including anisotropic thermal displacements and isotropic extinction.[4] The final disagreement index $R = \Sigma||F_o| - |F_c||/\Sigma|F_o|$ was 0.054, based on 651 nonzero intensities. The coordinates are:

	Position	x	y	z
Mg	2a	0	0	0
Cl	4i	0.3176(1)	0	0.6122(2)
O(1)	4i	0.2018(1)	0	0.1095(3)
O(2)	8j	−0.0429(1)	0.2066(2)	0.2233(2)
H(1)	4i	0.2372(3)	0	0.2583(6)
H(2)	4i	0.2693(4)	0	0.0083(8)
H(3)	8j	0.0209(2)	0.2998(3)	0.2784(4)
H(4)	8j	−0.1160(2)	0.1984(4)	0.3151(4)

The oxygen atoms form an almost perfect octahedron about the magnesium ion with Mg–O(1) and Mg–O(2) distances 2.056(1) and 2.062(1) Å, respectively, and angles ranging from 88.67(5) to 91.33(5)°. The inter-

atomic distances in the water molecules (in angstroms) are as follows, the correction for thermal motion being based on the riding model:

	Uncorrected	Corrected
O(1)–H(1)	0.947(4)	0.971(4)
O(1)–H(2)	0.935(4)	0.998(5)
O(2)–H(3)	0.958(2)	0.966(3)
O(2)–H(4)	0.942(2)	0.978(3)

The angles H(1)–O(1)–H(2) and H(3)–O(2)–H(4) are 113.2(4) and 110.3(2)°.

Andress and Gundermann pointed out that the structure can be considered as an arrangement of discrete groups,

$$Cl^-(H_2O)_3Mg^{2+}(H_2O)_3Cl^- .$$

Each group has crystallographic point symmetry $2/m$ and also shows a pseudosymmetry which is very nearly $\bar{3}m$ with the $\bar{3}$ axis in the $Cl^-...Mg^{2+}...Cl^-$ direction. The O(1)–H(2) and O(2)–H(4) bonds are roughly parallel to this axis and are directed toward the chloride ions within the group. The O(1)–H(1) and O(2)–H(3) vectors point away from the $\bar{3}$ axis and form short straight hydrogen bonds to chloride ions of neighboring groups. The distances and angles are:

	H...Cl	O–H...Cl
O(1)–H(1)...Cl	2.241(3) Å	179.1(3)°
O(1)–H(2)...Cl	2.483(5) Å	145.8(4)°
O(2)–H(3)...Cl	2.206(2) Å	174.5(2)°
O(2)–H(4)...Cl	2.500(3) Å	142.0(2)°

[1] W. R. Busing, *Chem. Div. Ann. Progr. Rept. May 20, 1968*, ORNL-4306, p. 139.

[2] V. M. Padmanabhan, W. R. Busing, and H. A. Levy, *Acta Cryst.* **16**, A26 (1963).

[3] K. R. Andress and J. Gundermann, *Z. Krist.* 87, 345 (1934).

[4] W. H. Zachariasen, *Acta Cryst.* 23, 558 (1967).

NEUTRON DIFFRACTION STUDIES OF CALCIUM CHLORIDE HEXAHYDRATE AND STRONTIUM CHLORIDE HEXAHYDRATE

P. A. Agron W. R. Busing

Jensen[1] determined the crystal structure of $SrCl_2 \cdot 6H_2O$ by x-ray diffraction methods and showed that $CaCl_2 \cdot 6H_2O$ is isostructural. We are presently completing neutron diffraction studies of these compounds to locate the hydrogen atoms and to improve the descriptions of the structures.

The compounds crystallize with the noncentrosymmetric trigonal symmetry of space group $P321$, one formula unit per cell. The lattice parameters of the strontium compound were determined by least-squares refinement based on x-ray diffractometer measurements of 12 high-angle reflections. They are a = 7.9593(2) Å and c = 4.1243(2) Å at 22°C, assuming λ = 1.54051 Å for Cu $K\alpha_1$ radiation. Preliminary lattice parameters for the calcium compound are a = 7.86 Å, c = 3.95 Å.

Neutron diffraction intensities were measured for 833 reflections from a 139-mg single crystal of the calcium compound. For the strontium compound, 793 reflections were measured using a 68-mg sample, and these measurements were later repeated on a 24-mg crystal. Calculated absorption corrections were applied, and the structure factor squares were obtained in the usual way. These were used for least-squares refinement of the structural parameters, including anisotropic temperature factors and an isotropic extinction correction.[2] The discrepancy factors $R = \Sigma\big||F_o| - |F_c|\big|/\Sigma|F_o|$ were reduced to 0.032 and 0.037 for the nonzero reflections of the calcium and strontium compounds respectively.

Although this agreement between observed and calculated structure factors appears to be excellent, some discrepancies remain among observations of equivalent reflections. It is thought that these may be due to anisotropic extinction,[3] and our least-squares refinement program is being revised to correct for this effect.

The structural parameters at this stage of refinement are:

Atom	Position	x	y	z
		$CaCl_2 \cdot 6H_2O$		
Ca	1a	0	0	0
Cl	2d	⅓	⅔	0.4248(2)
O_1	3e	0.3113(2)	0	0
O_2	3f	−0.2134(2)	0	½
H_1	6g	0.4323(3)	0.0984(3)	−0.0931(6)
H_2	6g	−0.2331(4)	0.1113(3)	0.4832(5)
		$SrCl_2 \cdot 6H_2O$		
Sr	1a	0	0	0
Cl	2d	⅓	⅔	0.4191(3)
O_1	3e	0.3230(2)	0	0
O_2	3f	−0.2217(2)	0	½
H_1	6g	0.4419(4)	0.0968(4)	−0.0899(7)
H_2	6g	−0.2419(4)	0.1099(3)	0.4895(5)

The arrangement of the water molecules in these crystals is intermediate between that in $MgCl_2 \cdot 6H_2O$[4] and that in $BaCl_2 \cdot 2H_2O$.[5] In the former compound each water molecule is coordinated to one Mg^{2+} ion, but in the latter, each water is shared by two Ba^{2+} ions. In the present compounds O(1) is coordinated to one metal ion, but O(2) is shared by two metal ions. In this way the cation is coordinated to nine water molecules.

Each hydrogen atom forms a rather short, straight hydrogen bond to the chloride ion. In doing this, the two kinds of hydrogen atoms come into van der Waals contact with each other.

Preliminary values for the distances and angles are listed below.

	$CaCl_2 \cdot 6H_2O$	$SrCl_2 \cdot 6H_2O$
Metal–O(1)	2.446 Å	2.572 Å
Metal–O(2)	2.592 Å	2.714 Å
O(1)–H(1)	0.949 Å	0.948 Å
H(1)–O(1)–H(1)	107.1°	107.2°
O(2)–H(2)	0.963 Å	0.967 Å
H(2)–O(2)–H(2)	104.2°	103.6°
H(1)...Cl	2.263 Å	2.285 Å
O(1)–H(1)...Cl	164.6°	162.7°
H(2)...Cl	2.274 Å	2.266 Å
O(2)–H(2)...Cl	163.7°	165.4°
H(1)...H(2)	2.265 Å	2.384 Å

[1] A. T. Jensen, *Kgl. Danske Videnskab. Selskab, Mat.-Fys. Medd.* 17, No. 9 (1940).

[2] W. H. Zachariasen, *Acta Cryst.* 23, 558 (1967).

[3] P. Coppens and W. C. Hamilton, *Acta Cryst.* (in press).

[4] P. A. Agron and W. R. Busing, preceding report.

[5] V. M. Padmanabhan, W. R. Busing, and H. A. Levy, *Acta Cryst.* 16, A26 (1963).

CORRECTING INTERATOMIC DISTANCES AND ANGLES FOR THERMAL MOTION

C. K. Johnson

A major source of error in the determination of interatomic distances and angles from the results of a crystal structure analysis is the apparent foreshortening of the interatomic distances by thermal motion. Busing and Levy[1] have discussed the difference between mean interatomic distances and the distances between the mean positions of the atoms and have proposed several models for estimating the mean interatomic distances. Their "riding" model is frequently used (often incorrectly, as pointed out by Brown[2]) for correcting bond distances. The only other models in extensive use at present are based on rigid-body libration. Schomaker and Trueblood[3] have derived an expression for calculating intramolecular distances d_c corrected for rigid-body libration. The matrix version of their equation, which was derived independently by Ellison and Levy,[4] is

$$d_c = |\mathbf{v}_0| \left\{ 1 + \frac{1}{2} \left[\operatorname{tr}(\mathbf{L}\,\mathbf{g}) - \mathbf{v}_0^t\,\mathbf{g}\,\mathbf{L}\,\mathbf{g}\,\mathbf{v}_0 / \mathbf{v}_0^t\,\mathbf{g}\,\mathbf{v}_0 \right] \right\} , \quad (1)$$

where $\mathbf{v}_0$ is the interatomic vector between the mean positions of two atoms in oblique crystal coordinates, and $\mathbf{L}$ is the rigid-body libration tensor, also expressed in contravariant components based on the crystal system. The matrix $\mathbf{g}$ is the metric tensor whose elements are $\mathbf{a}_i \cdot \mathbf{a}_j$, the scalar products of the unit-cell vectors. An alternate and equally valid formulation can be derived by noting that the libration in effect produces an affine distortion of space, so that a vector $\mathbf{v}_r$ between rest positions is related to a vector $\mathbf{v}_0$ between mean positions by

$$\mathbf{v}_r = \mathbf{M}\,\mathbf{v}_0 , \quad (2)$$

where

$$\mathbf{M} = \left[1 + \frac{1}{2} \operatorname{tr}(\mathbf{L}\,\mathbf{g}) \right] \mathbf{I} - \frac{1}{2} \mathbf{L}\,\mathbf{g} . \quad (3)$$

This result is simply a restatement of Schomaker and Trueblood's Eq. (21). The corrected interatomic distance is the square root of the inner product of $\mathbf{v}_r$ with itself:

$$d_c = (\mathbf{v}_0^t\,\mathbf{M}^t\,\mathbf{g}\,\mathbf{M}\,\mathbf{v}_0)^{1/2} . \quad (4)$$

Equation (2) also provides a direct method for calculating corrected interatomic angles between atoms within the rigid group. The corrected angle α_c between the uncorrected vectors $\mathbf{v}_0$ and $\mathbf{w}_0$ is

$$\alpha_c = \cos^{-1} \frac{\mathbf{v}_0^t\,\mathbf{M}^t\,\mathbf{g}\,\mathbf{M}\,\mathbf{w}_0}{(\mathbf{v}_0^t\,\mathbf{M}^t\,\mathbf{g}\,\mathbf{M}\,\mathbf{v}_0)^{1/2}\,(\mathbf{w}_0^t\,\mathbf{M}^t\,\mathbf{g}\,\mathbf{M}\,\mathbf{w}_0)^{1/2}} . \quad (5)$$

The bond-angle correction is a function of the anisotropy of libration, since isotropic libration, regardless of amplitude, does not distort bond angles. Equations (4) and (5) have been coded into the segmented-body[5] analysis program ORSBA. Tests on typical problems indicate that a bond-angle correction of ±0.2° is not

uncommon and that sometimes a correction is several times the estimated standard deviation for the uncorrected angle.

For certain types of covalent bonds, particularly the C–H bonds in aromatic hydrocarbons, the rigid-body model and the riding model can be combined to exploit the advantages of each. This "riding-on-rigid-group" model requires that a rigid body (or segmented body[5]) be fitted to the atoms in the molecule which do not display large amplitude displacements due to internal molecular motion within the group. The rigid-body description of motion is then used to calculate the displacements predicted at all atomic positions, including the riding atoms which were excluded from the rigid-body calculation. Riding corrections for appropriate bond distances are then made using the observed-minus-calculated residual thermal ellipsoids, and these corrections are added to the corrections made for the rigid-body motion. Table 9.3 gives a comparison of the C–H bond distances in the triclinic photodimer of isophorone[6] corrected with the riding model and the riding-on-rigid-group model. The superiority of the latter over the former is quite apparent from the table.

Table 9.3. Comparison of Various Estimates for C–H Bond Lengths in Triclinic Photodimers of Isophorone

Type of C–H Bond	Uncorrected Intermean Separation	Intermean plus Riding Correction[a]	Intermean plus Riding-on-Rigid-Group Correction[b]
$>$CH	1.093	1.125	1.115
$>$CH$_2$	1.089	1.144	1.130
	1.096	1.134	1.133
	1.094	1.131	1.126
	1.092	1.154	1.130
	1.075	1.130	1.113
	1.086	1.128	1.122
	1.074	1.127	1.110
	1.079	1.144	1.124
$-$CH$_3$	1.086	1.121	1.116
	1.084	1.134	1.126
	1.083	1.129	1.116
	1.067	1.116	1.111
	1.082	1.117	1.114
Average	1.084	1.131	1.120
Dispersion	0.008	0.010	0.007

[a]Values from column 1 corrected with riding model of Busing and Levy (ref. 1).

[b]Values from column 1 corrected with riding-on-rigid-group model.

Equations (1) and (4) are based on a distribution which is only slightly different from a rectilinear Gaussian distribution and are valid only for small librational amplitudes. It is important to characterize the librational range in which the equations are valid. Since the equations utilize only the lowest-order term in an infinite series expansion of the rotation operator, it is possible to add higher-order terms from the expansion; but if this is done, the physical and mathematical properties of the distribution become unclear. Instead, it is preferable to introduce new distribution functions which have a complete mathematical definition and a clear physical interpretation and to derive new distance corrections from these distributions which may be compared with those calculated from Eqs. (1) and (4). Let us examine the two extreme cases of librational anisotropy by considering distribution functions on a circle and on a sphere. The former corresponds to one-dimensional torsional oscillation and the latter to isotropic libration.

The closest analogs to a rectilinear Gaussian distribution for the circle are the wrapped-up normal,[7] defined by the probability density function

$$f(\theta) = \frac{1}{2\pi} + \frac{1}{\pi} \sum_{n=1}^{\infty} \cos n\theta \exp\left(-\frac{1}{2} n^2 \sigma^2\right), \qquad (6)$$

and the von Mises circular normal probability density function[7,8]

$$f(\theta) = \exp(k_c \cos\theta)/[2\pi I_0(k_c)] \ , \qquad (7)$$

where I_0 is the zero-order Bessel function of the first kind with pure imaginary argument. The von Mises probability density function represents a sinusoidal potential function,[9] and the wrapped-up normal represents a wrapped-up parabolic potential function. The term "wrapped-up" describes the cyclic overlap caused by placing a function onto a closed space such as the circle. The corresponding analogs for the sphere are the Brownian motion probability density function[10]

$$f(\theta,\phi) = \sum_{n=0}^{\infty} \frac{2n+1}{4\pi} P_n(\cos\theta) \times \exp\left[-\frac{1}{4} n(n+1) V\right], \qquad (8)$$

where P_n is the nth-order Legendre polynomial, and the Fisher spherical normal probability density function[10,11]

$$f(\theta,\phi) = k_s \exp(k_s \cos\theta)/[4\pi \sinh k_s] \ . \qquad (9)$$

The parameters σ^2 in Eq. (6) and V in Eq. (8) are the variances for those probability density functions. The parameters k_c in Eq. (7) and k_s in Eq. (9) are measures of concentration on the circle and sphere, such that when k is zero the probability density is uniformly distributed, and when k is large the density is concentrated around the modal vector at $\theta = 0$. For large k the total variance V for Eqs. (7) and (9) is approximately

$$V/C \approx 1/k\,, \tag{10}$$

where C is 1 for the circle and 2 for the sphere.

The bond-distance foreshortening problem is solved by determining the centers of gravity[12] g_c and g_s for the probability density functions, (6) to (9), which are

$$g_{c_1} = \exp(-\sigma^2/2)\,, \tag{11}$$

$$g_{c_2} = I_1(k_c)/I_0(k_c)\,, \tag{12}$$

$$g_{s_1} = \exp(-V/2)\,, \tag{13}$$

$$g_{s_2} = \coth k_s - \frac{1}{k_s}\,, \tag{14}$$

where $0 \leqslant g \leqslant 1$, and I_n is a Bessel function of order n. Since $g = d_0/d_r$, the corresponding values of g from the distance correction, Eq. (1), are

$$g_{c_3} = \frac{1}{1 + \psi^2/2}\,, \tag{15}$$

where $\psi^2 = L_{11}$ $(L_{22} = L_{33} = 0)$, and

$$g_{s_3} = \frac{1}{1 + \psi^2}\,, \tag{16}$$

where $\psi^2 = L_{11} = L_{22} = L_{33}$. In the derivation of Eqs. (1) and (4) an approximation was made replacing the distance between equilibrium positions by the observed distance between means. If this substitution is not made, we obtain the true quadratic approximation

$$g_{c_4} = 1 - \psi^2/2\,, \tag{17}$$

$$g_{s_4} = 1 - \psi^2\,. \tag{18}$$

The g values vs rms angular displacements derived from Eqs. (10) to (18) are given in Table 9.4. Although many interesting properties of the various probability density functions are shown by this table, the general conclusion of interest for bond distance corrections is that Eqs. (1) and (4) undercorrect bond distances compared with the two rigorous models and should be applied with caution when rms librational amplitudes exceed 10°. Note that the true quadratic approximation overcorrects, so that a linear combination of the two might provide a useful empirical correction factor. At present there is little to be gained in formulating a more elaborate correction, since the methods for determining librational amplitudes are limited to the quadratic approximation. However, work is under way to introduce higher-order effects into the rigid-body treat-

Table 9.4. Apparent Foreshortening of Interatomic Distances Due to Rigid-Body Libration: A Comparison of Different Models

The angle ψ is the rms angular displacement, and g is the foreshortening defined by $g = d_0/d_r$, where d_0 is the observed distance and d_r is the true distance. The eight models are described in the text. The entries for g_{s_2} and g_{c_2} are the angles which enclose a constant probability density consistent with the limiting case defined by Eq. (10).

Rms ψ (deg)	Isotropic Libration				One-Dimensional Torsional Oscillation			
	g_{s_1}	g_{s_2}	g_{s_3}	g_{s_4}	g_{c_1}	g_{c_2}	g_{c_3}	g_{c_4}
5	0.992	0.992	0.992	0.992	0.996	0.996	0.996	0.996
10	0.970	0.970	0.970	0.970	0.985	0.985	0.985	0.985
15	0.934	0.932	0.936	0.931	0.966	0.966	0.967	0.966
20	0.885	0.881	0.891	0.878	0.941	0.940	0.943	0.939
25	0.827	0.816	0.840	0.810	0.909	0.906	0.913	0.905
30	0.760	0.739	0.785	0.726	0.872	0.865	0.879	0.863
35	0.689	0.654	0.728	0.627	0.830	0.816	0.843	0.813
40	0.614	0.566	0.672	0.512	0.784	0.763	0.804	0.756
45	0.539	0.480	0.618	0.383	0.734	0.708	0.764	0.691
50	0.467	0.396	0.567	0.238	0.683	0.653	0.724	0.619

ment,[13] and there is hope for obtaining better estimates of the librational amplitudes with this approach.

[1] W. R. Busing and H. A. Levy, *Acta Cryst.* **17**, 142 (1964).

[2] G. M. Brown, *Acta Cryst.* **B24**, 294 (1968).

[3] V. Schomaker and K. N. Trueblood, *Acta Cryst.* B24, 63 (1968).

[4] R. D. Ellison and H. A. Levy, *Chem. Div. Ann. Progr. Rept. May 20, 1968,* ORNL-4306, p. 151.

[5] C. K. Johnson, *Chem. Div. Ann. Progr. Rept. May 20, 1968,* ORNL-4306, p. 143.

[6] C. K. Johnson and A. Vos, *Chem. Div. Ann. Progr. Rept. May 20, 1968,* ORNL-4306, p. 160.

[7] E. J. Gumbel, J. A. Greenwood, and D. Durand, *J. Am. Statist. Assoc.* **48**, 131 (1953).

[8] R. von Mises, *Phys. Z.* **19**, 490 (1918).

[9] M. V. King and W. N. Lipscomb, *Acta Cryst.* **3**, 155 (1950).

[10] P. H. Roberts and H. D. Ursell, *Phil. Trans. Roy. Soc.* **252**, 317 (1960).

[11] R. A. Fisher, *Proc. Roy. Soc. A* **217**, 295 (1953).

[12] K. J. Arnold, "Spherical Probability Distributions," Ph.D. dissertation, Massachusetts Institute of Technology, 1941.

[13] C. K. Johnson, "Higher-Order Effects in Rigid-Body Motion," following report.

HIGHER-ORDER EFFECTS IN RIGID-BODY MOTION

C. K. Johnson

The cumulant-expansion structure-factor equation[1] provides a general mathematical model for the experimental determination of higher-order thermal-motion effects in crystals. The equation, which can be used with either neutron or x-ray Bragg diffraction data, is

$$F(\mathbf{h}) = \sum_{\substack{\text{atoms}\\ \text{in}\\ \text{cell}}} f(\mathbf{h}) \exp\left[2\pi i \sum_{j=1}^{3} {}^{1}\kappa^{j} h_j + \frac{(2\pi i)^2}{2!} \sum_{j,k=1}^{3} {}^{2}\kappa^{jk} h_j h_k + \frac{(2\pi i)^3}{3!} \sum_{j,k,l=1}^{3} {}^{3}\kappa^{jkl} h_j h_k h_l + \ldots \right], \quad (1)$$

where $F(\mathbf{h})$ is the structure factor, $f(\mathbf{h})$ is the atomic scattering factor, $\mathbf{h}$ is the vector of Miller indices, and ${}^{r}\kappa$ ($r = 1, 2, 3 \ldots$) are symmetric cumulant tensors of order r. The first four cumulant tensors described the mean, the dispersion, the skewness, and the kurtosis of the probability density function for the thermal motion of an atom. The coefficients of the cumulant tensors are fitted by a least-squares procedure to the observed structure-factor amplitudes $|F_0(\mathbf{h})|$. If higher-order thermal-motion effects are absent, the third and all other higher-order cumulant tensor coefficients are zero.

The two major physical causes of higher-order thermal-motion effects are curvilinear motion and anharmonic vibration. A curvilinear motion is a nonrectilinear motion such as bond-bending or rigid-body libration. Anharmonic vibration results from a potential well which is not parabolic in shape. Many interesting aspects of chemical bonds are related to the shape of the potential well; hence it is desirable to attempt to separate the higher-order effects arising from anharmonicity from those arising from curvilinear motion.

The skewness (i.e., departure from a centrosymmetric shape) of a thermal-motion probability density function can be appreciable when large-amplitude curvilinear modes of vibration are present. Some experimentally determined thermal-motion probability density functions derived by using Eq. (1) terminated after the third cumulant are shown in Figs. 9.10 and 9.11.

It is of interest to see if the experimentally derived third-cumulant coefficients ${}^{3}\kappa^{jkl}$ ($j \leqslant k \leqslant l \leqslant 3$) describing the skewness can be predicted from a description of the curvilinear motion derived without using the third-cumulant coefficients. The simplest case is rigid-body libration, since a description of the mean-square libration tensor $\mathbf{L}$ can be determined from the experimentally derived atomic positions and anisotropic temperature factors (i.e., first and second cumulants), using the method of Schomaker and Trueblood.[2] A Cartesian tensor expression[3] relating ${}^{3}\kappa$ with $\mathbf{L}$ for a centrosymmetric rigid body undergoing harmonic libration is

$${}^{3}\kappa_{jkl} = 2 \sum_{m,n,p,q=1}^{3} L_{mp} L_{nq} (A_{jm} A_{kn} B_{lpq} + A_{lm} A_{jn} B_{kpq} + A_{km} A_{ln} B_{jpq}), \quad (2)$$

where

$$A_{jk} = \sum_{l=1}^{3} e_{jkl} r_l ,$$

$$B_{jkl} = \frac{1}{4} \sum_{m,n=1}^{3} e_{jml} e_{kmn} r_n + e_{jmk} e_{lmn} r_n ,$$

$\mathbf{r}$ = vector to the rest position of an atom from the center of symmetry in the molecule,

e_{jkl} = 1 when jkl is a cyclic permutation of 1,2,3
= −1 when jkl is a cyclic permutation of 3,2,1
= 0 for all other jkl.

ORNL-DWG. 68-6969

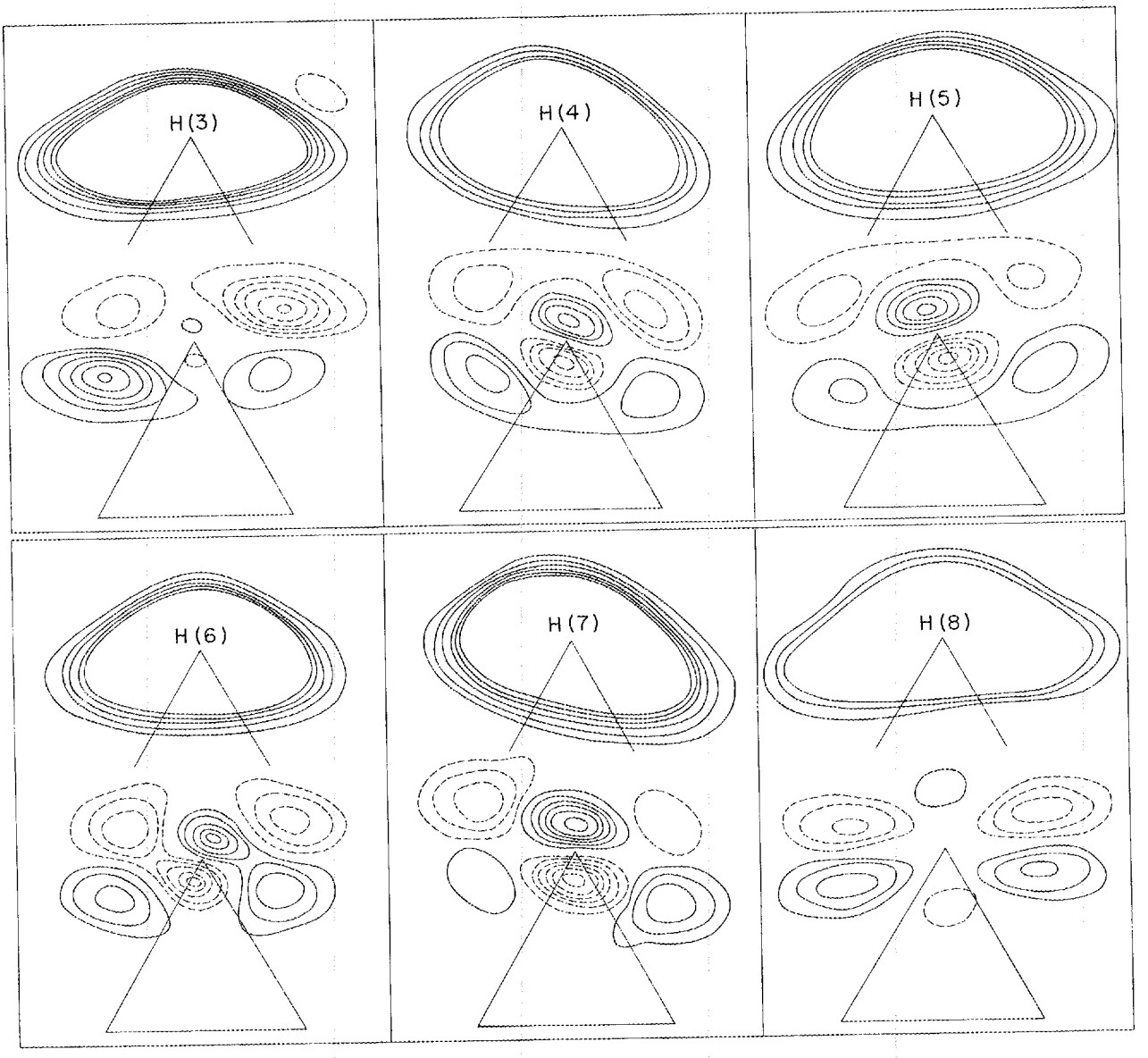

Fig. 9.10. Edgeworth Density Maps and Skew Density Maps for the Six Hydrogen Atoms on the Two Methyl Groups in Copper Acetate Monohydrate (R. Chidambaram and G. M. Brown, *Chem. Div. Ann. Progr. Rept. May 20, 1965,* **ORNL-3822, p. 121; G. M. Brown and R. Chidambaram,** *Chem. Div. Ann. Progr. Rept. May 20, 1966,* **ORNL-3994, p. 119).** The skew density maps display the antisymmetric component of the probability density functions for thermal motion, and the Edgeworth maps show the total probability density function. Each map is in the plane of the hydrogen atoms of the appropriate methyl group. The contour interval is 0.02 in units of 10^{-12} cm/Å^3. The zero contours and higher-level contours are omitted. The dashed contours in the skew maps signify the regions of subtraction. The vertices of the triangles designate the mean positions of the three hydrogen atoms in a methyl group.

Equation (2) was derived by expanding a rotation operator about **r** in a power series in the curvilinear librational components $(\lambda_1, \lambda_2, \lambda_3) \equiv \lambda$ to obtain the displacement **u** in rectilinear Cartesian components,

$$u_j = \sum_{k=1}^{3} A_{jk}\lambda_k + \sum_{k,l=1}^{3} B_{jkl}\lambda_k\lambda_l + \ldots . \qquad (3)$$

ORNL-DWG. 68-6971

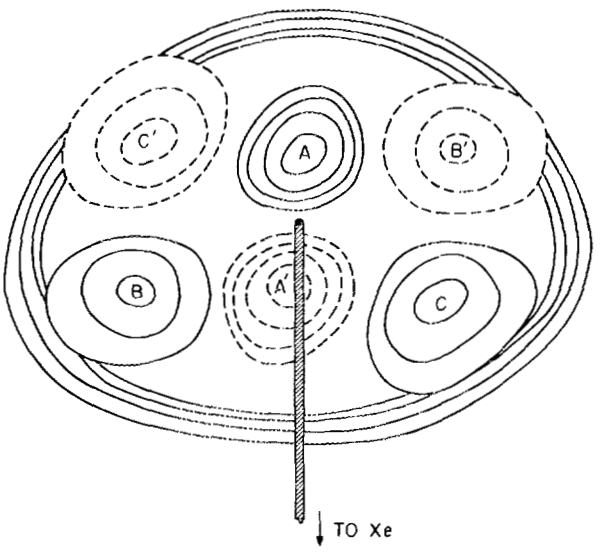

Fig. 9.11. Skew Density Map for Atom F(2) of XeF_4 Superimposed on the Edgeworth Density Map. The same contour levels are drawn in both maps, and higher contour levels for the Edgeworth density map are omitted. The contour interval is 0.02 in units of 10^{-12} cm/Å^3. Negative contours are dashed, and the zero contour is omitted. The heavy line designating the direction of the Xe-F bond originates at the mean of the fluorine atom. The map is in the plane of the XeF_4 molecule.

Moments about the equilibrium position of an atom at **r** are obtained by raising u_j in Eq. (3) to the appropriate power and averaging each term in the expanded equation. If the librational distribution has Gaussian form, the odd curvilinear moments $\langle\lambda_j\rangle$, $\langle\lambda_j\lambda_k\lambda_l\rangle$, etc., are zero, and the even curvilinear moments are all completely specified by the second curvilinear moment $\langle\lambda_m\lambda_n\rangle \equiv L_{mn}$. The fourth curvilinear moment, for example, is

$$L_{mnpq} = L_{mn}L_{pq} + L_{mp}L_{nq} + L_{mq}L_{np} . \qquad (4)$$

The cumulants can be calculated from the moments about any point, and all cumulants except the first are invariant to the choice of origin. The third cumulant, for example, is related to the first three moments μ_j, μ_{jk}, μ_{jkl} by

$$^3\kappa_{jkl} = \mu_{jkl} - \mu_j\mu_{kl} - \mu_k\mu_{lj} - \mu_l\mu_{jk} + 2\mu_j\mu_k\mu_l . \qquad (5)$$

All terms of higher order than $L_{mn}L_{pq}$ are omitted from Eq. (2). This is a reasonable approximation for the librational amplitudes found in most molecular crystals. A comparison of the experimentally derived third-cumulant coefficients for the two unique fluorine atoms in XeF_4 (refs. 1, 4) and those calculated by Eq. (2) is given in Table 9.5. Neutron data are being collected from crystals of benzene hexachloride to test further Eq. (2) and the hypothesis that rigid-body libration is a major contributor to skewness in the thermal-motion probability density function.

An assumption implicit in the derivation of Eq. (2) is that no interaction occurs between rigid-body libration

Table 9.5. Observed and Calculated Third-Cumulant Tensor Coefficients for XeF_4

The values tabulated are based on the crystal coordinate system and are multiplied by $(4\pi^2/3) \times 10^5$. Standard errors obtained from the inverted least-squares normal-equations matrix are in parentheses. The calculated values are from Eq. (2), using a libration tensor **L** derived by the Schomaker and Trueblood rigid-body method.

	κ^{111}	κ^{222}	κ^{333}	κ^{112}	κ^{122}	κ^{113}	κ^{133}	κ^{223}	κ^{233}	κ^{123}
F(1)										
Observed	−6	−16	16	25	3	−8	−5	5	2	4
σ(obs)	(12)	(7)	(8)	(6)	(5)	(6)	(6)	(4)	(5)	(4)
Calculated	−21	−13	12	5	3	−5	−1	3	−3	−6
F(2)										
Observed	−36	−4	−20	−16	−3	−1	13	−1	4	−1
σ(obs)	(12)	(5)	(5)	(6)	(5)	(5)	(3)	(4)	(3)	(3)
Calculated	−24	−1	−8	1	−3	−2	8	−4	0	1

Table 9.6. Tensor Moments About Equilibrium Position for Rigid-Body Motion with Harmonic Libration

The contributors of major and of minor importance to the first three rectilinear moments $\langle u \rangle$, $\langle uu \rangle$, and $\langle uuu \rangle$ of an atom are listed. A centrosymmetric site symmetry for the rigid body will allow only the even-polar and odd-axial tensors listed in the centrosymmetric column. If the site symmetry is noncentrosymmetric, the tensors listed in the "Additional" column are also allowed in addition to those for the centrosymmetric site. The libration vector λ is axial and the translation vector t is polar.

Rectilinear Moments for Individual Atoms		Moments for Rigid Body					
		Centrosymmetric			Additional		
		Even Polar and Odd Axial Tensors			Odd Polar and Even Axial Tensors		
		Trans.	Coupling	Libr.	Trans.	Coupling	Libr.
Mean $\langle u \rangle$	Major			$\langle \lambda\lambda \rangle$			
	Minor			$\langle \lambda\lambda \rangle^2$	$\langle t \rangle$		
Dispersion $\langle uu \rangle$	Major	$\langle tt \rangle \equiv T$		$\langle \lambda\lambda \rangle \equiv L$		$\langle \lambda t \rangle \equiv S$	
	Minor			$\langle \lambda\lambda \rangle^2$		$\langle \lambda\lambda t \rangle$	
Skewness $\langle uuu \rangle$	Major		$\langle \lambda tt \rangle$	$\langle \lambda\lambda \rangle^2$	$\langle ttt \rangle$	$\langle \lambda\lambda t \rangle$	
	Minor		$\langle \lambda\lambda tt \rangle$	$\langle \lambda\lambda \rangle^3$		$\langle \lambda\lambda\lambda t \rangle$	

and rigid-body translation when the molecule is on a crystallographic center of symmetry. This is not strictly true. In particular the third-rank axial tensor for the interaction $\langle \lambda tt \rangle$ (i.e., mean cubic libration-translation-translation) might be an important contributor to the skewness of thermal motion for an atom belonging to a centrosymmetric rigid molecule, since odd-rank axial tensors are not required to be zero by the center of symmetry. Table 9.6 lists the major and minor contributors to the first three moments (about the equilibrium positions) from which the cumulants are derived. Equation (2) is not applicable to the noncentrosymmetric case because $\langle ttt \rangle$, $\langle \lambda\lambda t \rangle$, and $\langle \lambda tt \rangle$ are all a function of the location of the origin and would have to be included to produce an invariant formulation.

[1] C. K. Johnson, *Acta Cryst.* **A25**, 187 (1969).

[2] V. Schomaker and K. N. Trueblood, *Acta Cryst.* **B24**, 63 (1968).

[3] C. K. Johnson, *Abstracts of the Am. Cryst. Assoc. Winter Meeting*, Seattle, Wash., Mar. 23–28, 1969, p. 55.

[4] J. H. Burns, P. A. Agron, and H. A. Levy, p. 211 in *Noble-Gas Compounds* (ed. by H. H. Hyman), University of Chicago Press, Chicago, 1963.

CRYSTAL AND MOLECULAR STRUCTURES OF TRI(*p*-FLUOROPHENYL)AMINE AND TRI(*p*-IODOPHENYL)AMINE[1]

G. R. Freeman[2] G. M. Brown
H. A. Levy

The molecular structure of triphenylamine has been the subject of some discussion in the chemical literature (for key references, see the electron-diffraction study of Sasaki, Kimura, and Kubo[3]). The questions of principal interest concern the geometrical configuration of the nitrogen valence bonds and the orientations of the phenyl rings about the nitrogen-carbon axes. The nitrogen valence geometry has been deduced by some authors to be trigonal plane and by others to be pyramidal, depending on the particular datum used for the electric dipole moment. The electron-diffraction study of Sasaki *et al.*,[3] on gaseous triphenylamine, led to the conclusion that the probable value of the valence angle C–N–C is 116 ± 2° and that the probable value of the twist angle of each ring from parallelism with the threefold axis of the molecule is 47 ± 5°. However, Sasaki *et al.* specifically admitted "a possibility that a triphenyl amine molecule has a flat trigonally bonded central nitrogen atom at equilibrium but appears pyramidal because of thermal bending motion."

X-ray analysis can in principle provide a complete description of the molecular structure of triphenylamine in the crystalline state. Unfortunately, however, the compound crystallizes with eight molecules per asymmetric unit, and the crystals are nearly always twinned.[4,5] Hence, we have turned our attention to the tri(*p*-halophenyl)amines, which are known to be more suitable candidates for x-ray analysis. The structural details in these amines may well be somewhat different from those of the unsubstituted compound, but they are of equal interest. We report here structure determinations on tri(*p*-fluorophenyl)amine (TFPA) and on tri(*p*-iodophenyl)amine (TIPA). These particular tri(*p*-halophenyl)amines were chosen with the thought that the difference of electronegativity between fluorine and iodine might be accompanied by some significant difference in molecular structure.

Schlemper and Hausmann[6] reported that TFPA crystals have the symmetry of the centric space group $P2_1/a$, with 4 molecules per cell, and that TIPA crystals have the symmetry of either the acentric group $R3$ or the centric group $R\bar{3}$, with 12 molecules per primitive rhombohedral cell. These assignments and Schlemper and Hausmann's approximate cell parameters were readily verified by preliminary precession photography. Precise values of the unit-cell parameters for each compound were obtained by the method of least squares from angle data recorded at about 23°C with the Oak Ridge computer-controlled x-ray diffractometer.[7] The angle data of 12 TFPA reflections in the range 110 to 119° 2θ (Cu $K\alpha_1$ radiation, λ = 1.54051 Å) yielded the following cell parameters: a = 10.436 ± 0.001 Å, b = 17.379 ± 0.002 Å, c = 8.487 ± 0.001 Å, β = 108.55 ± 0.01°. Data for 12 TIPA reflections in the range 34.7 to 51.4° 2θ at 24 to 25°C (Mo $K\alpha_1$ radiation, λ = 0.70296 Å) yielded: $a = b$ = 44.371 ± 0.009 Å, c = 10.130 ± 2 Å (hexagonal triply primitive cell).

Intensity data for 3020 independent reflections of TFPA were recorded by using the automatic diffractometer and Cu $K\alpha$ radiation to the limit 159.6° in 2θ. The crystal specimen was measured accurately to obtain the necessary data for making absorption corrections[8,9] and computing derivatives later used in applying extinction corrections. The value of the absorption coefficient used was 9.3 cm^{-1}; the absorption correction factors on the F_0^2 values ranged from 1.08 to 1.40. The raw intensity data were converted in the usual preliminary processing to a set of structure-factor squares and standard errors. The normalized structure factors[10] (E's) were also calculated.

Data for 4956 independent reflections of TIPA were recorded using Mo $K\alpha$ radiation and were processed in the same preliminary procedures as those used for the TFPA data. All reflections having $2\theta \leqslant 42°$ were recorded; reflections having $2\theta > 42°$ were recorded only if a preliminary observation indicated a peak count at least five times the background count. The absorption coefficient used was 30.9 cm^{-1}; the range of correction factors was from 2.56 to 3.23.

The solution for the structure of TFPA was obtained through use of Long's computer program for sign determination.[11] The 22 nitrogen, carbon, and fluorine atoms were identified with the 22 highest peaks in the E map computed with the "best" sign combination for the 371 normalized structure factors of magnitude $\geqslant$1.50.

Refinement by the method of least squares proceeded smoothly. After some preliminary cycles, starting coordinates for the hydrogen atoms were computed from structural considerations, and both coordinates and thermal parameters of the hydrogen atoms were adjusted thereafter. In the final refinement cycles, anisotropic thermal parameters were used for all atoms. Corrections for mild extinction were applied in the least-squares calculations.[12] The extreme correction on F_c^2 is 0.49; for 169 reflections the correction factor is less than 0.99. Final values of the usual measures of goodness of fit[13] are: $R(F)$ = 0.044; $R(F^2)$ = 0.040; $R_w(F^2)$ = 0.098; σ_1 = 2.12.

Statistical tests[14] on the normalized structure factors of TIPA gave a positive indication of centrosymmetry, thereby establishing the space group as $R\bar{3}$ and the number of molecules per asymmetric unit as 2, and suggesting the application of the Long program for solving the phase problem. The six iodine atoms of the asymmetric unit were identified with the six highest peaks of the E map based on the "best" sign combination for 534 E's $\geqslant$ 1.50. The nitrogen and carbon atoms were subsequently located by the Fourier method.

Refinement of the positional and thermal parameters of the 44 nitrogen, carbon, and iodine atoms was carried to convergence. The usual six anisotropic thermal parameters were adjusted for each nitrogen and carbon atom; in addition, the ten extra parameters of the third-cumulant model[15] were adjusted for each iodine atom in the final cycles. The final values of the measures of goodness of fit are: $R(F)$ = 0.098; $R(F^2)$ = 0.073; $R_w(F^2)$ = 0.101; σ_1 = 1.36. Hydrogen atoms were not included in the final refinement cycles because of a limitation of the least-squares program used. However, their inclusion at an earlier stage of refinement before use of the third-cumulant model had resulted in virtually no changes in the parameters of other atoms or in the measures of goodness of fit. The rather high values of the various discrepancy indices R

at convergence are judged to reflect mainly the fact that for many of the reflections recorded the net counts are very low.

Figure 9.12*a* shows a stereoscopic view of the TFPA molecule in the direction normal to the plane of the three carbon atoms attached to the central nitrogen atom; Figs. 9.12*b* and *c* show similar views of the two molecules of TIPA. Values of the valence angles at the nitrogen atoms and of the bond lengths C–N, C–C, C–F, and C–I are included in the molecular drawings. All other valence angles except those involving hydrogen atoms are shown in Table 9.7.

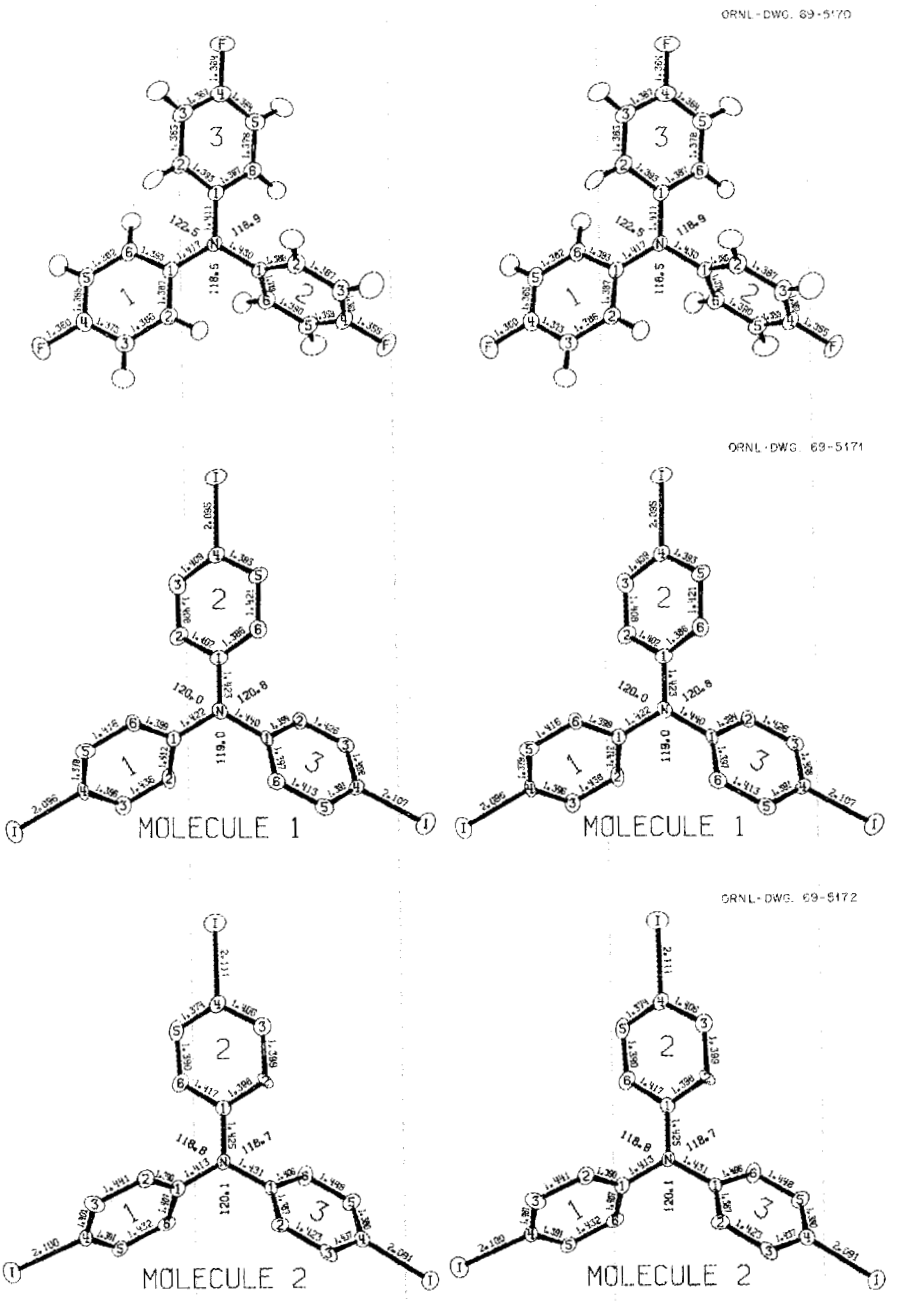

Fig. 9.12. Stereoscopic View of the Molecule of Tri(*p*-fluorophenyl)amine (*a*) and of the Two Different Molecules of Tri(*p*-iodophenyl)amine (*b* and *c*). Drawings are all to the same scale, and the view direction in each case is normal to the plane of the three carbons attached to nitrogen. The valence angles (deg) at nitrogen and all bond lengths (Å) are shown except those of TFPA involving hydrogen atoms. The standard errors of the angles are about 0.1 and 1° for TFPA and TIPA respectively; those of the bond lengths are about 0.002 and 0.02 Å, respectively, for the two compounds.

Table 9.7. Valence Angles (deg) at Carbon Atoms in TFPA and TIPA

Standard errors are from 0.10 to 0.16° for TFPA and from 1.1 to 1.7° for TIPA. For each molecule the angles for rings 1, 2, and 3 appear in successive columns from left to right.

Angle	TFPA			TIPA					
				Molecule 1			Molecule 2		
N-C(1)-C(2)	120.0	120.2	121.9	119.4	117.3	117.3	119.0	121.3	118.6
N-C(1)-C(6)	121.2	119.7	119.5	118.8	119.7	119.0	117.1	117.5	117.9
C(6)-C(1)-C(2)	118.8	120.0	118.6	121.8	123.0	123.6	123.9	121.2	123.5
C(1)-C(2)-C(3)	121.0	120.1	120.6	118.6	117.3	119.2	119.5	117.9	119.0
C(1)-C(6)-C(5)	120.5	120.0	120.8	119.3	119.9	117.4	117.3	121.2	119.2
C(2)-C(3)-C(4)	118.4	118.4	118.7	117.6	119.8	116.9	115.2	118.9	117.7
C(6)-C(5)-C(4)	119.0	118.5	119.1	118.6	117.3	119.6	117.7	116.3	116.8
C(3)-C(4)-C(5)	122.4	123.0	122.2	124.1	122.5	123.4	126.2	124.4	123.8
C(3)-C(4)-X	118.8	118.5	118.6	117.7	119.7	117.5	115.5	116.3	117.8
C(5)-C(4)-X	118.8	118.5	119.2	118.2	117.7	119.1	118.3	119.2	118.4

In TFPA the best planes through the carbon atoms of rings 1, 2, and 3 make angles with the plane defined by the three carbon atoms attached to nitrogen of 31.8, 59.1, and 30.6° respectively. In TIPA the corresponding angles are 43.4, 33.1, and 44.2° in molecule 1 and 56.6, 27.3, and 52.3° in molecule 2. These varied ring twists are obviously requirements for packing of the molecule into crystals.

It is clear from the values of the valence angles of the nitrogen atoms in Fig. 9.12 that the configurations of the C–N bonds in the TFPA molecule and in the two TIPA molecules are all nearly plane trigonal configurations. The nitrogen atom in TFPA is displaced from the plane of its three carbon neighbors by 0.029 Å. This displacement, though about 24 times the standard error (σ) of position of the nitrogen atom along the plane normal, is still quite small; it corresponds to bending of each C–N bond from a hypothetical plane configuration by only 1.2°. In molecule 1 of TIPA the nitrogen atom is 0.027 Å ($\sim 3\sigma$) from the plane of the three carbons, and the C–N bond configuration is barely distinguishable from the plane configuration. In molecule 2 the nitrogen atom is 0.129 Å (15σ) from the plane, corresponding to bending each C–N bond from a plane configuration by 4.8°. For comparison, the C–N–C valence angle of 116° reported for triphenylamine corresponds to a displacement of the nitrogen atom from the three-carbon plane of 0.29 Å and a bending of each C–N bond of 11.7°.

The fact that the TIPA crystal contains two molecules per asymmetric unit provides us with some very informative data as to what degree of deformation of the nitrogen valence geometry in triphenylamines may be expected from packing effects. The relative distortion between molecules 1 and 2 in TIPA is more than the slight distortion in the TFPA molecule or that in molecule 1 of TIPA from the hypothetical plane configuration. We conclude that there is no significant inherent difference between the nitrogen atoms in TFPA and TIPA so far as valence geometry is concerned and that it is possible that molecules of both compounds in solution or in the gaseous state have the plane valence configuration at nitrogen.

In these same molecules there are some other small distortions that surely are to be attributed to packing. For example, in TFPA the fluorine atom on ring 3 is displaced from the least-squares best plane through the six carbon atoms by 0.030 Å (30σ), more than three times the displacement of any carbon atom from its best plane. Similarly, the nitrogen atom is 0.022 Å (19σ) from the best plane through ring 1. In TIPA the iodine atom on ring 1 of molecule 2 is displaced 0.130 Å (65σ) from the best plane. The largest of the displacements of the carbon atoms from this best plane is 0.03 ($\sim 2\sigma$), and the indication is that the displacement of the iodine atom is real.

The hybridization of the nitrogen atoms must be very nearly the ideal sp^2 plane trigonal hybridization. Presumably the nearly plane configuration signifies some stabilization through π-orbital overlap between the nitrogen atoms and the adjacent carbon atoms, even though all the rings are twisted far from the orientations allowing maximum overlap. Since the degree of overlap of π orbitals is determined by the twist angles, one may expect the exact hybridization and valence geometry to depend on packing in an indirect manner through effects on the twist angles, as well as by way of direct strains.

The average C–N bond lengths in TFPA and TIPA are 1.419 ± 0.005 and 1.426 ± 0.008 Å respectively. These averages are shorter than the value 1.472 ± 0.008 Å reported from a microwave study of trimethylamine.[16] The C–N–C angle found in the microwave study was 108.7 ± 1°, nearly the angle of a regular tetrahedron. The difference in the C–N bond length between trimethylamine and the tri(*p*-halophenyl)amines is about that to be expected to accompany the difference in hybridization of the nitrogen and carbon atoms.

It is interesting that triphenylphosphine[17] and tri-*p*-tolylarsine[18] are known from x-ray studies to have pyramidal valence configurations at the central atoms. The average C–P–C angle in the triphenylphosphine molecule (point group 1) is 103.0 ± 0.7°, and the angle C–As–C in tri-*p*-tolylarsine (point group 3) is 102 ± 2°.

We thank Professor Robert I. Walter of the University of Illinois at Chicago Circle for suggesting this work and for supplying the samples of the tri(*p*-halophenyl)amines used.

---

[1] A preliminary report of this work was published in the *Abstracts of the Eighth International Congress of Crystallography, Buffalo and Stony Brook, New York, August 1969.*

[2] Oak Ridge Graduate Fellow from North Texas State University, Denton, under appointment with Oak Ridge Associated Universities.

[3] Y. Sasaki, K. Kimura, and M. Kubo, *J. Chem. Phys.* **31**, 477 (1959).

[4] E. R. Howells *et al.*, *Acta Cryst.* **7**, 298 (1954).

[5] V. I. Iveronova and C. M. Rojtburd, *Zh. Fiz. Khim.* **26**, 810 (1952).

[6] E. Schlemper and J. Hausmann, *Acta Cryst.* **16**, 1069 (1963).

[7] W. R. Busing *et al.*, *The Oak Ridge Computer-Controlled X-Ray Diffractometer*, ORNL-4143 (January 1968).

[8] W. R. Busing and H. A. Levy, *Acta Cryst.* **10**, 180 (1957).

[9] D. J. Wehe, W. R. Busing, and H. A. Levy, *A Fortran Program for Calculating Single-Crystal Absorption Corrections*, ORNL-TM-229 (1962).

[10] H. Hauptman and J. Karle, "Solution of the Phase Problem. I. The Centrosymmetric Crystal," *Amer. Cryst. Assoc. Monograph No. 3*, 1953.

[11] R. E. Long, Ph.D. dissertation, including the "Program for Sign Determination by Reiterative Application of Sayre's Equation," University of California at Los Angeles, 1965.

[12] A correction procedure based on the theory of W. H. Zachariasen, *Acta Cryst.* **23**, 558 (1967), has been inserted in our least-squares program ORFLS by A. Vos and C. K. Johnson.

[13] Definitions: $R(F)$ and $R(F^2)$ are defined by

$$\Sigma \left| |F^x_{\text{obs}}| - S^x |F^x_{\text{calc}}| \right| / \Sigma |F^x_{\text{obs}}| ,$$

with $x = 1$ and 2 respectively;

$$R_w(F^2) \equiv \left[\Sigma w (F^2_{obs} - S^2 F^2_{calc})^2 / \Sigma w F^4_{\text{obs}} \right]^{1/2} ,$$

$$\sigma_1 \equiv \left[\Sigma w (F^2_{\text{obs}} - S^2 F^2_{\text{calc}})^2 / (n - p) \right]^{1/2} ,$$

where p is the number of parameters fitted to the n observations. The factor S is the factor scaling the values $|F_{\text{calc}}|$ to the values $|F_{\text{obs}}|$.

[14] J. Karle and I. L. Karle, "Probability Methods for Centrosymmetric Crystals," chap. 17, in *Computing Methods in Crystallography*, J. S. Rollett, Ed., Pergamon, Oxford, 1965.

[15] C. K. Johnson, *Acta Cryst.* **A25**, 187 (1969).

[16] D. R. Lide, Jr., and D. E. Mann, *J. Chem. Phys.* **28**, 572 (1958).

[17] J. J. Daly, *J. Chem. Soc.* 3799 (1964).

[18] J. Trotter, *Canadian J. Chem.* **41**, 14 (1963).

CRYSTAL STRUCTURE OF SEDOHEPTULOSAN MONOHYDRATE[1]

G. M. Brown W. E. Thiessen[2]

Sedoheptulosan is an anhydride of sedoheptulose, a sugar important in the photosynthetic cycle and in carbohydrate metabolism which itself has not been crystallized. In 1938 Hudson[3] proposed the unusual structure **1** for sedoheptulosan. However, the combination of the three-membered epoxide ring and the seven-membered ring in **1** was in such striking contrast to the known combination of five- and six-membered rings in levoglucosan (**2**) and other aldosans that it prompted further exhaustive chemical work by Pratt, Richtmyer, and Hudson[4] which led to the conclusion that sedoheptulosan is indeed properly to be formulated as in **3**, with the five-six ring combination. This conclusion was reached even though it flatly contradicts a seeming experimental fact of an earlier investigation which was not otherwise suspect and which was basic to Hudson's original assignment[3] of formula **1**. Pratt *et al.*

ORNL-DWG. 69-6697

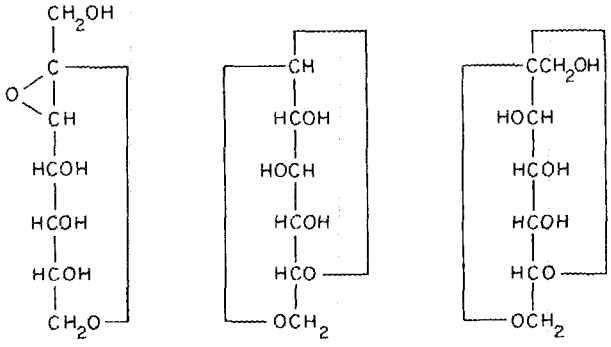

1 2 3

surmised that the earlier workers had accidentally interchanged two samples. Since this surmise could not at the time be checked directly, Pratt *et al.* were very careful to establish their structure **3** by several lines of chemical evidence. We have carried out an x-ray crystal-structure analysis of sedoheptulosan monohydrate which provides a completely independent proof of the correctness of structure **3** and also provides detailed metrical data on the crystal and molecular structure.

Crystals of sedoheptulosan monohydrate display in x-ray photographs the symmetry of the enantiomorphous pair of space groups $P4_1$ and $P4_3$. There are four formula units in a cell with parameters $a = b = 11.0739 \pm 0.0005$ Å and $c = 7.3746 \pm 0.0005$ Å. These parameters were obtained by the method of least squares from angle data for 12 reflections in the range 123 to 157° in 2θ recorded at about 23°C with the Oak Ridge computer-controlled diffractometer[5] (Cu $K\alpha_1$ radiation, $\lambda = 1.54051$ Å).

Intensity data for 1074 independent reflections were recorded by using the automatic diffractometer and Cu $K\alpha$ radiation to the limit 162.3° in 2θ. The 379 accessible Cu $K\beta$ reflections in the 2θ range 126 to 163.8° were also recorded, thereby extending the data to the limit 0.71 in $(\sin\theta)/\lambda$. Absorption correction factors ranging from 1.16 to 1.49 were calculated[6,7] and applied, and derivatives to be used later in correcting for extinction were calculated. A set of structure-factor squares with accompanying standard errors was calculated, as well as a set of normalized structure factors[8] (E's).

The solution for this noncentrosymmetric structure was found with remarkable ease by application of direct methods.[9] Space group $P4_1$ was assumed at the beginning. A basic set of ten phases, including eight calculated by the Σ_1 formula[10] and two chosen to fix the origin, was used in the tangent formula[10] as embodied in program PHASEM[11] to phase 157 of the 158 reflections with $E \leqslant 1.47$. The 14 highest peaks of the E map then calculated were identifiable with the 14 carbon and oxygen atoms of the asymmetric unit. Since the coordinates of these 14 peaks described a molecule of opposite configuration to the known absolute configuration,[4] the coordinates were inverted and the symmetry operations of space group $P4_3$ were used in subsequent calculations.

Refinement by the method of least squares led eventually to convergence with the following values of the usual measures of goodness of fit:[12] $R(F)$, 0.033; $R(F^2)$, 0.052; $R_w(F^2)$, 0.072; σ_1, 2.06. All hydrogen atoms were located; their coordinates and isotropic thermal parameters were adjusted in the refinement, along with the usual nine parameters for each of the other atoms. Satisfactory corrections[13] for rather severe extinction effects were made in the least-squares refinement. The largest correction factor on F_0^2 was 2.73; many reflections were corrected by smaller, yet substantial, factors.

The inclusion of the Cu $K\beta$ reflection data is an unusual feature of this determination. The 43 E's representing Cu $K\beta$ reflections that were included in the E map surely contributed to the solution; they may well have been very important. This point is of considerable interest and will be investigated by recalculation of the phases without the inclusion of the β data and by synthesis of another E map.

The spatial configuration of the sedoheptulosan molecule is displayed in the stereoscopic drawing of Fig. 9.13, which also shows the lengths of all C–C and C–O

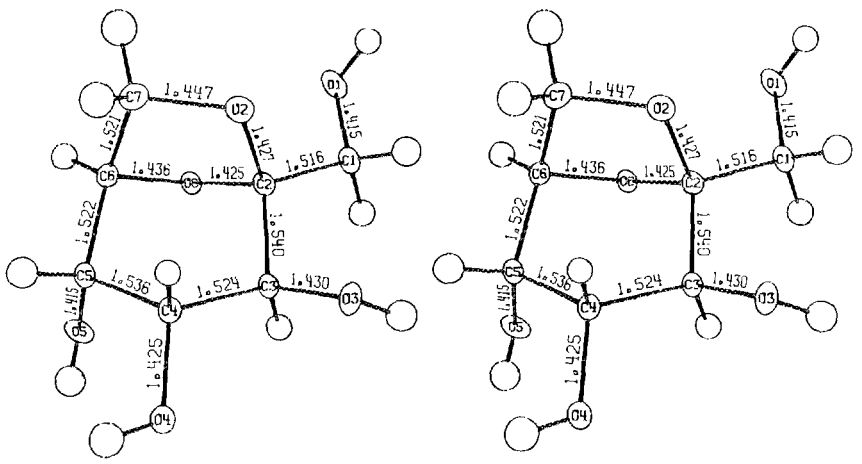

Fig. 9.13. Stereoscopic View of the Sedoheptulosan Molecule, Showing C–C and C–O Bond Lengths (Å). The standard errors of the bond lengths are ~0.002 Å or less.

bonds. The valence angles not involving hydrogen atoms and the conformation angles[14] of the ring bonds are given in Table 9.8. Each conformation angle is specified by four atoms. For example, the conformation angle O(6)-C(2)-C(3)-C(4) is the angle measured clockwise which the projection of vector C(3) → C(4) makes with reference to the projection of C(2) → O(6) when one views the bond system in the direction C(2) → C(3).

There are some variations among both the C–C and the C–O bond lengths that appear significant in relation to the standard errors of the bond lengths. However, we make no attempt at this time to explain these differences.

The valence angle of 102.8° at O(6) in the six-membered pyranose ring is substantially smaller than corresponding angles known in unbridged pyranose rings. In α-D-glucose,[15] for example, the corresponding angle is 113.7°; in sucrose[16] it is 116.1°. The small angle in sedoheptulosan is obviously a result of closure of the five-membered anhydride ring. Coincidentally, an angle of 101.8° at the oxygen atom of the pyranose ring in levoglucosan (2) has just been reported.[17]

The anhydride ring closure also forces some changes in the conformation angles of the pyranose ring. These angles vary in magnitude from 44.3 to 76.2° in sedoheptulosan, whereas, for example, they vary in α-D-glucose from 51.3 to 62.3° and in sucrose only from 54.8 to 56.0°. In sedoheptulosan the two angles of small magnitude, 44.3 and −44.8°, about bonds C(3)-C(4) and C(4)-C(5) reflect a flattening of the chair at C(4) from the configuration in an unbridged pyranose ring; and the two angles −76.2 and 76.0° reflect just the opposite effect at O(6).

The pattern of the bond lengths, the valence angles, and the conformation angles in the pyranose ring shows approximate mirror symmetry through a plane passing through O(6) and C(4). The small conformation angle for bond C(7)-O(2) in the five-membered ring shows that atoms C(2), O(2), C(7), and C(6) are nearly coplanar.

The apparent C–H bond lengths vary from 0.94 to 1.03 Å, and the apparent OH bond lengths of the sugar hydroxyl groups vary from 0.74 to 0.86 Å. The apparent O–H distances in the water molecule are 0.69 and 0.84 Å. Such short lengths are characteristically found in x-ray analyses for chemical bonds involving hydrogen atoms, presumably because the centroid of the electron distribution in the hydrogen atom is shifted by the bonding away from the hydrogen nucleus. However, the orientations of these bonds are determined well enough, for example, to identify unambiguously the pattern of hydrogen bonding.

A complex system of hydrogen bonds ties the sugar and water molecules into the crystal structure. Each of the four OH groups of the sugar molecule functions as donor and acceptor in hydrogen bonding; O(6) is an acceptor, but O(2) is not. The water molecules, H(a)-O(w)-H(b), are joined by bonds O(w)-H(a). . .O(w) into a helix centered on the axis 4_3 located at $\frac{1}{2}, \frac{1}{2}, z$; peripheral bonds O(w)-H(b). . . O(1) connect the helix to adjacent sugar molecules. Bonds O(1)-H. . .O(4) and O(3)-H. . .O(3) connect the molecules of the sugar helix centered on the axis 4_3 at 0,0,z. Bonds O(4)-H. . .O(5) and O(5)-H. . .O(6) connect the molecules of the sugar helix centered on the axis 2_1 at $\frac{1}{2}$,0,z. The length and angle parameters of these hydrogen bonds are given in Table 9.9. A stereoscopic view of the crystal structure is shown in Fig. 9.14.

Table 9.8. Valence Angles and Ring Conformation Angles (deg) in the Sedoheptulosan Molecule

Valence Angles			
O(6)-C(2)-C(3)	108.1	C(1)-C(2)-O(6)	108.3
C(2)-C(3)-C(4)	109.4	C(1)-C(2)-C(3)	112.7
C(3)-C(4)-C(5)	112.0	O(1)-C(1)-C(2)	111.3
C(4)-C(5)-C(6)	109.7	O(2)-C(2)-C(3)	111.0
C(5)-C(6)-O(6)	107.9	C(7)-C(6)-C(5)	113.4
C(6)-O(6)-C(2)	102.8	O(3)-C(3)-C(2)	111.4
O(6)-C(6)-C(7)	101.4	O(3)-C(3)-C(4)	107.9
C(6)-C(7)-O(2)	103.8	O(4)-C(4)-C(3)	108.5
C(7)-O(2)-C(2)	107.2	O(4)-C(4)-C(5)	109.7
O(2)-C(2)-O(6)	104.8	O(5)-C(5)-C(4)	110.8
C(1)-C(2)-O(2)	111.5	O(5)-C(5)-C(6)	107.0
Ring Conformation Angles			
O(6)-C(2)-C(3)-C(4)	−60.6	O(2)-C(2)-O(6)-C(6)	−42.5
C(2)-C(3)-C(4)-C(5)	44.3	C(2)-O(6)-C(6)-C(7)	43.2
C(3)-C(4)-C(5)-C(6)	−44.8	O(6)-C(6)-C(7)-O(2)	−28.5
C(4)-C(5)-C(6)-O(6)	60.7	C(6)-C(7)-O(2)-C(2)	3.3
C(5)-C(6)-O(6)-C(2)	−76.2	C(7)-O(2)-C(2)-O(6)	23.6
C(6)-O(6)-C(2)-C(3)	76.0	C(4)-C(3)-C(2)-O(2)	53.8
		C(4)-C(5)-C(6)-C(7)	−50.8

Table 9.9. Length and Angle Parameters of the Hydrogen Bonds in Sedoheptulosan Monohydrate

Hydrogen Bond	Distances (Å)			Angle (deg)
	O–O	O–H	H. . .O	
O(1)-H. . .O(4)	2.65	0.86	1.80	168
O(3)-H. . .O(3)	2.78	0.84	1.95	173
O(4)-H. . .O(5)	2.70	0.81	1.90	174
O(5)-H. . .O(6)	2.76	0.74	2.05	163
O(w)-H(a). . .O(w)	2.84	0.69	2.15	171
O(w)-H(b). . .O(1)	2.88	0.83	2.10	158

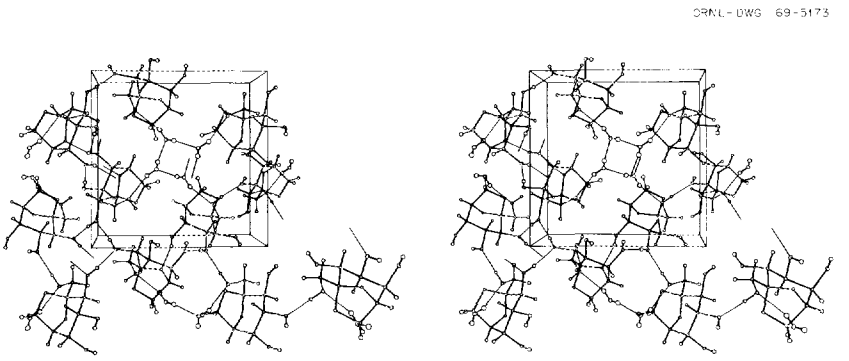

Fig. 9.14. Stereoscopic View of the Crystal Structure of Sedoheptulosan Monohydrate. The view direction is that of −c. The outline of one unit cell is shown.

[1]Collection of data for this structure determination was briefly noted in *Chem. Div. Ann. Progr. Rept. May 20, 1966,* ORNL-3994, p. 125. A preliminary report of this work was published in the *Abstracts of the Eighth International Congress of Crystallography, Buffalo and Stony Brook, New York, August 1969.* See *Acta Cryst.* **A25**(S3), S195 (1969).

[2]National Institutes of Health Special Postdoctoral Fellow.

[3]C. S. Hudson, *J. Am. Chem. Soc.* **60**, 1241 (1938).

[4]J. W. Pratt, N. K. Richtmyer, and C. S. Hudson, *J. Am. Chem. Soc.* **74**, 2200 (1952).

[5]W. R. Busing *et al., The Oak Ridge Computer-Controlled X-Ray Diffractometer,* ORNL-4143 (January 1968).

[6]W. R. Busing and H. A. Levy, *Acta Cryst.* **10**, 180 (1957).

[7]D. J. Wehe, W. R. Busing, and H. A. Levy, *A Fortran Program for Calculating Single-Crystal Absorption Corrections,* ORNL-TM-229 (1962).

[8]H. Hauptman and J. Karle, "Solution of the Phase Problem. I. The Centrosymmetric Crystal," *Amer. Cryst. Assoc. Monograph No. 3,* 1953.

[9]J. Karle and I. L. Karle, *Acta Cryst.* **21**, 849 (1966).

[10]J. Karle and H. Hauptman, *Acta Cryst.* **9**, 635 (1956).

[11]Program written by Michael Drew, Lawrence Radiation Laboratory, University of California, Berkeley.

[12]For definitions see the preceding report.

[13]A correction procedure based on the theory of W. H. Zachariasen, *Acta Cryst.* **23**, 558 (1967), has been inserted in our least-squares program ORFLS by A. Vos and C. K. Johnson.

[14]W. Klyne and V. Prelog, *Experientia* **16**, 521 (1960).

[15]G. M. Brown and H. A. Levy, *Science* **147**, 1038 (1965).

[16]G. M. Brown and H. A. Levy, *Science* **141**, 921 (1963).

[17]Y. J. Park, H. S. Kim, and G. A. Jeffrey, *Acta Cryst.* **A25**(S3), S197 (1969).

DIFFRACTION PATTERN AND STRUCTURE OF AQUEOUS AMMONIUM HALIDE SOLUTIONS

A. H. Narten

Among monovalent cations, the ammonium ion is unique in its similarity to water: ammonium ions and water molecules have very similar masses and sizes; because of the strong polarity of the O–H bond in water, the forces exerted on their nearest neighbors by a neutral water molecule and by a charged ammonium ion in aqueous solution are probably similar; and, finally, both H_2O and NH_4^+ form hydrogen bonds of about the same strength. Thus aqueous ammonium halide solutions may be considered to a good approximation as solutions of halide ions in water, and the effect of the salts on "water structure" may be regarded as arising primarily from the anions alone.

The scattering of x rays from aqueous ammonium chloride, bromide, and iodide solutions ($NH_4X \cdot \sim 8H_2O$) has been measured[1] at 25°C and analyzed. In Fig. 9.15 radial distribution functions (RDF) for the three solutions are compared with previously obtained results for ammonium fluoride solutions[2] ($NH_4F \cdot 3.57H_2O$ and $NH_4F \cdot 45.8H_2O$) and for pure water[3] at the same temperature. The curves for the ammonium fluoride solutions are very similar to the RDF of pure water, and the significance of small differences has been discussed elsewhere.[2] The maxi-

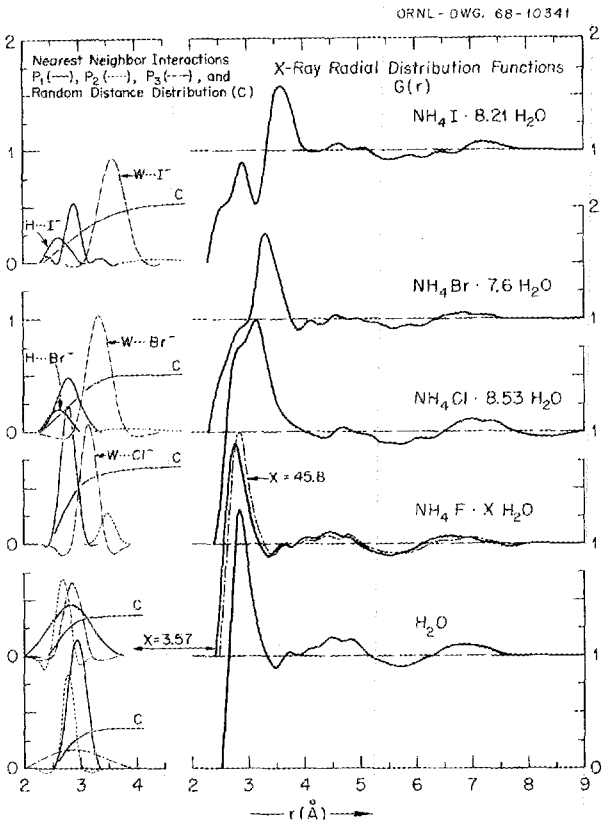

Fig. 9.15. Experimental Radial Distribution Functions of Water and Aqueous Ammonium Halide Solutions. Resolution of near-neighbor interactions based on ice I model (see Fig. 9.17).

mum at 2.85 Å in the water curve corresponds to ~4.4 interactions between oxygen atoms.[4] A corresponding water-water[5] interaction is visible as a shoulder in the chloride and bromide solutions and as a partially resolved maximum at 2.91 Å in the ammonium iodide solution. The halide-water interaction occurs at 3.2 Å for the chloride, 3.3 Å for the bromide, and 3.6 Å for the iodide solution. The expected distances, based on crystal radii,[6] are 3.19, 3.33, and 3.54 Å respectively. A distinct shoulder on the short-distance side of the water-water peak in the NH_4I solution (less pronounced in the NH_4Br solution and not visible in NH_4Cl and NH_4F) must be ascribed to interactions between hydrogen atoms and halide ions. In the iodide solution, this shoulder occurs near 2.6 Å; since this distance is very nearly equal to the difference between the W...I^- (3.6 Å) and the intramolecular W-H (~1 Å) distance, the conclusion is that some water molecules (or ammonium ions) have average orientations such that one W-H...I^- angle is close to 180°.

We can understand the changes in the radial distribution functions of Fig. 9.15 only if we make more detailed assumptions about the average arrangement of water molecules in the solutions. The proposed ice I model for water[4] provides this detailed description for the studied ammonium halide solutions, and intensity functions calculated for this model are in excellent agreement with the x-ray data (Fig. 9.16). The liquid phase is regarded as an extensive hydrogen-bonded network of water molecules (and ammonium ions), the details of which are short lived. Over short distances from any starting point, this network is closely related to a slightly expanded ice I lattice, each network molecule being tetrahedrally surrounded by four others. Three of these network neighbors occur at a distance P_1 and the fourth at a distance P_2 (in the solid $P_1 \cong P_2$). The average structure of this network is very open, with spaces between the groups of molecules in tetrahedral coordination sufficiently large to accommodate additional molecules at a distance P_3 from the nearest network molecule (these cavities are not occupied in solid ice I). In pure water,[4] about half the cavities are occupied by "interstitial" molecules which interact with the network by less specific, but by no means negligible, forces.

While the fluoride (and ammonium) ions are visualized as occupying both network and cavity positions, the chloride, bromide, and iodide ions are assumed to occupy cavity positions only. Some relevant parameters of the ice I model for water and the ammonium halide solutions are summarized in Table 9.10. Whereas the P_1 distance between network molecules remains nearly constant, the P_2 distance increases drastically from pure water to the iodide solution. The mean-square variation in the P_2 interaction shows a corresponding increase, indicating that there is a wide distribution of instantaneous P_2 distances about the mean value. This may be taken as an indication that the icelike network is severely distorted from the average, so that the cavities occupied by water molecules are smaller than those containing a halide ion.

While in pure water about 50% of the cavities are not occupied, this fraction decreases with ionic size until all cavities are occupied by water molecules or ions in the case of the iodide solution. At the same time, the interactions between cavity water molecules and the network, as well as between cavity water molecules and the chloride, bromide, or iodide ions, become so diffuse that they give rise to uniform distance distributions.

In terms of the ice I model the influence of halide ions on water structure can be summarized as follows: In order to accommodate the relatively large chloride,

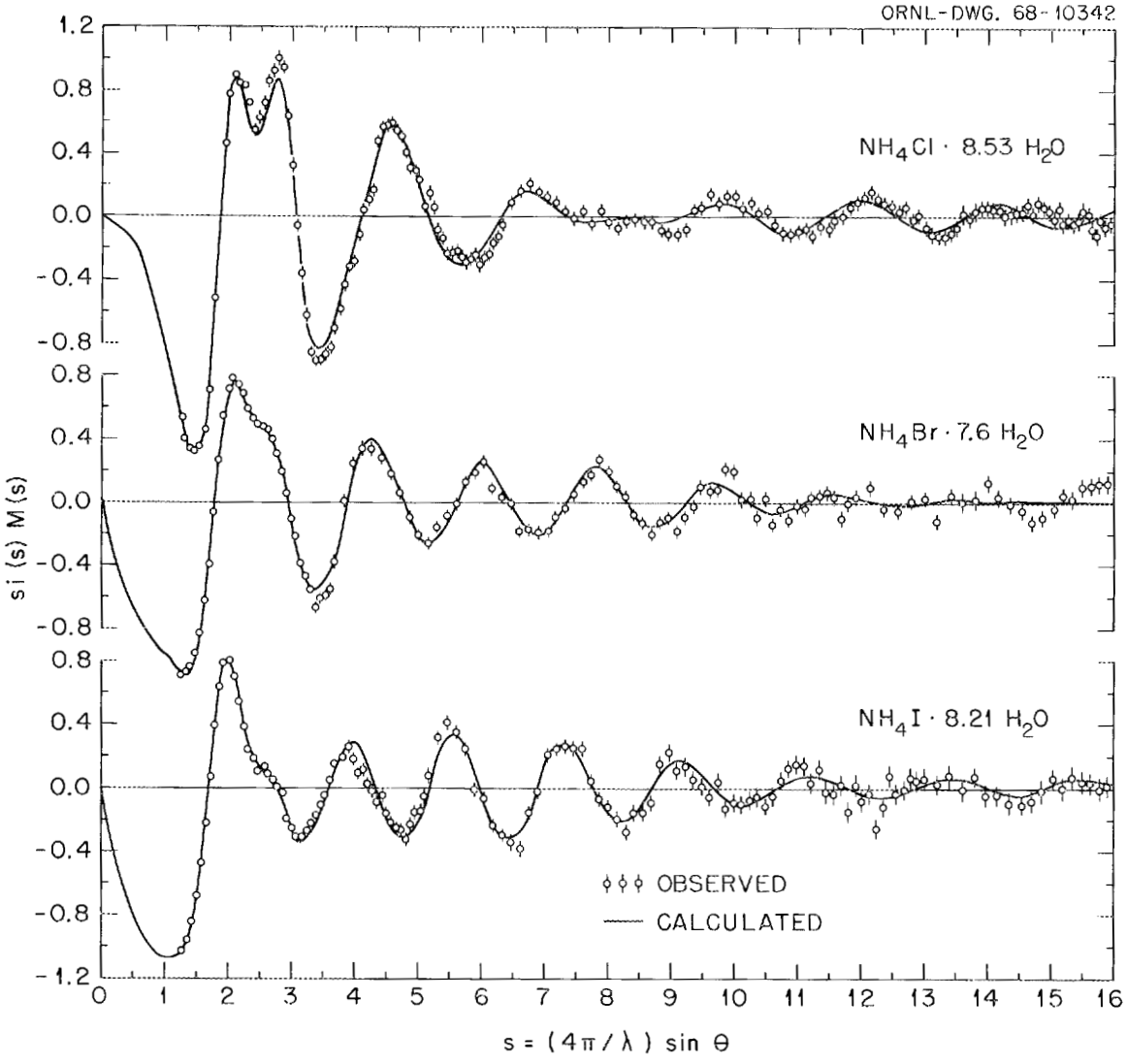

Fig. 9.16. Reduced Intensity Functions of Aqueous Ammonium Halide Solutions. Calculated curves based on ice I model.

Table 9.10. Some Relevant Parameters for the Ice I Model of Water and Aqueous Ammonium Halide Solutions

P_1, P_2, and P_3 are independently variable near-neighbor distances (see Fig. 9.17) characterized by an average distance r (Å) and an associated rms displacement $\langle \Delta r^2 \rangle^{1/2}$ (Å)

	H_2O		$NH_4F \cdot 3.57H_2O$		$NH_4Cl \cdot 8.53H_2O$		$NH_4Br \cdot 7.6H_2O$		$NH_4I \cdot 8.21H_2O$	
	r	$\langle \Delta r^2 \rangle^{1/2}$	r	$\langle \Delta r^2 \rangle^{1/2}$	r	$\langle \Delta r^2 \rangle^{1/2}$	r	$\langle \Delta r^2 \rangle^{1/2}$	r	$\langle \Delta r^2 \rangle^{1/2}$
P_1	2.94 ± 0.01	0.18 ± 0.01	2.88 ± 0.01	0.38 ± 0.01	2.80 ± 0.01	0.14 ± 0.01	2.82 ± 0.02	0.19 ± 0.02	2.91 ± 0.01	0.08 ± 0.01
P_2	2.78 ± 0.01	0.08 ± 0.01	2.69 ± 0.01	0.10 ± 0.01	3.50 ± 0.02	0.13 ± 0.02	4.11 ± 0.04	0.49 ± 0.07	4.70 ± 0.04	0.63 ± 0.08
P_3	2.96 ± 0.01	0.53 ± 0.04	2.87 ± 0.01	0.17 ± 0.01	3.17 ± 0.02	0.17 ± 0.01	3.36 ± 0.04	0.22 ± 0.01	3.61 ± 0.04	0.24 ± 0.01
Fraction of water molecules in network positions	0.80 ± 0.01		0.78 ± 0.01		0.85 ± 0.02		0.77 ± 0.02		0.66 ± 0.02	
Fraction of empty cavities	0.50 ± 0.02		0.45 ± 0.02		0.39 ± 0.03		0.07 ± 0.04		0	

ORNL-DWG. 68-10340

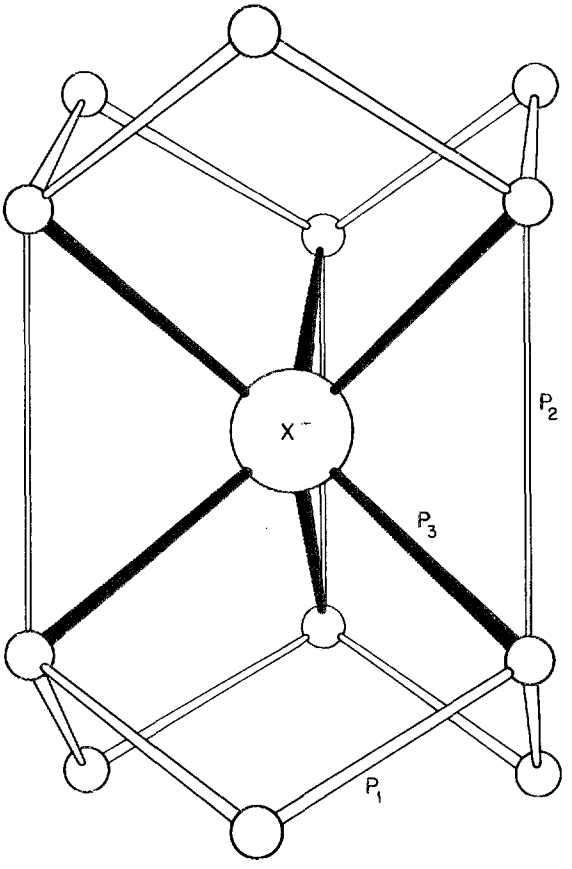

Fig. 9.17. Proposed Average Configuration of Water Molecules and Ammonium Ions Around a Cl^-, Br^-, and I^- Ion. P_1, P_2, and P_3 are the independently variable near-neighbor distances of the ice I model (Table 9.10). In the bromide and iodide solutions, the six water molecules (ammonium ions) are oriented in such a way that one hydrogen atom points in the P_3 direction.

bromide, and iodide ions, the hydrogen-bonded network of water molecules expands anisotropically; in this way, each water molecule in the network retains three nearest water neighbors within hydrogen-bond distance, while the bond corresponding to the P_2 distance is broken (Fig. 9.17). At the same time, the fraction of water molecules in cavity positions increases significantly from chloride to iodide, that is, the degree of randomness of the systems increases.

[1] A. H. Narten, *X-Ray Diffraction Data on Aqueous Ammonium Halide Solutions at 25°C*, ORNL-4367 (1969).

[2] M. D. Danford, *Diffraction Pattern and Structure of Aqueous Ammonium Fluoride Solutions*, ORNL-4244 (1968).

[3] A. H. Narten, M. D. Danford, and H. A. Levy, *X-Ray Diffraction Data on Liquid Water in the Temperature Range 4–200°C*, ORNL-3997 (1966).

[4] A. H. Narten, M. D. Danford, and H. A. Levy, *Discussions Faraday Soc.* **43**, 97 (1967).

[5] The term "water" (W) will subsequently be used for interactions involving oxygen atoms from water molecules and nitrogen atoms from ammonium ions (indistinguishable in this treatment).

[6] L. Pauling, *The Nature of the Chemical Bond*, Cornell University Press, Ithaca, N.Y., 1946.

OBSERVED DIFFRACTION PATTERN AND PROPOSED MODELS OF LIQUID WATER

A. H. Narten H. A. Levy

For heteroatomic liquids such as water the analysis of x-ray scattering data yields reduced intensity and radial distribution functions which contain information about average atomic and molecular configurations. This information cannot be deduced uniquely from the diffraction data. However, assumptions about the average arrangement of molecules with respect to each other may be made, and such a model of liquid structure can be tested against the observations. In order to test the validity of proposed water models with x-ray data, much detail is needed which is usually left unspecified; that is, most proposed water models cannot be tested with diffraction data because they are not sufficiently defined at the molecular level. Of the structures which have a sufficiently detailed basis to permit calculation of radial distribution functions, only the ice I model (Samoilov,[1] Danford and Levy[2]) has been shown to give agreement with both large- and small-angle x-ray scattering data. In the few other cases[3–8] in which radial distribution functions have been calculated, the apparent agreement with experimental curves for water is meaningless, since the computer curves do not describe radial distribution in the respective models correctly.

A comprehensive discussion of the subject will appear in *Science*.

[1] O. Y. Samoilov, *Zh. Fiz. Chim.* **20**, 12 (1946).

[2] M. D. Danford and H. A. Levy, *J. Am. Chem. Soc.* **84**, 3965 (1962).

[3] J. A. Pople, *Proc. Roy. Soc. (London)* **A205**, 163 (1964).

[4] G. Nemethy and H. A. Scheraga, *J. Chem. Phys.* **36**, 3382 (1962); **41**, 680 (1964).

[5] L. Pauling, in *Hydrogen Bonding*, D. Hadzi, ed., p. 1, Pergamon, New York, 1959.

[6] J. D. Bernal and R. H. Fowler, *J. Chem. Phys.* **1**, 515 (1933).

[7]C. M. Davis, Jr., and T. A. Litowitz, *J. Chem. Phys.* **42**, 2563 (1965).

[8]B. Kamb, in *Structural Chemistry and Molecular Biology*, A. Rich and N. Davidson, eds., p. 507, W. H. Freeman Co., San Francisco, Calif., 1968.

MOLECULAR BEAM STUDIES

INELASTIC SCATTERING OF ALKALI ATOMS AND IONS FROM HYDROGEN MOLECULES

Peter F. Dittner Sheldon Datz

Inelastic energy losses arising from knock-on collisions of both alkali ions and atoms with H_2 and D_2 molecules have been determined by time-of-flight measurements[1,2] of the projectile (K^+, K, Na^+, Na) velocity following collision with a target molecule (H_2, D_2, ^{4}He, ^{3}He). The apparatus is pictured in Fig. 9.18. The alkali atoms are ionized on an indirectly heated tungsten surface and subsequently accelerated and pulsed on for intervals ranging from 0.5 to 1.5 μsec. The pulsed ion beam is bent and passed through a chamber which can serve as an alkali oven for resonant charge exchange to produce a fast neutral beam. Following its path through the liquid-nitrogen-cooled scattering chamber and a flight tube, the ion impinges on an electron multiplier which initiates a "start" pulse in a time-to-pulse-height converter (TPHC). When the projectiles are fast neutrals, they are first surface ionized on a heated tungsten ribbon ($T \approx 500°C$) prior to entering the electron multiplier. The "stop" pulse is obtained from a delay generator triggered by the beam pulser. The output from the TPHC is fed into a multichannel analyzer yielding an intensity vs time display. Beam currents are adjusted so that less than one particle per pulse is measured at the detector (else only the fastest particle's time of flight is determined). For the experiments reported here, the detector aperture was directly in line with the primary beam, so that projectiles which were unscattered, forward scattered through center-of-mass (c.m.) angles between 0 and 10°, and back scattered through c.m. angles between 170 and 180° were detected.

With He as the scattering gas, only elastic scattering was observed; a typical spectrum is shown in Fig. 9.19. The time separation between the forward and backward peak is used as a calibration of the distance between scattering center and detector. Calibrations were done with ^{4}He in the relative energy range 9 to 28 eV and with ^{3}He from 7 to 42 eV. The spectra obtained with He can also be used to obtain model peaks for stripping the data obtained with D_2 and H_2. With projectiles of either Na or K, the back-scattered peaks remained relatively narrow, but a shift in peak position occurred corresponding to inelastic loss which increased with increasing relative energy. In Fig. 9.20 the relative energy E_r is plotted vs the energy expected following an elastic collision E_{el} minus the observed energy E_o. When this energy difference ΔE is less than the dissociation limit of hydrogen, translational energy has been transferred to vibrational excitation of the molecule. (The degree of rotational excitation is small at the small impact parameters required for backward scattering.) When ΔE is greater than the dissociation limit, excess energy ($\Delta E - D_0^0$) can also be carried off as translational energy by the two constituent atoms. For K^+ and K^0 on D_2 (Fig. 9.20*b*), the inelastic losses below $E_r = 22$ eV are not markedly different and give a value $\Delta E/E_r$ of ~0.2. Above 22 eV the predominant process is dissociation, and double peaks, tentatively ascribed[1] to electronic excitation of D atoms, are observed. Also sketched in Fig. 9.20*b* is the result of the exact classical calculation of Kelley and Wolfsberg[3] for a linear head-on collision of a mass 42 atom with a diatomic molecule (mass 2-2). (The force constant κ used was 10.6 millidynes/Å as compared with the harmonic constant for H_2 of 4.5 millidynes/Å.) In the case of Na^+ and Na^0 on H_2 (Fig. 9.20*a*), there is significantly more efficient energy transfer; that is, only 15 eV is required to dissociate the molecule.

For a given mass ratio, the energy transfer efficiency ($\Delta E/E_r$) in the exact classical calculation[4] depends only on the ratio E_r/L^2, where L is the potential parameter in the exponential potential $V(r) = A \exp(-r/L)$. The

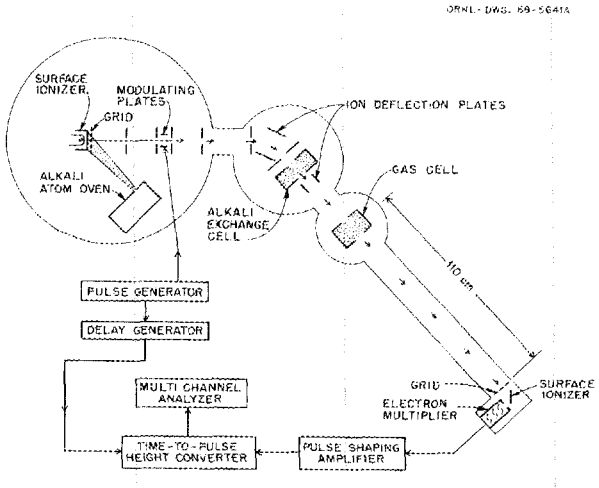

Fig. 9.18. Schematic of Time-of-Flight Apparatus.

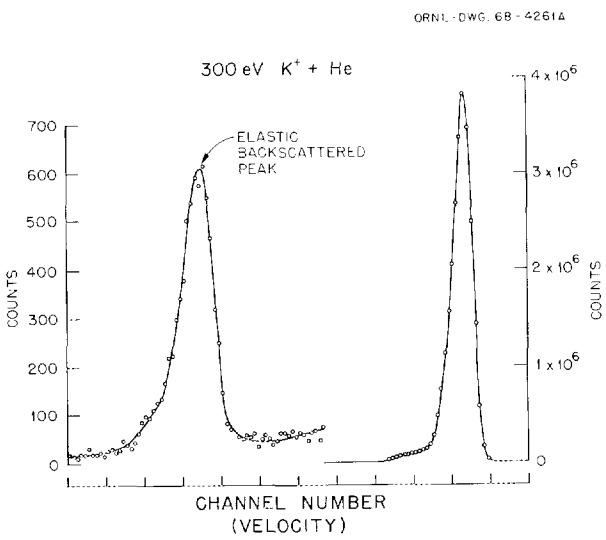

Fig. 9.19. Time Spectrum of K^+ Backscattered from ^4He at a Relative Energy of 28 eV (300 eV Laboratory System). The forward (unscattered) peak, shown at the right, is separated from the backward peak by 6.3 μsec (each point is 0.1 μsec).

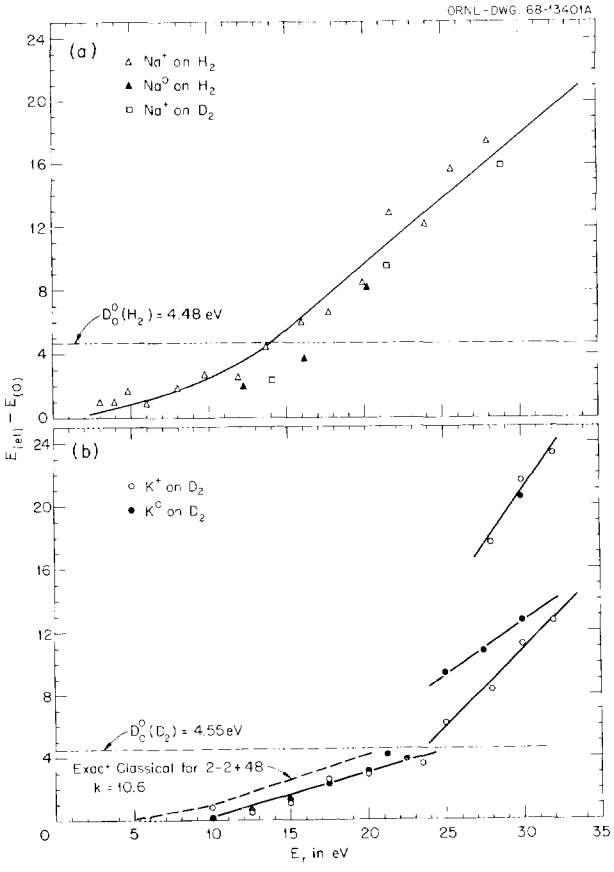

Fig. 9.20. Inelastic Energy Losses for (*a*) K^+ and K^0 on D_2 and (*b*) Na^+ and Na^0 on H_2 and D_2.

mass ratios for the K-D_2 and Na-H_2 systems are almost identical. The differences in behavior should therefore be attributable to differences in the potential parameter. From the data, an approximate L value for the Na^+-H_2 system of 0.21 Å and for K^+-D_2 of 0.39 Å is obtained, in qualitative accord with theoretical expectations.[5] The similarity between the atomic and ionic behavior is not understood, and studies on the Cs^+ and Cs^0 collisions with D_2 are under way.

---

[1] P. F. Dittner and S. Datz, *J. Chem. Phys.* 49, 1969 (1968).

[2] J. Schöttler and J. P. Toennies, *Z. Physik* **214**, 472 (1968).

[3] J. D. Kelley and M. Wolfsberg, *J. Chem. Phys.* 44, 324 (1966).

[4] D. Secrest, private communication.

[5] I. Amdur, private communication.

CROSSED-MOLECULAR-BEAM STUDIES OF BIMOLECULAR ASSOCIATION AND UNIMOLECULAR DECOMPOSITION REACTIONS

R. E. Minturn Sheldon Datz

Earlier attempts to observe, by crossed-molecular-beam methods, vibrationally excited product molecules in reactions of the type

$$R\text{–}NH_2 + BF_3 \rightarrow [R\text{–}NH_2\text{–}BF_3]^* ,$$

where R is an organic radical and the asterisk indicates vibrational excitation, were unsuccessful,[1] but the data did indicate that considerable unreactive scattering of the BF_3 into large angles had occurred. We have now investigated this scattering of BF_3 by ammonia, by methyl- and ethylamine, and by propane.

In the course of these experiments, considerable improvement in the equipment and in the experimental techniques was made. Chief among these was the design and development of a very accurate gating and pulse-counting system, which has reduced the errors in extracting the desired signal from noise levels two or three orders of magnitude higher to essentially those expected from statistical deviations only. One essential component of this system, a delayed steering gate, was designed by J. R. Tarrant of the Chemistry Division. The statistical errors have themselves been minimized by lowering the temperature of the liquid-nitrogen traps which capture ambient gases in the scattering center. This is done by reducing the pressure over the liquid nitrogen by continuous pumping and reduces the background counts by a factor of 10 or more.

The data on the four systems studied to date are shown graphically in the four panels of Fig. 9.21. In panel A, ammonia is the scattering gas and the intensity of BF_3, relative to its intensity at 40°, is plotted against the laboratory scattering angle, measured from the BF_3 beam. Panels B, C, and D of Fig. 9.21 are similar plots for the scattering gases methylamine, ethylamine, and propane, except that the curves are normalized with respect to the scattering of BF_3 by propane at 40° to reflect differences in absolute scattering intensities. The ammonia data were taken before several important improvements were made in equipment and technique; the error bars are correspondingly larger, and relative intensities cannot be extracted from the data. All error bars drawn in Fig. 9.21 are those corresponding to one standard statistical deviation.

Propane was chosen as an inert analog of similar mass to ethylamine, so that an elastically scattered BF_3 distribution was available for comparison. However, for elastic scattering, one would expect a smoothly decreasing intensity as one moves to larger scattering angles, much as exhibited by the methylamine curve, and not a curve with the inflection that apparently exists in the propane curve. The larger error bars for propane than for the two amines reflect the greater difficulty in cryogenically pumping propane with liquid nitrogen. The greater resulting ambient pressure causes appreciably higher background counts and correspondingly higher statistical deviations.

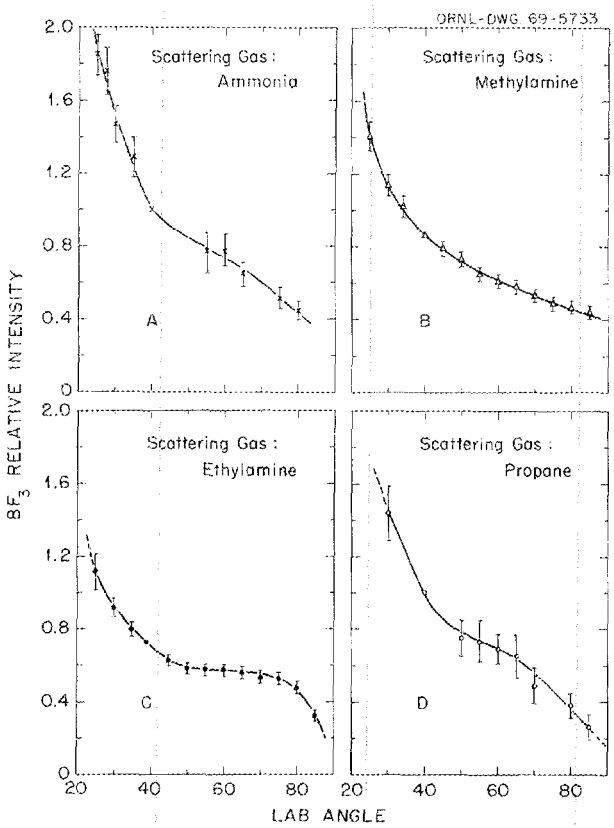

Fig. 9.21. Differential Scattering of BF_3. Plots of the relative intensity of BF_3 scattered into various angles by the scattering gases: *A*, ammonia; *B*, methylamine; *C*, ethylamine; and *D*, propane. Plot *A* is normalized to the intensity of BF_3 scattered into 40° by ammonia; plots *C* and *D* are normalized to the intensity of BF_3 scattered into 40° by propane.

The curve for ethylamine gives strong evidence for the existence of an activated reaction complex which lasts for several rotations following the collision before it again breaks up into the original reactants. A kinematic analysis of the mechanics for such "sticky collisions"[2] postulates that the intensity of the scattered BF_3 will peak at $\chi = 0$ and 180°, where χ is the scattering angle in the center-of-mass system. An accurate transformation of such a distribution into the laboratory system involves an integration over the beam velocity distributions as well as a consideration of the energy transfer that occurs because of the collision. However, if we assume that the initial and final relative translational energies are the same, we may calculate the laboratory angles corresponding to $\chi = 0$ and 180°. For ethylamine, they are 0 and 78° respectively. Figure 9.21*C*, for ethylamine, does indeed show a distinct peaking in the region of 78°. The expected peaking at 0° is obscured by the high intensity of the elastically scattered BF_3 in this region.

If a long-lived complex of methylamine and BF_3 is formed, a peak should occur at a laboratory angle of about 68°. The absence of any appreciable peak in this region may mean that the complex dissociates almost immediately into the original reactants, and the scattering appears essentially elastic. For ammonia, some perturbation of the curve occurs at large angles, although it cannot be directly correlated with a sticky collision peak, which should occur around 53°. The propane curve looks qualitatively very similar to the ammonia curve for reasons as yet unexplained.

To aid in the analysis of the data given above, experiments with heavier amines are currently being carried out. As the amine molecule increases in size, the probable lifetime of the collision complex also increases, and a knowledge of the effect that longer lifetimes have on the scattering distributions should be very helpful in the understanding of these complicated but interesting systems.

---

[1] R. E. Minturn and S. Datz, *Chem. Div. Ann. Progr. Rept. May 20, 1968*, ORNL-4306, p. 170.

[2]See, for example, D. R. Herschbach, *Discussions Faraday Soc.* 33, 149 (1962); and D. O. Ham and J. L. Kinsey, *J. Chem. Phys.* 48, 939 (1968).

"HOT" ATOMIC HALOGEN BEAMS FROM SPUTTERING OF SILVER HALIDES

S. Datz G. Ostrom[1] F. Schmidt-Bleek[1]

In sputtering of metals by ion bombardment, it is generally found that atoms of the target material are ejected with an energy distribution extending from thermal energies up to 40 or 50 eV and peaking at 0.5 to 2.5 eV.[2-5] The same sputtering mechanisms should apply as well to nonmetallic targets, but low thermal conductivity can cause thermal-spike sputtering, and low electrical conductivity can cause defocusing of the bombarding ion beam due to buildup of electrical charge.

Recently, fast atomic beams of potassium were produced by sputtering methods in two laboratories.[4,5] From the viewpoint of chemical reaction kinetics (hot-atom chemistry), it would be particularly desirable to have available fast beams of species which have already been studied by means of nuclear recoil techniques,[6] primarily monovalent iodine, bromine, and hydrogen (tritium). To this end we have investigated the sputtering of silver halides (AgI and AgBr).

AgI targets were produced by reacting I_2 with a metallic silver slab. A layer of iodide was formed (~0.05 mm thick) in good thermal and electrical contact with the backing. Electron diffraction showed the layer to be AgI, and electron microscopy indicated well-developed crystalline orientation.

Figure 9.22 depicts the apparatus used in this study. The silver halide targets were bombarded with beams of argon ions ranging in energy from 0.5 to 7 keV. Elements of "source 2" can be used to (1) repel ions coming directly from the target, (2) ionize emitted neutral species with an intersecting electron beam, (3) repel ionized neutrals after they have been formed in the ion source, (4) apply acceleration voltage to ions, and finally (5) focus the ions into the attached 60° mass spectrometer. The mass spectrometer was set to a resolution $\Delta M/M = \Delta E/E$ of 1 in 500. The translational energy of the sputtered particles was measured in two ways. First, the ionized beam was swept through a slowly decreasing acceleration voltage, at fixed magnetic field, for several mass units at a time. At 1 keV the energy resolution was 2 eV, and a detailed trace of the peaks showed high kinetic energy contributions (see Fig. 9.23, dashed lines). The second method utilized the repeller plate in source 2 to suppress ionized particles of low kinetic energy, thereby permitting the study of the transmitted beam as a function of the barrier potential. The solid lines in Fig. 9.23 represent acceleration voltage sweeps with stepwise increased repeller potentials. The virtual disappearance of masses 108, 110, 128, and 129 after the application of only 2 V barrier potential illustrates the effect of the repeller on peaks due to background gas in source 2. The spectrum taken in the AgI region contains the "cleanest" sputtering results, since there is no interfering background in this mass region.

The particles of greatest interest in the present study were halogen atoms. For iodine, inspection of the mass 127 peak in Fig. 9.23 shows not only a very large thermal energy contribution but, clearly, also a high-energy tail. The total 127 peak contains, in addition to the iodine atoms ejected directly from the target, a background due to ambient impurities at 127 as well as contributions from dissociative ionization of HI and I_2. Contributions from dissociative ionization of AgI are small, because the total AgI peak is only 10% of the corrected I atom peak. I_2 and HI are found to be produced in large quantities during the sputtering process; however, their energy distribution is almost completely thermal. These species are probably formed by secondary reactions of the sputtered atomic iodine with iodine atoms and water molecules adsorbed on the walls of the sputtering chamber. They are permanent gases and remain in the ion source region. The high-energy component in the composite mass 127 must originate from sputtered atomic iodine. In order to assess the "pure" sputtered mass 127 peak, we assumed the I energy distribution to be identical with the AgI distribution and underlaid the AgI and I peaks on a semilog plot. Subtracting the sputtered contribution in mass 127 on this basis yielded two results: (1)

ORNL-DWG. 69-3608A

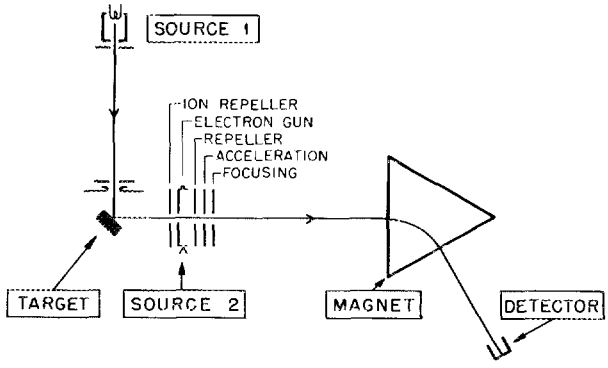

Fig. 9.22. Schematic of Ion Bombardment Source and Mass Spectrometer.

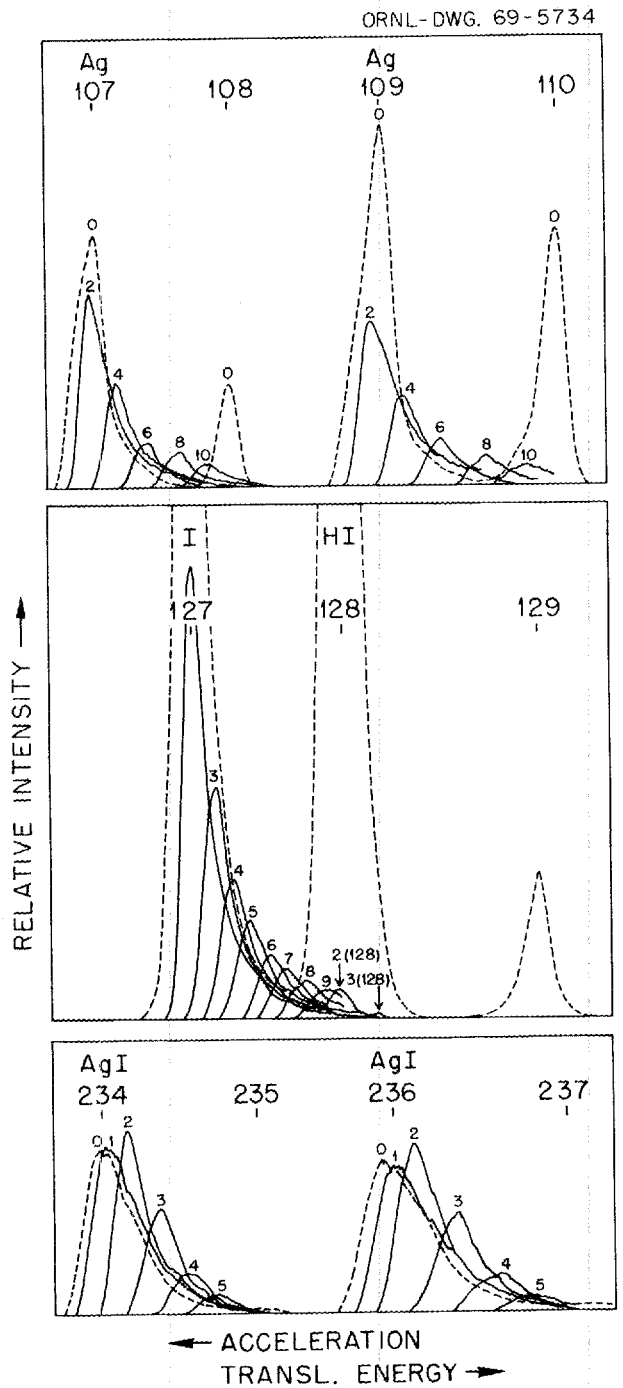

Fig. 9.23. Mass Spectra Obtained by Sweeping Acceleration Voltage at Fixed Magnetic Field. Electron bombardment ionization gives the number density distribution; $E^{-1/2}$ correction must be applied for flux distribution comparison with refs. 3 and 4.

the residual peak at mass 127 has a purely thermal shape, and (2) the net atomic yield of sputtered iodine is, within experimental error, identical to the sputtered atomic silver yield.

The energy distributions of sputtered I, Ag, and AgI resemble closely those observed for sputtered potassium.[4,5] For iodine atoms the sputtering yield is ~1 for bombardment with 3-keV argon ions, the neutral/ion ratio was estimated to be $>10^5$, and at a kinetic energy of 10 eV, >10% of the maximum intensity was observed. Results obtained with AgBr target were very similar to those described for AgI targets. Mechanical velocity selection is necessary with any sputtered beam source and in this case will eliminate interference from HI and I_2. Some fast Ag and AgI will accompany a fast velocity-selected I atom beam, but these can be discriminated by the detector.

---

[1] Department of Chemistry, Purdue University, Lafayette, Ind.

[2] R. V. Stuart and G. K. Wehner, *J. Appl. Phys.* **35**, 1819 (1964).

[3] M. W. Thompson, *Phil. Mag.* **18**, 377 (1968).

[4] J. Politick *et al.*, *Rev. Sci. Instr.* **39**, 1147 (1968).

[5] E. Hulpke, Ph.D. thesis, University of Freiburg, 1967.

[6] F. Schmidt-Bleek and F. S. Rowland, *Angew. Chem. Intern. Ed. Engl.* **3**, 769 (1964).

CROSSED-MOLECULAR-BEAM STUDIES OF REACTIONS OF ATOMIC DEUTERIUM WITH HALOGEN MOLECULES

George E. Moore Sheldon Datz
Robert M. Statnick[1]

Further modifications in the highly flexible general-purpose crossed-molecular-beam apparatus have been undertaken to improve the precision with which reactions of H atoms with halogen-containing molecules can be studied.

Detection of neutral product molecules resulting from reactive collisions of two intersecting molecular beams is carried out by ionizing the beam by electron bombardment, mass filtering the ions thus produced, and measuring the ion current by means of an electron multiplier. The previously described[2] modifications in the detection system (improved ion source and quadrupole mass filter and ultrahigh vacuum detection chamber) did indeed improve the sensitivity of signal detection.

However, the need for further improvements in the system became evident in the attempted study of the

crossed-beam reaction of D atoms with CH_3I, which was substituted for the Br_2 and F_2 previously used in order to avoid the complications of corrosive action. In all these systems, in order to discriminate the extremely small signals produced from the product molecules against the background, differential pulse counting had been employed.[3,4] However, mechanical chopping was found to be too imprecise for the very low signal levels in the present system. Anode pulses from the electron multiplier are fed into a fast-pulse linear amplifier whose output is now being fed into a precision gating circuit which utilizes a time base generator accurate to several parts per million to control the length of time a scaler will accept a given burst and which incorporates a delay circuit to eliminate undesirable end effects of the burst.

An additional problem in pulse counting is that a very small radio-frequency pickup (~0.4 mV) on the signal saturates the linear amplifier at a PHS level normally used to discriminate against electronic noise. Raising the PHS level to discriminate against the rf also discriminates against a substantial fraction of real signal pulses. Elimination of this problem by more efficient rf shielding and by electronic means is being investigated.

Of course, increases in flux of the colliding beams should lead to increased production of product molecules. Attempts to enhance the intensity of the crossed beam by use of Laval slits[5] and of the main-beam D atoms by electron-bombardment heating of a tungsten tube[6] for thermal dissociation of D_2 have met with some success.

[1] U.S. Atomic Energy Commission Postdoctoral Fellow under appointment with Oak Ridge Associated Universities.

[2] G. E. Moore and S. Datz, *Chem. Div. Ann. Progr. Rept. May 20, 1968*, ORNL-4306, p. 170.

[3] T. W. Schmidt, "A Study of the Reaction Between Deuterium Atoms and Bromine Molecules Using Crossed Molecular Beams," Ph.D. dissertation, University of Tennessee, Knoxville, March 1967.

[4] S. Datz and T. W. Schmidt, *Fifth Intern. Conf. Phys. Electronic and Atomic Collisions, Leningrad, U.S.S.R., July 17–23, 1967*, p. 247, "Nauka" Publishing House.

[5] M. C. Moulton and D. R. Herschbach, *J. Chem. Phys.* **44**, 3010 (1966).

[6] P. Kusch and V. W. Hughes, "Atomic and Molecular Beam Spectroscopy," p. 11 in *Atoms III – Molecules I*, vol. 37, Part 1 of *Handbuch der Physik*, S. Flügge, ed., Springer-Verlag, Berlin, 1959; also J. W. Heberle, H. A. Reich, and P. Kusch, *Phys. Rev.* **101**, 612 (1956).

MASS SPECTROMETRY AND RELATED TECHNIQUES

PRELIMINARY MASS SPECTRAL STUDIES OF SILANE

Russell Baldock Jay W. Pinson[1]
P. S. Rudolph Louie Idom

Prelusive to studying the radiolysis of SiH_4 in the wide-range radiolysis source[2] attached to a research mass spectrometer, the cracking pattern of SiH_4 in a conventional ionization source was determined at several electron energies. The results shown in Table 9.11 indicate that the ratios of the fragment ions change with the energy of the ionizing electrons. Above 70 eV the ratios were found to be quite constant.

Pressure studies from 3×10^{-8} to 7×10^{-8} torr showed no effect on the mass spectrum of SiH_4.

Our results are compared with those of previous workers[3,4] in Table 9.11. Although our relative abundances generally differ considerably from those of Saalfeld and Svec,[3] we agree with them that SiH_4^+ is

Table 9.11. The Mass Spectrum of SiH_4

Relative abundances at several energies of the ionizing electrons

Ion	This Work			Previous Work	
	50 eV	60 eV	75 eV	60 eV, ref. 3	100 eV, ref. 4
Si^+	26.7 ± 0.8	28.0 ± 0.5	31.8 ± 0.5	20.7	15.1
SiH^+	31.8 ± 0.8	32.6 ± 0.5	36.0 ± 0.5	20.3	33.6
SiH_2^+	100	100	100	100	31.0
SiH_3^+	72.7 ± 1.4	71.2 ± 0.3	71.7 ± 0.7	78.1	100
SiH_4^+	$\ll 1$	$\ll 1$	$\ll 1$	$\ll 1$	77.5

very low in abundance or nonexistent. These workers claim that Neuert and Clasen[4] made a mass error which would explain the noted discrepancies.

The electronics of the mass spectrometer have been extensively overhauled, and the instrument has been completely realigned in preparation for a detailed investigation of the radiolysis of silane.

[1] Oak Ridge Associated Universities Research Participant from the University of Southern Mississippi, Hattiesburg, Miss., summer 1968.

[2] P. S. Rudolph, p. 101 in *Radiation Chemistry – II, Advan. Chem. Ser.* No. 82 (1968).

[3] S. E. Saalfeld and H. J. Svec, *Inorg. Chem.* **2**, 46 (1963).

[4] H. Neuert and H. Clasen, *Z. Naturforsch.* **7a**, 410 (1952).

Publications

NUCLEAR CHEMISTRY

N. K. Aras,[1] E. Eichler, G. Chilosi,[2] G. D. O'Kelley, and N. R. Johnson, "Decay of ^{88}Rb," *Nucl. Sci. Appl.* 3(2), 58 (1968).

L. L. Riedinger,[3,4] N. R. Johnson, and J. H. Hamilton,[5] "The β- and γ-Vibrational Bands of ^{152}Sm and ^{154}Gd," *Phys. Rev.* **179**, 1214 (1969).

N. K. Aras,[1] E. Eichler, and G. Chilosi,[2] "Decay of ^{94}Tc Isomers into the Levels of ^{94}Mo," *Nucl. Phys.* **A112**, 609 (1968).

E. Eichler, P. H. Stelson,[6] and J. K. Dickens,[7] "A New Measurement of the Half-Life of the ^{72}Ge 0+ State," *Nucl. Phys.* **A120**, 622 (1968).

E. L. Robinson,[8] R. C. Hagenauer,[3,9] and E. Eichler, "Decay of ^{89}Zr and ^{89m}Zr and Levels of ^{89}Y," *Nucl. Phys.* **A123**, 471 (1969).

G. Chilosi,[2] E. Eichler, and N. K. Aras,[1] "Decay of ^{95}Tc Isomers to Levels in ^{95}Mo," *Nucl. Phys.* **A123**, 327 (1969).

N. R. Johnson, L. L. Riedinger,[3,4] and J. H. Hamilton,[5] "Properties of β- and γ-Vibrational Bands in Deformed Nuclei," *Proceedings of Conference on the Electron Capture and Higher Order Processes in Nuclear Decays, Debrecen, Hungary, July 15, 1968.*

N. T. Porile,[10] I. Fujiwara,[10] and R. L. Hahn, "Angular Distributions of ^{64}Cu Nuclei from the ^{65}Cu(^{3}He,α)^{64}Cu Reaction," *Phys. Rev.* **170**, 958 (1968).

S. M. Brahmavar,[5] J. H. Hamilton,[5] A. V. Ramayya,[5] E. F. Zganjar,[11] and C. E. Bemis, Jr., "The Decay of ^{110m}Ag: Gamma-Ray Energy and Intensity Standardization," *Nucl. Phys.* **A125**, 217 (1969).

S. C. Burnett,[3,12] R. L. Ferguson, F. Plasil,[6] and H. W. Schmitt,[6] "Prompt Neutrons from Fission of ^{233}U by 8.5 and 13.0 MeV Protons," *Phys. Rev. Letters* **21**, 1350 (1968).

Y. Y. Chu[13] and R. L. Hahn, "Production Cross Sections of Some I, Te, Ba, and Cs Isotopes from the Interactions of 1, 2, and 2.9 GeV Protons with Uranium," *J. Inorg. Nucl. Chem.* **30**, 2561 (1968).

---

[1] Guest scientist 1964–66; present address: Middle East Technical University, Ankara, Turkey.

[2] Visiting scientist 1964–65; present address: University of Naples, Italy.

[3] Oak Ridge Graduate Fellow under appointment with Oak Ridge Associated Universities.

[4] Present address: Niels Bohr Institute, Copenhagen, Denmark.

[5] Physics Department, Vanderbilt University, Nashville, Tenn.

[6] Physics Division.

[7] Neutron Physics Division.

[8] Department of Physics and Radiation Biology Laboratory, University of Alabama, Birmingham.

[9] Present address: Chemistry Department, Purdue University, Lafayette, Ind.

[10] Chemistry Department, Purdue University, Lafayette, Ind.

[11] Department of Physics and Astronomy, Louisiana State University, Baton Rouge.

[12] Present address: Los Alamos Scientific Laboratory, University of California, Los Alamos, N.M.

[13] Chemistry Department, Brookhaven National Laboratory, Upton, N.Y.

C. E. Bemis, Jr., and R. L. Hahn (book review), *Nuclear Chemistry,* vol. I (ed. by L. Yaffe), in *Nucl. Sci. Eng.* **34**, 349 (1968).

R. L. Hahn and C. E. Bemis, Jr. (book review), *Nuclear Chemistry,* vol. II (ed. by L. Yaffe), in *Nucl. Sci. Eng.* **36**, 460 (1969).

L. L. Riedinger, Jr.,[3,4] "Studies of the Collective States in ^{152}Gd, ^{152}Sm, and ^{154}Gd," Ph.D. thesis, Vanderbilt University, January 1969.

R. C. Hagenauer,[3,9] "The Decay of Neutron-Deficient Nuclides of Mass 89," Ph.D. dissertation, University of Tennessee, Knoxville, March 1969.

G. D. O'Kelley, B. J. Dropesky,[14] C. W. Townley,[15] and G. R. Choppin,[16] "Status of Nuclear and Radiochemistry," National Academy of Sciences–National Research Council, April 1969.

M. H. Lietzke and R. W. Stoughton, "Atomic Number," in *The Encyclopedia of the Chemical Elements* (ed. by C. A. Hampel), Reinhold, New York, 1968.

R. W. Stoughton and M. H. Lietzke, "Polonium," in *The Encyclopedia of the Chemical Elements* (ed. by C. A. Hampel), Reinhold, New York, 1968.

CHEMISTRY AND PHYSICS OF TRANSURANIUM ELEMENTS

C. E. Bemis, Jr., J. Halperin, and R. E. Eby,[17] "The Alpha Decay Half-Lives of ^{242}Pu and ^{244}Pu," *J. Inorg. Nucl. Chem.* **31**, 599 (1969).

C. E. Bemis, Jr., and J. Halperin, "The Alpha Decay of ^{253}Cf and ^{254}Cf," *Nucl. Phys.* **A121**, 433 (1968).

R. L. Hahn, M. F. Roche,[18] and K. S. Toth,[18] "New Neptunium Isotopes, ^{230}Np and ^{229}Np," *Nucl. Phys.* **A113**, 206 (1968), and *Contributions to International Symposium on Nuclear Structure,* Report D-3893, p. 58, Dubna, U.S.S.R. (July 1968).

L. J. Nugent, J. L. Burnett, R. D. Baybarz,[19] G. K. Werner,[6] S. P. Tanner,[20] J. R. Tarrant, and O. L. Keller, Jr., "Intramolecular Energy Transfer and Sensitized Luminescence in Actinide(III) β-Diketone Chelates," *J. Phys. Chem.* **73**, 1540 (1969).

L. J. Nugent, R. D. Baybarz,[19] and J. L. Burnett, "Electron-Transfer Spectra and the II-III Oxidation Potentials of Some Lanthanide and Actinide Halides in Solution," *J. Phys. Chem.* **73**, 1177 (1969).

L. J. Nugent, R. D. Baybarz,[19] and J. L. Burnett, "Lanthanide and Actinide Standard II-III Oxidation Potentials and the Optical Absorption Spectra of Some Lanthanide and Actinide Trihalides in Ethanol," *Proceedings of the Symposium on Transuranium Elements, University of Liege, Liege, Belgium, April 21–22, 1969.*

J. R. Peterson[21] and B. B. Cunningham,[22] "Crystal Structures and Lattice Parameters of the Compounds of Berkelium. IV. Berkelium Trifluoride," *J. Inorg. Nucl. Chem.* **30**, 1775–84 (1968).

J. R. Peterson[21] and J. H. Burns, "Preparation and Crystal Structure of Californium Oxyfluoride, CfOF," *J. Inorg. Nucl. Chem.* **30**, 2955 (1968).

R. M. Harbour, "Nuclear-Charge Distribution: Fractional Cumulative Yields of ^{99}Nb from the Low-Energy Fission of ^{233}U, ^{235}U, ^{238}U, and ^{252}Cf. Mass Distribution: Cumulative Yields of Masses 95, 99, 103, 105, 131, 132, 133, 140, 141, 143, 144, and 147 from ^{252}Cf Fission," Ph.D. thesis, University of Missouri, November 1968.

---

[14] Los Alamos Scientific Laboratory, University of California, Los Alamos, N.M.

[15] Battelle Memorial Institute, Columbus, Ohio.

[16] Chemistry Department, Florida State University, Tallahassee.

[17] Analytical Chemistry Division.

[18] Electronuclear Division.

[19] Chemical Technology Division.

[20] Guest scientist from the University of West Florida, Pensacola.

[21] Consultant; Chemistry Department, University of Tennessee, Knoxville.

[22] Lawrence Radiation Laboratory, University of California, Berkeley.

ISOTOPE CHEMISTRY

D. A. Lee, W. L. Taylor,[23] W. J. McDowell,[19] and J. S. Drury, "Solvent Extraction of Lithium," *J. Inorg. Nucl. Chem.* **30**, 2807 (1968).

A. A. Palko and J. S. Drury, "The Chemical Fractionation of Boron Isotopes," p. 40 in *Isotope Effects in Chemical Processes,* Advan. Chem. Ser. No. 89 (1969).

D. A. Lee, "The Enrichment of Lithium Isotopes by Extraction Chromatography," p. 57 in *Isotope Effects in Chemical Processes,* Advan. Chem. Ser. No. 89 (1969).

RADIATION CHEMISTRY

C. J. Hochanadel, J. A. Ghormley, and J. W. Boyle, "Vibrationally Excited Ozone in the Pulse Radiolysis and Flash Photolysis of Oxygen," *J. Chem. Phys.* **48**, 2416 (1968).

J. A. Ghormley, C. J. Hochanadel, and J. W. Boyle, "The Yield of Ozone in the Pulse Radiolysis of Gaseous Oxygen at Very High Dose Rate. Use of This System as a Dosimeter," *J. Chem. Phys.* **50**, 419 (1969).

C. J. Hochanadel, J. A. Ghormley, J. W. Boyle, and J. F. Riley,[24] "Short Duration Flash Photolysis Lamp," *Rev. Sci. Instr.* **39**, 1144 (1968).

T. J. Sworski, R. W. Matthews,[25] and H. A. Mahlman, "Radiation Chemistry of Concentrated $NaNO_3$ Solutions: Dependence of $G(HNO_2)$ on $NaNO_3$ Concentration," Advan. Chem. Ser. No. 81, p. 164 (1968).

R. W. Matthews,[25] H. A. Mahlman, and T. J. Sworski, "Oxidation of Cerium(III) in Sulfuric Acid Solutions Induced by ^{60}Co Gamma Radiation," *J. Phys. Chem.* 72, 3704 (1968).

G. E. Boyd and Q. V. Larson, "Chemistry of ^{38g}Cl Recoils in Neutron Irradiated Crystalline $KClO_2$, $KClO_3$, and $KClO_4$," *J. Am. Chem. Soc.* **90**, 5092 (1968).

L. C. Brown and G. E. Boyd, "Production of ClO_4^- and ClO_2^- Ions in Crystalline $KClO_3$ Irradiated with ^{60}Co γ-Rays," *J. Phys. Chem.* 73, 396 (1969).

L. C. Brown, G. M. Begun, and G. E. Boyd, "Production of Bromite and Perbromate Ions in Crystalline $CsBrO_3$ Irradiated with ^{60}Co γ-Rays and the Vibrational Spectrum of BrO_4^- Ion," *J. Am. Chem Soc.* **91**, 2250 (1969).

G. E. Boyd (book review), *Interaction of Radiation with Solids* (ed. by A. Bishay), Plenum, New York, 1967, in *J. Am. Ceram. Soc.* **51**, 328 (1968).

ORGANIC CHEMISTRY

H. Kwart,[26] E. N. Givens,[3] and C. J. Collins, "Stereospecificity of Carbonium Ions Related to Solvation Factors," *J. Am. Chem. Soc.* **90**, 7162 (1968).

M. D. Eckart,[3] "The Deamination of Deuterated-2-hydroxy-2-phenyl-3-amino-norbornanes," Ph.D. thesis, University of Tennessee, December 1968.

CHEMISTRY OF AQUEOUS SYSTEMS

M. H. Lietzke and R. W. Stoughton, "A Comparison of Several Different Models for Fitting Data on the Solubility of Silver Sulfate in Aqueous Solutions Containing Various Supporting Electrolytes," ORNL-4325 (October 1968).

M. H. Lietzke and H. A. O'Brien, Jr.,[27] "Electromotive Force Studies in Aqueous Solutions at Elevated Temperatures. X. The Thermodynamic Properties of HCl-KCl, HCl-RbCl, HCl-CsCl, HCl-$MgCl_2$, HCl-$CaCl_2$, HCl-$SrCl_2$, and HCl-$AlCl_3$ Mixtures," *J. Phys. Chem.* 72, 4408 (1968).

---

[23] Oak Ridge Associated Universities Research Participant from Mt. Vernon Nazarene College, Mt. Vernon, Ohio.

[24] Present address: Lockheed Palo Alto Research Laboratory, Palo Alto, Calif.

[25] Guest scientist from Australian Atomic Energy Research Establishment, Sydney.

[26] Chemistry Department, University of Delaware, Newark.

[27] Isotopes Division.

H. A. O'Brien,[27] "Thermodynamic Properties of Aqueous Binary Mixtures of Hydrochloric Acid with a Series of Metal Chlorides as Calculated from Electromotive Force Measurements," Ph.D. thesis, University of Tennessee, June 1968.

M. H. Lietzke and R. W. Stoughton, "On the Existence of the Complex $AgSO_4^-$ in Aqueous Solutions," *J. Phys. Chem.* 73, 745 (1969).

Y. C. Wu,[28] R. M. Rush, and G. Scatchard,[29] "Osmotic and Activity Coefficients for Binary Mixtures of Sodium Chloride, Sodium Sulfate, Magnesium Sulfate, and Magnesium Chloride in Water at 25°. I. Isopiestic Measurements on the Four Systems with Common Ions,"[30] *J. Phys. Chem.* 72, 4048 (1968).

R. M. Rush, "Parameters for the Calculation of Osmotic and Activity Coefficients and Tables of These Coefficients for Twenty-two Aqueous Mixtures of Two Electrolytes at 25°C.," ORNL-4402 (April 1969).

C. V. Linderstrøm-Lang[31] and F. Vaslow, "Isotope Effect on the Vapor Pressures of H_2O-C_2H_5OH and D_2O-C_2H_5OD Mixtures," *J. Phys. Chem.* 72, 2645 (1968).

A. J. Shor,[32] K. A. Kraus,[33] W. T. Smith, Jr.,[34] and J. S. Johnson, Jr., "Hyperfiltration XI. Salt-Rejection Properties of Dynamically Formed Hydrous Zirconium(IV) Oxide Membranes,"[35] *J. Phys. Chem.* 72, 2200 (1968). (Joint contribution of ORNL and the Chemistry Department, University of Tennessee.)

J. S. Johnson, Jr., K. A. Kraus,[33] S. M. Fleming,[36] H. D. Cochran,[36] and J. J. Perona,[19] "Hyperfiltration XIV. Porous Tubes Precoated with Filteraids as Supports for Dynamically Formed Membranes,"[30] *Desalination* 5, 259 (1968).

H. C. Savage,[32] N. E. Bolton,[37] H. O. Phillips, K. A. Kraus,[33] and J. S. Johnson, Jr., "Hyperfiltration of Plant Effluents (Hyperfiltration XV),"[30] *Water Sewage Works* **116**, 102 (1969).

A. J. Shor,[32] K. A. Kraus,[33] J. S. Johnson, Jr., and W. T. Smith, Jr.,[34] "Reply by the Authors to Comments of Cooney and Rabe Concerning 'Hyperfiltration VII. Concentration Polarization in Tubular Systems with Dynamically Formed Membranes,' " *Ind. Eng. Chem., Fundamentals* 7, 44 (1968). Reply appeared in same journal 7, 528 (1968).[35]

K. A. Kraus[33] and J. S. Johnson, Jr., "Colloidal Hydrous Oxide Hyperfiltration Membranes,"[38] U.S. Pat. 3,413,219 (Nov. 30, 1968).

J. S. Johnson and K. A. Kraus,[33] "Hyperfiltration Process Having Ion Exchange Pretreatment,"[38] U.S. Pat. 3,431,201 (Mar. 4, 1969).

J. S. Johnson, K. A. Kraus,[33] A. E. Marcinkowsky,[39] H. O. Phillips, and A. J. Shor,[32] "Method of Making a Salt Rejecting Membrane,"[38] Canada Pat. 795,274 (Sept. 24, 1968).

K. A. Kraus[33] and J. S. Johnson, "Method of Making a Salt Rejecting Membrane,"[38] Argentina Pat. 162,754 (Aug. 28, 1968).

J. S. Johnson and K. A. Kraus,[33] "Hyperfiltration Process,"[38] Egypt Pat. 8516 (July 14, 1968).

G. E. Boyd, Q. V. Larson, and S. Lindenbaum, "Heat Capacity Changes in Ion-Exchange Reactions: The Exchange of Tetra-*n*-butylammonium with Sodium Ion in Cross-Linked Polystyrenesulfonate," *J. Phys. Chem* 72, 2651 (1968).

---

[28] Present address: National Bureau of Standards, Washington, D.C.

[29] Consultant; Professor of Physical Chemistry, Emeritus, Massachusetts Institute of Technology, Cambridge.

[30] Jointly sponsored by the Office of Saline Water, U.S. Department of the Interior, and the U.S. Atomic Energy Commission.

[31] Danish Atomic Energy Commission, Risø, Denmark.

[32] Reactor Chemistry Division.

[33] Director's Division.

[34] Chemistry Department, University of Tennessee, Knoxville.

[35] Sponsored by the Office of Saline Water.

[36] Oak Ridge Station, MIT School of Chemical Engineering Practice.

[37] Health Division.

[38] Based on work performed in the Chemistry Division under the Water Research Program.

ELECTROCHEMICAL KINETICS AND ITS APPLICATION TO CORROSION

G. H. Cartledge, "Passivation and Activation of Iron in the Presence of Molybdate Ions," *Corrosion* **24**, 223 (1968).

E. J. Kelly, "The Active Iron Electrode. II. Anion Adsorption and Its Effects on the Iron Dissolution and Hydrogen Evolution Reactions," *J. Electrochem. Soc.* **115**, 1111 (1968).

R. E. Meyer, F. A. Posey, and P. M. Lantz, "Chronopotentiometry of the Ag-AgCl System and Analysis for the Chloride Ion," [38] *J. Electroanal. Chem.* **19**, 99 (1968).

NONAQUEOUS SYSTEMS AT HIGH TEMPERATURE

A. S. Dworkin, H. R. Bronstein, and M. A. Bredig, "Miscibility of Liquid Metals with Salts VIII. Strontium–Strontium Halide and Barium–Barium Halide Systems," *J. Phys. Chem.* 72, 1892 (1968).

H. R. Bronstein, "Electromotive Force Measurements on Solutions of Rare Earth Metals in Their Molten Halides. I. The Ce-$CeCl_3$, Pr-$PrCl_3$, and Nd-$NdCl_3$ Solutions," *J. Phys. Chem.* 73, 1320 (1969).

S. Cantor[32] (ed.), J. W. Cooke,[40] A. S. Dworkin, G. D. Robbins,[32] R. E. Thoma,[32] and G. M. Watson,[32] "Physical Properties of Molten-Salt Reactor Fuel, Coolant, and Flush Salts," ORNL-TM-2316 (August 1968).

CHEMICAL PHYSICS

W. C. Waggener, A. J. Weinberger, and R. W. Stoughton, "Spectrophotometry of Aqueous HNO_3, H_2SO_4, and $DClO_4$ from 25° to 250°C," *Appl. Spectry.* **22**, 545 (1968).

P. Erman,[41] B. Sigfridsson,[41] T. A. Carlson, and Kjell Fransson,[41] "Auto-Ionization in β^- Decay," *Nucl. Phys.* **A112**, 117 (1968).

T. C. Tucker,[42] L. D. Roberts,[6,43] C. W. Nestor, Jr.,[42] T. A. Carlson, and F. B. Malik,[44] "Calculation of the Electron Binding Energies and X-Ray Energies for the Superheavy Elements 114, 126, and 140 Using Relativistic Self-Consistent-Field Atomic Wave Functions," *Phys. Rev.* **174**, 118 (1968).

T. C. Tucker,[42] L. D. Roberts,[6,43] C. W. Nestor, Jr.,[42] T. A. Carlson, and F. B. Malik,[44] "Relativistic Self-Consistent-Field Calculation of the Wave Functions, Eigenvalues, Isotope Shifts, and the *6s* Hyperfine-Structure Coupling Constant as a Function of Pressure for Metallic Gold in the Wigner-Seitz Model," *Phys. Rev.* **178**, 998 (1969).

R. H. Busey, E. D. Sprague,[45] and R. B. Bevan, Jr., "Enthalpy of Hydrolysis of Rhenium Trichloride. Enthalpy and Free Energy of Formation of Rhenium Sesquioxide," *J. Phys. Chem.* **73**, 1039 (1969).

Henry Zeldes and Ralph Livingston, "Paramagnetic Resonance Study of Liquids During Photolysis. VI. Aliphatic Nitroanions," *J. Am. Chem. Soc.* **90**, 4540 (1968).

Ralph Livingston and Henry Zeldes, "Paramagnetic Resonance Study of Liquids During Photolysis. VII. Nitriles," *J. Magnetic Resonance* **1**, 169 (1969).

M. M. Abraham,[46] G. W. Clark,[47] C. B. Finch,[47] R. W. Reynolds,[46] and H. Zeldes, "Ground-State Splitting of Trivalent Gd and Cm in $ZrSiO_4$, $HfSiO_4$, and $ThSiO_4$ Determined by ESR," *J. Chem. Phys.* **50**, 2057 (1969).

---

[39] Present address: Technical Center, Union Carbide Corp., South Charleston, W.Va.

[40] Reactor Division.

[41] Research Institute for Physics and Research Institute of National Defence, Stockholm, Sweden.

[42] Mathematics Division.

[43] Present address: Physics Department, University of North Carolina, Chapel Hill.

[44] Physics Department, Yale University, New Haven, Conn.

[45] Temporary employee, summer 1967.

[46] Solid State Division.

[47] Metals and Ceramics Division.

C. K. Johnson, "Addition of Higher Cumulants to the Crystallographic Structure-Factor Equation: A Generalized Treatment for Thermal-Motion Effects," *Acta Cryst.* **A25**, 187 (1969).

H. G. Smith,[46] S. W. Peterson,[48] and H. A. Levy, "Neutron-Diffraction Study of Lithium Sulfate Monohydrate," *J. Chem. Phys.* **48**, 5561 (1968).

F. Madaule-Aubry[49] and G. M. Brown, "Crystal Structures of Complexes of Nickel Perchlorate with Substituted Pyridines. I. Bisperchlorotetrakis(3,5-dimethylpyridine)nickel(II)," *Acta Cryst.* **B24**, 745 (1968).

F. Madaule-Aubry,[49] W. R. Busing, and G. M. Brown, "Crystal Structures of Complexes of Nickel Perchlorate with Substituted Pyridines. II. Tetrakis(3,4-dimethylpyridine)nickel(II) Perchlorate," *Acta Cryst.* **B24**, 754 (1968).

J. M. Williams,[48] S. W. Peterson,[48] and G. M. Brown, "A Neutron Diffraction Study of the Reaction Product of Acetonitrile and Hydrogen Chloride: Chloroacetiminium Chloride, $[CH_3C(Cl) = NH_2{}^+]Cl^{-1}$," *Inorg. Chem.* **7**, 2577 (1968).

G. M. Brown and R. Chidambaram,[50] "The Structure of Copper Ammonium Sulfate Hexahydrate from Neutron-Diffraction Data," *Acta Cryst.* **B25**, 676 (1969).

J. H. Burns, H. A. Levy, and O. L. Keller, "The Crystal Structure of Rubidium Hexafluoroprotactinate(V), $RbPaF_6$," *Acta Cryst.* **B24**, 1675 (1968).

A. H. Narten, "X-Ray Diffraction Data on the System Tetra-*n*-butylammonium Fluoride–Water at 25°C," ORNL-4333 (December 1968).

A. H. Narten, "X-Ray Diffraction Data on Aqueous Ammonium Halide Solutions at 25°C," ORNL-4367 (February 1969).

A. H. Narten, "Diffraction Pattern and Structure of the System Water-Ammonia at 4°C," *J. Chem. Phys.* **49**, 1692 (1968).

P. F. Dittner and S. Datz, "Vibrational Excitation and Fragmentation of Molecular Hydrogen from Slow K^+ Ion Collisions," *J. Chem. Phys.* **49**, 1969 (1968).

S. Datz and H. O. Lutz,[51] "Interactions of Heavy Particles with Solids," in *Methods of Experimental Physics*, vol. 7, p. 231 (B. Bederson and W. Fite, eds.), Academic, New York, 1968.

C. D. Moak,[6] H. O. Lutz,[51] L. B. Bridwell,[52] L. C. Northcliffe,[53] and S. Datz, "Equilibrium Charge States of Br and I Ions in Solids and Gases in the Energy Range 10–180 MeV," *Phys. Rev.* **176**, 427 (1968).

S. Datz, C. D. Moak,[6] T. S. Noggle,[46] B. R. Appleton,[46] and H. O. Lutz,[51] "Potential Energy and Differential Stopping Power Functions from Energy Loss Spectra of Fast Ions Channeled in Gold Single Crystals," *Phys. Rev.* **179**, 315 (1969).

C. D. Moak,[6] L. B. Bridwell,[52] H. O. Lutz,[51] S. Datz, and L. C. Northcliffe,[53] "Charge State Distributions of Ion Energy from Solids and Gases in the Energy Range 20–150 MeV," in *Beam Foil Spectroscopy*, vol. 1, p. 157 (ed. by S. Bashkin), Gordon and Breach, New York, 1968.

R. Baldock, "Isotopes. I. Pre-World War I Status; Isotopes. II. Post-World War I Status," in *Encyclopedia of the Chemical Elements* (ed. by C. A. Hampel), pp. 313–30, Reinhold, New York, 1968.

P. S. Rudolph, "The Radiolysis of Methane in a Wide-Range Radiolysis Source," p. 101 in *Radiation Chemistry – II*, Advan. Chem. Ser. No. 82 (1968).

---

[48] Present address: Chemistry Division, Argonne National Laboratory, Argonne, Ill.

[49] Guest scientist 1966; present address: Centre de Recherche de Chimie, Ecole Centrale des Arts et Manufactures, Paris.

[50] Guest scientist 1964–65 from Bhabha Atomic Research Centre, Trombay, Bombay-74, India.

[51] Present address: Max Planck Institut für Kernphysik, Heidelberg, Germany.

[52] Oak Ridge Associated Universities Research Participant from Murray State University, Murray, Ky.

[53] Texas A & M University, College Station.

Papers Presented at Scientific and Technical Meetings

NUCLEAR CHEMISTRY

F. Plasil,*[1] R. L. Ferguson, Frances Pleasonton,[1] and H. W. Schmitt,[1] "Search for an Asymmetric Component in the Mass Distribution from Proton-Induced Fission of ^{209}Bi," American Physical Society Meeting, Miami Beach, Fla., Nov. 25–27, 1968; *Bull. Am. Phys. Soc.* **13**, 1408 (1968).

F. Plasil,*[1] R. L. Ferguson, and H. W. Schmitt,[1] "Neutron Emission in the Fission of ^{209}Bi Induced with 53.25-MeV ^{4}He Ions," American Physical Society Meeting, Washington, D.C., Apr. 28–May 1, 1969; *Bull Am. Phys. Soc.* **14**, 536 (1969).

N. R. Johnson,* L. L. Riedinger, Jr.,[2,3] and J. H. Hamilton,[4] "Mixing of Vibrational Bands in ^{152}Sm and ^{154}Gd," Informal Physics Conference, Stockholm, Sweden, June 26–28, 1968.

N. R. Johnson,* L. L. Riedinger,[2,3] and J. H. Hamilton,[4] "Properties of β- and γ-Vibrational Bands in Deformed Nuclei," Conference on the Electron Capture and Higher Order Processes in Nuclear Decays, Debrecen, Hungary, July 15–18, 1968.

N. R. Johnson, "Vibrational Properties of Nuclei in the Transitional Region," Southeastern Section, American Physical Society, Meeting, Athens, Ga., Oct. 9–11, 1968 (invited).

L. L. Riedinger,[2,3] N. R. Johnson, A. F. Kluk,[2,5] and J. H. Hamilton,*[4] "Decay of ^{158}Eu," American Physical Society Meeting, Washington, D.C., Apr. 28–May 1, 1969.

G. D. Benson,*[4] R. G. Albridge,[4] A. V. Ramayya,[4] P. V. Rao,[6] and G. D. O'Kelley, "Conversion Coefficients of Gamma Rays of ^{194}Pt," 35th Meeting of the Southeastern Section, American Physical Society, Athens, Ga., Oct. 9–11, 1968; *Bull. Am. Phys. Soc.* **13**, 1722 (1968).

A. V. Ramayya,*[4] G. D. Benson,[4] R. G. Albridge,[4] P. V. Rao,[6] and G. D. O'Kelley, "Levels of ^{194}Pt from the Decay of ^{194}Hg," American Physical Society Meeting, Miami Beach, Fla., Nov. 25–27, 1968; *Bull. Am. Phys. Soc.* **13**, 1469 (1968).

M. F. Roche,*[7] K. S. Toth,[7] R. L. Hahn, and C. E. Bemis, "Levels in ^{172}Yb Populated in the Decay of ^{172}Lu," American Physical Society Meeting, Washington, D.C., Apr. 28–May 1, 1969; *Bull. Am. Phys. Soc.* **14**, 586 (1969).

K. S. Toth,*[7] R. L. Hahn, M. F. Roche,[7] and D. S. Brenner,[8] "New Erbium Isotope, ^{155}Er," American Physical Society Meeting, Miami Beach, Fla., Nov. 25–27, 1968.

---

*Speaker.

[1] Physics Division.

[2] Oak Ridge Graduate Fellow under appointment with Oak Ridge Associated Universities.

[3] Present address: Niels Bohr Institute, Copenhagen, Denmark.

[4] Physics Department, Vanderbilt University, Nashville, Tenn.

[5] From Vanderbilt University, Nashville, Tenn.

[6] Department of Physics, Emory University, Atlanta, Ga.

[7] Electronuclear Division.

[8] Chemistry Department, Clark University, Worcester, Mass.

R. L. Hahn,* M. F. Roche,[7] and K. S. Toth,[7] "Alpha Decay of ^{227}U," American Physical Society Meeting, Washington, D.C., Apr. 28–May 1, 1969.

G. D. O'Kelley, "Recent Nuclear Research on Technetium Isotopes," Nuclear Applications in Chemistry Award Symposium, 157th National Meeting, American Chemical Society, Minneapolis, Minn., Apr. 14–18, 1969 (invited).

G. D. O'Kelley,* J. S. Eldridge,[9] P. R. Bell,[10] K. A. Richardson,[10] and E. Schonfeld,[10] "Gamma-Ray Spectrometry of Returned Lunar Samples," Symposium on Plans for Chemical Analysis of Returned Lunar Samples, 157th National Meeting, American Chemical Society, Minneapolis, Minn., Apr. 14–18, 1969 (invited).

J. S. Eldridge,*[9] P. R. Bell,[10] V. A. McKay,[11] G. D. O'Kelley, and R. E. Wintenberg,[11] "Low-Level Radiation Counting Facility for Geochemical and Returned Lunar Samples," Twelfth Conference on Analytical Chemistry in Nuclear Technology, Gatlinburg, Tenn., Oct. 8–10, 1968.

G. E. Boyd, "Nuclear Energy Centers," Symposium on Recent Developments in Nuclear Instrumentation, Exhibition on Nuclear Instrument Systems and Components, U.S. Trade Center, London, England, Sept. 19–20, 1968 (invited).

G. E. Boyd, "Award Address," ACS Award for Nuclear Applications in Chemistry, 157th National Meeting, American Chemical Society, Minneapolis, Minn., Apr. 13–18, 1969 (invited).

CHEMISTRY AND PHYSICS OF TRANSURANIUM ELEMENTS

R. L. Ferguson,* F. Plasil,[1] Frances Pleasonton,[1] and H. W. Schmitt,[1] "Fragment Energy Correlation Measurements in the Fission of ^{232}Th, ^{238}U, and ^{239}Pu by 8- to 12.5-MeV Protons," American Physical Society Meeting, New York, Feb. 3–6, 1968; *Bull. Am. Phys. Soc.* **14**, 57 (1969).

R. L. Hahn,* M. F. Roche,[7] and K. S. Toth,[7] "New Neptunium Isotopes, ^{230}Np and ^{229}Np," International Symposium on Nuclear Structure, Dubna, U.S.S.R., July 4–11, 1968.

E. T. Chulick,*[12] P. L. Reeder,[13] E. Eichler, and C. E. Bemis, Jr., "Delayed Neutron Yields and Spectra from ^{252}Cf Spontaneous Fission," American Physical Society Meeting, St. Louis, Mo., Feb. 27, 1969; *Bull. Am. Phys. Soc.* **14**, 190 (1969).

C. B. Finch,*[14] L. J. Nugent, G. K. Werner,[1] and M. M. Abraham,[15] "Self-Excited Thermoluminescence and Optical Bleaching in Rare-Earth Doped Thorium Dioxide Crystals," The Seventh Rare-Earth Research Conference, San Diego, Calif., Oct. 28–30, 1968.

J. L. Burnett, R. D. Baybarz,[16] and L. J. Nugent,* "Charge Transfer Spectra of Lanthanide and Actinide Trihalides in Solution," The Seventh Rare-Earth Research Conference, San Diego, Calif., Oct. 28–30, 1968.

S. P. Tanner*[17] and L. J. Nugent, "Self Excitation and Luminescence from $^{244}CmCl_3$ in the H_2O-D_2O System," Southeastern Regional Meeting, American Chemical Society, Tallahassee, Fla., Dec. 4–7, 1968.

L. J. Nugent,* R. D. Baybarz,[16] and J. L. Burnett, "Lanthanide and Actinide Standard II-III Oxidation Potentials and the Optical Absorption Spectra of Some Lanthanide and Actinide Trihalides in Ethanol," Symposium on Transuranium Elements, University of Liege, Liege, Belgium, Apr. 21–22, 1969.

M. D. Danford,* J. H. Burns, O. L. Keller, Jr., J. R. Stokely,[9] and W. H. Baldwin, "Preparation, Volatility and Crystallography of Some Rare Earth and Americium Chelates," Southeastern Regional Meeting, American Chemical Society, Tallahassee, Fla., Dec. 4–7, 1968.

---

[9] Analytical Chemistry Division.

[10] NASA Manned Spacecraft Center, Houston, Tex.

[11] Instrumentation and Controls Division.

[12] Graduate student from Washington University, St. Louis, Mo.

[13] Chemistry Department, Washington University, St. Louis, Mo.

[14] Metals and Ceramics Division.

[15] Solid State Division.

[16] Chemical Technology Division.

[17] Guest scientist from the University of West Florida, Pensacola.

J. H. Burns* and M. D. Danford, "Crystal and Molecular Structure of Cesium Tetrakishexafluoroacetylacetonato Europate(III) and Americate(III)," American Crystallographic Association Summer Meeting, State University of New York at Buffalo, Buffalo, N.Y., Aug. 11–16, 1968.

O. L. Keller, Jr., "The ORNL High Flux Isotope Reactor," 157th National Meeting, American Chemical Society, Minneapolis, Minn., Apr. 13–18, 1969.

ISOTOPE CHEMISTRY

L. L. Brown, "Enrichment of ^{13}C by Chemical Exchange Between Cyanide and Cyanohydrin" Gordon Research Conference on the Chemistry and Physics of Isotopes, Plymouth, N.H., June 24–28, 1968.

RADIATION CHEMISTRY

C. J. Hochanadel, J. A. Ghormley, and P. J. Ogren,*[18] "Pulse Radiolysis of NO: Production of NO_2 and N_2O_3 and the Production and Relaxation of Vibrationally Excited NO," Southeastern Regional Meeting, American Chemical Society, Tallahassee, Fla., Dec. 4–6, 1968.

T. J. Sworski,* R. W. Matthews,[19] and H. A. Mahlman, "Radiation Chemistry of Concentrated $NaNO_3$ Solutions: Dependence of $G(HNO_2)$ on $NaNO_3$ Concentration," International Conference on Radiation Chemistry, Argonne National Laboratory, Argonne, Ill., Aug. 12–15, 1968.

H. A. Mahlman,* R. W. Matthews,[19] and T. J. Sworski, "Kinetics of Ce(IV) Reduction by H_2O_2 in Sulfuric Acid Solutions," 157th National Meeting, American Chemical Society, Minneapolis, Minn., Apr. 14–18, 1969.

R. W. Matthews,[19] H. A. Mahlman, and T. J. Sworski,* "Kinetic Evidence for a Primary Yield of SO_4^- Radicals in the Radiolysis of Aqueous Sulfuric Acid Solutions," 17th Annual Meeting, Radiation Research Society, Cincinnati, Ohio, May 18–22, 1969.

L. C. Brown* and G. E. Boyd, "The Production of Perhalate and Halite Ions in Crystalline Alkali-Metal Halates Irradiated with ^{60}Co Gamma-Rays," 157th National Meeting, American Chemical Society, Minneapolis, Minn., Apr. 13–18, 1969.

CHEMISTRY OF AQUEOUS SYSTEMS

J. S. Johnson, "Hyperfiltration Studies at ORNL," 2nd Symposium on Reverse Osmosis, Sponsored by Office of Saline Water, Miami, Apr. 20–25, 1969 (invited paper; speaker substituted for K. A. Kraus).

J. S. Johnson, "Desalination and Other Projected Applications of Hyperfiltration (Reverse Osmosis)," Greenville, S.C., Section of American Society of Mechanical Engineers, Jan. 10, 1969 (invited).

J. I. Padova,[20] "The Thermodynamics of Mixed Chloride Nitrate Systems," 156th National Meeting, American Chemical Society, Atlantic City, N.J., Sept. 9–13, 1968.

S. Lindenbaum, "Thermodynamic Studies of Aqueous Solutions of Tetraalkylammonium Halides," Southeastern Regional Meeting, American Chemical Society, Tallahassee, Fla., Dec. 2–7, 1968 (invited).

R. W. Hendricks*[14] and S. Lindenbaum, "A Small-Angle X-Ray Scattering Investigation of Aqueous Solutions of Tetraalkylammonium Halides," 157th National Meeting, American Chemical Society, Minneapolis, Minn., Apr. 13–18, 1969.

---

[18] Oak Ridge Associated Universities Research Participant from Maryville College, Maryville, Tenn., summer 1968.

[19] Guest scientist from Australian Atomic Energy Research Establishment, Sydney.

[20] Present address: Soreq Nuclear Research Centre, Yavne, Israel.

ELECTROCHEMICAL KINETICS AND ITS APPLICATION TO CORROSION

G. H. Cartledge, "The Mechanistic Action of Inhibitors," Southeastern Regional Meeting, National Association of Corrosion Engineers, Atlanta, Ga., Sept. 18–20, 1968 (invited).

E. J. Kelly, "Mechanism of Iron Dissolution With and Without Inhibitors," Symposium on Corrosion Kinetics and Mechanisms, Gordon Research Conference on Corrosion, New London, N.H., July 22, 1968 (invited).

F. A. Posey, "Pitting and Crevice Corrosion of Titanium and Its Alloys," Symposium on Corrosion in Desalination, 134th Meeting, Electrochemical Society, Montreal, Quebec, Canada, Oct. 8, 1968 (invited).

F. A. Posey, "Electrochemical Aspects of the Corrosion of Metals," Symposium on Kinetics of Corrosion Processes, 25th Annual Conference, National Association of Corrosion Engineers, Houston, Tex., Mar. 10, 1969 (keynote address, invited).

NONAQUEOUS SYSTEMS AT HIGH TEMPERATURE

M. A. Bredig, "The Experimental Evidence for 'Complex Ions' in Some Molten Salt Mixtures," Symposium on Characterization and Analysis in Molten Salts, Analytical Division, 156th National Meeting, American Chemical Society, Atlantic City, N.J., Sept. 9–13, 1968 (invited).

CHEMICAL PHYSICS

W. C. Waggener,* A. J. Weinberger, and R. W. Stoughton, "Mathematical Resolution of the 0.86–1.34 μ Absorption Spectrum of Liquid H_2O at Temperatures from 250° to 0°C," 156th National Meeting, American Chemical Society, Atlantic City, N.J., Sept. 9–13, 1968.

T. A. Carlson, "Use of Electron Spectroscopy in Determination of Electron Studies in Molecules," Mid-America Symposium on Spectroscopy, Chicago, May 12–15, 1969 (invited).

T. A. Carlson, "Electron Structures of Solids and Gaseous Molecules by Electron Spectroscopy," Southeastern Section, American Physical Society, Meeting, Athens, Ga., Oct. 9–11, 1968 (invited).

R. H. Busey* and R. A. Gilbert, "Enthalpy of Potassium Pertechnetate and Potassium Perrhenate from 0 to 900°C. Evidence of Order-Disorder Transitions Just Below Their Melting Points," Twenty-third Annual Calorimetry Conference, Midland, Mich., Aug. 13–15, 1968.

R. H. Busey, "The Chemical Thermodynamic Properties of Technetium and Rhenium," Nuclear Applications in Chemistry Award Symposium, 157th National Meeting, American Chemical Society, Minneapolis, Minn., Apr. 13–18, 1969 (invited).

Ralph Livingston* and Henry Zeldes, "Paramagnetic Resonance Study of Liquids During Photolysis," Conference on ESR in Radiation Chemistry, Chalk River, Canada, May 7, 1969.

C. K. Johnson, "Sources of Error in the Calculated Structure Factors Due to Atomic Motion," International Meeting on Accurate Determination of X-Ray Intensities and Structure Factors, Cambridge, England, June 24–28, 1968 (invited).

C. K. Johnson, "Generalized Treatments for Thermal Motion," International Summer School on the Accurate Determination of Neutron Intensities and Structure Factors, Harwell, England, July 1–5, 1968 (invited).

C. K. Johnson, "Higher Moments and Cumulants for Rigid-Body Motion," American Crystallographic Association Meeting, Seattle, Wash., Mar. 23–28, 1969.

G. M. Brown, "The Crystal Structure of Leucoxine Hydrobromide," American Crystallographic Association Summer Meeting, State University of New York at Buffalo, Buffalo, N.Y., Aug. 11–16, 1968.

S. Datz, "Inelastic Atom-Molecule Scattering," American Physical Society Meeting, Miami Beach, Fla., Nov. 25, 1968 (invited).

S. Datz, "Penetration of Energetic Particles in Ordered Lattices," American Physical Society Meeting, Washington, D.C., May 1, 1969 (invited).

S. Datz, "Molecular Beam Studies of Chemical Reactions," Southeastern Regional Meeting, American Chemical Society, Tallahassee, Fla., Dec. 5, 1968 (invited).

S. Datz, "Interatomic Stopping Parameters from Channeled Ion Energy Loss Spectra," Gordon Research Conference on Particle Solid Interactions, Meriden, N.H., July 15, 1968 (invited).

S. Datz, G. Ostrom,[21] and F. Schmidt-Bleek,*[21] "Hot Halogen Atoms by Sputtering," 157th National Meeting, American Chemical Society, Minneapolis, Minn., Apr. 13–18, 1969.

P. S. Rudolph, "The Radiolysis of Methane in a Wide-Range Radiolysis Source," International Conference on Radiation Chemistry, Argonne National Laboratory, Argonne, Ill., Aug. 12, 1968 (invited).

---

[21] Chemistry Department, Purdue University, Lafayette, Ind.

Lectures

CHEMISTRY AND PHYSICS OF TRANSURANIUM ELEMENTS

J. L. Burnett, "Some Aspects of Lanthanide and Actinide Thermodynamics," Rocky Flats Division, Dow Chemical Company, Boulder, Colo., Dec. 2, 1968.

J. R. Peterson,[1] "Microchemical Techniques Used in Transuranium-Element Research," Chemical Technology Division Summer Lecture Series, Oak Ridge National Laboratory, Oak Ridge, Tenn., July 29--Aug. 2, 1968.

J. R. Peterson,[1] "Transuranium Elements: Synthesis, Separation, and Research," Department of Chemistry General Seminar, University of Tennessee, Knoxville, Tenn., Jan. 23, 1969.

ORGANIC CHEMISTRY

C. J. Collins, "Memory Effects During Deaminations," University of Sheffield, England, Feb. 7, 1969; King's College, London, England, Feb. 11, 1969; Queen's University of Belfast, Ireland, Feb. 12, 1969; L'Université de Paris, France, Apr. 21, 1969.

C. J. Collins, "The Use of Isotopes in Organic Chemistry," King's College, London, England, Feb. 10, 1969; L'Université de Paris, France, Apr. 16, 1969.

C. J. Collins, "The Use of Isotopes to Study Organic Reaction Mechanisms," University of Padova, Italy, Feb. 24, 1969.

C. J. Collins, "Erinnerungseffekte während Desaminierungen," Gesellschaft Deutscher Chemiker, Tübingen, Germany, May 30, 1969; Institut für Organische Chemie der Universität Karlsruhe, Germany, Feb. 1, 1969.

C. J. Collins, "Der Gebrauch von Isotopen in der Organischen Chemie," Two lectures at Technische Universität Clausthal, Germany, Nov. 28, 1968.

C. J. Collins, "Aufklärung von Reaktionsmechanismen in der organischen Chemie," Naturwiss.-Technische Akademie, Isny, May 7, 1969.

C. J. Collins, seminars "Uber aktuelle Forschungsprobleme," "Isotopen Effekte," University of Tübingen, Germany, Jan. 8 and 22, 1969.

CHEMISTRY OF AQUEOUS SYSTEMS

M. H. Lietzke, "Thermodynamics of Aqueous Solutions at High Temperatures and Pressures," University of North Carolina, Chapel Hill, July 1, 1968.

M. H. Lietzke, "Desalination," University of North Carolina, Chapel Hill, July 2, 1968.

M. H. Lietzke, "Desalination and Water Recovery," Central Pennsylvania Section, American Chemical Society, Bloomsburg, Pa., Feb. 12, 1969.

J. S. Johnson, "Membrane Separation," Fall Study Course, Charleston, West Virginia, Section of American Institute of Chemical Engineers, Nov. 8, 1968.

---

[1] Consultant; Department of Chemistry, University of Tennessee, Knoxville.

J. S. Johnson, "Dynamic Membranes, Theory and Experiment," Short Course on Desalination, Methods and Applications, sponsored by Continuing Education in Engineering, University Extension and College of Engineering, University of California, Berkeley, Mar. 24–28, 1969.

R. J. Raridon, "The Problems of Water," The University of Tennessee at Martin, Martin, Tenn., May 2, 1969.

NONAQUEOUS SYSTEMS AT HIGH TEMPERATURE

M. A. Bredig, "The Molten Alkaline Earth Metal–Metal Halide Systems in Perspective with the Alkali Metal and Rare Earth Metal–Metal Halide Systems," Department of Chemistry and Institute for Atomic Research, Iowa State University, Ames, Apr. 21, 1969.

CHEMICAL PHYSICS

T. A. Carlson, "Dependence of Internal Conversion on Chemical Surroundings and Its Relationship to Mössbauer Isomer Shift," Vanderbilt University, Nashville, Tenn., Oct. 5, 1968.

T. A. Carlson, "Electron Spectroscopy: An Exciting New Tool for Determining the Nature of Chemical Binding," University of Alabama, Birmingham, Apr. 25, 1969.

R. Livingston, "Nuclear Magnetic Resonance," University of Tennessee–Oak Ridge Graduate School of Biomedical Sciences, Aug. 13, 1968.

R. Livingston, "Paramagnetic Resonance Studies of Short-Lived Radicals Formed in Liquids by Photolysis," seminar, Department of Chemistry, University of Alabama, Tuscaloosa, Mar. 20, 1969.

H. A. Levy, "Crystallography and Chemistry," Welch Foundation Lecture Tour: Baylor University, Waco, Tex., Mar. 24, 1969; Stephen F. Austin State College, Nacogdoches, Tex., Mar. 25, 1969; and University of Texas at El Paso, El Paso, Tex., Mar. 26, 1969.

R. D. Ellison, "The Crystal Structure and an Interpretation of the Thermal Motion of Glycolic Acid from Neutron Diffraction Data," Experimental Station, E. I. du Pont de Nemours & Co., Wilmington, Del., Apr. 21, 1969.

R. D. Ellison, "The Oak Ridge Computer-Controlled Diffractometer," Buffalo Medical Foundation, Buffalo, N.Y., May 2, 1969.

S. Datz, "Molecular Beam Studies of Chemically Reactive Collisions," Chemistry Seminar, University of Colorado, Boulder, Jan. 13, 1969.

S. Datz, "Molecular Beam Experiments in Chemical Dynamics," American Chemical Society Lecture, Knoxville, Tenn., Feb. 25, 1969; Madison, Wis., Mar. 10, 1969.

R. Baldock, "Some Considerations of the Reaction of Ions and Molecules in the Gas Phase: Methane," ORAU Traveling Lecture: Auburn University, Auburn, Ala., Nov. 15, 1968.

Supplementary Activities

STAFF

PROFESSIONAL AND EDUCATIONAL ACTIVITIES

Russell Baldock	Editorial Board, *International Journal of Mass Spectrometry and Ion Physics,* 1968–present.
G. E. Boyd	American Chemical Society Award for Nuclear Applications in Chemistry, April 1969.
	American Nuclear Society Representative to the Division of Chemistry and Chemical Technology, National Academy of Sciences–National Research Council, 1966–1969.
	Editorial Advisory Board, *Radiochimica Acta,* 1963–present.
	Honorary Editorial Board, *Radiokhimiia,* Pergamon Press, Inc., 1961–present.
R. H. Busey	Secretary-Treasurer, Calorimetry Conference, 1963–present.
W. R. Busing	Professor of Chemistry, part time (temporary assignment), University of Tennessee, Knoxville, October 1968–April 1969.
T. A. Carlson	Lecturer in Physics, University of Tennessee, Oak Ridge Extension, October 1968–June 1969.
C. J. Collins	Professor of Chemistry, part time, University of Tennessee, Knoxville, January 1964–present.
S. Datz	Symposium Chairman, Conference on Cross Sections in Chemical Dynamics, Industrial Associates, California Institute of Technology, Pasadena, Calif., Feb. 27–28, 1969.
	International Committee for "Conference on Atomic Collisions in Solids," International Atomic Energy Agency.
	Steering Committee for International Conference on the Physics of Electronic and Atomic Collisions, International Union of Pure and Applied Physics, 1963–present.
O. L. Keller, Jr.	USAEC Transplutonium Program Committee, 1969–1972.
K. A. Kraus	Editorial Board, *Journal of Chromatography,* 1958–present.
	Editorial Advisory Board, *Journal of Inorganic and Nuclear Chemistry,* 1958–present.
	Editorial Board, *Desalination,* 1966–present.
M. H. Lietzke	Professor of Chemistry, part time, University of Tennessee, Knoxville, January 1964–present.
Ralph Livingston	Professor of Chemistry, part time, University of Tennessee, Knoxville, January 1964–present.
	ORNL liaison officer for ORNL–University of Tennessee part-time teaching programs, 1968–present.
G. E. Moore	Instructor in Chemistry, National Science Foundation In-Service Institute for Secondary School Science Teachers, Knoxville College, Knoxville, Tenn., 1967–present.
G. D. O'Kelley	Professor of Chemistry, part time, University of Tennessee, Knoxville, January 1964–present.
	Subcommittee on Radiochemistry, National Academy of Sciences–National Research Council, 1962–present.
	Lunar Sample Preliminary Examination Team, an advisory committee to the NASA Manned Spacecraft Center, Houston, Tex., 1967–present.
	Committee on Major Nuclear Facilities, Division of Nuclear Chemistry and Technology, American Chemical Society, 1967–present.
R. J. Raridon	State Sponsor of the Collegiate Division, Tennessee Academy of Science, 1965–present.
L. L. Riedinger	National Science Foundation Postdoctoral Fellowship to the Niels Bohr Institute, Copenhagen, Denmark, 1968.
R. W. Stoughton	Editorial Advisory Board, *Journal of Inorganic and Nuclear Chemistry,* 1958–present.
E. H. Taylor	Board of Directors, Institute of Catalysis.

FOREIGN MEETINGS AND ACTIVITIES

Meeting and/or Activity	Location	Staff Member(s)
International Meeting on Accurate Determination of X-Ray Intensities and Structure Factors, June 24–28, 1968	Cambridge, England	C. K. Johnson
Informal Physics Conference, June 26–28, 1968	Stockholm, Sweden	N. R. Johnson
International Summer School on the Accurate Determination of Neutron Intensities and Structure Factors, July 1–5, 1968	Harwell, England	C. K. Johnson
International Symposium on Nuclear Structure, July 4–11, 1968	Dubna, USSR	R. L. Hahn N. R. Johnson
Conference on the Electron Capture and Higher Order Processes in Nuclear Decays, July 15–18, 1968	Debrecen, Hungary	N. R. Johnson
Guest scientist, Niels Bohr Institute (August 1968–August 1969)	Copenhagen, Denmark	E. Eichler
Visiting Professor of Chemistry, Chemisches Institut der Universität Tübingen (September 1968–July 1969)	Tübingen, West Germany	C. J. Collins
Symposium on Recent Developments in Nuclear Instrumentation, Exhibition on Nuclear Instrument Systems and Components, U.S. Trade Center, Sept. 19–20, 1968	London, England	G. E. Boyd
Symposium on Corrosion in Desalination, 134th Meeting of Electrochemical Society, Oct. 6–11, 1968	Montreal, Canada	F. A. Posey
Symposium on Transuranium Elements, University of Liege, Apr. 21–22, 1969	Liege, Belgium	L. J. Nugent
Conference on Electron Spin Resonance in Radiation Chemistry, May 5–9, 1969	Chalk River, Canada	R. Livingston

COLLABORATIVE RESEARCH

Institution	Collaborator(s)	Subject	Staff Member(s)
Abbott Laboratories, North Chicago, Ill.	L. H. Niece	Independent yields of ^{95}Zr from the thermal-neutron fission of ^{233}U and ^{235}U	R. L. Ferguson
Andrews University	M. C. Kelley J. R. Van Hise	Search for the 0^+ member of the two-phonon vibrational state in ^{110}Cd	N. R. Johnson
Cleveland State University and Case Western Reserve University	K. J. Kasper	Search for E0 transitions by nuclear spectroscopy	E. Eichler
University of Delft, The Netherlands	B. van Nooijen	Properties of radioactive ^{84}Y and ^{86}Y	N. R. Johnson
University of Delhi, India	S. C. Pancholi	Investigations of the decay properties of ^{75}Se and ^{59}Fe	N. R. Johnson
Florida State University	R. K. Sheline	Nuclear reaction spectroscopy on deformed rare-earth nuclei	N. R. Johnson G. D. O'Kelley
Gesellschaft f. Strahlenforschung MBH, Munich, Germany	K. Bunzl	Dilatometric measurements of volume changes in ion exchange reactions	G. E. Boyd
Institute of Nuclear Research, Amsterdam, The Netherlands	J. Konijn	Properties of radioactive ^{84}Y	N. R. Johnson
Lawrence Radiation Laboratory, Berkeley	B. B. Cunningham	Preparation and properties of einsteinium compounds	J. R. Peterson[1]

[1] Consultant.

Institution	Collaborator(s)	Subject	Staff Member(s)
Lawrence Radiation Laboratory, Livermore	E. K. Hulet R. Lougheed	Search for ^{258}Fm	C. E. Bemis, Jr.
Los Alamos Scientific Laboratory	S. C. Burnett	Determination of prompt neutrons emitted from fission fragments by intermediate-energy proton fission of ^{233}U and ^{238}U	R. L. Ferguson
University of Louisiana at New Orleans	J. H. Stocker	Stereochemistry of glycols	B. M. Benjamin
Louisiana State University	E. F. Zganjar	Use of ^{110m}Ag as a standard for gamma-ray energies and intensities	C. E. Bemis, Jr.
Michigan Technological University	L. Leifer	Thermal and solute effects on solvent hydrogen bonding: variation of osmotic coefficients of aqueous R_4NX solutions with temperature	S. Lindenbaum G. E. Boyd
Middle East Technical University, Ankara, Turkey	N. K. Aras	Level properties of ^{184}W	N. R. Johnson
		Study of the excited levels of some Mo isotopes populated in radioactive decay	E. Eichler G. D. O'Kelley
University of Missouri, Columbia	D. E. Troutner	Some aspects of fission	R. L. Ferguson
University of Naples, Italy	G. G. Chilosi	Study of the excited levels of some Mo isotopes populated in radioactive decay	E. Eichler G. D. O'Kelley
NASA Manned Spacecraft Center, Houston	Various personnel	Design of experiments to determine the gamma-ray spectra of returned lunar samples	G. D. O'Kelley
	W. Greenwood K. A. Richardson	Measurement of the gamma-ray spectra induced in simulated lunar materials by protons of energy appropriate to solar flares	G. D. O'Kelley
Purdue University	F. Schmidt-Bleek	Chemical accelerator sources	S. Datz
University of Rhode Island	S. Kupferman	Measurement of the gamma-ray spectra induced in simulated lunar materials by protons of energy appropriate to solar flares	G. D. O'Kelley
Rose Polytechnic Institute	B. S. Benjaminov	*Endo*-Hydrogen migration in reactions of a norbornyl system	B. M. Benjamin C. J. Collins
Savannah State College	M. P. Menon	Decay of 86-sec ^{136}I	E. Eichler N. R. Johnson G. D. O'Kelley
Soreq Nuclear Research Center, Yavne, Israel	J. I. Padova	Physical chemistry of polyelectrolyte systems	G. E. Boyd S. Lindenbaum
St. John's University	R. J. Beshinske	Monte Carlo calculations of the thermodynamic properties of water	M. H. Lietzke
University of Tennessee	W. E. Bull G. K. Schweitzer	Use of electron spectroscopy for investigating molecular structure[2]	T. A. Carlson
	J. F. Eastham	Calculations of conformational equilibrium of methyl-substituted hexahydropyrimidine	B. M. Benjamin
Vanderbilt University	R. G. Albridge	Nuclear spectroscopy	G. D. O'Kelley
	S. M. Brahmavar J. H. Hamilton A. V. Ramayya	Use of ^{110m}Ag as a standard for gamma-ray energies and intensities	C. E. Bemis, Jr.
	J. H. Hamilton	Properties of vibrational states in deformed nuclei	N. R. Johnson

[2]In collaboration with the Physics Division.

Institution	Collaborator(s)	Subject	Staff Member(s)
Washington University	P. L. Reeder	Delayed-neutron emitters from fission	E. Eichler
	P. L. Reeder E. T. Chulick	Measurement of delayed-neutron abundances and the energy spectra from the spontaneous fission of ^{252}Cf	C. E. Bemis, Jr.
	D. Sarantites	Level properties of ^{110}Cd	N. R. Johnson
West Georgia College	H. W. Boyd	Level properties of ^{110}Cd	N. R. Johnson

ANNUAL INFORMATION MEETING AND ADVISORY COMMITTEE

The Annual Information Meeting of the Chemistry Division was held October 9–11, 1968. Reports presented at the Meeting were:

Wednesday, Oct. 9, 1968

E. H. Taylor	Introduction
R. L. Hahn	New Transuranium Nuclides Produced at ORIC and HFIR
S. P. Tanner[3]	Self-Excited and UV-Excited Luminescence from $^{244}CmCl_3$ in the H_2O-D_2O System
L. L. Brown	Fractionation of Carbon Isotopes: CYANEX System
W. C. Waggener	The Near-Infrared Absorption of Liquid Water from 0 to 250° – Mathematical Resolution of the Spectrum
S. Lindenbaum	Unusual Behavior of Large Organic Ions in Aqueous Solution
M. H. Lietzke	A Two-Region Model for Electrolytic Solutions

Thursday, Oct. 10, 1968

J. Halperin	Some Recently Measured Neutron Cross Sections
R. W. Matthews[4]	Radiation-Induced Oxidation of Cerium(III) in Sulfuric Acid Solutions
E. J. Kelly	Electrodics of Zone-Refined Metals–Anion Adsorption on Iron; Corrosion of Titanium
C. K. Johnson	Generalized Methods of Thermal Motion Analysis Using Neutron Bragg Diffraction Data
B. M. Benjamin	A Study of Rotational Isomerism of Allyl Compounds by NMR
R. W. Holmberg	Studies by Paramagnetic Resonance of Gamma-Irradiated Single Crystals at Low Temperatures

Members of the Advisory Committee were:

Dr. Joseph J. Katz (1965–1968)
Argonne National Laboratory
9700 South Cass Avenue
Argonne, Illinois 60439

Prof. Joseph E. Mayer (1965–1968)
Department of Chemistry
University of California
La Jolla, California 92038

Prof. Harry H. Sisler, Dean (1966–1969)
College of Arts and Sciences
University of Florida
Gainesville, Florida 32601

Dr. Gerhart Friedlander, Chairman (1966–1969)
Department of Chemistry
Brookhaven National Laboratory
Upton, Long Island, New York 11973

---

[3] Visiting scientist from the University of West Florida, Pensacola.

[4] Visiting scientist from the Australian Atomic Energy Commission Research Establishment, Lucas Heights, N.S.W.

Prof. Paul D. Bartlett (1966–1969)
Department of Chemistry
Harvard University
Cambridge, Massachusetts 02138

Prof. Franklin A. Long (1967–1970)
Vice President for Research and Advanced Studies
Cornell University
Ithaca, New York 14850

VISITING SCIENTISTS

Name	Affiliation	ORNL Research Program	Sponsor
M. C. Banta	East Texas Baptist College	Electrochemical Kinetics	ORAU Faculty Research Participation Program
D. S. Brenner	Clark University	Nuclear Chemistry	ORAU Faculty Research Participation Program
R. G. Lanier		Nuclear Chemistry	U.S. AEC Postdoctoral Fellowship Program
P. G. Laubereau	Anorganisch-Chemisches Laboratorium, Technische Hochschule München, Munich, Germany	Transuranium Research Laboratory	German Ministry of Science
Zeev Luz	Weizmann Institute of Science, Rehovoth, Israel	Microwave and Radio-Frequency Spectroscopy	Weizmann Institute
R. W. Matthews	Australian Atomic Energy Commission Research Establishment, Lucas Heights, N.S.W.	Radiation Chemistry	Australian Atomic Energy Commission
P. J. Ogren	Maryville College	Radiation Chemistry	ORAU Faculty Research Participation Program
M. J. Pikal	University of Tennessee	Physical Chemistry of Polyelectrolyte Systems	ORAU Faculty Research Participation Program
J. W. Pinson	University of Southern Mississippi	Mass Spectrometry	ORAU Faculty Research Participation Program
Nelva G. Runnalls	Stout State University	Transuranium Research Laboratory	ORAU Faculty Research Participation Program
S. B. Sachs	Weizmann Institute of Science, Rehovoth, Israel	Water Research Program	Temporary Employee
F. K. Schmidt-Bleek	Purdue University	Molecular Beam	Purdue University
R. M. Statnick		Molecular Beam	U.S. AEC Postdoctoral Fellowship Program
D. V. Subrahmanyam	Indian Institute of Science, Bangalore	Water Research Program	Temporary employee
S. P. Tanner	University of West Florida	Transuranium Research Laboratory	Summer employee
W. E. Thiessen		Neutron and X-Ray Crystallography	National Institutes of Health Special Postdoctoral Fellow
D. E. Troutner	University of Missouri	Transuranium Research Laboratory	ORAU Faculty Research Participation Program; temporary employee
M. O. Workman	University of Virginia	Transuranium Research Laboratory	ORAU summer employee

STUDENTS

GRADUATE

Name	Major Professor and/or Institution	Staff Advisor	Field of Research	Sponsor
E. T. Chulick	P. L. Reeder, Washington University	E. Eichler	Delayed-neutron emitters from fission	
M. D. Eckart	C. J. Collins, University of Tennessee	C. J. Collins	The Deamination of Deuterated-2-hydroxy-2-phenyl-3-amino-norbornanes (Ph.D. thesis, December 1968)	Oak Ridge Graduate Fellowship Program
J. A. Fahey	J. R. Peterson, University of Tennessee	J. R. Peterson[1]	Transuranium Research Laboratory	
L. Finkel	J. A. Marinsky, State University of New York at Buffalo	G. E. Boyd E. Eichler R. L. Ferguson	Independent fission yields of ^{101}Tc, ^{104}Tc, and ^{105}Tc from thermal-neutron fission of ^{235}U	
G. R. Freeman	Robert Desiderato, Jr., North Texas State University	H. A. Levy G. M. Brown	X-ray crystal structure of triaryl amines	Oak Ridge Graduate Fellowship Program
D. W. Gosbin	M. H. Lietzke, University of Tennessee	M. H. Lietzke	Monte Carlo calculations of thermodynamic properties of electrolyte solutions	
R. C. Hagenauer	G. D. O'Kelley, University of Tennessee	G. D. O'Kelley E. Eichler	The Decay of Neutron-Deficient Nuclides of Mass 89 (Ph.D. thesis, March 1969)	Oak Ridge Graduate Fellowship Program
R. M. Harbour	D. E. Troutner, University of Missouri		Transuranium Research Laboratory	NDEA Fellowship
C. E. Harding	C. J. Collins, University of Tennessee	C. J. Collins	Solvolyses of ^{14}C-labeled 2-(Δ^3-cyclopentenyl)ethyl tosylates	Oak Ridge Graduate Fellowship Program
R. J. Herdklotz	M. H. Lietzke, University of Tennessee	M. H. Lietzke	Thermodynamic investigations of aqueous HCl-NaCl-$MgCl_2$ solutions	
H. B. Hupf[5]	M. H. Lietzke, University of Tennessee	M. H. Lietzke	Thermodynamic properties of HCl-CsCl-$BaCl_2$ mixtures	ORNL
N. Kashihira	F. Schmidt-Bleek, Purdue University	S. Datz	Chemical accelerator sources	
A. F. Kluk	J. H. Hamilton, Vanderbilt University	N. R. Johnson	Gamma-ray spectra of deformed rare-earth nuclei	U.S. AEC Fellow in Health Physics
R. A. Kuebbing	Case Western Reserve University	E. Eichler J. K. Dickens[6]	$(p,n\gamma)$ reactions on Zr nuclei and a search for E0 radiation in the decay of excited states of ^{80}Kr	Oak Ridge Graduate Fellowship Program
C. W. Linsey	R. B. Escue, North Texas State University	R. H. Busey R. A. Gilbert	High-temperature enthalpies of the lead halides -- enthalpies and entropies of fusion	Oak Ridge Graduate Fellowship Program
W. E. Moddeman	W. E. Bull and G. K. Schweitzer, University of Tennessee	T. A. Carlson	Measurement of the absolute energies of electrons in molecular orbitals[2]	

[5]Isotopes Division.

[6]Neutron Physics Division.

Name	Major Professor and/or Institution	Staff Advisor	Field of Research	Sponsor
H. A. O'Brien[5]	M. H. Lietzke, University of Tennessee	M. H. Lietzke	Thermodynamic properties of aqueous binary mixtures from emf measurements (Ph.D. thesis, June 1968)	ORNL
B. P. Pullen	W. E. Bull and G. K. Schweitzer, University of Tennessee	T. A. Carlson	Photoelectron spectroscopy of simple molecules[2]	Oak Ridge Graduate Fellowship Program
L. L. Riedinger, Jr.	J. H. Hamilton, Vanderbilt University	N. R. Johnson	Studies of the Collective States in ^{152}Gd, ^{152}Sm, and ^{154}Gd (Ph.D. thesis, January 1969)	Oak Ridge Graduate Fellowship Program

UNDERGRADUATE

Name	Institution	ORNL Research Program	Sponsor
H. Bryan Alphin	Sweet Briar College	Organic Chemistry	ORAU Summer Student Trainee Program
E. R. Black	Westminster College	Chemistry of Aqueous Systems	ORAU Summer Student Trainee Program
D. E. Chyba	LaSalle College	Solution Spectrophotometry	ORAU Summer Student Trainee Program
Ellen J. Elliott	Centre College	Water Research Program	ORAU Summer Student Trainee Program
L. Howdyshell	University of Tennessee	Transuranium Research Laboratory	UT Senior Honors Research Program
Miriam E. McShan	Southeastern Louisiana College	Transuranium Research Laboratory	ORAU Summer Student Trainee Program
J. G. Porterfield	University of Tennessee	Chemistry of Aqueous Systems	Cooperative Education Program

ORNL-4437
UC-4 – Chemistry

INTERNAL DISTRIBUTION

1. Biology Library
2–4. Central Research Library
5. Laboratory Shift Supervisor
6. MIT Practice School
7–8. ORNL – Y-12 Technical Library Document Reference Section
9–41. Laboratory Records Department
42. Laboratory Records, ORNL R.C.
43. H. I. Adler
44. P. A. Agron
45. C. R. Baldock
46. W. H. Baldwin
47. C. E. Bemis
48. D. S. Billington
49. F. F. Blankenship
50. E. G. Bohlmann
51. C. J. Borkowski
52–56. G. E. Boyd
57. M. A. Bredig
58. R. B. Briggs
59. H. R. Bronstein
60. A. R. Brosi
61. G. M. Brown
62. J. H. Burns
63. R. H. Busey
64. W. R. Busing
65. T. A. Carlson
66. G. H. Cartledge
67. C. J. Collins
68. D. R. Cuneo
69. F. L. Culler
70. M. D. Danford
71. S. Datz
72. J. S. Drury
73. A. S. Dworkin
74. E. Eichler
75. R. L. Ferguson
76. J. L. Gabbard
77. J. A. Ghormley
78. R. A. Gilbert
79. J. H. Gillette
80. W. R. Grimes
81. R. L. Hahn
82. J. Halperin
83. R. F. Hibbs
84. C. J. Hochanadel
85. H. P. Carter
86. J. S. Johnson
87. N. R. Johnson
88. W. H. Jordan
89. M. A. Kastenbaum
90. O. L. Keller
91. M. T. Kelley
92. B. H. Ketelle
93. K. A. Kraus
94. J. A. Lane
95. E. Lamb
96. H. A. Levy
97. M. H. Lietzke
98. T. A. Lincoln
99. S. Lindenbaum
100. R. Livingston
101. R. S. Livingston
102. R. N. Lyon
103. H. G. MacPherson
104. Peter Mazur
105. J. R. McNally, Jr.
106–116. G. E. Moore
117. K. Z. Morgan
118. A. H. Narten
119. L. J. Nugent
120. G. D. O'Kelley
121. G. W. Parker
122–123. R. B. Parker
124. J. J. Pinajian
125. F. A. Posey
126. Helen Raaen
127. R. J. Raridon
128. S. A. Reynolds
129. P. S. Rudolph
130. H. E. Seagren
131. C. H. Secoy
132. E. D. Shipley
133. M. J. Skinner
134. A. H. Snell
135. R. W. Stoughton
136. D. A. Sundberg
137. T. J. Sworski
138–167. E. H. Taylor
168. R. E. Thoma
169. P. F. Thomason
170. F. Vaslow
171. G. M. Watson
172. A. M. Weinberg

173. T. E. Willmarth
174. F. A. Long (consultant)
175. H. H. Sisler (consultant)
176. Gerhart Friedlander (consultant)
177. P. D. Bartlett (consultant)
178. G. Scatchard (consultant)
179. J. J. Katz (consultant)

EXTERNAL DISTRIBUTION

180. H. Miller, Office of Isotope Development, AEC, Washington
181. R. H. Schuler, Radiation Research Laboratories, Mellon Institute, 4400 Fifth Ave., Pittsburgh 13, Pa.
182. Division of Research and Development, AEC, Washington
183. Laboratory and University Division, AEC, ORO
184. Boeing Airplane Company
185. Union Carbide Corporation, Chemicals Division (South Charleston)
186. North American Aviation, Inc.
187. Masaharu Kondo, Professor of Chemistry, Radiation Chemistry Laboratory, Tokyo Metropolitan University, 1-950, Fukasawa-cho, Setagaya-ku, Tokyo, Japan
188. M. Daniels, Department of Chemistry, University College of West Indies, Kingston 7, Jamaica
189. J. P. W. Houtman, Reactor Institute Delft, Technische Hogeschool, Delft, The Netherlands
190. Technion, Israel Institute of Technology, Department of Nuclear Science, Haifa, Israel
191. W. T. Smith, Jr., Department of Chemistry, University of Tennessee, Knoxville
192. J. H. Green, Department of Nuclear and Radiation Chemistry, The University of New South Wales, P.O. Box 1, Kensington, N.S.W., Australia
193. Ingmar Bergstrom, Nobel Institute of Physics, Stockholm 50, Sweden
194. Riki Kobayashi, William Marsh Rice University, Houston, Texas
195. J. A. Swartout, 270 Park Avenue, New York 17, New York
196. W. W. Grigorieff, Assistant to the Executive Director, Oak Ridge Associated Universities
197. Enrico Cerrai, CISE, Milan, Italy
198. H. E. Podall, U.S. Department of the Interior, Office of Saline Water, Washington, D.C.
199. D. E. Troutner, Chemistry Department, University of Missouri, Columbia, Missouri
200. J. H. Hamilton, Physics Department, Vanderbilt University, Nashville, Tennessee
201. W. H. McCoy, Office of Saline Water, U.S. Department of the Interior, Washington, D.C.
202. Sidney Johnson, Office of Saline Water, U.S. Department of the Interior, Washington, D.C.
203. F. H. Coley, Office of Saline Water, U.S. Department of the Interior, Washington, D.C.
204. W. A. Schwartz, Cincinnati Water Research Laboratory, 4676 Columbia Parkway, Cincinnati, Ohio
205. Sidney Langer, Gulf General Atomic, San Diego, California
206. J. R. Peterson, Department of Chemistry, University of Tennessee, Knoxville, Tennessee
207. S. B. Sachs, Gulf General Atomic, San Diego, California
208. Library, Wah Chang Albany Corporation, P.O. Box 460, Albany, Oregon

209–413. Given distribution as shown in TID-4500 under Chemistry category (25 copies – CFSTI)